

Diss. ETH No. 14890

Operation and Control of Azeotropic Distillation Column Sequences

A dissertation submitted to the
Swiss Federal Institute of Technology (ETH)
Zurich

for the degree of
Doctor of Technical Sciences
(Dr. sc. techn.)

presented by
Jan Ulrich
Dipl.-Ing. (Universität Karlsruhe)
born 18.01.1972
citizen of Germany

accepted on the recommendation of
Prof. Manfred Morari, examiner
Prof. Marco Mazzotti, co-examiner

November, 2002

© 2002
Jan Ulrich
All Rights Reserved

Preface

This doctoral thesis is the result of my work as a research and teaching assistant at the Automatic Control Laboratory (IfA), Swiss Federal Institute of Technology (ETH) Zürich. I would like to take the opportunity to thank the people who accompanied me during these years.

First of all, I am most thankful to Prof. Manfred Morari for accepting me as a PhD student, for giving me the opportunity to study control of distillation columns in great detail, and for the freedom he allowed me for my research. Our discussions always sharpened my ideas and brought my research to life. Further, I thank Prof. Marco Mazzotti for his willingness to be my co-advisor and the interesting discussions about my work and chemical engineering in general.

I would like to thank Dr. Thomas E. Güttinger for initiating the contact to Lonza AG, Walliser Werke, Visp and laying the basis together with Jimmy Wells for my first project. I would like to thank Dr. Ralf Proplesch, Claudio Arnold, Dr. Kishore Nedungadi, and Dr. Felix Previdoli (Lonza AG) for the opportunity to work on an industrial problem. Thanks go to the students Jörg Loeser and Daniel Nüssli for their contributions in that project.

The almost daily discussions with my colleague in distillation Dr. Cornelius Dorn gave me an excellent start and always sharpened both of our ideas about our research projects and life in general. Thanks, Cornelius! I also thank Dr. Oliver Kaiser for his scientific and non-scientific support of my work and Eleonora Bonanomi for being a helpful colleague and for keeping the spirit of chemical engineers in an electrical engineering department. Further, I thank Dr. Ron Pearson for the interesting discussions and advices. Many

thanks go also to the rest of the lunch group (Dr. Domenico Mignone, Kazuro Tsuda, Dr. Toru Kawabe, Tobias Geyer, Mato Baotic, Dominik Niederberger, Jordi Bonet, Frank Christophersen, Rainer Möbus) for the interesting discussions that contributed to this thesis in one way or the other. Finally, I thank the people of the Informatic Support Group for the good collaboration during my time as informatic coordinator and our secretaries Esther Hagenow, Martine D'Emma, Alice Vyskocil und Danielle Couson for their support.

My deepest gratitude goes to my parents and my sister for all their support that enabled me to reach this point of my scientific career, and to Susana for her love, support and understanding. It is them this thesis is dedicated to.

Abstract

Distillation is the most widely used unit operation in chemical industries to separate multi-component fluid mixtures. For zeotropic mixtures, a simple sequence of distillation columns will give pure products. For azeotropic mixtures, the column sequences often have product recycles that change the steady state and dynamic behavior. In this thesis, a theoretical asymptotic case is used to understand the behavior of homogeneous and heterogeneous azeotropic distillation column sequences and to propose control schemes for them. The results are then validated using rigorous simulations.

First, a concept is presented for the design of heterogeneous distillation columns under aspects of operability. The column behavior is analyzed using residue curve maps and a theoretical finite reflux/infinite length column. In particular, the influence of impurities on the operation of the column is discussed. Depending on the impurities, different control schemes with different designs of the process have to be used to guarantee robust performance. Here, robustness is not against modeling errors, but against typical nonlinear phenomena such as the disappearance of the phase split in the decanter.

The key idea of the control schemes is that the overall feed composition has to be adjusted to changes in the crude feed by manipulating the entrainer flow rate, and in the presence of impurities by manipulating an additional flush stream. The theoretical findings are illustrated by steady state and dynamic simulations of an industrial column where a heavy boiling organic substance is dewatered using MTBE as light entrainer.

Second, a self-optimizing control concept is provided for a sequence of three homogeneous azeotropic distillation columns with two recycles (boundary separation scheme). This se-

quence separates a three component 020 mixture, which has two simple distillation regions, into pure components. The residue curve boundary that separates the two simple distillation regions can be crossed by simple mixing of products because it is curved. Studying a case with reduced complexity (columns of infinite length operated at infinite reflux), one of the two recycles (the recycle of the entrainer) is identified as the key manipulated variable to ensure the feasibility and optimality of the process. Similar to the results for the heterogeneous columns, the key aspect is that the overall feed composition of one column of the sequence has to be changed by manipulation of the entrainer recycle such that the distillate composition is at the optimal point. For a finite sequence, the distillate composition of that particular column indicates the entrainer holdup in the system that plays a central role for the success of the process and can be manipulated via the entrainer recycle. Based on this insight, a control scheme is introduced that is robust towards uncertainties in the curvature of the residue curve boundary.

The theoretical results are validated with rigorous simulations of a three column sequence for a 020 mixture: methanol, 2-propanol and water. Dynamic simulations confirm that the process operates robust using standard control for the individual columns and one additional control loop that controls the entrainer holdup. Dynamic simulations also confirm that column profiles can cross residue curve boundaries, distillation boundaries and even azeotropes if the feed composition is changed such that a column profile is only feasible in the other distillation region.

Further, a short cut method is developed to compare the performance of homogeneous and heterogeneous sequences based on the sum of the reboiler duties for identical equipment. A general result is that the homogeneous boundary separation scheme has a lower energy consumption for low contents of the intermediate boiler of 020 mixtures compared to heterogeneous sequences with the same equipment. These results are illustrated with the methanol–2-propanol–water mixture and cyclohexane as heterogeneous entrainer showing that the boundary separation scheme is the best alternative up to 15 mass-% 2-propanol in the crude feed.

Zusammenfassung

Destillation und mehrstufige Rektifikation sind die in der chemischen Industrie am weitesten verbreiteten Prozesse zur Trennung fluider Mehrkomponentengemische. Bei zeotropen Gemischen können die Gemische durch einfache Reihenschaltung von Rektifikationskolonnen in reine Produkte aufgetrennt werden. Für Gemische mit einem azeotropen Punkt haben die Kolonnensequenzen oft Produkt- und Schleppmittelrückführungen, die das stationäre und dynamische Verhalten der Sequenzen ändern. In dieser Arbeit wird das Verhalten von homogenen und heterogenen azeotropen Rektifikationskolonnensequenzen mit Hilfe eines asymptotischen Grenzfalles untersucht. Auf der Basis dieser Untersuchungen werden Konzepte zur Regelung dieser Prozesse erarbeitet, die dann mit rigorosen Prozesssimulationen validiert werden.

Zuerst wird ein Konzept zur Auslegung und Konstruktion von heterogenen Destillationsskolonnen unter Berücksichtigung des Betriebsverhaltens vorgestellt. Das Betriebsverhalten der Kolonne wird mit Rückstandskurvendiagrammen und einer theoretischen Kolonne, die mit endlichem Rückfluss betrieben wird und unendlich lang ist, untersucht. Besonders wird der Einfluss von Verunreinigungen auf das Betriebsverhalten der Kolonnen diskutiert. Je nach Verunreinigung müssen verschiedene Regelungskonzepte in Verbindung mit verschiedenen Anlagenkonfigurationen gewählt werden, um ein robustes Betriebsverhalten zu ermöglichen. Robustheit ist in diesem Zusammenhang nicht Robustheit gegen Modellierungsfehler, sondern gegen typische nichtlineare Phänomene wie das Verschwinden des Phasensplits im Dekanter.

Die Kernidee des Regelungsschemas ist, die Zusammensetzung des Gesamtzulaufs an Änderungen des zu trennenden Rohzulaufs durch Veränderung des Schleppmittelzulaufs anzu-

passen. Bei gewissen Verunreinigungen im Rohzulauf kann dies nur mit Hilfe eines zusätzlichen Spülstromes erreicht werden. Die theoretischen Ergebnisse werden mit stationären und dynamischen Simulationen einer industriell betriebenen Rektifikationskolonne veranschaulicht. Die industrielle Kolonne entwässert einen organischen Schwersieder mit der Hilfe von MTBE als leichtsiedendes Schleppmittel.

Im zweiten Teil der Arbeit wird ein selbstoptimierendes Regelungskonzept für eine Sequenz aus drei Kolonnen mit zwei Produktrückführungen vorgestellt. Die Sequenz trennt ein ternäres 020 Gemisch, das zwei Destillationsgebiete hat, in die reinen Komponenten. Die Grenzurückstandskurve, die die beiden Destillationsgebiete trennt, kann durch einfaches Mischen von Produkten überwunden werden, da sie gekrümmt ist. Bezüglich der Machbarkeit und dem optimalen Betriebspunkt der Sequenz wurde mit Hilfe eines asymptotischen Grenzfalls (Kolonnen mit unendlicher Länge, die mit unendlich hohem Rückfluss betrieben werden) eine der beiden Produktrückführungen (die des Schleppmittels) als die Kernvariable identifiziert. Ähnlich wie bei den heterogenen Kolonnen muss auch bei einer der Kolonnen der homogenen Sequenz die Zusammensetzung des Gesamtzulaufs zu dieser Kolonne durch Ändern des Schleppmittelzulaufs derart verändert werden, dass in diesem Fall die Destillatzusammensetzung am optimalen Punkt bleibt. Bei einer Sequenz endlich langer Kolonnen mit endlichem Rückfluss ist diese Destillatzusammensetzung ein Mass für die Schleppmittelmenge im System. Diese spielt eine zentrale Rolle für den Erfolg der Trennaufgabe und muss separat geregelt werden. Aufgrund dieser Erkenntnisse wird ein Regelungsschema vorgestellt, das robust gegenüber Unsicherheiten in der Kenntnis der Krümmung der Grenzurückstandskurve ist.

Die theoretischen Ergebnisse werden mit rigorosen Simulationen einer 020 Mischung bestehend aus Methanol, 2-Propanol und Wasser validiert. Dynamische Simulationen zeigen, dass der Prozess robust mit Standardregelungsschemata für die einzelnen Kolonnen und einem zusätzlichem Regelkreis, der die Schleppmittelmenge in der Sequenz regelt, betrieben werden kann. Ferner wird mit dynamischen Simulationen gezeigt, dass Kolonnenprofile Grenzurückstandskurven, Grenzdestillationslinien und sogar Azeotrope überwinden können, wenn die Zulaufzusammensetzung so geändert wird, dass ein machbares Kolonnenprofil nur in dem anderen Destillationsgebiet liegt.

Zuletzt wird eine Short-Cut Methode vorgestellt, mit der die Wirtschaftlichkeit homogener und heterogener Kolonnensequenzen anhand der benötigten Verdampferleistung bei gleicher Anlagenausstattung verglichen werden kann. Ein allgemein gültiges Ergebnis ist, dass die homogene Drei-Kolonnensequenz für geringe Mengen des Mittelsieders einer 020 Mischung den geringsten Energieverbrauch im Vergleich zu heterogenen Sequenzen mit der gleichen Ausstattung aufweist. Die Anwendung dieser Methode auf das Gemisch Methanol, 2-Propanol und Wasser mit Cyclohexan als heterogenes Schleppmittel zeigt, dass die homogene Sequenz (ohne das Schleppmittel Cyclohexan) für 2-Propanol-Gehalte bis zu 15 Masse-% im Rohzulauf die beste Alternative ist.

Contents

Preface	iii
Abstract	v
Zusammenfassung	vii
1 Introduction	1
1.1 Motivating Example	3
1.2 Thesis Overview	6
2 Preliminaries, Concepts and Tools	9
2.1 Distillation	9
2.1.1 Residue Curve Maps	12
2.1.2 ∞/∞ Analysis	15
2.2 Boundary Separation Scheme	18
2.2.1 Definitions	19
2.2.2 Review	21
2.3 Heterogeneous Distillation	24

2.3.1	Definitions	24
2.3.2	Review on Control of Heterogeneous Distillation	26
2.4	Self-Optimizing Control	28
2.4.1	Requirements for Controlled Variables	28
2.4.2	Procedure for Selection	29
2.4.3	Implementation of Controlled Variables	30
I	Control of Heterogeneous Azeotropic Distillation Columns	33
3	Analysis and Controller Design of a Heterogeneous Azeotropic Distillation Column	35
3.1	Industrial Plant	35
3.2	Steady State Analysis	38
3.2.1	Degrees of Freedom	38
3.2.2	Analysis with the ∞/∞ Column	39
3.2.3	Analysis with the Finite/ ∞ Column	42
3.3	Influence of Impurities	43
3.3.1	Light Impurity – LL	43
3.3.2	Intermediate Impurity 1 – LI	47
3.3.3	Intermediate Impurity 2 – IH	49
3.3.4	Heavy Impurity – HH	50
3.3.5	Summary	51

3.4	Control Schemes	51
3.4.1	Specifications	52
3.4.2	Two Point Control for the Three Component Mixture	53
3.4.3	Problems with Two Point Control for a Four Component Mixture	56
3.4.4	Three Point Control for the Four Component Mixture	57
4	Simulations of a Heterogeneous Azeotropic Distillation Column	61
4.1	Modeling	61
4.1.1	Column Model	61
4.1.2	Industrial Plant–Model Comparison	63
4.1.3	Composition of the Ternary Azeotrope	64
4.2	System MTBE/Water/MBI	66
4.2.1	Validation of Finite/ ∞ Column Predictions	66
4.2.2	Selection of Operation Point	69
4.2.3	Controller Implementation	70
4.2.4	Dynamic Simulations	73
4.3	System MTBE/Acetone/Water/MBI	75
4.3.1	Validation of Finite/ ∞ Column Predictions	75
4.3.2	Two Point Control	79
4.3.3	Three Point Control	82
4.3.4	Industrial Plant	84

II	Azeotropic Distillation Column Sequences	89
5	Design and Control of the ∞/∞ Boundary Separation Schemes	91
5.1	Problem Statement	91
5.2	Cost Function	96
5.3	Degrees of Freedom and Constraints	97
5.3.1	Sequence A: Three Columns in a Row	97
5.3.2	Sequence B: Three Columns with One Recycle	100
5.3.3	Sequence C: Three Columns with Two Recycles	105
5.4	Optimization	108
5.4.1	Sequence B	108
5.4.2	Sequence C	110
5.5	Selection of Controller Pairings	122
5.6	Evaluation of the Controlled Variable x^{D_1}	123
5.6.1	Sequence C Setup 1	123
5.6.2	Sequence C Setup 2	129
5.7	Boundary Separation Scheme with Three Recycles	132
6	Design and Control of the Finite Boundary Separation Scheme	135
6.1	Degrees of Freedom	135
6.2	Cost Function and Constraints	136
6.3	Identification of Important Disturbances	136

6.4	Optimization	137
6.5	Selection of Controlled Variables	139
6.6	Evaluation of the Sets of Controlled Variables	142
6.6.1	Set 1	143
6.6.2	Feed 1	145
6.6.3	Feed 2	146
6.6.4	Feed 3	147
6.6.5	Feed Variation	148
6.7	Model Uncertainties	150
6.7.1	Influence on the ∞/∞ Column Sequence	150
6.7.2	Influence on Set 2a	152
6.7.3	Influence of Pressure	153
6.7.4	Comparison to Experiments	157
6.8	Implementation of the Concept in a Process Simulator	159
6.8.1	Control of Column 1	161
6.8.2	Control of Column 2	167
6.8.3	Control of Column 3	170
6.8.4	Control of the Three Column Sequence	173
7	Performance of Homogeneous and Heterogeneous Sequences	177
7.1	Boundary Separation Scheme	178

7.2	Heterogeneous Sequences	181
7.2.1	Methanol Removal Column	182
7.2.2	Direct Heterogeneous Sequence	184
7.2.3	Indirect Heterogeneous Sequence	187
7.2.4	Comparison of the Direct with the Indirect Sequence	190
7.3	Comparison of the Homogeneous Sequences with the Heterogeneous Sequences	191
8	Conclusions	195
A	System Acetone/Water/MBI/MTBE	209
A.1	Thermodynamic Data	209
A.1.1	Pure Component Data of MBI	209
A.1.2	Vapor–Liquid Equilibrium	209
A.1.3	Liquid–Liquid Equilibrium	211
A.2	Optimization of the Column Sequences	211
A.2.1	Heterogeneous Sequence	211
A.2.2	Boundary Separation Scheme	217
B	System Methanol/2-Propanol/Water/Cyclohexane	219
B.1	Residue Curve Maps	219
B.2	Boundary Separation Scheme	221
B.2.1	Analysis of Column 1	221
B.2.2	Further Sets of Controlled Variables	226

<i>Contents</i>	xvii
B.2.3 Effect of the Recycle R_2	229
B.2.4 Continuum of Solutions	230
B.3 Simulations of the Direct Heterogeneous Sequence	236
B.3.1 Methanol-Free B_1	236
B.3.2 Methanol polluted B_1	238
B.4 Simulations of the Indirect Heterogeneous Sequence	239
B.4.1 Methanol-Free B_1	239
B.4.2 Methanol polluted B_1	241
C Simple Examples for Illustration	243
C.1 Quadratic Residue Curve Boundary for the BSS	243
C.1.1 Sequence B	243
C.1.2 Sequence C: Setup 1	244
C.1.3 Sequence C: Setup 2	245
C.2 Intermediate Entrainer State Multiplicities	246
C.3 Models for Input and Output Multiplicities	246
C.4 Inverse Response Behavior	250

Chapter 1

Introduction

In the chemical industry, distillation is the most common process to separate multicomponent mixtures. If the mixtures are zeotropic, they can be separated into pure components by a simple distillation sequence. If the mixture is azeotropic, a simple sequence cannot separate the mixture into its pure components. A common technique is to break the azeotrope by a third component, the entrainer, which is added to the mixture. The key idea is to remove one component in the first column and to process the other component enriched with the entrainer to a second column. In the second column, the entrainer is recovered and recycled to the first column while the second component is retrieved. Hence, azeotropic distillation sequences exhibit recycles. Product recycles change the steady state and dynamic properties of the system (Luyben, 1993a; Luyben, 1993b; Luyben, 1993c; Luyben, 1993d), which make operation and control of the sequences with recycles more difficult than sequences without recycles.

One of the most difficult tasks in designing a separation sequence is the proper choice of entrainers which has been extensively discussed in literature (Doherty and Calderola, 1985; Stichlmair et al., 1989; Laroche et al., 1991; Laroche et al., 1992b; Foucher et al., 1991; Wahnschafft and Westerberg, 1993) and is also subject of chemical engineering textbooks about separation processes (Doherty and Malone, 2001; Stichlmair and Fair, 1998). There are four different kinds of entrainers (Laroche et al., 1991):

Homogeneous Entrainers. They alter the relative volatility of the two azeotropic com-

ponents without inducing a liquid immiscibility with either one of the components.

Heterogeneous Entrainers. They alter the relative volatility of the two azeotropic components and induce a liquid immiscibility with one of the components that is used as an additional separation step.

Reactive Entrainers. They react reversibly and preferentially with only one of the azeotropic components changing the components involved in the separation.

“Salting” Entrainers. They dissociate ionically in the solution altering the azeotropic composition of the mixture to be separated.

Homogeneous and heterogeneous entrainers are the most common in chemical industry. Homogeneous entrainers can be subdivided into three classes for separating a minimum boiling azeotrope depending on the boiling temperature compared to the azeotropic components: light, intermediate and heavy entrainers. These entrainers are extensively discussed by Laroche et al. (1991), the key points are briefly summarized:

The most common entrainer is the heavy entrainer that may outperform a heterogeneous sequence (Knight and Doherty, 1989), but operation is difficult because a high purity of the heavy entrainer recycle is required (see Knight and Doherty (1989) for details), and in operation it is difficult to determine the best amount of recycle and reflux as discussed by Andersen et al. (1995).

Intermediate entrainers are rarely used. They hardly change the relative volatility because of the small boiling point differences, which leads to long columns with a high energy consumption.

Light entrainer topologies are also common in the chemical industry. When two components react with each other to form a third component, the third component is often a larger molecule with a higher boiling temperature that can build a minimum-boiling azeotrope with one of the reactants. The best entrainer candidates to break a possible azeotropes of the products are then either the reactants or side products of the reaction. Though these light entrainers have the advantage that no additional component has to be introduced to the process, they are hardly used in industries for two reasons. They

are often economically worse than heterogeneous schemes and they are difficult to operate because of a large uncertainty in a physical property of the mixture: the curvature of the residue curve boundary. There are different names in literature for the light entrainer scheme:

- processes with border crossing (Stichlmair, 1988; Stichlmair et al., 1989; Stichlmair and Herguijuela, 1992),
- the light entrainer scheme (Laroche et al., 1991; Laroche et al., 1992b),
- boundary separation scheme (Güttinger and Morari, 1996).

Since the scheme is the same for a heavy entrainer used for the separation of a maximum boiling azeotrope (Stichlmair, 1988; Stichlmair et al., 1989), the general term of Güttinger and Morari (1996) is used: boundary separation scheme.

Heterogeneous entrainers alter the relative volatility more than homogeneous ones (a large difference in the activity coefficients is needed to introduce the instability of the liquid phase). Hence, they are preferred in industry. However, the operation of the decanter is not easy. The phase split might disappear as a result of a disturbance. This leads to severe upsets in plant operation. An opposite effect is that the liquid-liquid split can occur on the trays of the column leading to efficiency losses (Kovach III and Seider, 1987).

1.1 Motivating Example

The motivating example for this work is the dewatering of methyl isobutanol (MBI) in the presence of unreacted acetone. MBI is an intermediate product for isoprene and vitamin A production. MBI is produced by the reaction of acetylene with acetone in the presence of ammonia as solvent and aqueous KOH as catalyst (Tedeschi et al., 1963; De Malde et al., 1964). Hence, the product stream contains MBI, acetylene, ammonia, acetone, water and some byproducts, which are mainly heavy boilers. Figure 1.1 shows the separation sequence of the industrial plant (Kürüm, 1996). Ammonia and acetylene are recovered first

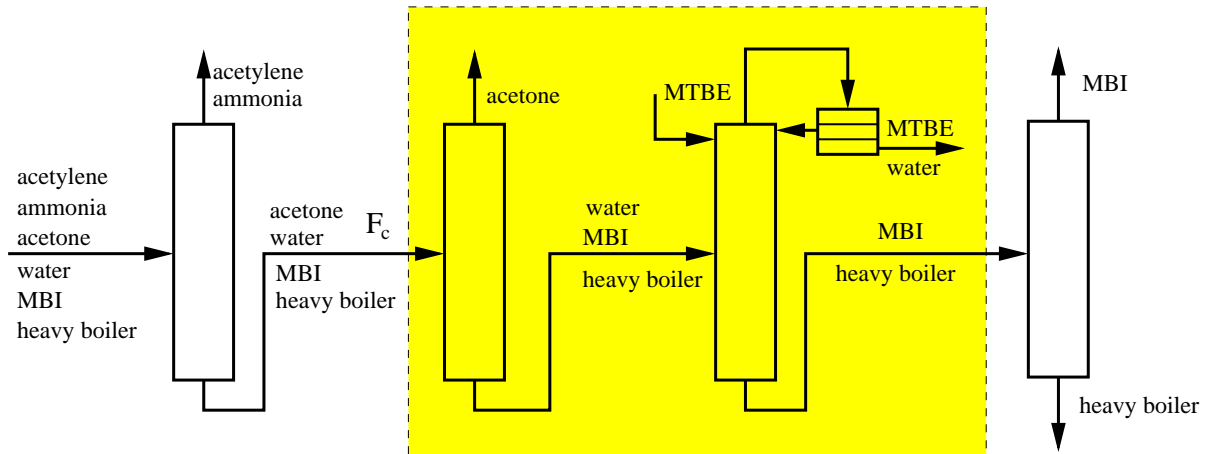


Figure 1.1: Separation sequence of MBI production.

and recycled to the reactor. In a second step, acetone is separated from the product stream and recycled. After the removal of some very heavy boilers by simple flashing, the product stream contains mainly MBI ($x_{MBI} \approx 0.95$ kg/kg), little amount of water ($x_{water} \approx 0.02$ kg/kg), traces of acetone ($x_{acetone} < 0.001$ kg/kg), and heavy boilers ($x_{hb} \approx 0.03$ kg/kg). Because MBI and water form a minimum boiling azeotrope, the product stream is fed to an azeotropic distillation column to dewater the product MBI with the light entrainer MTBE. The dewatered product stream leaves the azeotropic column through the bottom and enters a succeeding column where the heavy boiling byproducts are removed.

The first motivation to analyze this process was a problem with the operation of the heterogeneous column. It was operated with two point control and the two controllers were difficult to tune. Part I of this thesis analyzes this process in detail and the results have already been published (Ulrich and Morari, 2002).

The same process is also the motivation for Part II of this thesis. The separation of acetone, water, and MBI as indicated by the dashed box in Figure 1.1 is further analyzed. For an arbitrary feed¹ as given in Table 1.1, the heterogeneous two column sequence consumes

¹While the feed to the azeotropic column is known (Ulrich and Morari, 2002), the feed to the acetone column is proprietary. Based on the thesis of Kürüm (1996), the acetone mass fraction of the acetone recycle is about 0.99. If all the heavy boilers are lumped to MBI, then the feed to the acetone column has to lie on the mass balance line that connects the concentration of the acetone recycle with the feed of the heterogeneous column. By this, the feed was arbitrarily set to the values given in Table 1.1.

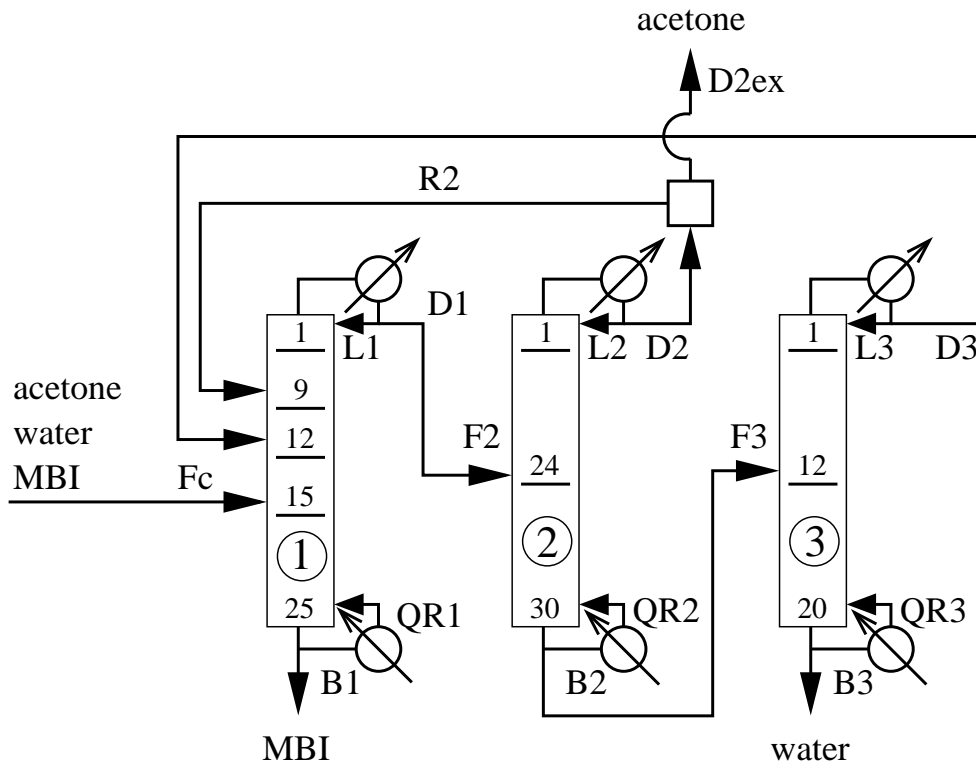


Figure 1.2: Boundary separation scheme.

Table 1.1: Arbitrary base case crude feed F_C for the mixture acetone/water/MBI.

flow rate	$x_{acetone}^{F_C}$	$x_{water}^{F_C}$	$x_{MBI}^{F_C}$	pressure	temperature
2200 kg/h	0.27 kg/kg	0.02 kg/kg	0.71 kg/kg	1.1 bar	80° C

763.8 kW. For the same feed, a boundary separation scheme as shown in Figure 1.2 needs only 558.3 kW. Figure 1.3 shows a comparison of the sum of the reboiler duties of the two sequences for different crude feed compositions (a detailed study of these two schemes can be found in appendix A.2). Both sums are proportional to the water mass fraction in the crude feed. For the boundary separation scheme, the proportionality factor is higher than for the heterogeneous sequence. For water mass fractions up to 0.04 kg/kg, the boundary separation scheme consumes less energy than the heterogeneous sequence and is the better alternative for these feed compositions.

The goals of this work are

- to understand the dependency of the reboiler duties on the crude feed composition,

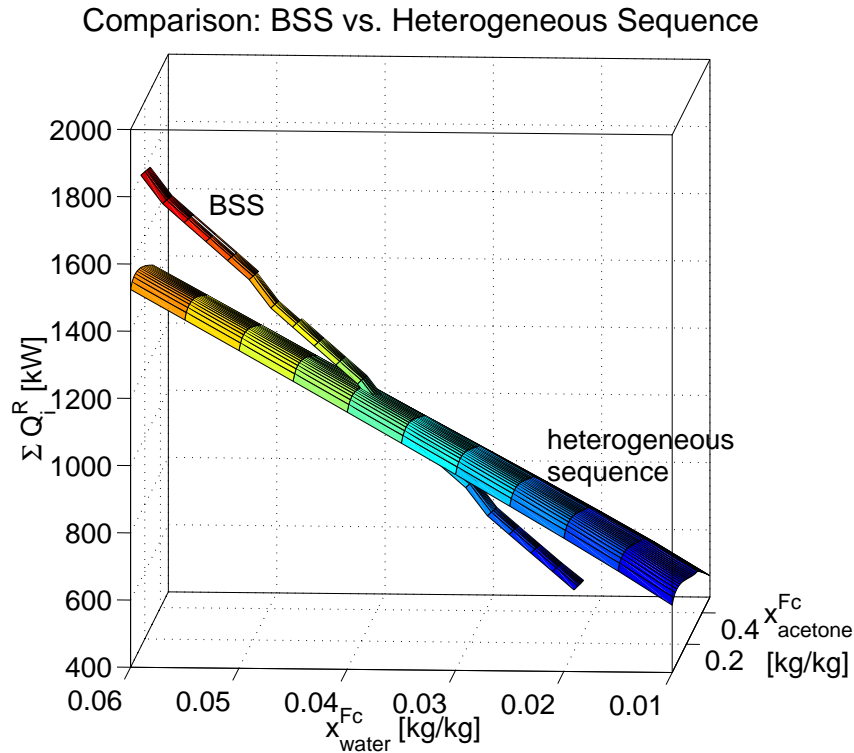


Figure 1.3: Comparison of the sum of the reboiler duties of the heterogeneous sequence with the boundary separation scheme (BSS).

- to understand the steady state and dynamic behavior of the boundary separation scheme and column sequences with recycles in general,
- to propose an optimal operation point for these sequences,
- and to propose an optimal operation strategy for these sequences.

1.2 Thesis Overview

The thesis is structured in two parts: In **Part I**, the design of a heterogeneous distillation column under aspects of operability is discussed. In **Part II** a self-optimizing control concept is developed for the boundary separation scheme.

Before these two parts, **Chapter 2** introduces some basics of distillation and in particular the concept of the ∞/∞ analysis (Bekiaris et al., 1993; Bekiaris et al., 1996) that is a very

useful tool to predict the product paths of distillation columns by analyzing an asymptotic case (section 2.1). The results available in literature about the boundary separation scheme are presented and discussed (section 2.2). Section 2.3 introduces heterogeneous column sequences and gives short review about operation and control of heterogeneous distillation columns. Section 2.4 summarizes the concept of self-optimizing control that will be used to propose a robust operation strategy for the boundary separation scheme.

Part I starts with **Chapter 3**. Section 3.1 introduces the specific industrial heterogeneous column. In section 3.2, this column is analyzed using theoretical finite and infinite reflux / infinite length columns, which are useful to predict the behavior of heterogeneous azeotropic distillation columns. In section 3.3, the limitations of operability caused by impurities are analyzed. Control schemes, which are robust against impurities, are presented in section 3.4 for this class of heterogeneous mixtures. **Chapter 4** validates the results of Chapter 3 for a the finite heterogeneous column separating water from methyl isobutanol. First, the model of the industrial process is described (section 4.1). In the sections 4.2 and 4.3, simulations of the industrial process validate the predictions of the finite reflux / infinite length column.

Part II studies the boundary separation scheme. In **Chapter 5**, a self-optimizing control scheme is developed for a sequence with reduced complexity: a sequence of ∞/∞ columns. The problem statement is given in section 5.1 where the three possible setups of the boundary separation scheme are introduced. Then, a cost function for the ∞/∞ columns is derived (section 5.2). The analysis of the degrees of freedom and of the feasible feed regions (section 5.3) of the sequence lay the basics for the optimization (section 5.4). An optimal operation point is identified for two of the three setups that is independent of the crude feed composition. A set of controller pairings is selected (section 5.5) and analyzed (section 5.6). The influence of an additional manipulated variable is discussed (section 5.7).

In **Chapter 6**, the results of chapter 5 are applied to a real system: the separation of methanol, 2-propanol and water. Again, the first steps of the self-optimizing control concept are applied (degrees of freedom, cost function, constraints, disturbances and optimization, section 6.1 to section 6.4). Different sets of controlled variables are introduced (section 6.5) and analyzed (section 6.6). In section 6.7, the model uncertainty is discussed.

Section 6.8 shows the implementation of one set of controlled variables as decentralized linear single-loop controllers. Dynamic simulations validate that this scheme works well. Further, dynamic simulations show that distillation boundaries and even azeotropes can be crossed if the feed composition is changed such that the mass balance forces the column profile to cross these boundaries.

Chapter 7 transfers the concept of finding an optimal operation point from the homogeneous boundary separation scheme to heterogeneous schemes. The results are discussed on the basis of the separation of methanol, 2-propanol, and water using cyclohexane as entrainer.

Chapter 8 summarizes and concludes the thesis.

Chapter 2

Preliminaries, Concepts and Tools

2.1 Distillation

Distillation is one of the oldest unit separation processes. The key idea of this separation process is that there is a difference between the composition of the liquid phase and of the vapor phase when these two phases are in equilibrium. Figure 2.1a shows a simple flash unit. A feed F of a liquid mixture with the composition vector x^F enters the flash unit and is partially vaporized. If the vapor and the liquid phase are in equilibrium, then the vapor will have a different composition than the liquid phase for zeotropic mixtures.

Definition 1. Zeotropic mixture: *A two component mixture of L and H with L lighter boiling than H is called zeotropic mixture if the difference between the vapor phase composition y_L and the liquid phase composition x_L is always greater than zero.*

For a zeotropic mixture, L will be enriched in the vapor stream V . If the vapor is condensed and partially vaporized again, L will further enrich. For a cascaded process where the vapor is condensed and vaporized upstream while the remaining liquid L is recycled to the flash unit down stream (Figure 2.1b), pure L can be obtained at the upper end of this process, and pure H at the lower end. For an azeotropic mixture, this is not possible.

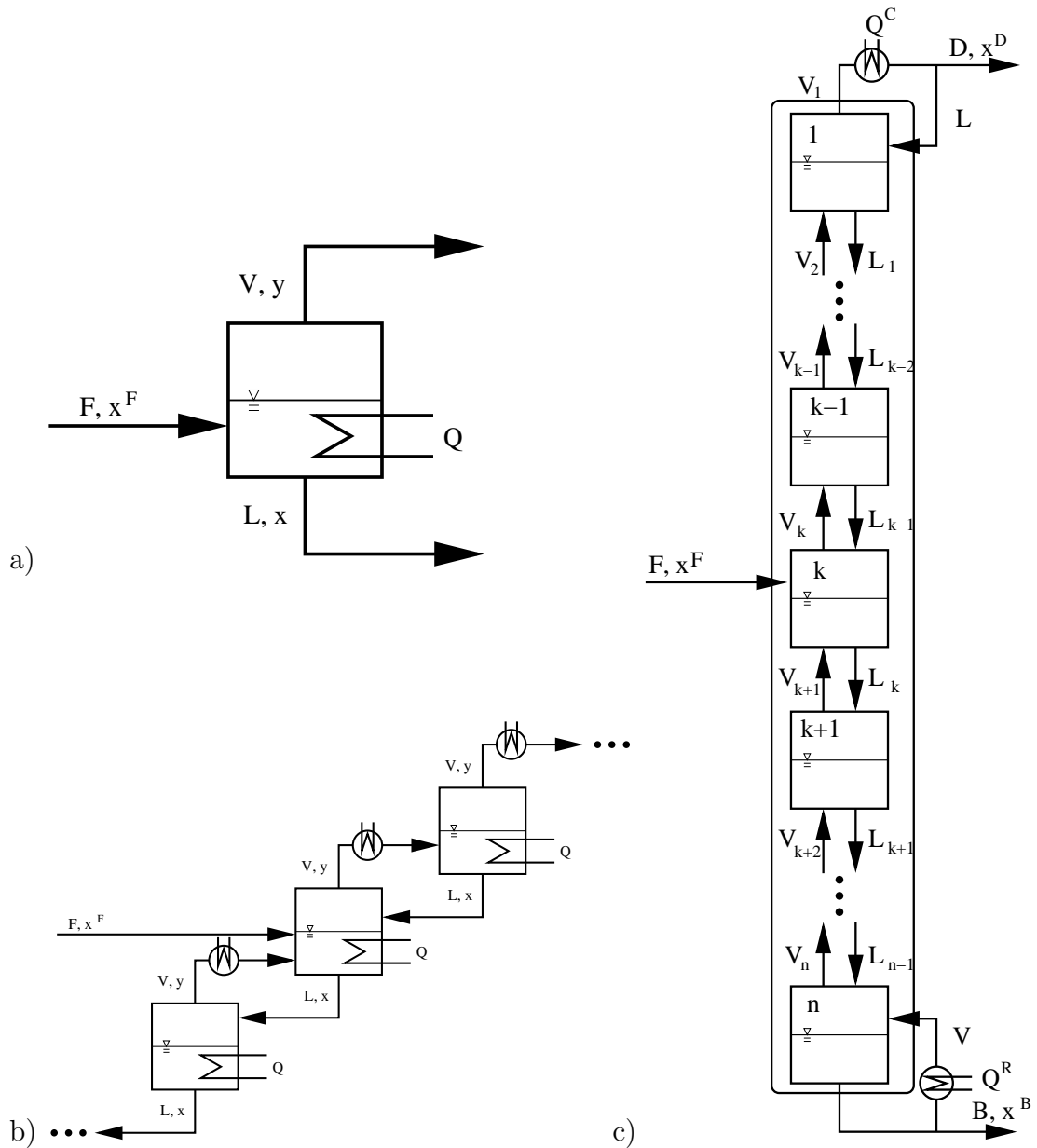


Figure 2.1: a) Simple flash unit, b) flash cascade, c) distillation column.

Definition 2. Azeotropic mixture: A two component mixture of L and H with L lighter boiling than H is called azeotropic mixture if the difference between the vapor phase composition y_L and the liquid phase composition x_L is zero at some point apart from the pure components.

If $y_L - x_L$ is zero at some point, the mixture cannot be further separated which leads to the fact that either pure L or pure H cannot be obtained in a cascaded process as shown

in Figure 2.1b.

Figure 2.1c shows the cascaded process where the heat exchange between the vapor and liquid phase is combined the flash units. This is a distillation column. There is a continuous counter-current flow of vapor and liquid. A feed of flow rate F with the composition vector x^F is split into a distillate product of flow rate D with the composition vector x^D and a bottom product of flow rate B with the composition vector x^B . The mass balance for the distillation column is:

$$x^F F = x^D D + x^B B \quad (2.1)$$

The liquid that flows down the column and does not leave the column as B is evaporated as V and condensed in the top of the column. The distillate product D is removed and the remaining liquid stream is recycled to the column as reflux L .

The model of a distillation column can be found in every standard chemical engineering textbook about separation processes (Doherty and Malone, 2001; Seader and Henley, 1997; Stichlmair and Fair, 1998). Therefore it is not repeated here. In general, the model consists of mass and energy balances for each flash unit assuming that the vapor and the liquid phase that leave the flash unit (tray of a distillation column) are in equilibrium. There are many derivatives of this model with simplifications such as the assumption of constant molar overflow (see e.g. Dorn (2000)), which eliminates the energy balances, or constant relative volatility, which eases the phase equilibrium calculation and enables an easy implementation in Matlab (Skogestad, 1997). Modern process simulators such as AspenPlus and AspenDynamics model the process very detailed down to the heat capacity of the equipment giving a model with hundreds of states and thousands of algebraic constraints. Using the implemented solvers, steady state and dynamic simulations can be performed.

In this thesis, a theoretical approach (∞/∞ analysis, section 2.1.2, which is an asymptotic case to reduce the complexity of the problem) is used to predict the steady state and dynamic behavior of the columns based on graphical considerations and interpretations. The theoretical findings are then validated with simulations of rigorous models as implemented in AspenPlus and AspenDynamics. A central model used by the ∞/∞ analysis is a residue curve map, which is discussed next.

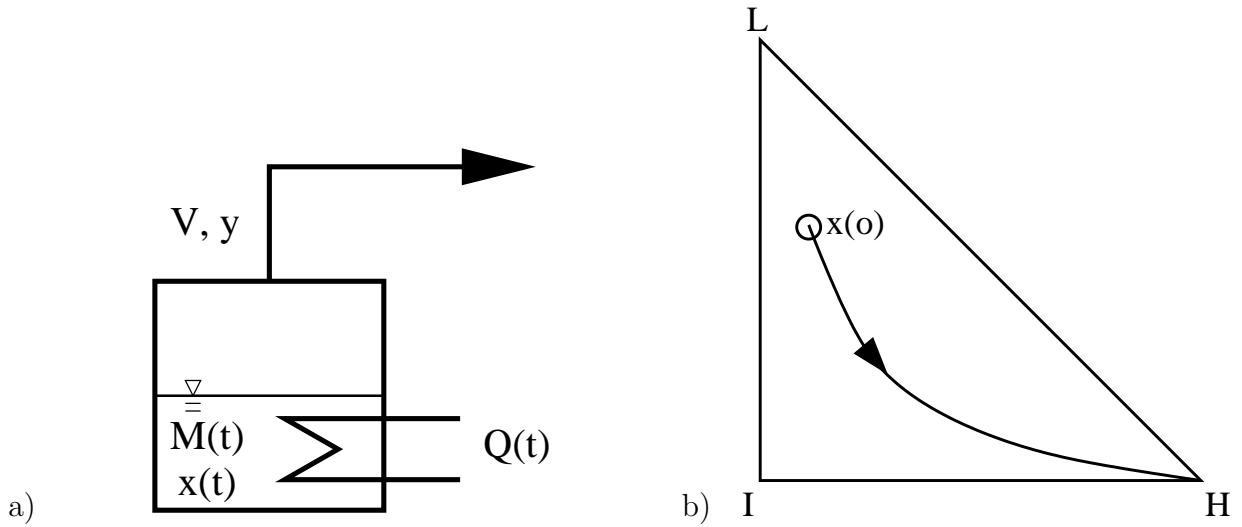


Figure 2.2: a) Simple batch distillation still, b) the Gibbs triangle of the components L, I, and H showing the evolution of the residue composition x .

2.1.1 Residue Curve Maps

Figure 2.2a shows a simple batch distillation still. The initial amount $M(0)$ of a liquid mixture of initial composition $x(0)$ is brought to its boiling point at the given pressure p by heating. By further heating, the liquid is vaporized and removed from the system. The vapor is assumed to be in equilibrium with the liquid phase. Because the vapor is enriched with the more volatile species, the least volatile species are enriched in the residue. For a ternary mixture, the evolution of the composition of the residue can be plotted in a Gibbs triangle giving a residue curve (Figure 2.2b). In the Gibbs triangle, each corner represents a pure component (L for low boiling, I for intermediate boiling, and H for high boiling). Each point inside a triangle stands for a certain composition in mass or mole fractions, which all sum up to 1.

The component wise mass balances of the system are

$$\frac{d}{dt}(Mx_i) = -Vy_i(x) \quad i = 1, \dots, n_c \quad (2.2)$$

or

$$x_i \frac{d}{dt}M + M \frac{d}{dt}x_i = -Vy_i(x) \quad i = 1, \dots, n_c \quad (2.3)$$

$y_i(x)$ is the composition of the vapor in equilibrium with the liquid of composition x at

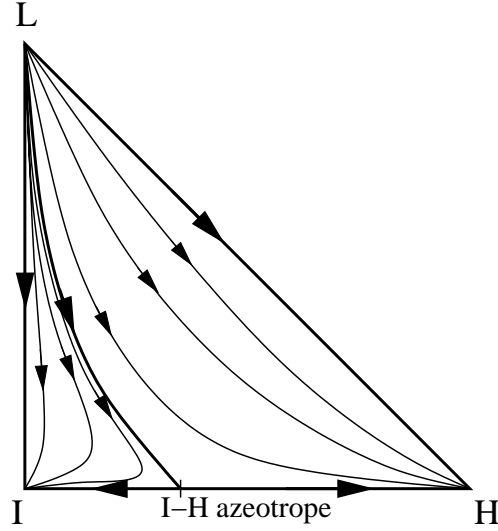


Figure 2.3: Residue curve map of the L, I, and H forming a 020 mixture (Matsuyama and Nishimura, 1977).

pressure p . Of those n_c mass balance equations, only $n_c - 1$ are linearly independent because the two component wise summations $\sum_{i=1}^{n_c} x_i = 1$ and $\sum_{i=1}^{n_c} y_i = 1$ must hold. With the global mass balance $\frac{d}{dt}M = -V$ follows

$$\frac{d}{dt}x_i = -\frac{V}{M}(y_i(x) - x_i) \quad i = 1, \dots, n_c \quad (2.4)$$

M and V are both functions of time. They are connected to the heat input $Q(t)$ by the energy balance. Therefore, system 2.4 of coupled nonlinear differential equations is non-autonomous. However, the heat input $Q(t)$ is not of interest, but the evolution of the composition of the residue. By defining a dimensionless (“warped”) time

$$\xi = \frac{V}{M}t \quad (2.5)$$

an autonomous system of $n_c - 1$ linear independent nonlinear differential equations is obtained:

$$\frac{d}{d\xi}x_i = -(y_i(x) - x_i) \quad i = 1, \dots, n_c - 1 \quad (2.6)$$

The evolution of $x(\xi)$ defined by system 2.6 to the initial condition $x(\xi = 0)$ is called a residue curve through $x(\xi = 0)$. The residue curve map is a plot of all characteristic residue curves in the composition space. Figure 2.3 shows the residue curve map of a ternary mixture. Matsuyama and Nishimura (1977) investigated and classified all feasible

topologies of residue curve maps. According to their classification, the mixture shown in Figure 2.3 is of class 020. Applying the theory of dynamical systems and topology to equation 2.6, Doherty and Perkins (1978) deduced a couple of interesting and useful properties of residue curve maps.

Singular Points. The singular point of a residue curve map are the equilibria of equation 2.6, i.e, the solution of $0 = y(x) - x$. Thus, the singular points are the pure components and the azeotropes in the composition space. For the isobaric case, there are only isolated singular points. Generic singular points have real nonzero eigenvalues. They can be categorized as stable nodes (all eigenvalues negative), unstable nodes (all eigenvalues positive), and saddles (both positive and negative eigenvalues). Residue curves originate from unstable nodes and end at stable nodes. At saddles, residue curves end and start. By definition, residue curves do not intersect. Therefore, there are no closed cycles.

Distillation Regions. A simple distillation region is defined as the union of all residue curves that start at the same unstable node and end at the same stable node. If there exists more than one node of the same kind (stable or unstable), there will be at least as many simple distillation regions as there are nodes of that same kind. The residue curve that separates two simple distillation regions is called a residue curve boundary. At least one of the ends of a residue curve boundary must be a saddle. The residue curve map shown in Figure 2.3 has two simple distillation regions. The pure component L is the only unstable node where all residue curves originate. The residue curves either end in pure I or pure H, which are the two stable nodes of this mixture. Thus, there are two simple distillation regions that are separated by the residue curve boundary, which originates from pure L and ends in the I-H azeotrope, the saddle of the system.

Temperature Surface. For a constant pressure, the temperature always increases along a residue curve, as one would expect to happen according to the original definition of residue curves. The liquid phase depletes in the more volatile components which increases the boiling temperature of the residue. If the boiling point temperatures are plotted over the composition space giving a temperature surface, the unstable nodes represent the local minima of this surface while the stable nodes represent the local maxima of this surface. The globally lowest (highest) boiling point is always at an unstable (stable) node.

The key advantage of the residue curve maps is that their topological properties can be easily calculated or experimentally determined. The ∞/∞ analysis connects these properties to the more complex process, the distillation column. This is discussed next.

2.1.2 ∞/∞ Analysis

The ∞/∞ analysis is a framework that predicts possible product paths of a distillation column based on residue curve map information only. A product path is obtained by the continuation of solutions found by varying, for example, the distillate flow rate D from 0 to its maximum, the feed flow rate F . In general, this product path can be generated by either a series of case studies using a distillation column model implemented in a commercial simulator such as AspenPlus, or by a “continuation” of solutions using a simplified model (Güttinger, 1998; Dorn, 2000) or a rigorous model as implemented in AspenPlus (Vadapalli and Seader, 2001). To predict the product path based on residue curve map information only, two main simplifying assumptions¹ are necessary: Infinite reflux (internal flow rates) and infinite length of the column / number of trays.

Infinite Reflux. If a column is operated at infinite reflux, the composition profile of a packed column will follow a part of a residue curve (Van Dongen and Doherty, 1985; Laroche et al., 1992a). Hence, a feed F of composition x^F can be split into two products D and B with compositions x^D and x^B if x^D and x^B lie on one residue curve and are collinear according to the mass balance of the column (equation 2.1). This implies that the distillate and the bottom product have to lie in the same distillation region. Note that the feed composition x^F does not necessarily have to lie in the same distillation region. This one of the key features of the boundary separation scheme, which is reviewed in section 2.2 and thoroughly analyzed in part II of this thesis. For a column with trays, the composition profile follows a distillation line which has qualitatively the same properties as a residue curve (Bekiaris et al., 1996).

Infinite Length. For an infinitely long column, the profile must contain a pinch. In this context, the column profile contains a pinch if it exhibits a zone where the composition

¹A very detailed review about all the assumptions and simplifications is given by Dorn (2000).

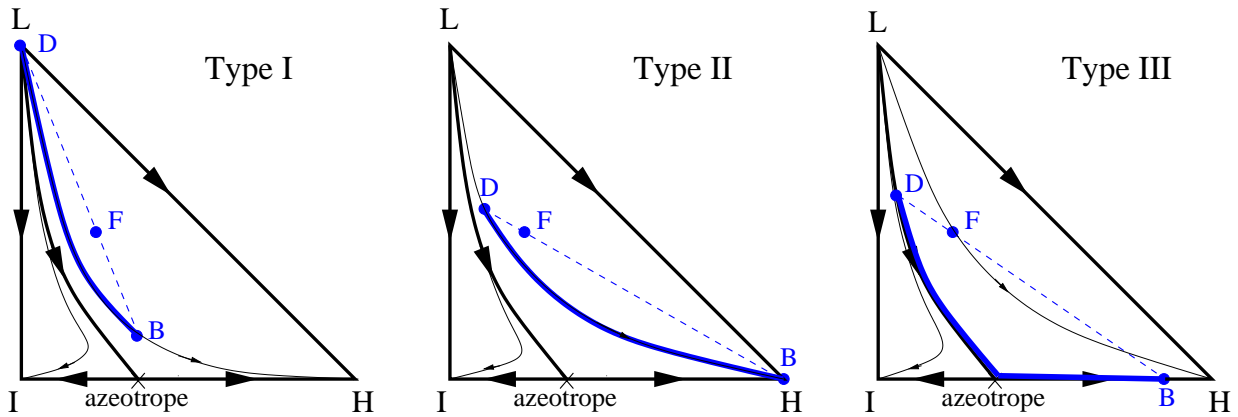


Figure 2.4: Three possible ∞/∞ column profiles illustrated for a 020 mixture.

is constant. Probably the most well known pinch in distillation is the pinch at minimum reflux. At this point, the number of stages goes to infinity.

Infinite Reflux / Infinite Length. The combination of these two asymptotic cases is the basis of the ∞/∞ analysis. If a column of infinite length is operated at infinite reflux, then the pinch must be a singular point in the residue curve map. This combination was studied first by Petlyuk and Avet'yan (1971), but without a significant impact on the western research community. About 20 years later, Bekiaris et al. (1993) developed this combination into a tool that can be used to predict the product path of distillation columns based on residue curve map information only. Using this framework, the existence of multiple steady states was predicted and explained for homogeneous azeotropic distillation columns (Bekiaris et al., 1993) and heterogeneous azeotropic distillation columns (Bekiaris et al., 1996). A complete review about research on multiple steady states in distillation up to 1998 can be found in the thesis of Güttinger (1998).

There are three possible profiles for an ∞/∞ column (Bekiaris et al., 1993) which are shown in Figure 2.4:

Type I. The column profile is a type I profile if the distillate composition x^D is at the unstable node (L in this case). The column profile starts at L and follows the indicated residue curve until it is at x^B that is collinear with x^F and x^D . For a different split D/F , the profile would follow a different residue curve.

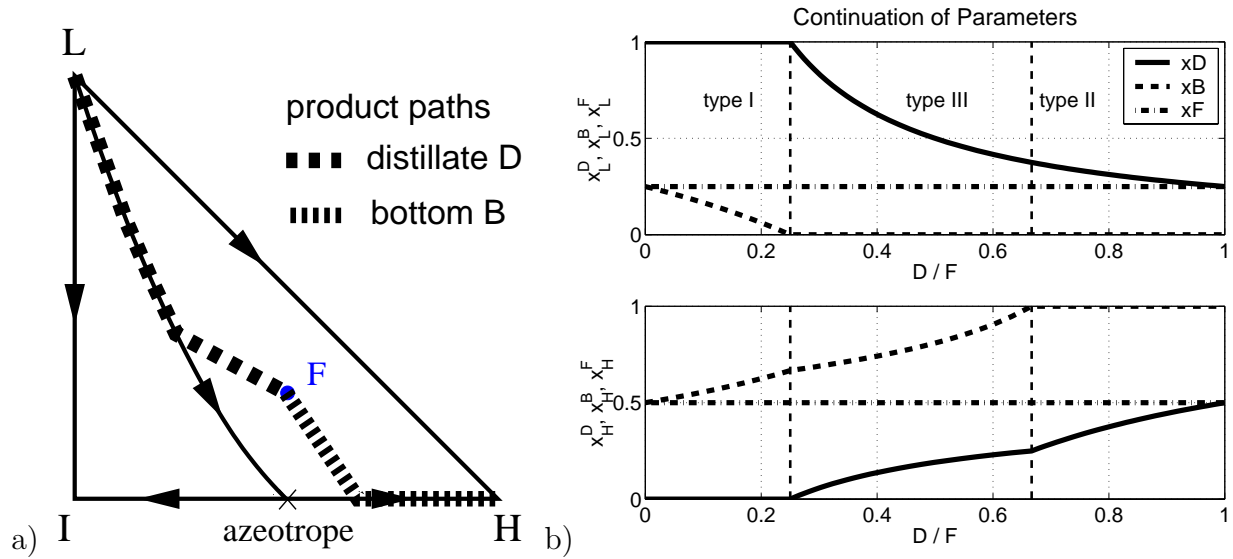


Figure 2.5: a) ∞/∞ product paths of the distillate and bottom composition for a 020 mixture, b) distillate and bottom compositions for a continuation of D/F .

Type II. The column profile is a type II profile if the bottom composition x^B is at the stable node (H in this case). The column profile starts at an arbitrary point x^D that is collinear with x^F and x^B and follows the indicated residue curve until it is at the stable node (H in this case).

Type III. The column profile is a type III profile if the profile contains at least one saddle (the I-H azeotrope in this case). The column profile starts either at the edge of the triangle or on a residue curve boundary, as in this case. It follows the residue curve boundary, passes the I-H azeotrope, and ends somewhere at the binary I-H edge.

For a given feed composition x^F and flow rate F , the distillate flow D , which is the only unspecified parameter, can be varied from 0 to F to track all possible product compositions x^D and x^B . This gives the product paths for the distillate and the bottom (Figure 2.5a). Figure 2.5b shows the distillate and bottom compositions x^D and x^B for a continuation of the parameter D/F . There are no multiple steady states.

Bekiaris et al. (1996) elaborated also a framework for heterogeneous distillation columns. This is discussed in detail in section 3.2 when the industrial heterogeneous column is analyzed.

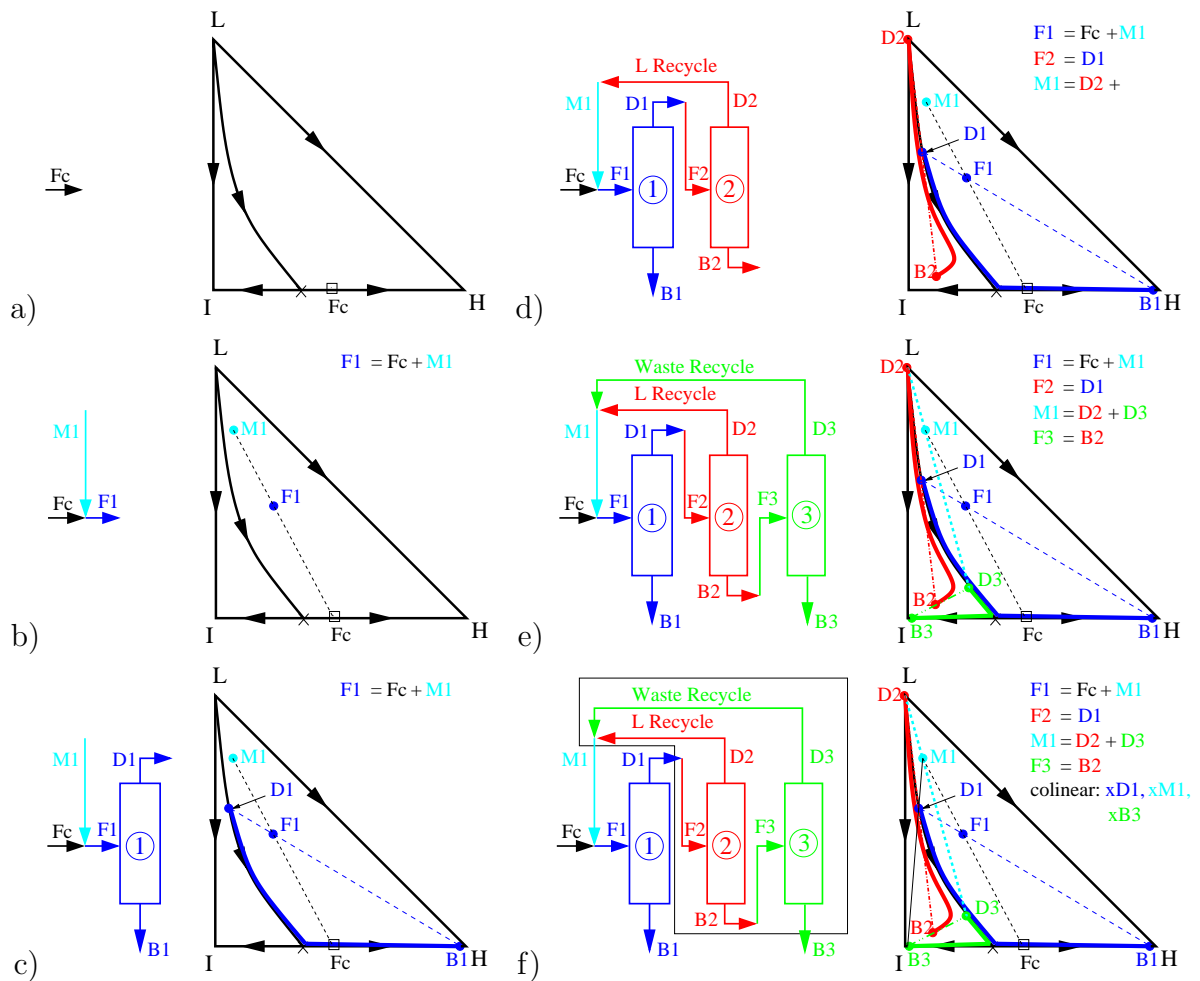


Figure 2.6: Boundary separation scheme separating a binary feed with three ∞/∞ columns.

2.2 Boundary Separation Scheme

The boundary separation scheme was first introduced as a sequence of three columns that breaks a binary minimum boiling azeotrope using a light entrainer that is recycled inside the system. The setup is shown in Figure 2.6 for a 020 mixture (Matsuyama and Nishimura, 1977). The binary I-H feed F_C lies in the convex set of the mixture (Figure 2.6a). To break the azeotrope, F_C is mixed with some recycle M_1 (Figure 2.6b) and fed into column 1 (Figure 2.6c). The ∞/∞ profile (Petlyuk and Avet'yan, 1971; Bekiaris et al., 1993) of column 1 starts somewhere on the boundary, runs through the saddle azeotrope and ends close to or in pure H (type III and type II profile). H leaves as B_1 and the distillate D_1 is fed into column 2. Here, the entrainer L is recovered through the distillate and recycled

to the feed of column 1 (Figure 2.6d). The profile is a type I profile, ending somewhere in the non-convex set. The bottom B_2 is fed into column 3, where pure I is removed and the rest (waste) is recycled to the feed of column 1 (Figure 2.6e). As column 1, column 3 may also contain two pinch points: pure I and the saddle I-H azeotrope. This sequence is characterized by two columns lying in the concave set and one column lying in the convex set of the residue curve map. Based on the idea of Doherty and Caldarola (1985), a subsystem around column 2 and 3 is created (Figure 2.6f). The mass balance of this subsystem is:

$$x^{D_1} D_1 = x^{M_1} M_1 + x^{B_3} B_3 \quad (2.7)$$

x defines the composition vector (mass fraction) of the stream, which is indicated by the superscript. From equation 2.7 follows that x^{M_1} , x^{D_1} and x^{B_3} have to be collinear for a feasible operation of the sequence.

2.2.1 Definitions

Concerning the residue curve boundary, the term convex and concave is used in two opposite ways in literature (Doherty and Caldarola, 1985; Laroche et al., 1992a; Güttinger and Morari, 1996). To clarify this, the following definition is made:

Definition 3. Usage of Convex / Concave: *Figure 2.7 shows a residue curve map that is divided into two regions by the boundary Γ (020 mixture). **A** lies in the convex set and **B** lies in the concave (non-convex) set.*

According to Doherty and Caldarola (1985), a residue curve boundary cannot be crossed by simple mixing, if it is straight. This is illustrated with Figure 2.8. As mentioned above, the subsystem around column 2 and 3 (Figure 2.6f) shows that compositions of M_1 , D_1 , and B_3 have to be collinear. If the boundary is “straightened”, the collinearity condition forces x^{D_1} , which has to lie on the residue curve boundary, to move towards x^{M_1} if all other compositions except x^{F_1} remain constant, as shown in Figure 2.8. From the mass balance of column 1 follows that x^{F_1} also has to move towards x^{M_1} . For constant flows F_C , B_1 , and B_3 , the flows D_1 , M_1 and all other interconnecting flows, which are flows that connect

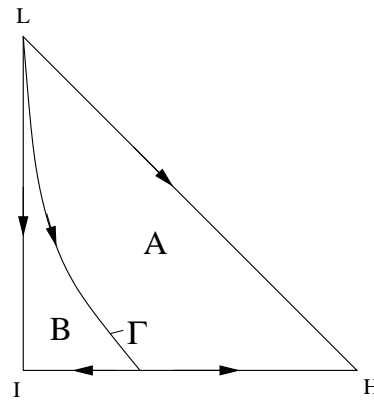


Figure 2.7: Residue curve map of a 020 mixture with boundary to illustrate convex and concave.

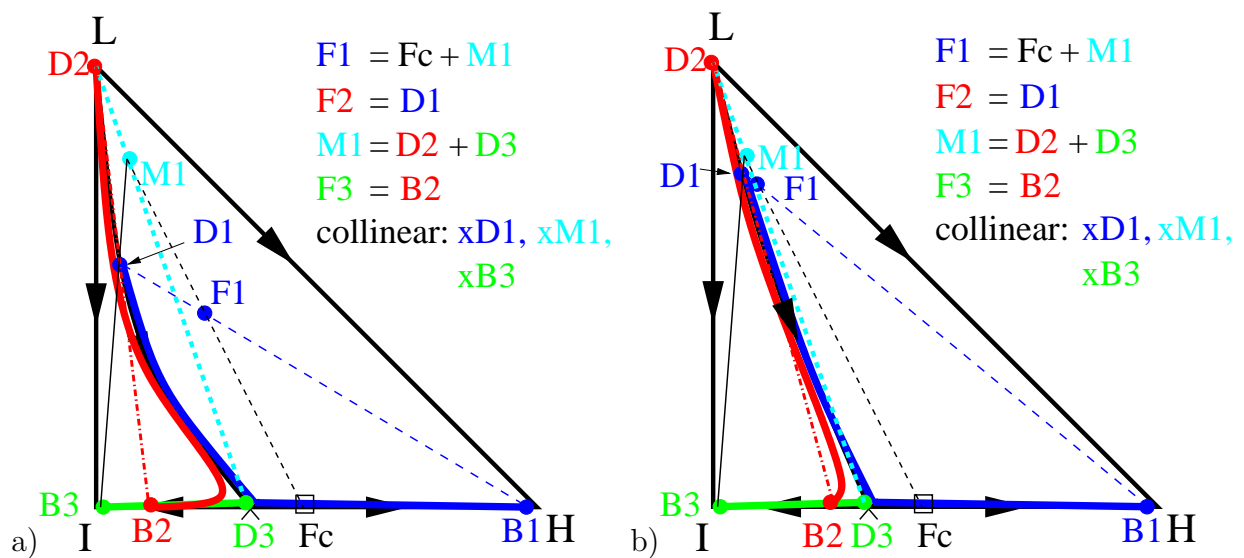


Figure 2.8: Boundary separation scheme for a) a curved and b) an almost straight boundary.

two columns, have to approach infinity to move x^{F_1} towards x^{M_1} . For a straight boundary, they are at infinity. This leads to the following definition:

Definition 4. Feasibility of Boundary Separation Scheme. *The set up of the boundary separation scheme is called feasible if there exist products different from the feed for all flow rates between the columns smaller than infinity.*

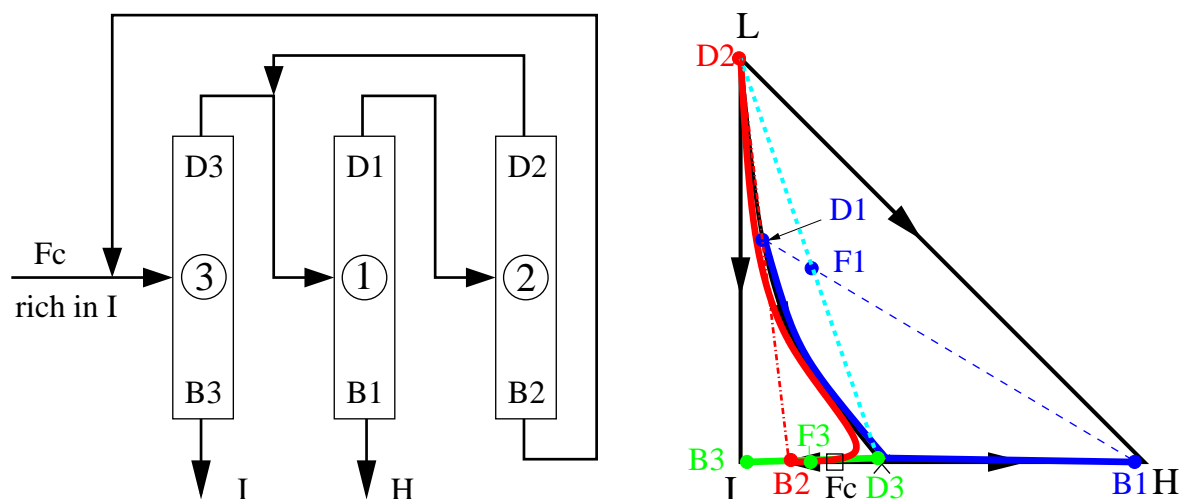


Figure 2.9: Boundary separation scheme of a 020 mixture for a feed rich in I. Feed and I are in the concave set.

2.2.2 Review

The boundary separation scheme was first reported by Doherty and Caldarola (1985). Here, the separation of the minimum boiling ethanol-water azeotrope with an entrainer resulting in a 120 mixture is discussed. Because of convergence difficulties, Doherty and Caldarola (1985) divided the three column sequence into two subsystems and showed that the boundary cannot be crossed by simple mixing of recycles if the boundary is straight. This result also applies to 020 mixtures (boundary separation scheme), as discussed above.

Stichlmair and co-workers (Stichlmair, 1988; Stichlmair et al., 1989) show that a three column sequence is able to separate a maximum boiling azeotrope with a heavy entrainer (400) and a minimum boiling azeotrope with a light entrainer (020) for a curved boundary (Figure 2.6). A succeeding paper introduces two different setups of this process that depend on the feed composition (Stichlmair and Herguijuela, 1992). Figure 2.8a shows that a binary I–H feed lying in the convex set is separated into pure H (B_1) and pure I (B_3). The proposed second setup for a crude feed rich in I is shown in Figure 2.9. Stichlmair and Herguijuela (1992) suggest to place M_1 (M_2 in their paper) at an optimal position such that the recycles are minimal to reduce the energy consumption. This is not further elaborated.

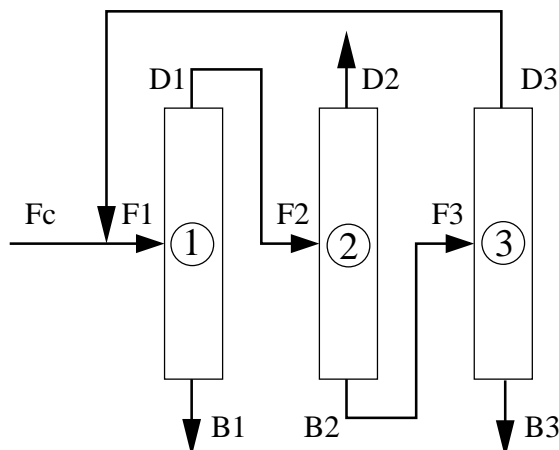


Figure 2.10: Three column sequence with one recycle.

Laroche et al. (1992a) also analyzed the boundary separation scheme. They found that there is only one setup (as indicated by the numbering of the columns in Figure 2.9). The difference between the two setups illustrated in Figure 2.6 and 2.9 is that the feed is either introduced to column 1 or to column 3. Both options are feasible for every binary I–H feed. However, for some crude feed compositions, it is of economical advantage to either introduce the crude feed to column 1, whereas for other compositions, the crude feed should be introduced to column 3. The analysis of three component feeds for this setup (section 5.3.3) will show that a feed to column 3 leads to fewer recycle flows than a feed to column 1 for some compositions. But introducing the feed to column 3 is always worse than introducing it to column 2 except for the binary case, where the recycles are the same. The option of introducing the recycle to column 2 has not been discussed in literature before.

Serafimov et al. (1992b) analyzed the separation of a ternary feed of a 020 mixture with a three column sequence with one recycle as shown in Figure 2.10. Using the necessary condition for system functionality (Serafimov et al., 1992a), a region for feasible feeds is derived. The composition space is divided into two regions by the tangent to the separatrix in the saddle azeotrope. For a feed outside the feasible region, they show that a second recycle is needed. The core results are the same as the ones that will be derived later in this thesis using the ∞/∞ framework and graphical arguments (Sections 5.3.2.1 and 5.3.3).

Wahnschafft and co-workers developed algorithms for the design and synthesis of azeotropic sequences including the boundary separation scheme (Wahnschafft et al., 1992; Wahnschafft and Westerberg, 1993; Wahnschafft et al., 1993; Wahnschafft et al., 1994). They focussed on the product regions and possible profiles of finite, single columns.

Güttinger and Morari (1996) analyzed this system with the ∞/∞ framework (Bekiaris et al., 1993). They introduced the idea that an optimal operation point for a sequence of ∞/∞ columns is where the recycle flows are minimal. They found that the scheme is not only feasible for a light entrainer, but also for a heavy entrainer that introduces a minimum-boiling binary azeotrope, whose boiling point is lower than the one of the azeotrope that has to be broken. To capture this general behavior, they introduced the term boundary separation scheme. The main focus of their paper was the possible existence of multiple steady states in two column sequences. In particular, they looked at the two column boundary separation scheme with a side stream in the second column. They did not find any new multiplicities introduced by the presence of recycles. They showed that for the mixtures where output multiplicities are present for the single columns, the output multiplicities of that two column sequence disappeared by closing the recycles.

Bauer and Stichlmair analyzed the design of the boundary separation scheme (Bauer and Stichlmair, 1996; Frey et al., 1997; Bauer and Stichlmair, 1998). They showed for a sequence with a ternary feed (methanol, ethanol, and water) and three product streams (a configuration that will be discussed later) using Mixed Integer NonLinear Programs (MINLP) that the optimal flow rates, optimal feed stage locations and optimal number of recycle streams depend on the feed composition. The observation that the optimal number of recycle stream depends on the feed composition will be explained with the topology of the residue curve map in section 5.4.2.1.

Recently, the design of azeotropic column sequences has attracted more researchers (Tyner and Westerberg, 2001a; Tyner and Westerberg, 2001b; Thong and Jobson, 2001a; Thong and Jobson, 2001b; Thong and Jobson, 2001c; Yeomans and Grossmann, 2000). The procedures presented there can be used to design a sequence, but for operation, less complex physical knowledge is necessary.

The control of the classical heavy entrainer scheme was thoroughly investigated (Andersen et al., 1991; Andersen et al., 1995). Here, the main control problems are the change of the gain for the entrainer recycle: If the reflux or entrainer flow rates are too large, the separating effect disappears. This is the reason that the scheme is only feasible at finite reflux, but not at infinite reflux. Contrary to that, heterogeneous distillation schemes and the boundary separation scheme are less sensitive to overrefluxing because they are also feasible for infinite reflux. Hence, they should be easier to operate. For the boundary separation scheme, the presence of two recycles makes control more complicated. A result of this thesis is that one recycle is the key manipulated variable for robust operation of the scheme.

Though light entrainer topologies are nearly as common as heavy entrainers (Laroche et al., 1992b), they are rarely used in industries. Up to recently, only one experiment for a sequence has been reported in literature (Hunek et al., 1989). The feasibility of this sequence strongly depends on the curvature of the boundary and has attracted researchers to measure it (Pelkonen et al., 1997; Pelkonen et al., 2001). Just recently, experimental column profiles that cross distillation boundaries have been reported and validated by non-equilibrium thermodynamics (Springer, Baur and Krishna, 2002; Springer, Buttinger, Baur and Krishna, 2002). These results are discussed in detail in section 6.7. Further, an experiment is reported that uses the boundary separation scheme to separate methanol, ethanol, and water (Bai et al., 2001). Bai et al. (2001) point out the necessity of controlling the methanol recycle to save energy. Section 5.3.3 derives this fact using the ∞/∞ analysis.

2.3 Heterogeneous Distillation

2.3.1 Definitions

The concept of using a sequence of heterogeneous distillation columns to break a minimum-boiling azeotrope is very old. Kubierschky (1915) introduced two and three column sequences for the separation of ethanol and water using benzene as entrainer which is a heterogeneous 222-m mixture. Figure 2.11a shows the core sequence of Kubierschky's

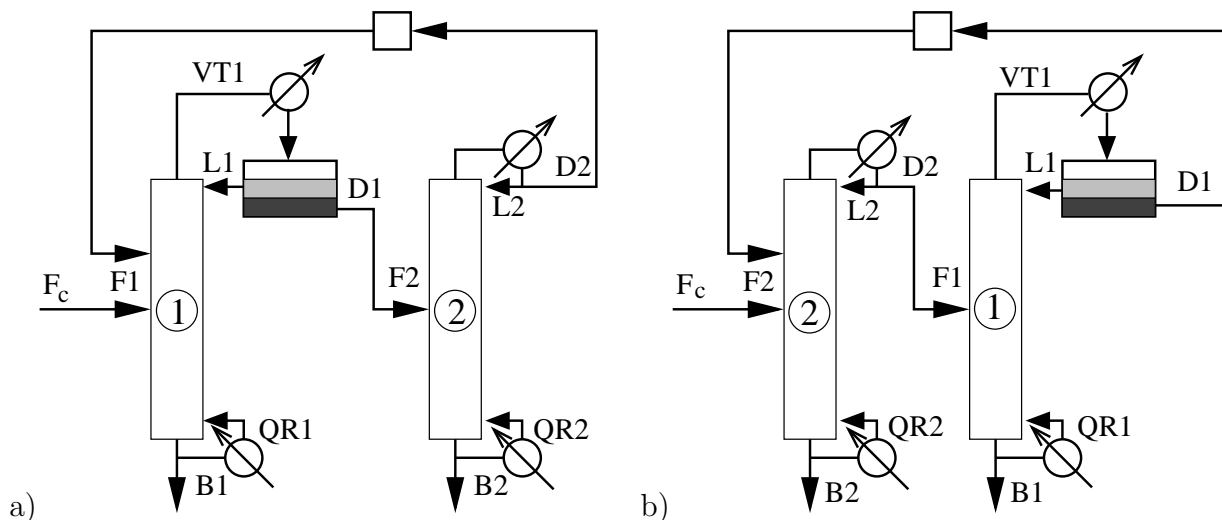


Figure 2.11: Heterogeneous two-column sequences: a) the core sequence of Kubierschky's three column sequence, and b) Kubierschky's two column sequence.

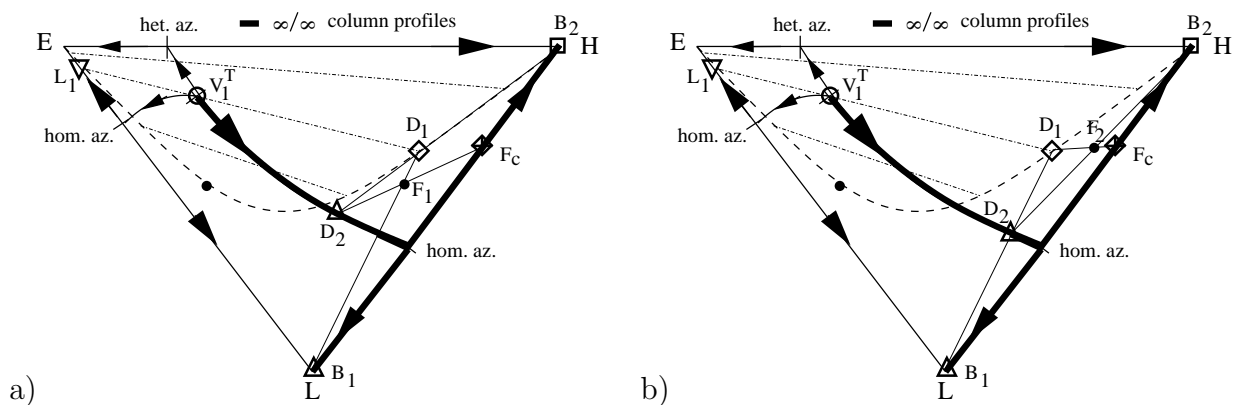


Figure 2.12: Ternary residue curve maps of a 222-m system illustrating the ∞/∞ column profiles and mass balances of a) the core sequence of Kubierschky's three column sequence, and b) Kubierschky's two column sequence.

three column sequence without the first column (the preconcentrator). Figure 2.11b shows the Kubierschky's two column sequence which just differs by the location of the crude feed. Figure 2.12 shows the ∞/∞ column profiles and mass balances for a 222-m mixture of L (light boiler), H (heavy boiler), and E (entrainer). As stated by e.g. Doherty and Caldarola (1985), distillation column sequences are named direct and indirect schemes depending on which component is removed first. If the lightest component is removed first, the scheme is called direct, if the heaviest component is the first one that is removed the scheme is

called indirect sequence. Analog to this definition, the following terms are defined.

Definition 5. Direct Heterogeneous Sequence: *A sequence separating two components that build a minimum boiling azeotrope using an heterogeneous entrainer is called **direct** sequence when the lighter boiling component is removed first (first column has the decanter).*

Definition 6. Indirect Heterogeneous Sequence: *A sequence separating two components that build a minimum boiling azeotrope using an heterogeneous entrainer is called **indirect** sequence when the heavier boiling component is removed first (second column has the decanter).*

According to these definitions, the scheme shown in Figure 2.11a is referred to as direct heterogeneous sequence and the one in Figure 2.11b is the indirect heterogeneous sequence.

2.3.2 Review on Control of Heterogeneous Distillation

Bozenhardt (1988) studied the dewatering of an unspecified alcohol in the presence of its complementary ether as entrainer. He described temperature and on-line composition control in an industrial plant, which resulted in improved economic operation.

Rovaglio et al. (1992) proposed control strategies for the ethanol dewatering column (Prokopakis and Seider, 1983b; Prokopakis and Seider, 1983a) where the entrainer benzene is recovered in a separate column. To maintain the desired product purity, the position of a temperature front in the stripping section of the dewatering column was fixed by controlling the average of two temperatures via the reboiler duty. By manipulating the entrainer flow, a second temperature front was fixed in the rectifying section to ensure the liquid-liquid phase split in the decanter. In a succeeding paper, Rovaglio et al. (1993) reported the importance of the entrainer inventory for good controller performance. In particular, the entrainer makeup flow was adjusted to the water content in the feed by a feed forward controller.

Corrêa and Jørgensen (1992) studied the same column with two different control schemes: Manipulation of decanter bypass and reboiler duty, and manipulation of decanter bypass and entrainer makeup flow. Their analysis showed that the first scheme is better conditioned for control than the second one.

Tonelli et al. (1997) analyzed the control strategy of a whole column train that dewateres 2-propanol using cyclohexane as entrainer. For the heterogeneous column, they found that controlling a temperature close to the top via manipulation of the reboiler duty and a temperature close to the bottom via manipulation of the reflux (inverse pairing (Chien et al., 1999)) was less interactive than the opposite (conventional (Chien et al., 1999)) pairing, which is normally used. They provided no clear statement about the adjustment of entrainer makeup flow. We suspect that the entrainer makeup flow was manipulated by controlling the decanter level, as is done in most industrial applications (Tyréus, 1992). This level control can either be continuous or discontinuous. In the latter case, the decanter is refilled with the entrainer when its level drops below a specified value as the result of entrainer loss.

Chien et al. (1999) presented simulation results for dewatering 2-propanol using cyclohexane as entrainer. Temperature fronts were fixed by manipulating reflux flow and reboiler duty. The entrainer makeup flow was manipulated to control the level of the buffer tank. Like Tonelli et al. (1997), they found that the inverse pairing is less interactive than the conventional one. The experimental validation of the simulation results was published recently (Chien et al., 2000).

All of the above mentioned heterogeneous distillation columns have one point in common: At the nominal operation point, the top composition of the column is close to the “unstable node” (the global temperature minimum in the three component mixtures) which is a heterogeneous azeotrope. The aqueous phase of the overhead is separated in a decanter and leaves the process as distillate. In the aforementioned control studies, the heterogeneous columns are operated with two point control. The entrainer flow rate is manipulated directly as a continuous variable (Rovaglio et al., 1992), or indirectly (Bozenhardt, 1988; Corrêa and Jørgensen, 1992; Tonelli et al., 1997; Chien et al., 1999). In the case of indirectly manipulated entrainer flow rate, the reflux is the continuously manipulated variable and

the process is operated pseudo-continuously. The process is not in steady state because the entrainer loss causes the decanter level to decrease. The decanter is refilled with entrainer when its level drops below a specified value. The importance of manipulating the entrainer flow rate will be studied in detail in Part I.

2.4 Self-Optimizing Control

A central issue in process control is to select the controller structure, as already stated by Foss (1973): *“Perhaps the central issue to be resolved by the new theories of chemical process control is the determination of control system structure.”* Once, the controller structure is selected, all the new control theories can be applied. However, there is no clear rule on how to select the best controller structure that operates the process optimally. About twenty year ago, Morari et al. (1980) postulated the following: *“in attempting to synthesize a feedback optimizing control structure, our main objective is to translate the economic objectives into process control objectives. In other words, we want to find a function c of the process variables which when held constant, leads automatically to the optimal adjustments of the manipulated variables, and with it, the optimal operating conditions.”*

Skogestad and Postlethwaite (1996) devoted chapter 10 in their book about multivariable feedback control to the importance of control structure selection. Following these ideas, a self-optimizing control concept is postulated (Skogestad, 2000b; Skogestad, 2000c; Skogestad, 2000a; Larsson et al., 2001).

2.4.1 Requirements for Controlled Variables

Requirement 1. Its optimal value should be insensitive to disturbances (so that the setpoint error is small).

Requirement 2. It should be easy to measure and control accurately (so that the implementation error is small).

Requirement 3. Its value should be sensitive to changes in the manipulated variables u , that is, the gain from u to c is large (so that even a large error in the controlled variable c results in only a small error in u). The optimum should be flat with respect to the variable c .

Requirement 4. For cases with two or more controlled variables, the selected controlled variables should not be closely correlated.

2.4.2 Procedure for Selection

Step 1: Degree of Freedom Analysis. Determine the number of degrees of freedom and a set of manipulatable variables that can be independently specified.

Step 2: Cost function and Constraints. Define a scalar cost function J to be minimized for optimal operation and specify the constraints that need to be satisfied.

Step 3: Identify the most important disturbances and uncertainties which are

- disturbances in operation,
- errors in the process model,
- implementation errors.

Step 4: Optimization. Find the optimal operation point according to the proposed cost function.

Step 5: Identify Candidate Controlled Variables. The controlled variables have to fulfill the requirements mentioned in Section 2.4.1. Larsson et al. (2001) give eight useful rules to reduce the number of candidate variables.

1. Variables with no effect on steady state (economics) should be eliminated.
2. Variables that are directly associated with equality constraints should be controlled.
3. Variables with active constraints should be controlled.

4. Closely related variables should be eliminated/grouped.
5. Use insight and experience to reduce variables.
6. Variables that would yield infeasibility for some disturbances if they had constant set points should be eliminated.
7. Combinations of variables that result in infeasibility should be eliminated.
8. Variables whose combination results in small singular values of the steady state gain matrix should be eliminated.

Step 6: Evaluation of Loss for Alternative Collections of Controlled Variables.

Here, the controlled variables have to be chosen and the loss of performance (cost function) for alternative setpoints for the selected controlled variables c has to be evaluated using steady state simulation.

Step 7: Further Analysis and Selection. Select the sets with acceptable loss to investigate the feasibility and expected dynamic control performance (input-output controllability).

2.4.3 Implementation of Controlled Variables

Once the variables with the best performance are chosen, it should be analyzed how control concept can be implemented. Since there is always an implementation error of the controlled variables caused by a measurement error, the influence of the selected controlled variables has to be analyzed. Concerning this, three cases are possible as shown in Figure 2.13 (Skogestad, 2000c).

1. Figure 2.13a shows a constrained optimum. The minimum value of J is for $c = c_{min}$ which is normally very easy to implement in a real plant. A constraint could be: control valve fully shut.
2. Figure 2.13b shows an unconstrained flat optimum. The cost function is insensitive to the controlled variable, which makes implementation easy.

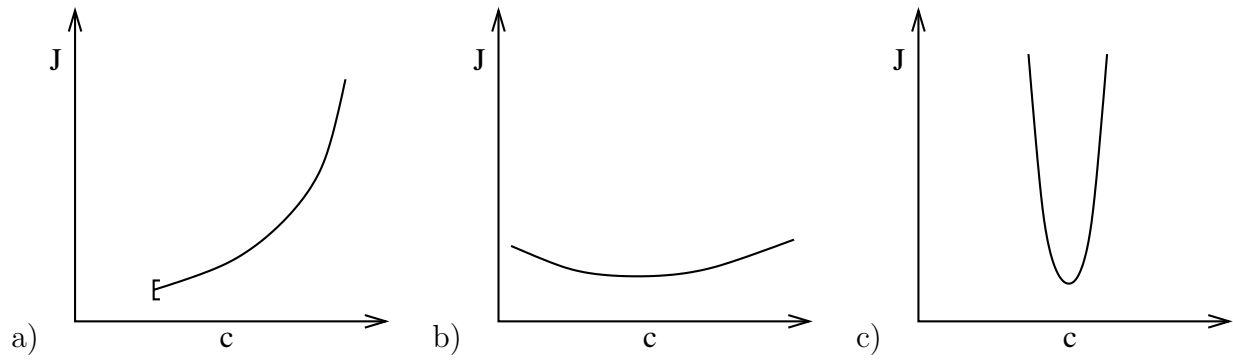


Figure 2.13: Three different cases of the cost function J : a) constrained optimum, b) unconstrained flat optimum, and c) unconstrained sharp optimum

3. Figure 2.13c shows an unconstrained sharp optimum. Here, the implementation is difficult because the cost function is very sensitive to the controlled variable.

Part I

Control of Heterogeneous Azeotropic Distillation Columns

Chapter 3

Analysis and Controller Design of a Heterogeneous Azeotropic Distillation Column

A concept for the design of heterogeneous distillation columns under aspects of operability is provided. The influence of additional components in the feed (impurities) on the design and operation of the process is discussed. This study was motivated by an actual industrial process, the production of methyl-isobutanol (MBI).

3.1 Industrial Plant

Figure 3.1 shows the heterogeneous distillation column. The crude feed F_C containing methyl-isobutanol and water is dewatered using methyl *tert*-butyl-ether (MTBE) as a light, heterogeneous entrainer. The column is operated at 1 bar. The crude feed F_C enters the column as saturated vapor. The rectifying section is filled with structured packing and the stripping section has 20 sieve trays. In the decanter, the aqueous phase (distillate) is separated from the organic phase (reflux). Like many heterogeneous columns, this column is operated with a two point control structure:

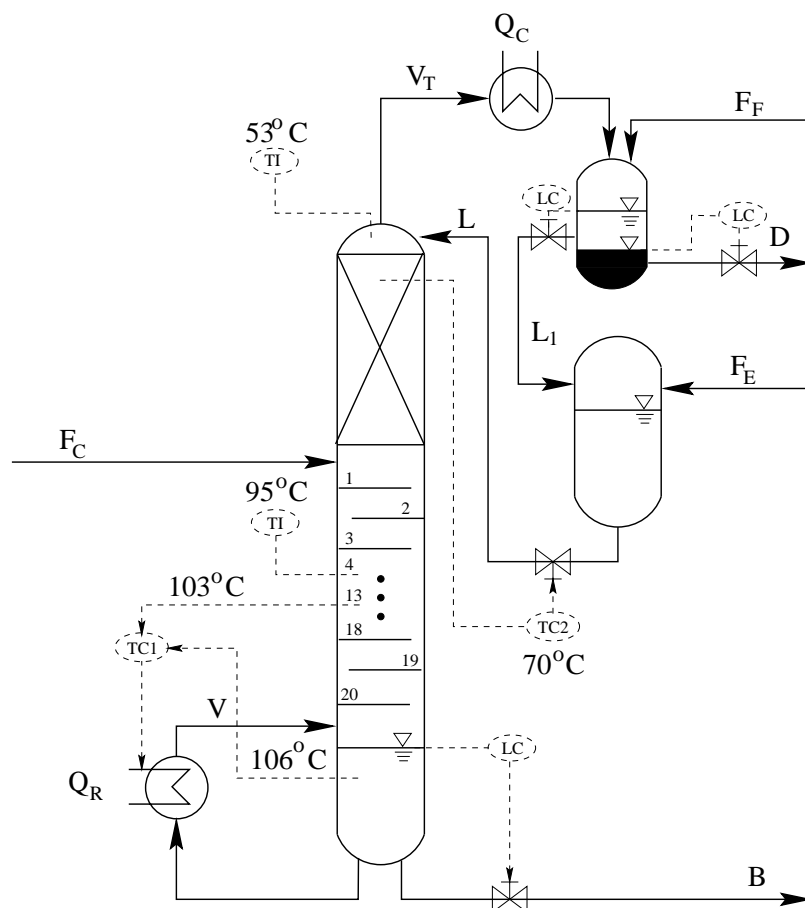


Figure 3.1: Setup of the industrial dewatering column.

TC1 controls the average of the bottom temperature and the temperature on tray 13 by manipulating the temperature of the steam in the reboiler, i.e. the reboiler duty, in order to guarantee the bottom purity. Temperature on tray 13 was included to improve performance: Down-coming disturbances are detected before they can affect the bottom purity.

TC2 controls a temperature in the structured packing by manipulating the reflux. This is done to ensure that the overhead vapor composition lies in the heterogeneous region and to prevent the product (MBI) from leaving the column through the distillate (bad recovery).

For this column, a buffer tank is used to absorb possible disturbances and differences between the required reflux (L) and the organic phase leaving the decanter (L_1). The effect of the large holdup of the entrainer MTBE in the buffer tank is that it suffices to add

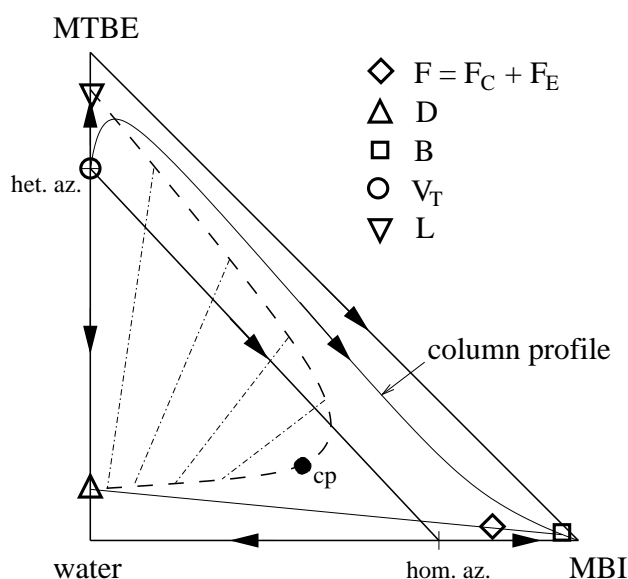


Figure 3.2: Illustration of the separation concept for the system MTBE–water–MBI using a residue curve map. The feed F is split into bottom B and the overhead vapor V_T . The condensed V_T splits in two phases: reflux L and distillate D . The dashed line indicates the binodal curve of the liquid-liquid equilibrium surrounding the heterogeneous region and the dashed-dotted lines indicate the tie lines.

the entrainer makeup F_E discontinuously to the process. In operation, this control scheme did not work satisfactorily because of the strong interactions between the two control loops. Currently, the temperature in the rectifying section is controlled by manually changing the reflux. This corresponds to a very detuned loop TC2. In addition, it was observed that from time to time the light boiling impurity acetone accumulates in the decanter and in the buffer tank. If the acetone content in the decanter (and in the buffer tank) is too high, the phase split in the decanter will disappear. To avoid this, the decanter is flushed with water (F_F) when the acetone content exceeds a certain value. In this manner, acetone leaves the process via the distillate.

Figure 3.2 illustrates the separation concept through a qualitative representation of the residue curve map of the main components MTBE (entrainer), water, and MBI. The overall feed $F = F_C + F_E$ is split into a water-rich distillate D and nearly pure MBI at the bottom B . The column profile runs from the unstable node (the MTBE–water azeotrope) along the indicated residue curve toward the stable node MBI. The overhead vapor V_T consisting

of the MTBE–water azeotrope is condensed and sub-cooled. In the decanter, it splits up into a water-rich phase, the distillate D, and an entrainer-rich phase, which is recycled as reflux (L). The key feature of this column is that the overhead vapor composition lies inside the heterogeneous region. Through the phase split, a separation with a very high MBI recovery and relatively small entrainer loss is possible

The analysis presented hereafter is not restricted to the MTBE–water–MBI mixture, which is a heterogeneous mixture of class 120 (Matsuyama and Nishimura, 1977), but it is valid for any heterogeneous azeotropic mixture where the unstable node is heterogeneous and the column is operated such that the top composition is at the unstable node. Hence, it can also be applied to other mixtures, e.g. class 222–m, such as water–ethanol–benzene(or cyclohexane) or 2-propanol–cyclohexane–water. A general design procedure for heterogeneous columns is proposed, which is based on residue curve map information and a theoretical finite reflux/infinite length column only. To emphasize the generality of the results, the notation is changed to

- LE for the light entrainer (MTBE in the industrial case)
- I for the intermediate boiler (water in the industrial case)
- H for the heavy boiler (MBI in the industrial case)

In chapter 4, the specific industrial process is used as an example to illustrate the implementation of the design and its dynamic behavior.

3.2 Steady State Analysis

3.2.1 Degrees of Freedom

Figure 3.3a shows a homogeneous distillation column. At steady state, this column has two degrees of freedom for a fixed feed (composition, flow rate, and quality). For example, D and V can be specified to ensure product recovery and bottom purity. If D and V are specified, all other streams (B, V_T and L) are defined.

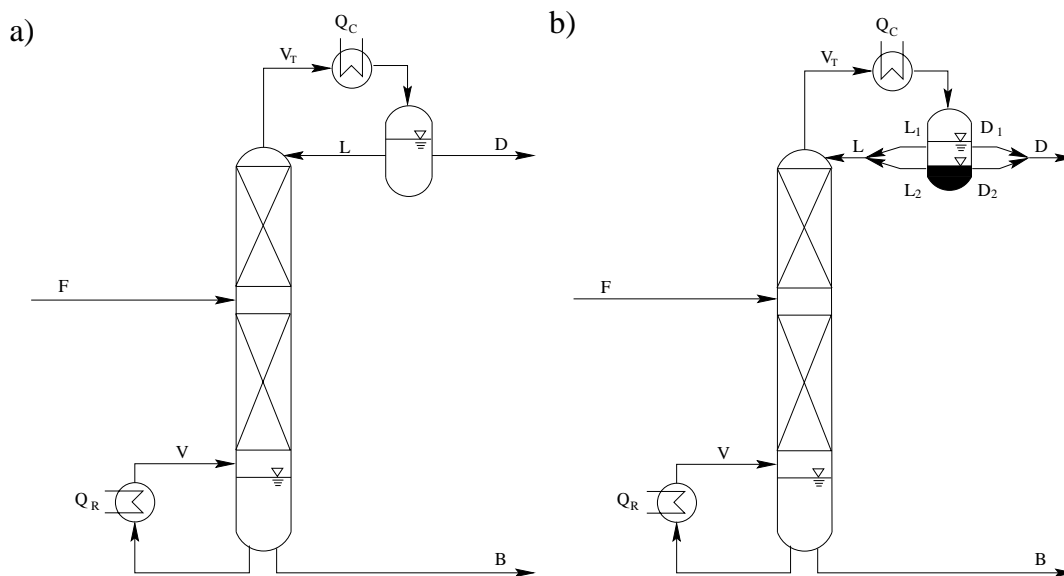


Figure 3.3: a) Homogeneous distillation column: Two degrees of freedom for a fixed feed F . Specifying e.g. D and V defines B , V_T , and L . b) Heterogeneous distillation column: Three degrees of freedom for a fixed feed F . Specifying D_1 , L_2 (e.g. both equal to zero), and e.g. V defines V_T , D_2 , L_1 .

A heterogeneous distillation column, Figure 3.3b, has three degrees of freedom at steady state for a fixed feed. The third degree of freedom is introduced by the second liquid phase in the decanter. With the decanter policy of the industrial example, where the I-rich phase is distillate and the LE-rich phase is reflux, two variables, D_1 and L_2 , are specified to be zero. Hence, only one degree of freedom remains at steady state. For example, specifying V (via Q_R) gives V_T . Because $D_1=L_2=0$ for the proposed decanter policy, D_2 and L_1 result from the liquid-liquid phase split in the decanter. B follows from the overall mass balance ($F = B + D_2$). In order to specify two variables independently, for example, the bottom purity and the top composition, another degree of freedom is needed. The impact of this fact on the control of the column will be discussed in section 3.4.2.

3.2.2 Analysis with the ∞/∞ Column

The process is analyzed using the ∞/∞ framework (Petlyuk and Avet'yan, 1971; Bekiaris et al., 1993; Bekiaris et al., 1996) that uses a distillation column with infinite internal flows

and an infinite number of stages in the rectifying section as well as in the stripping section. The composition profile of a packed column operated with infinite internal flows follows a residue curve. For a column with trays, the composition profile also follows a residue curve, but not exactly. A column with an infinite number of stages contains at least one pinch point. For a column operated with infinite internal flows, the pinch points are singular points in the residue curve map. For the heterogeneous ∞/∞ column (Figure 3.3b), two variables are specified: reflux L is infinite and D_1 is zero. As a result of the infinite reflux, both phases must be returned from the decanter to the column, i.e., $L_1 = L_2 = \infty$. Hence, this ∞/∞ column has only one degree of freedom for a fixed feed F for a given flow rate, composition and quality. For a column with one degree of freedom, only one specification is allowed. Either the finite distillate flow rate D_2 , which is only a part of the flow rate of phase two, or B can be varied to specify the bottom purity. If two specifications are needed, an additional degree of freedom must be introduced. For this column, the entrainer flow rate F_E can be used as a second degree of freedom.

The task of the column is to separate I from a crude I - H feed F_C by the use of the light entrainer LE that is separately fed to the column (stream F_E). There are two specifications on the process:

1. The bottom composition should be close to pure H .
2. The distillate should consist only of LE and I (no product H in distillate).

For the ∞/∞ column, Figure 3.4 illustrates a possible profile in the residue curve map with a distillate consisting of LE and I and pure H at the bottom. Without the need for detailed simulations, the following statements can be deduced:

1. The ternary overall column feed $F = F_C + F_E$ is located at the intersection of the column mass balance line connecting distillate with bottom and the line connecting the binary I - H feed with LE . Applying the lever rule gives an exact LE makeup flow rate F_E for every composition of the binary I - H feed F_C . Note that this column profile is possible for I contents in F_C between 0 and 1, i.e., for compositions on both sides of the I - H azeotrope.

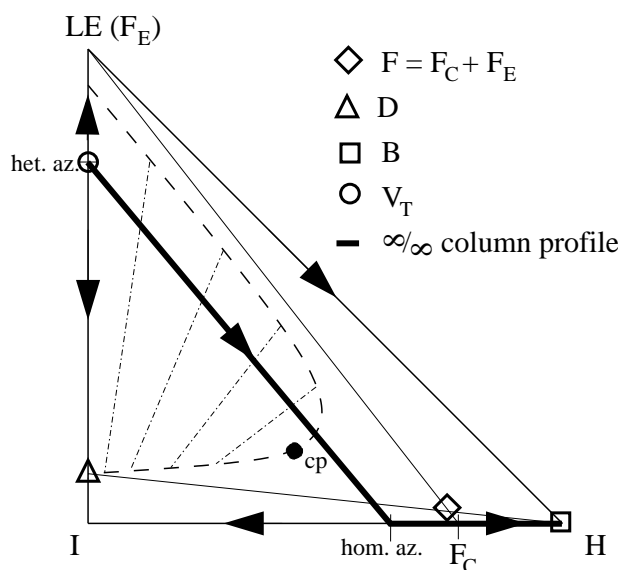


Figure 3.4: Residue curve map of the three component mixture LE–I–H with an ∞/∞ column profile (thick line) running from the unstable node along the boundary to the stable node H.

2. The recovery of H is perfect, because the bottom is pure H and the distillate consists only of LE and I.
3. The distillate composition is fixed, and all I leaves the column as distillate.
4. As a result of statements 2 and 3, the distillate flow rate D is proportional to the I flow rate in the crude feed F_C .
5. From statements 3 and 4, it follows that the required entrainer (LE) flow rate F_E is proportional to the I flow rate in the crude feed F_C .

The most important result is point 1: To reach a steady state that matches the two specifications, the entrainer flow rate F_E has to be adjusted to the I flow rate in F_C . The key point is that the phase split determines the entrainer loss. This argumentation also holds for all of the systems where the column is operated such that the upper pinch point of the column is the unstable node, which is heterogeneous. In operation of such columns, the entrainer flow rate F_E has to be adjusted to flow rate changes and to composition changes of F_C .

3.2.3 Analysis with the Finite/ ∞ Column

Most industrial columns are operated close to the maximum allowed vapor and/or liquid load to maximize the throughput. Hence, variations in column load can induce operational problems. Defining a finite reflux/ ∞ length column enables the prediction of column loads based on residue curve map information only.

The finite/ ∞ column is defined as a column with finite reflux and with the decanter policy that all of the LE-rich phase is used as reflux and all of the I-rich phase as distillate. This means $D_1 = L_2 = 0$ and specifying Q_R fixes all degrees of freedom, i.e., gives V_T , D_2 and B . Using the mass balance of the decanter, the reflux-to-distillate flow ratio of the finite/ ∞ column is determined by the liquid-liquid equilibrium that yields the concentrations of reflux and distillate. The reflux is assumed to be large enough so that the column profile still follows a residue curve. Because the number of stages is infinite, the finite/ ∞ column has the same pinch points as the ∞/∞ column. Hence, the finite/ ∞ column profile is exactly the same as the ∞/∞ column profile shown in Figure 3.4, and all five statements from the previous section hold also for the finite/ ∞ column. In addition, two more can be deduced:

6. The ratio D/L is determined by the phase split. With statement 4 follows that reflux L and reboiler duty Q_R are proportional to the I content in F_C .
7. As a result of statement 6, the column load depends directly on the I content in F_C .

These results predicted by the finite/ ∞ column will be confirmed by simulations of a real column with the industrial mixture in section 4.2.1. Note that problems such as load constraints in operation for certain crude feed compositions can be identified. In this case, the column load increases for increasing I content in the crude feed.

3.3 Influence of Impurities

Using the finite/ ∞ column, the effects of different impurities on the column operation are illustrated in this section using residue curve map information only. For a structured approach, the impurities are classified by their boiling points. For the three component LE–I–H mixture, there are four possibilities for the location of the boiling point of the impurity:

1. Lowest boiling (LL): $LL < LE < I < H$
2. Intermediate boiling 1 (LI): $LE < LI < I < H$
3. Intermediate boiling 2 (IH): $LE < I < IH < H$
4. Highest boiling (HH): $LE < I < H < HH$

In most cases, additional temperature minimum azeotropes are introduced by the impurity. To explain the effect of the impurity on column operation, the most common cases are used as examples. For all examples, a ternary Impurity–I–H feed F_C enters a finite/ ∞ column. The entrainer LE (stream F_E) is fed separately yielding a four–component overall feed F . The analysis is based on the following assumption: An arbitrary controller is able to fix either the top composition at the unstable node or the bottom composition at the stable node: If the number of stages is sufficiently large (or infinite as used for this analysis), then, the pinch has to coincide with a singular point in the residue curve map as reflux is increased. In some cases of the analysis, it is not clear whether the profile should be fixed at the unstable or the stable node. Then, both options are discussed.

3.3.1 Light Impurity – LL

Figure 3.5 shows the residue curve map for the simplest case of a light impurity: no further azeotropes are introduced. The tetrahedron is divided into two regions by a boundary represented by the shaded surface. One of the key features of the ternary LE–I–H mixture (Figure 3.4) is that the upper pinch point (unstable node) of the column profile is the

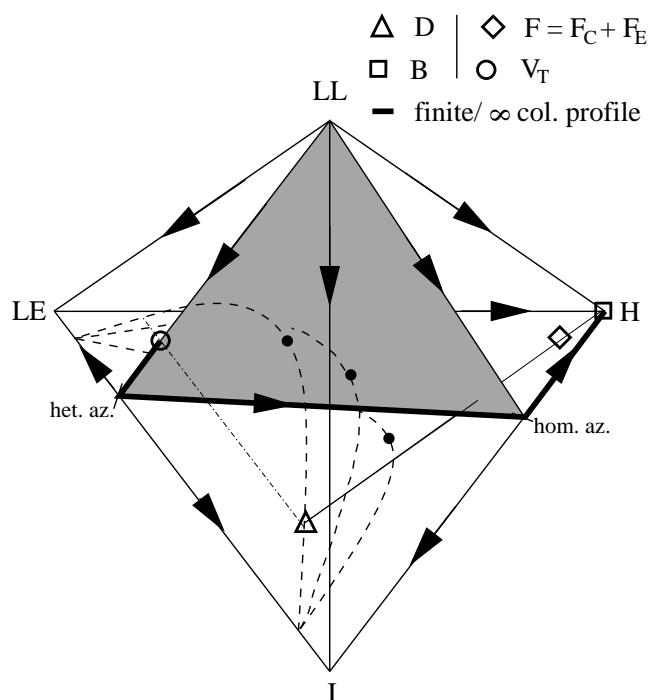


Figure 3.5: Example 1: LL–LE–I–H. A possible finite/ ∞ column profile starts at the circle, passes the LE–I and I–H azeotropes and ends at the stable node H.

desired LE–I azeotrope. For the four component mixture containing LL, this is no longer the case: The unstable node is now pure component LL. A column profile with the unstable node as upper pinch point and the stable node as bottom pinch would only be possible if the overall feed F lied on the binary LL–H edge. However, the overall feed F is a four component feed. The desired finite/ ∞ column profile runs as indicated with the thick line in Figure 3.5. The composition of the overhead vapor V_T lies inside the heterogeneous region on the residue curve boundary connecting LL with the heterogeneous LE–I azeotrope. The profile passes the LE–I and the I–H azeotrope, and ends at pure H.

A possible operation problem for this impurity is that the phase split in the decanter can disappear. This is illustrated by the following scenario. If an arbitrary controller fixes the bottom purity at pure H and if the LL concentration in the crude feed F_C increases, the LL concentration in the distillate has to increase as a result of the overall mass balance. This leads to an increase of LL in the top of the column. In the composition space, the top composition of the finite/ ∞ column has to move along the boundary residue curve toward LL. As long as the top composition stays inside the heterogeneous region, the decanter

will operate as desired. Note that the reflux-to-distillate ratio increases as a result of the changed liquid-liquid equilibrium when the top composition moves toward the binodal curve (see section 4.3.1 for a detailed discussion). If the LL concentration in the feed is too high, the overall mass balance forces the top composition to leave the heterogeneous region. This, however, causes a major disturbance in decanter operation: The phase split disappears. Hence, the liquid-liquid equilibrium limits the maximum allowed amount of LL in the ternary LL-I-H feed, if the bottom is fixed at pure H. This aspect must be considered for the design of the control system. It will be discussed in section 3.4.4 using an LE-LI-I-H mixture that is described in the next section and exhibits the same problems. If LL is very light boiling, then its concentration is expected to be small because the separation in the upstream column is very effective. However, if the boiling point of the impurity is close to the boiling point of LE, its concentration can fluctuate as a result of upstream disturbances. In addition, close boiling substances of different chemical nature are very likely to exhibit azeotropic behavior. Figure 3.6 shows such a case. LL introduces one additional minimum boiling LL-LE azeotrope, but the unstable node remains at the heterogeneous LE-I azeotrope.

For this mixture, two scenarios are possible. Figure 3.6 shows the first one: The bottom purity is fixed at pure H. As for the mixture shown in Figure 3.5, the tolerable LL content in the crude feed is limited by the heterogeneous envelope. A second scenario is shown in Figure 3.7. The controller fixes the top composition at the upper pinch point, the heterogeneous LE-I azeotrope. This always ensures a phase split in the decanter. A separation into a distillate only containing LE and I and a bottom containing only the light boiling impurity LL and H is possible for every ternary LL-I-H feed. A downstream separation of the bottom stream into the impurity LL and H is easy because of the large difference in boiling points. For this case, it is desired to fix the top composition and to remove the light boiling impurity LL in a subsequent column.

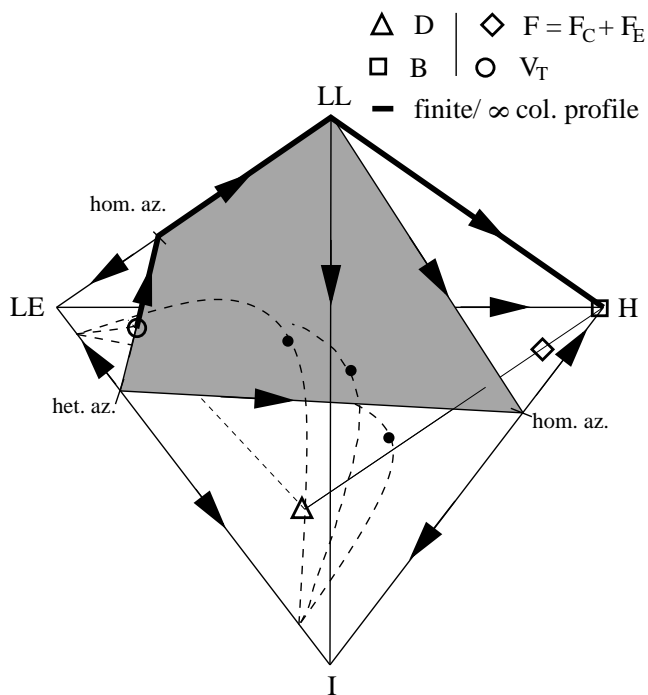


Figure 3.6: Example 2: LL-LE-I-H. A possible finite/ ∞ column profile starts on the boundary in the heterogeneous region and runs via LL to H.

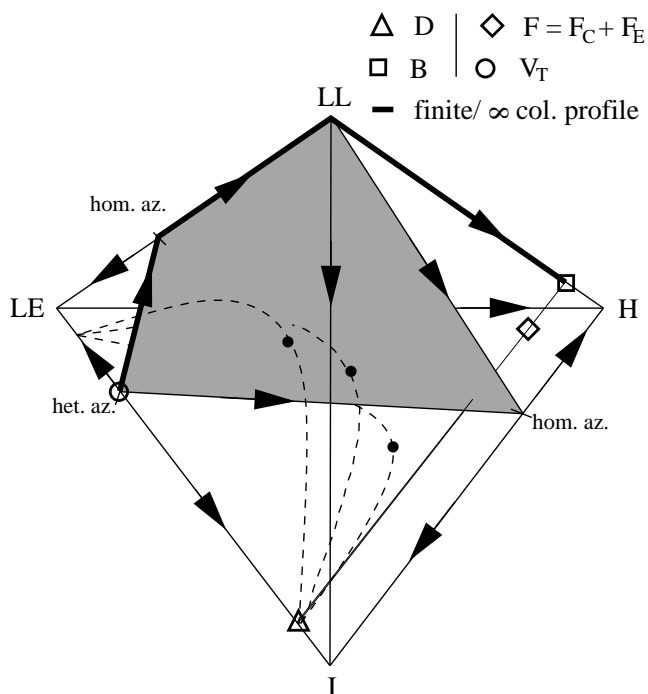


Figure 3.7: Example 3: LL-LE-I-H. A possible finite/ ∞ column profile runs from the unstable node via LL toward H.

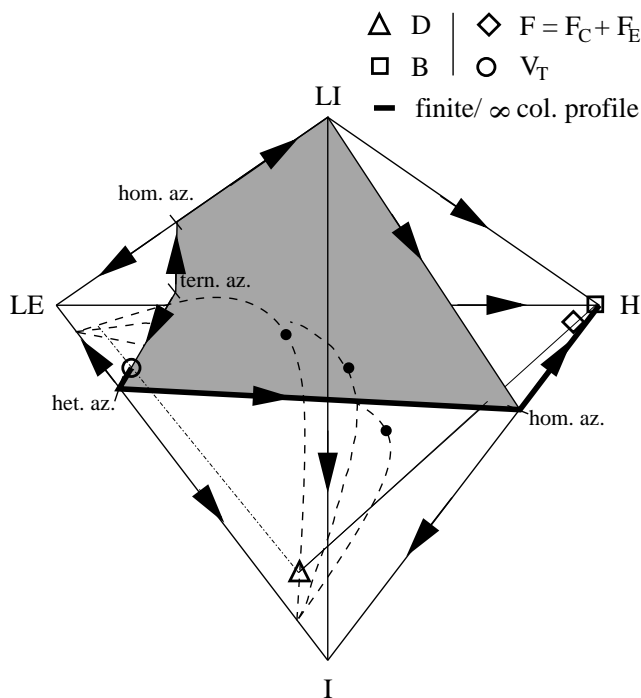


Figure 3.8: Example 4: LE–LI–I–H. A possible finite/ ∞ column profile starts at the circle, passes the LE–I and I–H azeotropes and ends at the stable node H.

3.3.2 Intermediate Impurity 1 – LI

The two cases pictured in Figures 3.6 and 3.7 is also possible for LI. The results are the same as those discussed for LL.

In Figure 3.8, the residue curve map for a different intermediate boiling impurity is shown. The impurity LI introduces a binary LE–LI and a ternary LE–LI–I azeotrope. Both are minimum boiling. The topology of this mixture corresponds to the one of the real industrial mixture. The key feature of this residue curve map is that the ternary azeotrope is the unstable node. The locus of this ternary azeotrope plays an important role: If it is outside the heterogeneous region as shown in Figure 3.8, then a separation with a column profile starting at the unstable node is not desired: There is no phase split, hence the entrainer loss is high and the entrainer LE needs to be recovered in another column. In contrast, column profiles starting between the ternary and the heterogeneous LE–I azeotrope and ending at the stable node H are generally possible if the concentration of LI in the crude feed is small enough. The limitation is that the overhead vapor composition can leave

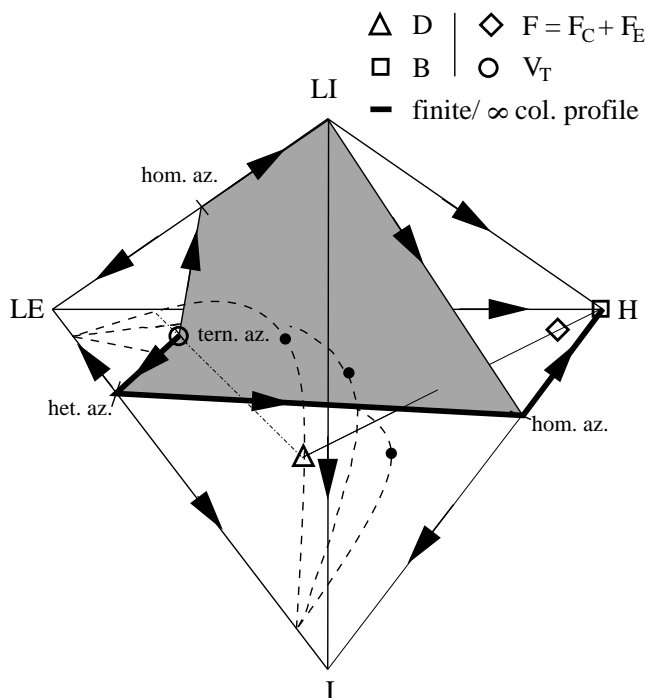


Figure 3.9: Example 5: LE–LI–I–H. For small amounts of LI, a possible finite/ ∞ column profile runs from the unstable node via the LE–I and I–H azeotrope to H.

the two phase region if the impurity in the feed is increased as a result of an upstream disturbance. The means to deal with these limitations are presented in section 3.4.4 for this specific mixture as example.

If the ternary azeotrope lies inside the heterogeneous region, the column profile can run as shown in Figure 3.9 if the crude ternary LI–I–H feed is such that the quaternary feed F lies on the line connecting the bottom B at H with the distillate which is the I–rich phase of the ternary LE–LI–I azeotrope. For smaller amounts of LI in the crude feed, the top composition will lie as shown in Figure 3.8 on the boundary between the ternary LE–LI–I azeotrope and the binary LE–I azeotrope, if the controller fixes the bottom composition at H. This is the desired case for small amounts of impurity. For larger amounts of LI, there again two possible scenarios. If the top composition is fixed at the ternary LE–LI–I azeotrope, the overall mass balance forces the whole profile to shift to the one pictured in Figure 3.10. The bottom stream now contains LI and H. If the bottom composition is fixed at H, then the top composition can leave the heterogeneous region for increasing amounts of LI similar to example 2 shown in Figure 3.6. This leads to a loss of the phase

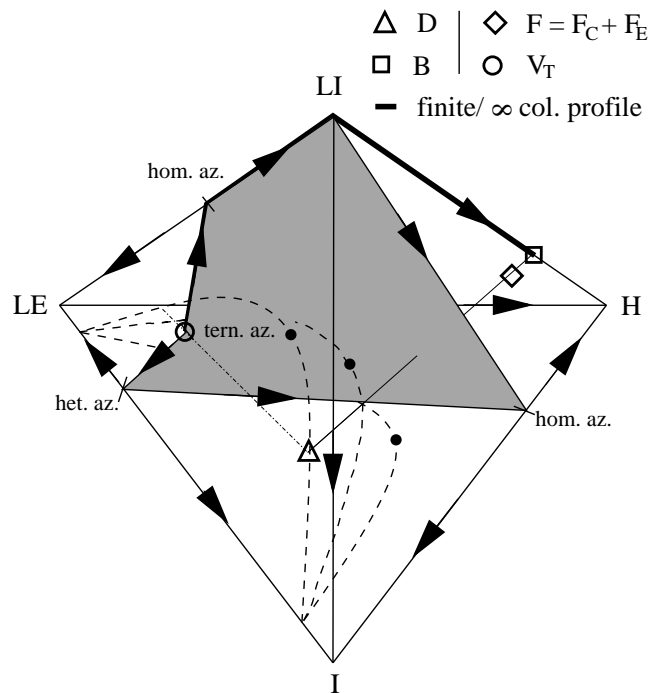


Figure 3.10: Example 6: LE–LI–I–H. For large amounts of LI, a possible finite/ ∞ column profile runs from the unstable node via the LE–LI azeotrope and LI toward H.

split in the decanter which is undesired. Hence, a different control scheme has to be used to prevent these changes in operation.

If there is an additional binary temperature minimum LI–I azeotrope, the described effects of LI on the decanter operation are the same, except that the column profile might run along a different path.

3.3.3 Intermediate Impurity 2 – IH

As Figure 3.11 shows, IH introduces two more binary azeotropes and a ternary azeotrope. All are minimum boiling. Despite that complicated behavior, the desired process (removal of I from H) is possible, because the unstable node remains at the LE–I azeotrope. A column profile that separates I from the product stream exists for all ternary I–IH–H feeds. However, depending on the relation of IH and H and the composition of the IH–H azeotrope, the bottom is either rich in H (Figure 3.11), or rich in IH (not shown). In both

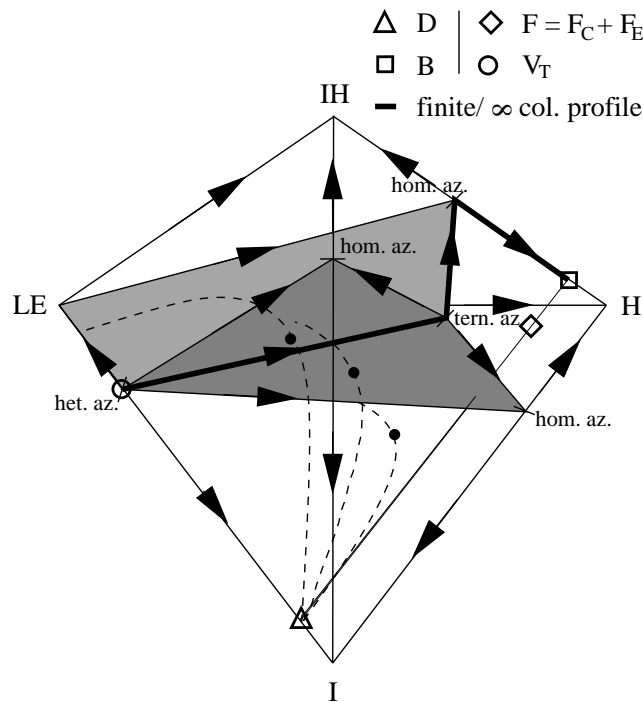


Figure 3.11: Example 7: LE–I–IH–H. A possible finite/ ∞ column profile runs from the unstable node via the ternary I–IH–H azeotrope and the binary IH–H azeotrope toward H.

cases, the subsequent separation of IH and H is not an easy task.

3.3.4 Heavy Impurity – HH

Figure 3.12 shows the residue curve map for a heavy boiling impurity. HH introduces one additional azeotrope with I. The unstable node remains at the LE–I azeotrope, which is the desired top composition. HH and I are the two stable nodes. The desired profile runs along the boundary in the LE–I–H plane, and passes the two saddles, I–H azeotrope and pure H. The profile finally ends on the edge of the tetrahedron connecting H with HH. Therefore, the heavy boiling impurity leaves the column through the bottom, as H does. Because HH forms no azeotrope with H, the separation of H and HH can be realized by zeotropic distillation in a subsequent column.

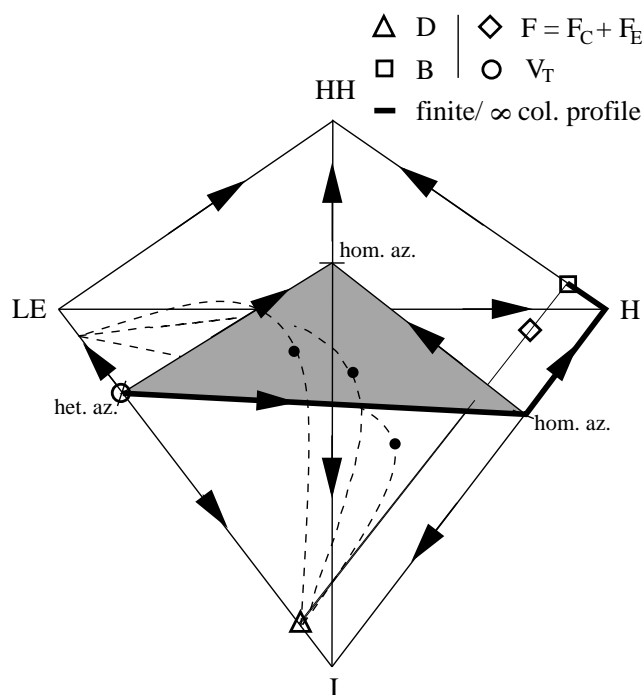


Figure 3.12: Example 8: LE–I–H–HH. A possible finite/ ∞ column profile runs from the unstable node via the binary I–H azeotrope and H toward HH.

3.3.5 Summary

Several impurities have been analyzed. Light to intermediate boiling impurities tend to change the locus of the unstable node. If they change the locus, their influence on the process has to be investigated further. Heavy boiling impurities normally do not change the locus of the unstable node. In this case, they can be lumped with H, i.e., neglected without losing significant aspects in a more detailed study of the heterogeneous distillation column.

3.4 Control Schemes

In this section, control schemes for the process are presented. In section 3.4.1, the specifications for the control schemes are defined. In section 3.4.2, a two point control scheme is proposed for the three component system LE–I–H (Figure 3.4). The key point for this system is that if the real finite column operates at maximum achievable separation, the

condensed overhead vapor will lie very close to the unstable node, and hence always inside the heterogeneous region if there is enough entrainer LE in the system. In section 3.4.3, problems with the two point control scheme for a four component system LE–LI–I–H as shown in Figure 3.8 are discussed. Here, the unstable node lies outside the heterogeneous region. In section 3.4.4, a three point control scheme is proposed based on knowledge of the steady state behavior of the finite/ ∞ column: If an impurity that changes the locus of the unstable node is present, the feasible overall feed composition is limited. The third manipulated variable changes the overall feed in a way so that the overall feed stays inside the feasible region. This three point control scheme is not restricted to this process. It enables robust performance for all heterogeneous distillation processes where the impurity changes the locus of the unstable node from the desired heterogeneous azeotrope to a singular point that lies outside the heterogeneous region.

The argumentation for the choice of the control loops is based on physical process insight gained by an analysis using the finite/ ∞ column. The procedure focuses on the *feasibility* and *robustness* of the control concept. The core results of this section are of qualitative nature. They are quantitatively illustrated with the industrial mixture in sections 4.2 and 4.3.

3.4.1 Specifications

The purpose of the heterogeneous column is to remove I from the crude feed F_C containing I, H, and a possible impurity using the miscibility gap between LE and I as illustrated in Figure 3.4. There are two specifications for the design of the process:

1. The I content of the bottom stream (the product stream) must be below a specified value.
2. The product loss through the distillate should be small.

In addition, for exploiting the phase split the overhead vapor (top) composition must lie inside the heterogeneous region. Then, the condensed and sub-cooled overhead vapor can

be separated in the decanter into reflux and distillate at their desired purities and flow rates. This coincides with specification 2 because the product loss through the distillate is minimal when the top composition is at the heterogeneous LE–I azeotrope. Another key point for reaching the LE–I azeotrope is that there is enough entrainer LE in the system. A constraint for operation is that the column load must stay below a certain value to prevent flooding.

A control scheme has to be robust in that sense that it ensures the operation of the column at the optimal point for different feed flow rates and compositions. Here, robustness is not robustness against modeling errors, but robustness against nonlinear phenomena like the disappearance of the phase split in the decanter or flooding. The control system must ensure that the phase split remains in the decanter for all possible feed compositions. In addition, it must ensure that the phase split returns if it disappears as the result of an unexpected disturbance. Whereas robustness against modeling errors can be obtained by controller tuning, it is shown in sections 3.4.2–3.4.4 that robustness against the disappearance of the phase split in the decanter can only be achieved by choosing the correct manipulated variables together with the proper design of the decanter, i.e., that there is enough entrainer LE and component I in the system. While I is contained in the crude feed, LE has to be adjusted separately. For the control schemes presented hereafter, we assume perfect control of all levels and of the column pressure. The decanter is assumed to be equipped with automatic phase detection where the level of the I rich phase is controlled in such a way that the distillate is set to zero if the phase split disappears, i.e., that the column is operated at total reflux.

3.4.2 Two Point Control for the Three Component Mixture

As discussed in section 3.2.1, the heterogeneous column has only one degree of freedom for the proposed decanter policy. To ensure the bottom purity, the reboiler duty Q_R is chosen as manipulated variable. Note that the reflux-to-distillate ratio is given by the phase split in the decanter. Hence, increasing Q_R leads to an immediate rise of reflux L if the top composition does not change. Critical for the top composition is that the amount

of entrainer LE is correct. Therefore, the entrainer makeup flow F_E is chosen as a second, directly manipulated variable. To reach a steady state, the entrainer flow rate has to be adjusted to different flow rates and I contents of F_C , because the LE flow in distillate D depends directly on the I flow in F_C , as deduced in section 3.2.2. The best location of F_E is directly after the decanter for the following reasons:

1. F_E will interfere the least with the bottom purity, if it is located furthest away from the bottom, i.e., at the top. Hence, the coupling between these two controllers is smallest for this location.
2. F_E makes up for the losses through the distillate leaving the decanter. Therefore, it should be located after the decanter. If the makeup is added before, part of the makeup is directly lost through the distillate.

Figure 3.13 presents a possible control scheme for this process with two single loop controllers. The binary I-H feed (F_C) enters the column in the middle, whereas the entrainer feed (F_E) is located after the decanter.

For the ∞/∞ column, a temperature profile can be predicted based only on residue curve map information: A temperature plateau is the part of the temperature profile at a pinch point, a temperature front is a part of the temperature profile where a sharp change in temperature occurs along a finite length (Dorn et al., 1998). Figure 3.14 shows the temperature profile of the finite/ ∞ column profile (Figure 3.4) obtained using these two definitions. Plateau 1 corresponds to the LE-I azeotrope. Front 1 connects plateau 1 with plateau 2 that corresponds to the I-H azeotrope. Front 2 is the connection of plateau 2 with plateau 3 that corresponds to pure H. To ensure the bottom purity, TC1 controls the temperature front in the stripping section (front 2 in Figure 3.14) by manipulating Q_R . The bottom temperature is added to the controlled temperature because it is an indicator for the bottom purity. TC2 has to control the LE inventory by manipulating F_E . A good indicator for LE is the temperature front in the rectifying section (front 1 in Figure 3.14). The choice of the actual sensor locations will be discussed in section 4.2.3.

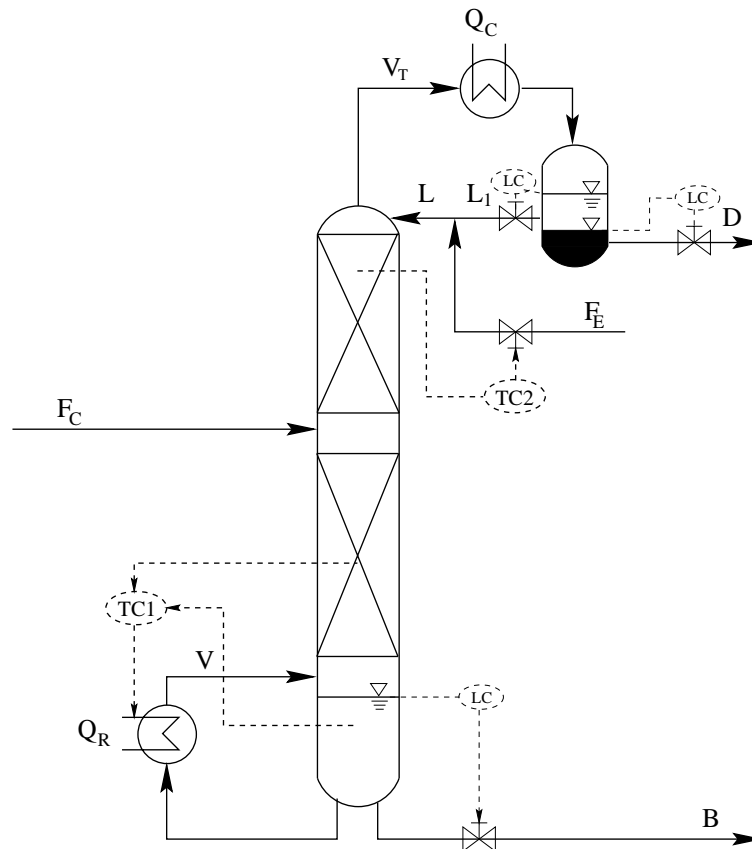


Figure 3.13: Two point control scheme for the finite/ ∞ column for the LE–I–H mixture. TC1 controls an average temperature by manipulating the reboiler duty. TC2 controls a temperature by manipulating the entrainer makeup F_E .

The decanter is designed so that the column operates at total reflux if the phase split disappears. By this, the control scheme can return the phase split by the following mechanism. If TC1 keeps the bottom purity at H, I has to collect in the top. With the proper amount of LE added by TC2, the heterogeneous LE–I azeotrope will finally appear in the top and reestablish the phase split.

Another option is to use the reflux L as manipulated variable and adjust the variable F_E , which is critical for success, indirectly via a level controller of the LE rich phase in the decanter. This will be discussed in section 4.3.4.

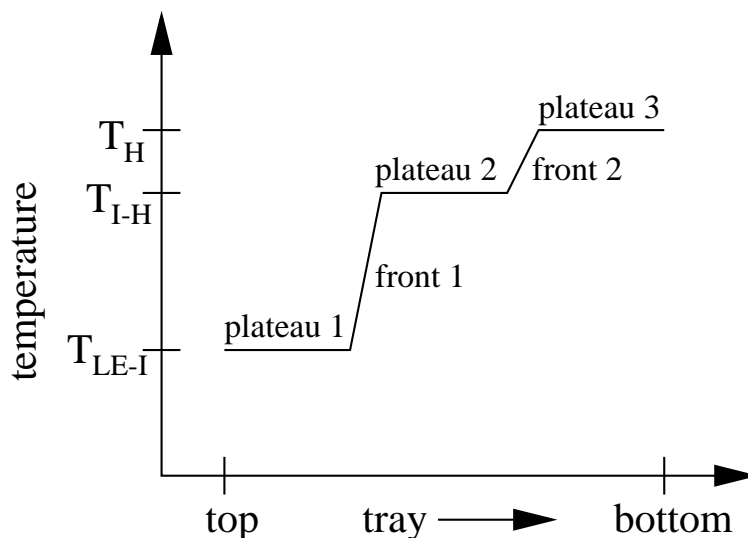


Figure 3.14: Predicted temperature profile for the ∞/∞ (finite/ ∞) column for the LE-I-H mixture (Figure 3.4).

3.4.3 Problems with Two Point Control for a Four Component Mixture

For the three component mixture, F_E has to be adjusted to the content of I in F_C to keep the operation of the column within specifications. The controller TC2 is robust against all possible disturbances, i.e., keeps the top composition inside the heterogeneous region, if the decanter is designed properly. For a four component mixture including a light (LL) or intermediate (LI) boiling impurity, TC2 cannot ensure that the top composition stays inside the heterogeneous region. As discussed in sections 3.3.1 and 3.3.2, the top composition can leave the heterogeneous region for high contents of the impurity in the crude feed. With the four component LE-LI-I-H mixture shown in Figure 3.8 that corresponds to the industrial example, it is illustrated why the two point control scheme cannot handle large changes of the impurity concentration in the crude feed.

Figure 3.8 shows that for small amounts of LI (acetone in the industrial case) in the overall feed, the overhead vapor of the finite/ ∞ column is still close to the binary LE-I azeotrope, and the bottom is pure H. For increasing LI contents in F_C and constant product purity in the bottom, the LI content in the distillate has to increase to fulfill the overall mass

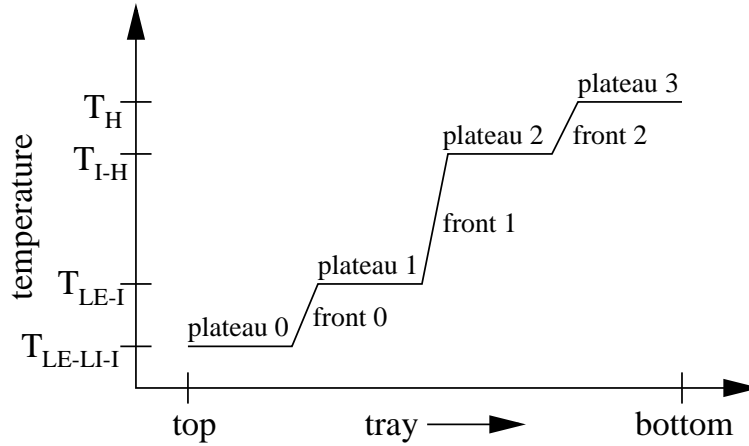


Figure 3.15: Predicted temperature profile for the ∞/∞ (finite/ ∞) column for the LE-LI-H mixture (Figure 3.8).

balance. Hence, the overhead vapor composition has to move along the residue curve toward the ternary azeotrope to increase the LI content in the decanter and the distillate. If the LI content is too high, the phase split in the decanter will disappear. Unfortunately, TC2 does not “see” that the overhead vapor composition approaches the binodal curve:

Figure 3.15 shows the temperature profile for a finite/ ∞ column with the top composition at the ternary LE-LI-I azeotrope and the bottom composition at pure H. In addition to the existing plateaus and fronts (as shown in Figure 3.14), plateau 0 corresponds to the ternary LE-LI-I azeotrope and front 0 connects it with plateau 1. TC2 fixes front 1, but does not see the appearance of front 0. Hence, LI can accumulate and the phase split can disappear. Note that the reflux will increase as the top composition approaches the binodal curve. This result does not depend on controller tuning and also applies to the Q_{RL} scheme of the industrial column (compare section 3.1). To avoid these operational problems, a third manipulated variable has to be introduced.

3.4.4 Three Point Control for the Four Component Mixture

For correct operation of the column, the control system must ensure that the overhead vapor composition lies inside the heterogeneous region. To keep reflux (and Q_R) small, the top composition should lie at some distance from the binodal curve. Figure 3.16 shows a

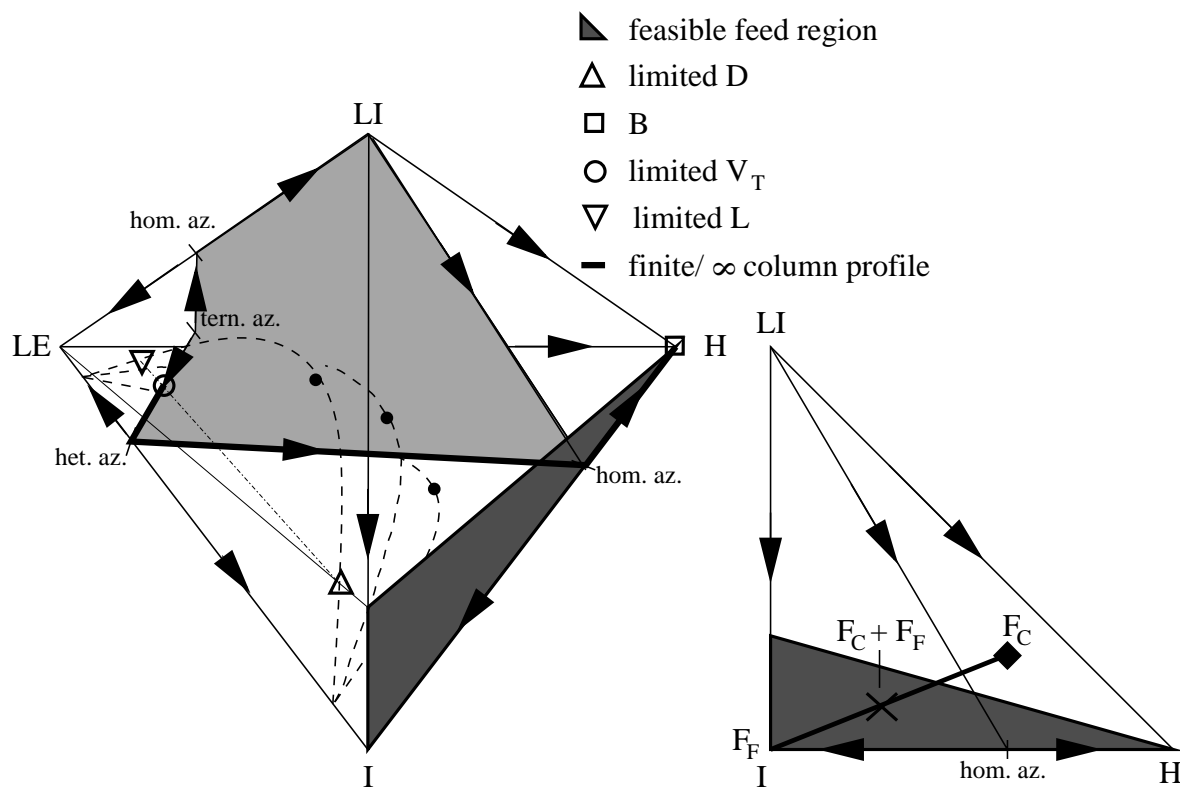


Figure 3.16: Residue curve map of the system LE–LI–I–H (Figure 3.8) picturing the feasible region (darkly shaded) for ternary crude feeds with a limited LI content in the overhead vapor.

region of feasible ternary LI–I–H feeds F_C (darkly shaded). This region is constructed as follows: The LI content in the overhead vapor is limited. Hence, the quaternary overall feed F has to lie on the surface connecting pure H with the possible locations of the distillate on the binodal curve. Since these quaternary feeds are obtained by mixing ternary LI–I–H crude feeds F_C with the entrainer (LE) makeup flow F_E , the surface of feasible quaternary feeds is projected on the LI–I–H plane by connecting the boundaries of the surface with LE giving the darkly shaded region in Figure 3.16, the region of feasible ternary LI–I–H feeds.

As the right part of Figure 3.16 shows, every ternary LI–I–H feed F_C that is outside this region can be brought into this region if I is added to F_C . In order to reject fluctuations of the LI content in F_C , the control scheme for the four component system has to be extended by a third loop, which manipulates an additional feed F_F that adds I to the process to keep

the ternary feed ($F_C + F_F$) inside the darkly shaded region of Figure 3.16. This corresponds to what is done in the industrial process: The decanter is flushed with I (water) when LI (acetone) accumulates in the top of the column.

A common operation strategy for heterogeneous 222-m mixtures is to reflux some of the distillate to ensure the phase split. For the three component heterogeneous 120 mixture (Figure 3.4), the upper pinch point is the desired LE-I heterogeneous azeotrope (unstable node). Here, refluxing some of the distillate, which sharpens the column profile, might be used to ensure that the overhead vapor is at the unstable node. For the four component mixture shown in Figure 3.8, refluxing part of the distillate does not work: Refluxing some of the distillate leads to a decrease of the distillate flow. If a controller fixes the bottom purity at pure H, less impurity LI leaves the process. Hence, LI accumulates faster. Together with the profile sharpening caused by the increased reflux, the top composition moves faster toward the homogeneous ternary azeotrope. The point where the phase split disappears is reached even faster. Therefore, the phase split cannot be ensured by refluxing some of the distillate, I has to be added as explained above.

Contrary to the location of F_E , the optimal location of F_F is before the decanter, because then the added I leaves the process directly through the distillate removing only the desired LI and some LE. Hence, its influence on the bottom purity is the smallest. Figure 3.17 shows the process including the I feed F_F . The process is now a three-input three-output system. Even though the inputs and outputs are coupled, three single loop controllers are chosen in a first approach: The bottom purity controller (TC1), the rectifying section controller (TC2) and the overhead vapor composition controller (CC3). TC1 and TC2 work as explained in section 3.4.2. CC3 controls the LI content in the overhead vapor feed by manipulating F_F to ensure that the ternary LI-I-H feed ($F_C + F_F$) is inside the feasible region (Figure 3.16). CC3 acts as an override controller: If the LI content in the top is less than a specified value, CC3 will set F_F to zero. If the LI content is above a specified value, CC3 will increase F_F to remove LI from the process via the distillate.

The composition controller CC3 can also be replaced by a temperature controller (TC3): If the top composition moves from the desired binary LE-I azeotrope to the undesired ternary LE-LI-I azeotrope, a temperature front (front 0 in Figure 3.15) will appear in the top.

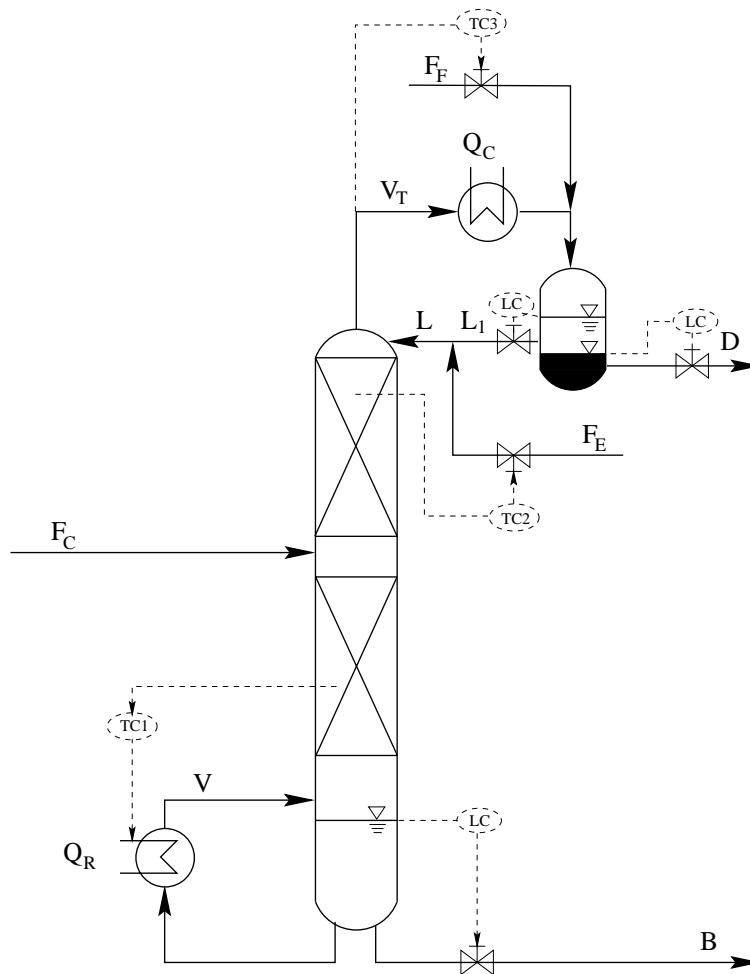


Figure 3.17: Process setup for the system LE–LI–I–H. In addition to TC1 and TC2, TC3 (CC3) manipulates the I feed F_F that is added to the sub-cooled liquid to control LI concentration in the overhead.

TC3 has to prevent the occurrence of front 0. The setpoint of TC3 should be close to the temperature of the binary LE–I azeotrope (T_{LE-I}). TC3 also acts as an override controller: If the top temperature is above the setpoint, F_F is set to zero. If it is below the setpoint, F_F is increased, i.e., greater than zero. These qualitative results are now illustrated with simulations of a real plant.

Chapter 4

Simulations of a Heterogeneous Azeotropic Distillation Column

4.1 Modeling

First, the column model that was used in all simulations is introduced. Using the qualitative analysis of section 3.3, the number of components is reduced to four. Second, the model is compared to actual plant data. The model matches well the key features of the plant behavior. Finally, the composition of the ternary MTBE–acetone–water whose location plays a major role on the plant operation is discussed.

4.1.1 Column Model

The column model used in the following simulations is based on the industrial plant (Figure 3.1). As mentioned in section 1.1, there are light and heavy boiling impurities. Following the analysis of section 3.3.4, the heavy boiling impurities leave the column via the bottom as MBI. Therefore, they can be lumped with MBI. As discussed in sections 3.3.2 and 3.4.3, an intermediate boiling impurity can change the column behavior. Therefore, acetone, which is intermediate boiling, is modeled as an individual component. The buffer tank is not included in the model because it is irrelevant at steady state. It is not neces-

Table 4.1: Data table for the column model RadFrac in Aspen Plus and Aspen Dynamics. The heights of the liquid phases on each tray calculated by the Francis weir formula.

top	pressure: 1 bar, condenser: sub cool to 45° C, no holdup
decanter	adiabatic with holdup: 1.131 m ³ , aqueous phase: distillate D, organic phase: reflux L, makeup F _E : added to reflux with T = 45° C, buffer tank (if used): adiabatic, holdup: 4 m ³
rectifying section	8 theoretical stages, $\Delta p = 1.2$ mbar/stage, diameter = 600 mm, weir height = 1 mm, tray spacing = 450 mm, holdup ≈ 0.003 m ³ /stage
feed F _C	saturated vapor, p = 1.015 bar
stripping section	20 stages with Murphree efficiency of 0.5, $\Delta p = 2.9$ mbar/stage, diameter = 600 mm, weir height = 25 mm, tray spacing = 180 mm, holdup ≈ 0.009 m ³ /stage
bottom	one theoretical stage, holdup: 1.178 m ³

sary to use a buffer tank in a real plant, if the decanter is designed in a way that it always provides reflux, for example with automatic phase detection. The column is modeled in Aspen Plus for steady state analysis and in Aspen Dynamics for the dynamic simulations using the block RadFrac. Table 4.1 describes the setup of the column (the AspenPlus and AspenDynamics files can be obtained from the authors upon request). At this stage, the manual flushing with water is not modeled. In the simulations presented hereafter, stage 1 always refers to the first stage of the column counting from the top. Hence, the entrainer makeup F_E and the reflux L enter the column above stage 1 (compare Figure 3.13), the crude feed F_C enters the column above stage 9, the bottom is stage 29.

The physical parameters are taken from the databases of Aspen Plus (Asp, 1999b) for all pure components except for MBI, which is not in the database. The parameters for MBI provided by our industrial partner are listed in Appendix A.1. The vapor–liquid equilibrium is calculated using the Wilson activity coefficient model for the liquid phase and the ideal gas equation for the vapor phase. The Wilson parameters of the binary subsystems were partly taken from literature, partly regressed to experimental binary VLE data from our industrial partner. They are also listed in Appendix A.1. Although the Wilson activity

coefficient model cannot provide a vapor–liquid–liquid equilibrium, it was chosen because steady state simulations of the industrial plant showed that Wilson parameters give a description closer to reality than simulations with a set of NRTL parameters.

The liquid–liquid equilibrium in the decanter is calculated using the UNIQUAC activity coefficient model. In order to give an adequate description of the four component liquid–liquid equilibrium, the set of UNIQUAC parameters was regressed to experimental four component liquid–liquid equilibrium data (MTBE, acetone, water, and MBI) supplied by our industrial partner. The parameters are listed in Appendix A.1.

4.1.2 Industrial Plant–Model Comparison

For all steady state simulations, the following specifications are made as for the industrial plant:

1. The bottom purity of MBI is specified to be 0.9996.
2. The temperature on stage 3 (T_3) is specified to be 70° C.

The bottom flow rate B and the entrainer makeup flow rate F_E are the free variables, which are adjusted by the steady state solver in order to meet these specifications.

As mentioned in section 3.1, the column is operated with manual adjustment of reflux and discontinuous entrainer makeup flow. Hence, the column is never at steady state. The water content in the crude feed F_C varies between 0.016 and 0.03, the acetone content between 0.0002 and 0.0010. Table 4.2 shows that the agreement between plant and model is quite good for the main streams of the process (flow rate and composition). The reflux varies in the simulations from 2772 kg/h for 0.016 water in F_C and 3505 kg/h for 0.03 water in F_C . The reflux–to–distillate ratio is approximately 85 on a mass basis. Figure 4.1a compares simulated temperature profiles of the column for different water and constant acetone contents in F_C with the predicted profile for the finite/ ∞ column (Figure 3.14) and actual plant data. Figure 4.1b compares simulated temperature profiles of the column for different acetone and constant water contents in F_C . The actual lengths of the plateaus and

Table 4.2: Comparison of plant measurements with the corresponding steady state from Aspen Plus for $F_C = 1600$ kg/h, 0.9795 MBI, 0.02 water, and 0.0005 acetone and $F_E = 0.72$ kg/h, pure MTBE. Concentrations are given in mass fractions.

component	bottoms		distillate		reflux	
	plant	model	plant	model	plant	model
MBI	0.9998	0.99973	0.0010	0.0009	0.0200	0.0044
MTBE	–	trace	0.0300	0.0217	0.9350	0.9593
water	0.0002	0.0001	0.9450	0.9576	0.0150	0.0135
acetone	–	0.0002	0.0240	0.0197	0.0300	0.0226
flow rate [kg/hr]	1566.9	1567.5	33.0	33.1	3040	2809

fronts of the finite/ ∞ column profile were chosen such that they fit well to the simulated data. For high acetone and/or water contents, the simulated column profile shows plateau 2 which corresponds to the binary water–MBI azeotrope at 89.8° C.

Figure 4.1 illustrates the strong dependence of the temperature profiles on the crude feed composition for constant bottom and almost constant distillate compositions. As for the finite/ ∞ column, the reflux of the real column depends on the water and acetone content in the crude feed. If the contents increase, reflux increases leading to a sharpening of the temperature profile. The effect of the tray efficiencies on the internal flow rates and hence on the column profile plays a minor role compared to the changes in crude feed composition that determine the reflux via the liquid–liquid equilibrium in the decanter.

4.1.3 Composition of the Ternary Azeotrope

A key problem in the operation of the plant is the presence of acetone. A ternary homogeneous MTBE–acetone–water azeotrope is predicted by the Wilson parameter set (Table 4.3). Using a set of NRTL parameters, the ternary azeotrope is also homogeneous (VLE) but it lies inside the heterogeneous region (LLE) for 45° C (Ulrich and Morari, 2000). The calculation of ternary azeotropes using VLLE or VLE has been discussed extensively (Pham and Doherty, 1990a; Pham and Doherty, 1990b). To our knowledge, the

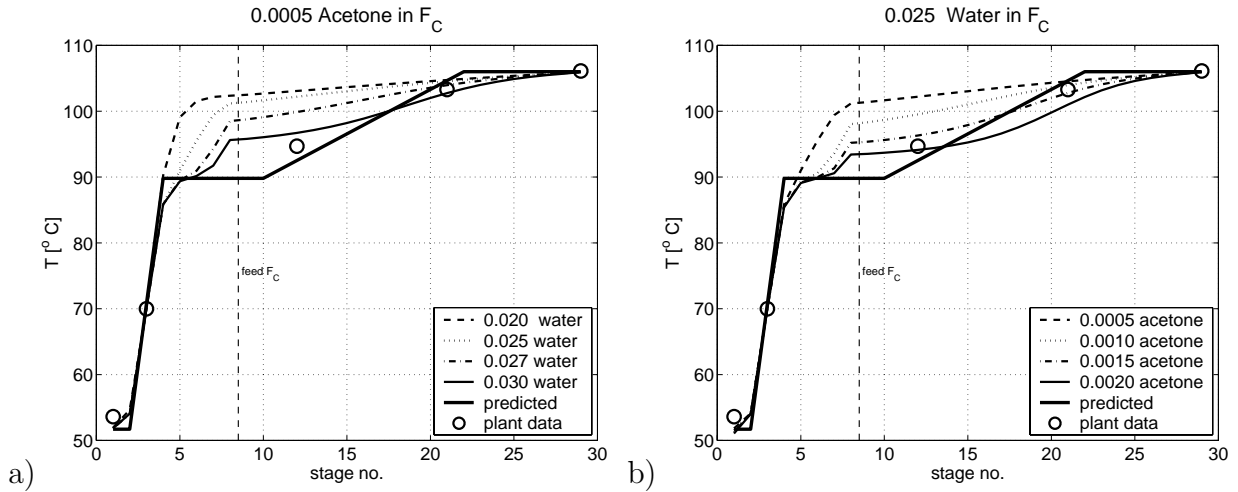


Figure 4.1: Comparison of the model with the predictions from the finite/ ∞ column and the industrial plant: a) temperature profiles of the column for different water contents in F_C at constant acetone content, b) temperature profiles of the column for different acetone contents in F_C at constant water content.

Table 4.3: Homogeneous ternary MTBE–acetone–water azeotrope predicted with the Wilson parameters (concentrations in mass fractions).

T [° C]	p [bar]	x_{MTBE}	$x_{Acetone}$	x_{Water}
49.82	1.000	0.7352	0.2489	0.0159

existence and location of the azeotrope has not been confirmed experimentally. Hence, there are three possibilities for the composition of the ternary azeotrope: Outside or inside the heterogeneous region, or not existent. The influences on the plant behavior are the following:

1. If the real ternary azeotrope lies outside the heterogeneous region, the phase split can disappear as a result of a high acetone concentration. This matches the observation of the operation staff that the phase split used to disappear in the decanter. The reason was a high acetone concentration.
2. If the real ternary azeotrope lies inside the heterogeneous region, the phase split cannot disappear as a result of a high acetone concentration. However, this is contradictory to the experience of the operating staff of the plant that the phase split

Table 4.4: Comparison of calculated binary azeotropes with data from literature.

mixture	T [$^{\circ}$ C]	p [bar]	x_1 [kg/kg]	kind	source
MTBE (1) – acetone (2)	50.57	1.013	0.675	homogeneous	Wilson
	50.70	1.0132	0.6589	homogeneous	experiment
MTBE (1) – water (2)	52.02	1.013	0.971	homogeneous	Wilson
	51.07	0.9795	0.971	homogeneous	Wilson
	51.25	0.9795	0.9678	heterogeneous	experiment
water (1) – MBI(2)	90.52	1.027	0.265	homogeneous	Wilson
	91.00	1.0266	0.2900	homogeneous	experiment

disappears as a result of a high acetone concentration.

3. If the ternary azeotrope does not exist in reality, the influence of acetone is the same as that if it lies outside the heterogeneous region. Based on the experimental data (Gmehling et al., 1994) shown in Table 4.4, the boiling temperature of the homogeneous MTBE–acetone azeotrope is lower than that of the heterogeneous MTBE–water azeotrope. Hence, the upper pinch point of the column profile is the homogeneous MTBE–acetone azeotrope and the desired separation is no longer possible for high acetone contents in the feed, because the overhead vapor composition lies outside the heterogeneous region.

To summarize, the predicted ternary azeotrope qualitatively describes the observed plant behavior. Therefore, we assume for the rest of the paper that the predicted ternary azeotrope exists and lies outside the heterogeneous region.

4.2 System MTBE/Water/MBI

4.2.1 Validation of Finite/ ∞ Column Predictions

The following predictions will be validated:

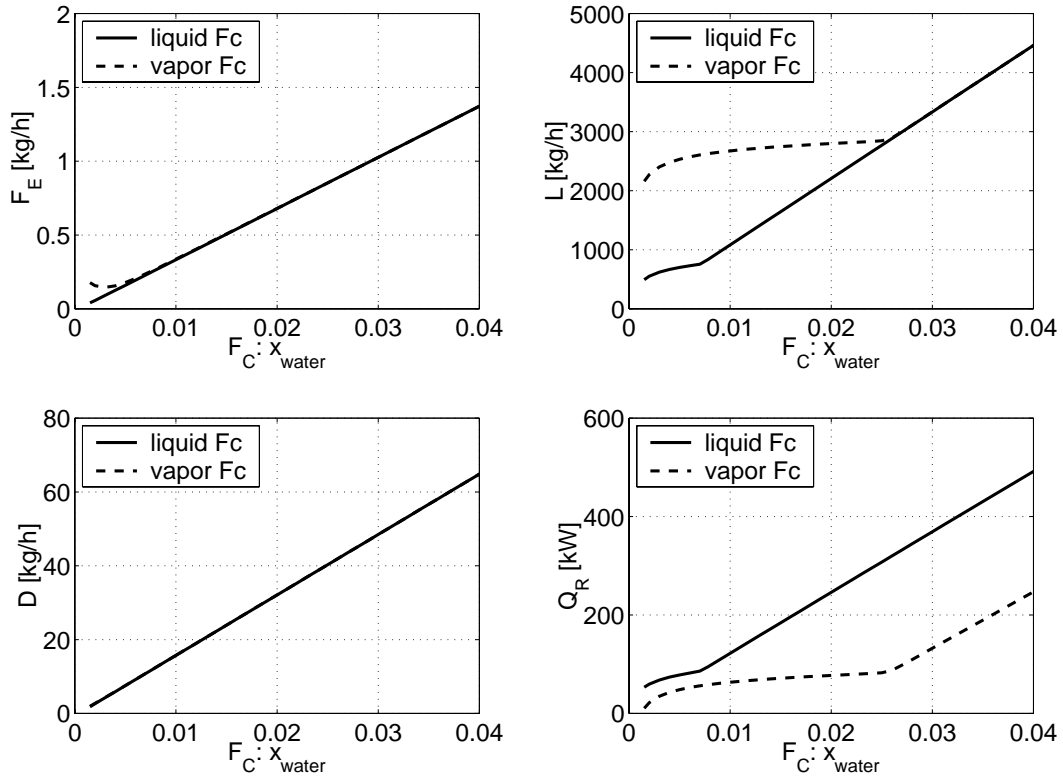


Figure 4.2: MTBE makeup flow rate F_E , distillate D , reflux L , and reboiler duty Q_R as a function of the water content in the binary water–MBI crude feeds for two conditions: boiling liquid and saturated vapor.

1. The required entrainer makeup F_E is proportional to the water flow rate in the crude feed.
2. The distillate flow rate D , reflux L and reboiler duty Q_R are proportional to the water flow rate in the crude feed.

Figure 4.2 shows F_E , D , L , and Q_R as a function of the water content in F_C for a flow rate of 1600 kg/h. Two feed conditions are pictured: boiling liquid F_C and saturated vapor F_C . As predicted from finite/ ∞ column, the required entrainer makeup F_E and the distillate flow rate D depend linearly on the water content in F_C for the real column. This is independent of the condition of F_C .

For water contents greater than 0.025, L and Q_R are proportional to the water content in F_C . For water contents smaller than 0.025, L and Q_R do not change proportional to the

water content in the feed for the saturated vapor feed. There are two reasons for that. The first reason is that the vapor feed F_C has to be condensed in the rectifying section. This requires a minimum reflux. Note that reflux L and reboiler duty Q_R are coupled because the column has only one degree of freedom for a fixed overall feed. The second reason is the specification of T_3 . If L is too small, the separation is not sharp enough. Hence, for decreasing values of L , the top composition moves slightly away from the MTBE–water azeotrope which causes a change of the reflux ratio through the liquid–liquid equilibrium. This effect also appears for the liquid feeds, but it occurs at lower water contents. The difference in the necessary reboiler duty between the two feeds for water contents greater than 0.025 is roughly the duty that is needed to evaporate the feed F_C . Since there is also a required minimal reboiler duty, the two curves approach each other for water contents smaller than 0.025. Simulations for water contents higher than 0.04 confirm the linear dependence of all four variables shown in Figure 4.2 for water contents up to 1 (pure water).

Based on the above results, a steady state composition profile of the real column is expected to be close to the one predicted by the finite/ ∞ column for water contents larger than 0.025. This is validated by comparing composition profiles for binary feeds containing 0.02 water and 0.03 water (Figure 4.3). The profile for 0.03 water runs close to the residue curve boundary as predicted by the finite/ ∞ column.

Reboiler duty as well as column load are roughly proportional to the water content in the feed. In a real plant, vapor and liquid load as well as reboiler duty are limited. A feasible operation range for the water content in the feed at a constant flow rate can be determined from the maximum vapor (F–factor) and liquid loads for each section and the limited reboiler duty. According to manufacturer data, the packing and the sieve trays work at constant efficiency up to a vapor load with an F-factor of $3 \text{ m/s} \sqrt{\text{kg/m}^3}$ and a liquid load below $40 \text{ m}^3/(\text{m}^2 \text{ h})$. Flooding occurs for a vapor load of F-factor of about $3.5 \text{ m/s} \sqrt{\text{kg/m}^3}$. The column can easily tolerate water contents in the feed of up to 0.05 for the current throughput, if the reboiler is designed for this necessary duty. If either the water content is above 0.05 or the reboiler is at its limit, the feed flow rate has to be reduced. This will be discussed in further detail in section 4.3.1, where the influence of

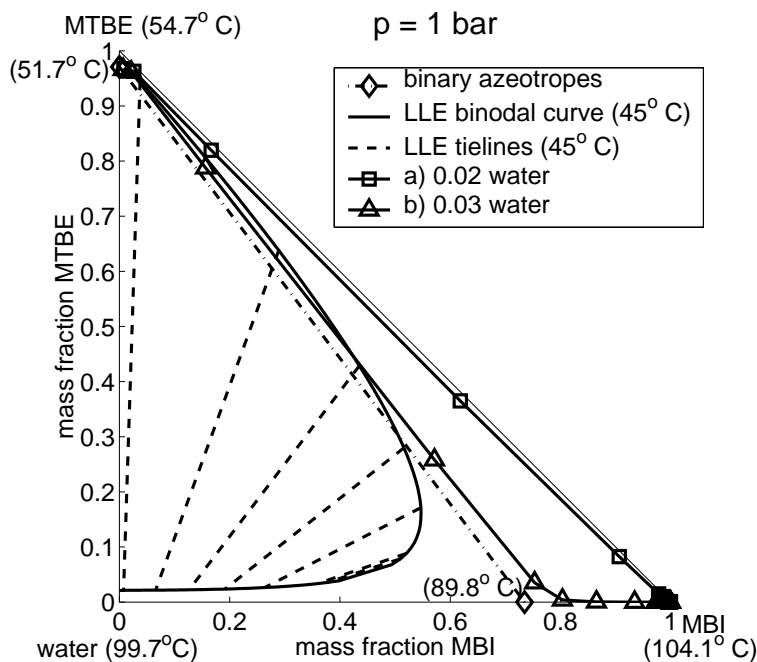


Figure 4.3: Residue curve map of the ternary mixture MTBE–water–MBI with liquid–liquid equilibrium at 45° C. Column profiles for two ternary overall feeds $F=F_C + F_E$: a) 0.9795 MBI, 0.0200 water and 0.0005 MTBE, and b) 0.9694 MBI, 0.0300 water and 0.0006 MTBE. Compare with the finite/ ∞ column profile (Figure 3.4).

acetone on the column operation is discussed.

4.2.2 Selection of Operation Point

The MTBE–water–MBI mixture exhibits multiple steady states for a fixed overall feed (Güttinger, 1998). Case studies were performed using Aspen Plus by varying Q_R at constant F_E and varying F_E at constant Q_R for $F_C = 1600$ kg/h, 0.97 MBI, and 0.03 water to detect possible multiple steady states and to identify possible operation points. The results are shown in Figure 4.4. The plots on the top of Figure 4.4 show the controlled variables, the plots on the bottom show the resulting concentrations of MBI in bottom and distillate. On the left side, possible operation points are shown for constant Q_R using F_E as bifurcation parameter. On the right side, possible operation points are shown for constant F_E using Q_R as bifurcation parameter. The solid lines represent stable steady

states. The unstable steady states are indicated by the dashed lines. The stars indicate fold bifurcation points. The stability of the steady states was determined with dynamic simulations.

A good bottom purity and a high MBI recovery (no MBI in distillate) can only be obtained if T_3 is between 52°C and 80°C . If T_3 is in that interval, there exists only one steady state for a given T_3 . The operation point that is currently used in industries ($T_3 = 70^\circ\text{C}$) is open loop unstable for constant Q_R and F_E . This is not a problem. In azeotropic distillation, unstable steady states can be stabilized by simple temperature control if the steady state can be uniquely identified by the chosen temperature (Dorn et al., 1998). For zeotropic binary distillation, detailed concepts for stabilizing an open loop unstable distillation column in the presence of multiple steady states were discussed earlier (Jacobsen and Skogestad, 1995). As Figure 4.4 shows, there is only one steady state for $T_3 = 70^\circ\text{C}$. To make the results comparable to the industrial plant, $T_3 = 70^\circ\text{C}$ is chosen as the nominal operation point in all subsequent simulations (except for the principal component analysis in the next section which requires a perturbation around a stable operation point).

4.2.3 Controller Implementation

At the industrial plant, the two temperature fronts are fixed by controlling $T_3 = 70^\circ\text{C}$ via the reflux and the average of the bottom temperature (stage 29) and the temperature on tray 13 (stage 21). For stable operation points, the temperature sensitivity matrix

$$\mathbf{K} = \begin{bmatrix} \left. \frac{\partial \mathbf{T}}{\partial Q_R} \right|_{F_E} & \left. \frac{\partial \mathbf{T}}{\partial F_E} \right|_{Q_R} \end{bmatrix}$$

with $\mathbf{T} = [T_1 \ T_2 \ \dots \ T_{29}]^T$ can be calculated. Then, the principal component analysis, which is based on singular value decomposition of the temperature sensitivity matrix: $\mathbf{K} = \mathbf{U}\mathbf{\Sigma}\mathbf{V}^T$, can be used to identify the best sensor locations (Moore, 1992). As Figure 4.4 shows, the industrial operation point with $T_3 = 70^\circ\text{C}$ is open loop unstable. Hence, a stable operation point with $F_C = 0.03$ water and 0.97 MBI, and $T_3 = 60^\circ$ was chosen for the principal component analysis. Figure 4.5 shows the first two left singular vectors U_1 and U_2 . They confirm that T_3 and T_{21} are reasonable choices as controlled temperatures.

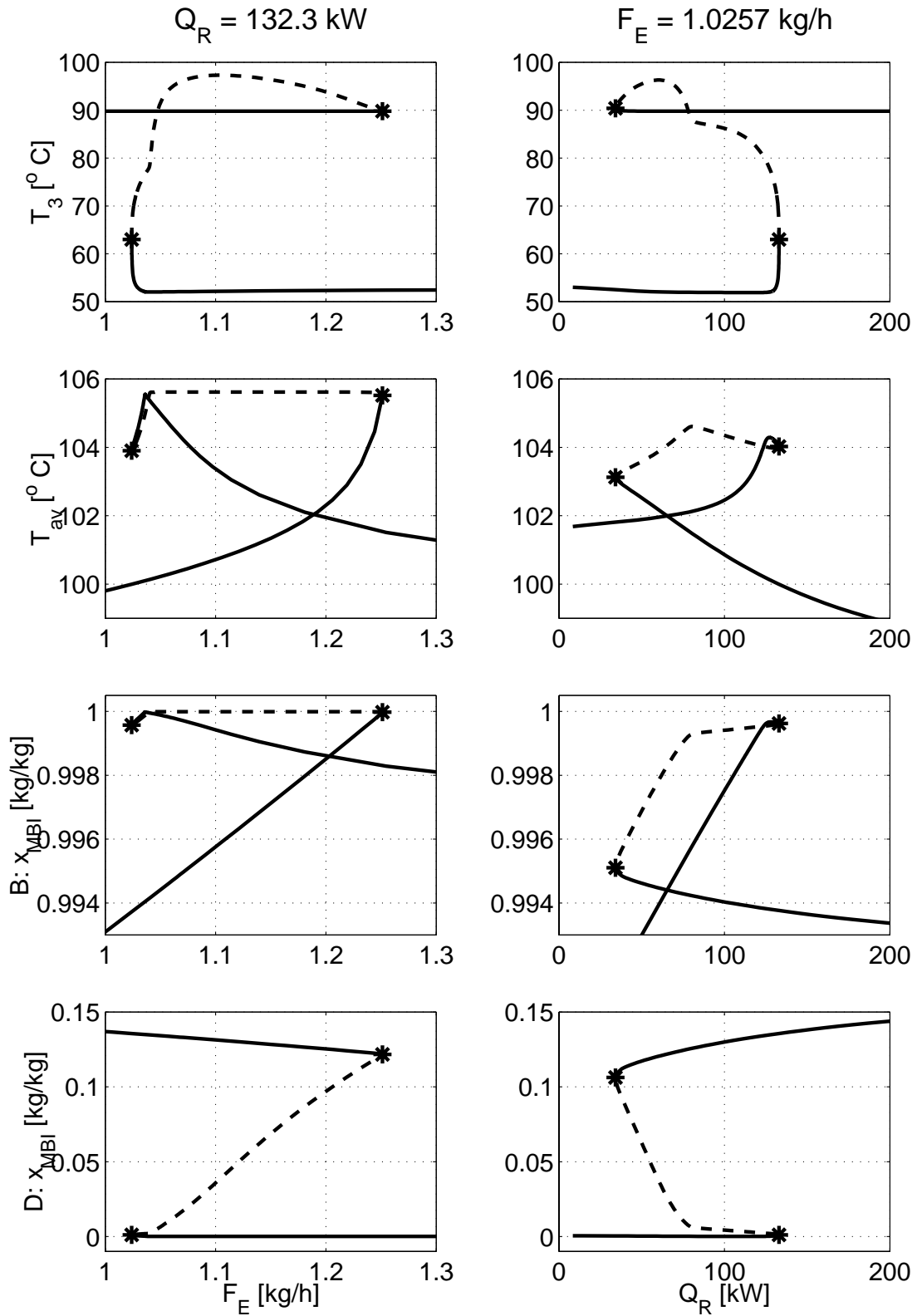


Figure 4.4: Case study of the system MTBE–water–MBI, composition of crude feed F_C : 0.03 water, 0.97 MBI. The solid lines represent stable steady states, and the dashed lines represent unstable steady states.

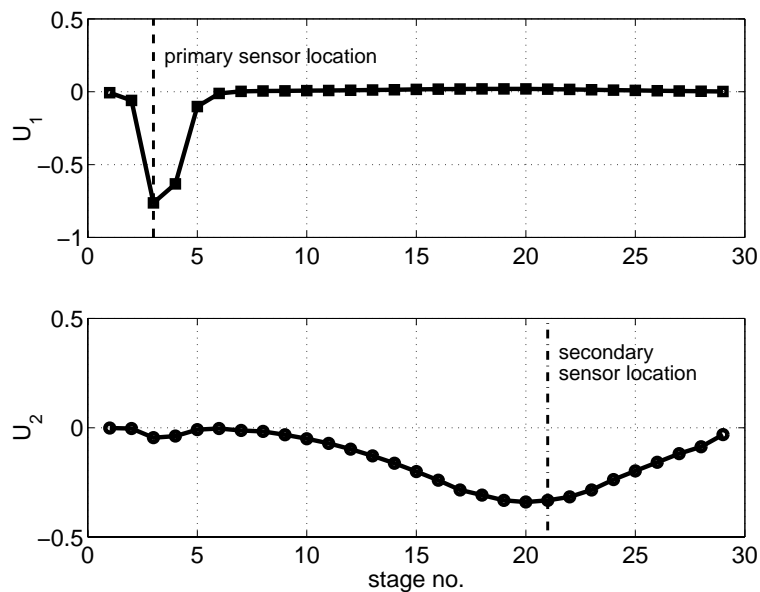


Figure 4.5: First two left singular vectors U_1 and U_2 of the temperature sensitivity matrix for F_C : 0.03 water, 0.97 MBI and $T_3 = 60^\circ \text{C}$ (stable operation point).

The bottom temperature was added to T_{21} , because it is a good indicator of the bottom purity. Further use of the temperature sensitivity matrix such as a relative gain array analysis will not be pursued in this paper for the following reason. As Figure 4.4 showed, the desired operation points (T_3 between 52°C and 80°C) are close to the fold bifurcation. This is similar to the behavior of the 2-propanol–water–cyclohexane column (Chien et al., 1999). Any small perturbation in the operation parameters causes a drastic change in the column conditions (change of stability properties). Thus, the steady state gain matrix does not have a useful meaning.

The process is designed with the two point control scheme as proposed in section 3.4.2 with the sensor locations of the industrial plant:

TC1 controls the average of temperature at stage 21 and stage 29 by manipulating the steam temperature in the reboiler, i.e. Q_R .

TC2 controls the temperature on stage 3 by manipulating F_E .

Table 4.5: Controller parameters for the controllers TC1, TC2, CC3 and TC3 of the $Q_R F_E(F_F)$ schemes.

	K_c	τ_I
TC1	$12 \frac{kW}{K}$	2 min
TC2	$2 \frac{kg/h}{K}$	10 min
CC3	$2500 \frac{kg/h}{kg/kg}$	20 min
TC3	$50 \frac{kg/h}{K}$	20 min

Both controllers are linear PI (proportional–integral) controllers with the transfer function

$$K = K_c \left(1 + \frac{1}{\tau_I s} \right)$$

and the parameters as listed in Table 4.5. No lags are modeled in the control loops. Top pressure, condenser duty and all levels were controlled with high gain simulating perfect control. The dynamic simulations appear here for illustration. The focus is to validate the choice of the manipulated variables, which are critical for success. Hence, the controllers were tuned only using rules of thumb and observation of closed loop responses for feed flow changes and feed composition changes in dynamic simulations. A detailed case study on controller tuning for heterogeneous distillation columns was recently published (Chien et al., 1999; Chien et al., 2000).

4.2.4 Dynamic Simulations

Figure 4.6 shows the process dynamics for changes of the flow rate F_C (the simulations took between 2 and 48 hours on a 400 MHz Pentium II processor). The product concentrations stay within the specifications. The slight difference in the bottom concentration results from the fact that TC1 controls an average temperature and not the bottom concentration. There are two competing effects which influence the temperature front: The change of pressure as a result of the change of the vapor load (small) and the change of the composition profile as a result of the internal flows. Therefore, there is no one–to–one relationship between the controlled average temperature and the bottom purity.

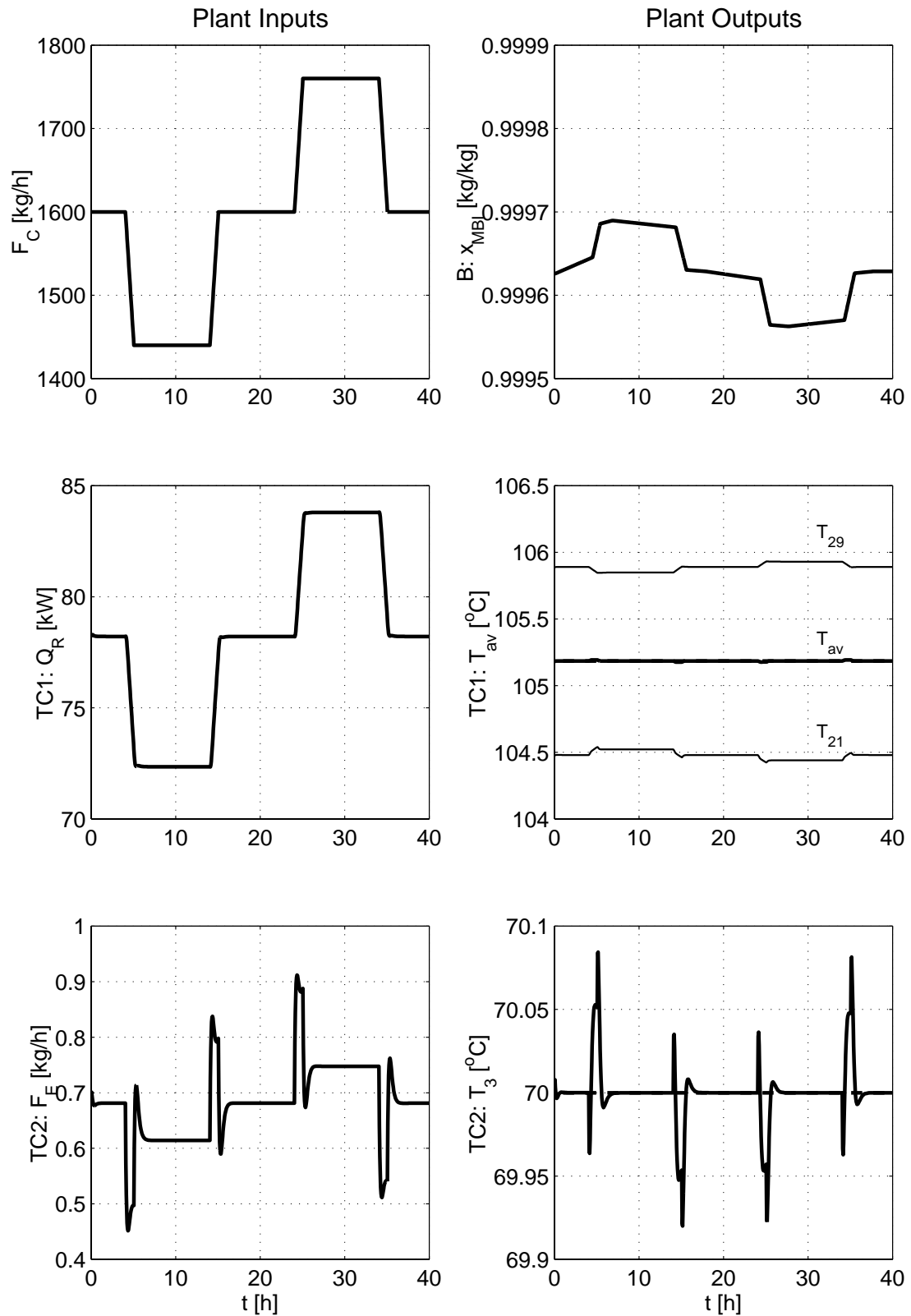


Figure 4.6: System MTBE–water–MBI, crude feed composition: 0.02 water, 0.98 MBI. Dynamic simulation of two point control scheme (Figure 3.13) for changes of the crude feed flow rate.

Figure 4.7 shows the process dynamics for changes of the water content in F_C . Again, the controllers are able to adjust Q_R and F_E to the changed operation conditions reaching the desired steady states. As shown in Figure 4.2, the difference in Q_R between 0.02 and 0.03 water content is significantly higher than that between 0.01 and 0.02. From Figure 4.1a, it follows that the average temperature decreases with increasing water content in F_C for a constant bottom purity. The dynamic simulations show that the bottom purity changes for the constant average temperature. A “robust setpoint” for changes in feed composition is a high one, e.g. 105.4°C , because then the bottom product is purer than required.

In these two simulations, the temperature control is very tight. Repeating the simulations with detuned controller gains (TC1 with 20% of original gain and TC2 with 7.5 % of original gain) showed qualitatively the same results. Hence, in all subsequent simulations, the controller parameters as listed in Table 4.5 are used.

4.3 System MTBE/Acetone/Water/MBI

4.3.1 Validation of Finite/ ∞ Column Predictions

In section 3.4.3, the finite/ ∞ column analysis predicted that the two point control scheme cannot operate the column in presence of the impurity acetone. The reflux goes to infinity as the overhead vapor composition approaches the binodal curve for increasing acetone contents in F_C . This is illustrated in Figure 4.8, which shows a part of the ternary residue curve map with the heterogeneous region. When the boundary residue curve connecting the MTBE–water azeotrope with the ternary MTBE–acetone–water azeotrope crosses the binodal curve, the aqueous distillate has the maximum acetone concentration and, as a result of the lever rule, the reflux is infinite. For this particular case, the compositions of the overhead vapor, distillate, and reflux are given in Table 4.6. From the overall mass balance, the maximum tolerable acetone content in F_C can be calculated for each water content in the ternary acetone–water–MBI feed in the same way as described in section 3.4.4 for a limited acetone concentration (Figure 3.16). For 0.02 water in the crude ternary acetone–water–MBI feed, the maximum acetone content is 0.0053, and, for 0.03

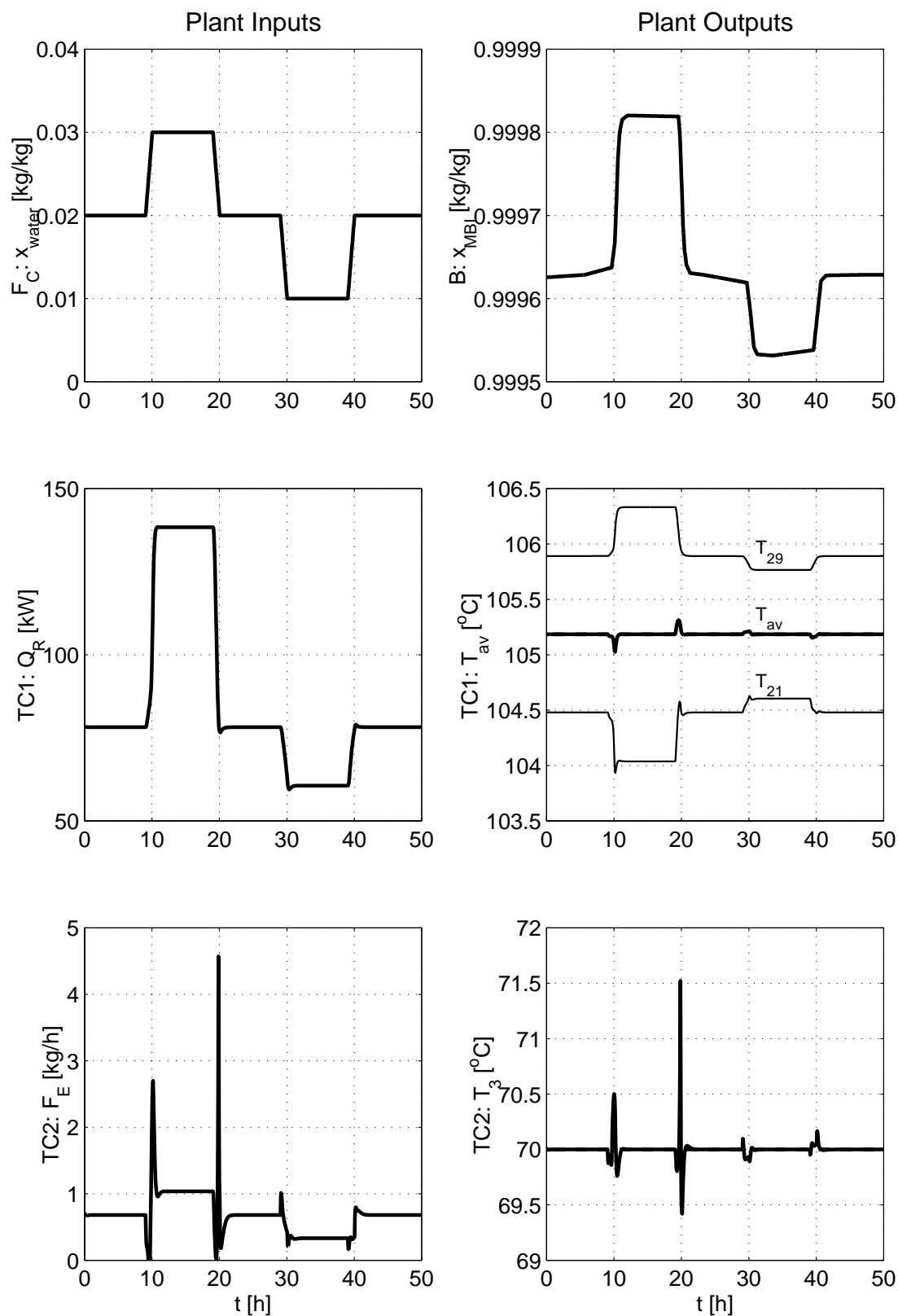


Figure 4.7: System MTBE–water–MBI, crude feed flow rate: 1600 kg/h. Dynamic simulation of two point control scheme (Figure 3.13) for changes of the water content in the crude feed.

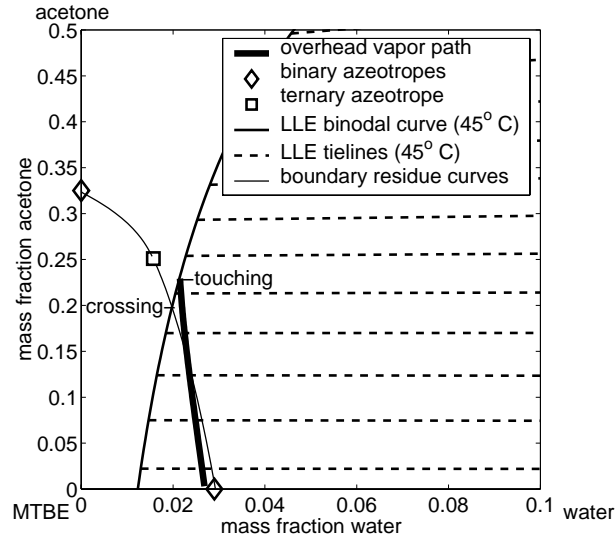


Figure 4.8: Residue curve map of the system acetone–MTBE–water to illustrate the crossing of the boundary residue curve and of the overhead vapor composition for 0.03 water and varying acetone contents in the crude feed with the heterogeneous envelope.

Table 4.6: Compositions of overhead vapor, reflux, and distillate when the boundary residue curve connecting the MTBE–water azeotrope with the ternary MTBE–acetone–water azeotrope crosses the binodal curve (see also Figure 4.8).

mass fraction	overhead vapor	reflux	distillate
x_{MTBE}	0.78205	0.78205	0.02907
$x_{acetone}$	0.19820	0.19820	0.20380
x_{water}	0.01975	0.01975	0.76713

water, it is 0.008. This also confirms that adding water increases the acetone tolerance of the column.

Figure 4.9 shows the reboiler duty and the reflux of the real column as a function of the acetone feed concentration for two different water contents (0.02 and 0.03). For the real column, the maximal tolerable acetone content in F_C is 0.00656 acetone for 0.02 water, and 0.00990 acetone for 0.03 water. The acetone contents predicted from the finite/ ∞ column for the limiting case of infinite reflux are smaller than those in the real column. This can be explained from Figure 4.8, which also shows the path of the overhead vapor composition for

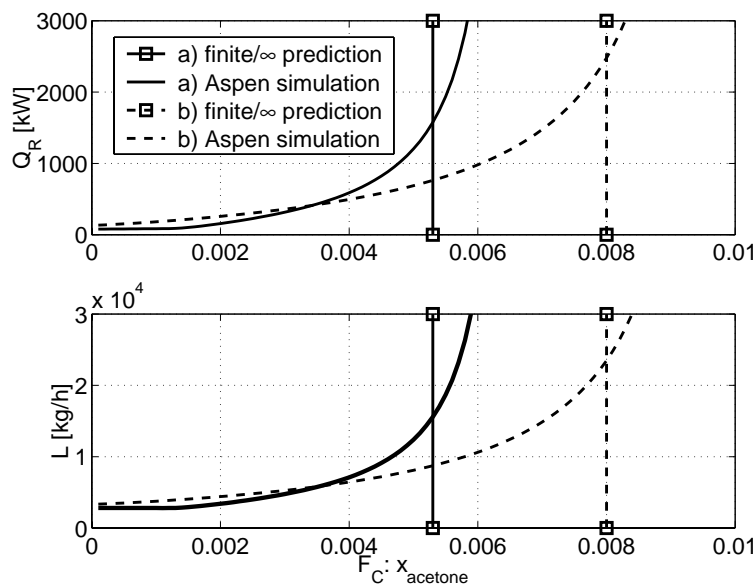


Figure 4.9: Comparison of finite/ ∞ column predictions with steady state simulation. Reboiler duty Q_R and reflux L as a function of the acetone crude feed concentration for a) 0.02 water and b) 0.03 water in the crude feed F_C (saturated vapor).

increasing acetone contents and constant water content (0.03) in F_C . The overhead vapor composition touches the binodal curve at the point where the reflux of the real column goes to infinity. Because the column is modeled with trays, the column profiles do not exactly follow residue curves. Therefore, the overhead vapor composition does not exactly follow the boundary residue curve toward the ternary azeotrope for increasing acetone contents in F_C . In this case, it touches the binodal curve at higher acetone contents giving a higher acetone concentration in the distillate. Thus, the predicted acetone content of finite/ ∞ column at the limiting case of infinite reflux is smaller than for the real column at this limiting case.

Figure 4.10a shows the required reboiler duty Q_R as a function of the composition of F_C . For a moderate water and acetone content, Q_R remains nearly constant whereas Q_R increases significantly for higher water and acetone content. Since reflux L and Q_R are strongly coupled (only one degree of freedom for fixed overall feed), vapor and liquid load increase for high acetone contents. Parts b and c of Figure 4.10 show a second effect of acetone on the process behavior. As mentioned in section 4.2.1, the column load is constrained.

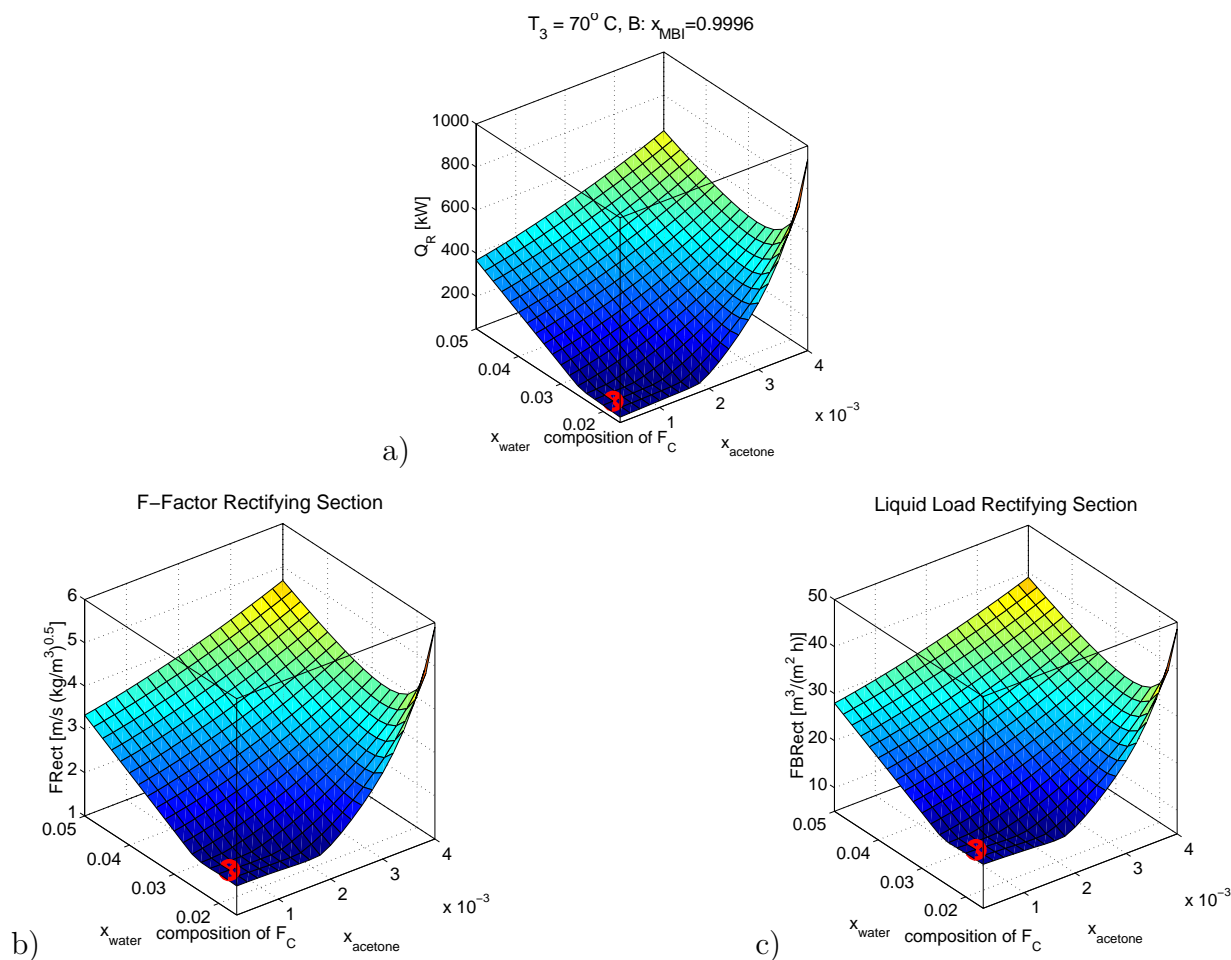


Figure 4.10: Operating parameters for different crude feed compositions: a) reboiler duty, b) vapor load (F-factor), and c) liquid load.

The column can tolerate water contents up to 0.05, if no impurity is present. However, as Figure 4.10b shows, flooding can already occur in the rectifying section for smaller water contents if more than 0.004 acetone is present in F_C . The load in the stripping section is less than the one in the rectifying section because the feed enters as saturated vapor. As for the binary water–MBI feeds, the “ideal” setpoint of TC1 depends on the composition of the ternary acetone–water–MBI feeds.

4.3.2 Two Point Control

Simulations for changes in water contents in the presence of small acetone contents (0.0005) show a similar behavior of the controlled process as reported in section 4.2.4, Figure 4.7,

for changes of the water content in F_C in the absence of the impurity acetone. In both cases, the two point control scheme can adjust the manipulated variables well to the new steady states. However, simulations show that the process adjusts only slowly to changes of the acetone content in F_C (Figure 4.11). The new steady state for 0.002 acetone is just reached after 140 hours. The bottom product is still within specification. Note the large undershoot of T_3 (despite anti-windup in TC2). After a while, T_3 increases again as a result of the increased reboiler duty. Note that the reflux L always increases simultaneously with Q_R . Even though T_3 remains at 70°C , acetone accumulates further in the overhead. As mentioned in section 3.4.4, TC2 does not “see” the accumulation of acetone.

For 0.004 acetone, the control scheme overreacts. Apart from the fact that the column load is beyond what the real column can cope with, the controller increases Q_R above the necessary value. The reason is the setpoint of TC1. As mentioned in sections 4.3.1, the ideal setpoint depends on the composition of F_C . For this change, the setpoint of TC1 is too high, Q_R is increased too much. The setpoint of TC1 can only be reached by the plant because of the significant increase of the bottom temperature (T_{29}). This increase is mainly caused by the pressure increase which is a result of the high column load. The bottom purity actually decreases slightly.

The difference between the slow process reaction toward changes in the acetone content in F_C and the fast response for water changes in F_C can be explained with the “inventory time constants” of the two components. The inventory time constant is defined as the change in holdup of one component divided by the imbalance in supply of this component. (Skogestad and Morari, 1987) Using the rigorous model, the inventories of each component can be computed for different supplies of the component in F_C . These inventory time constants are the minimum transient times that the process requires to adjust to the new operation conditions (neglecting all other effects). If the holdup of one component has to increase by 100 kg and the additional component feed flow rate is 10 kg/h, then the transition time to the new steady state is at least 10 hours neglecting all other effects. For all operation points, the inventory time constant is about 20 minutes for step changes in the water content and about 24 hours for step changes in the acetone content. This explains the big difference in the transient times observed in Figure 4.7 and 4.11.

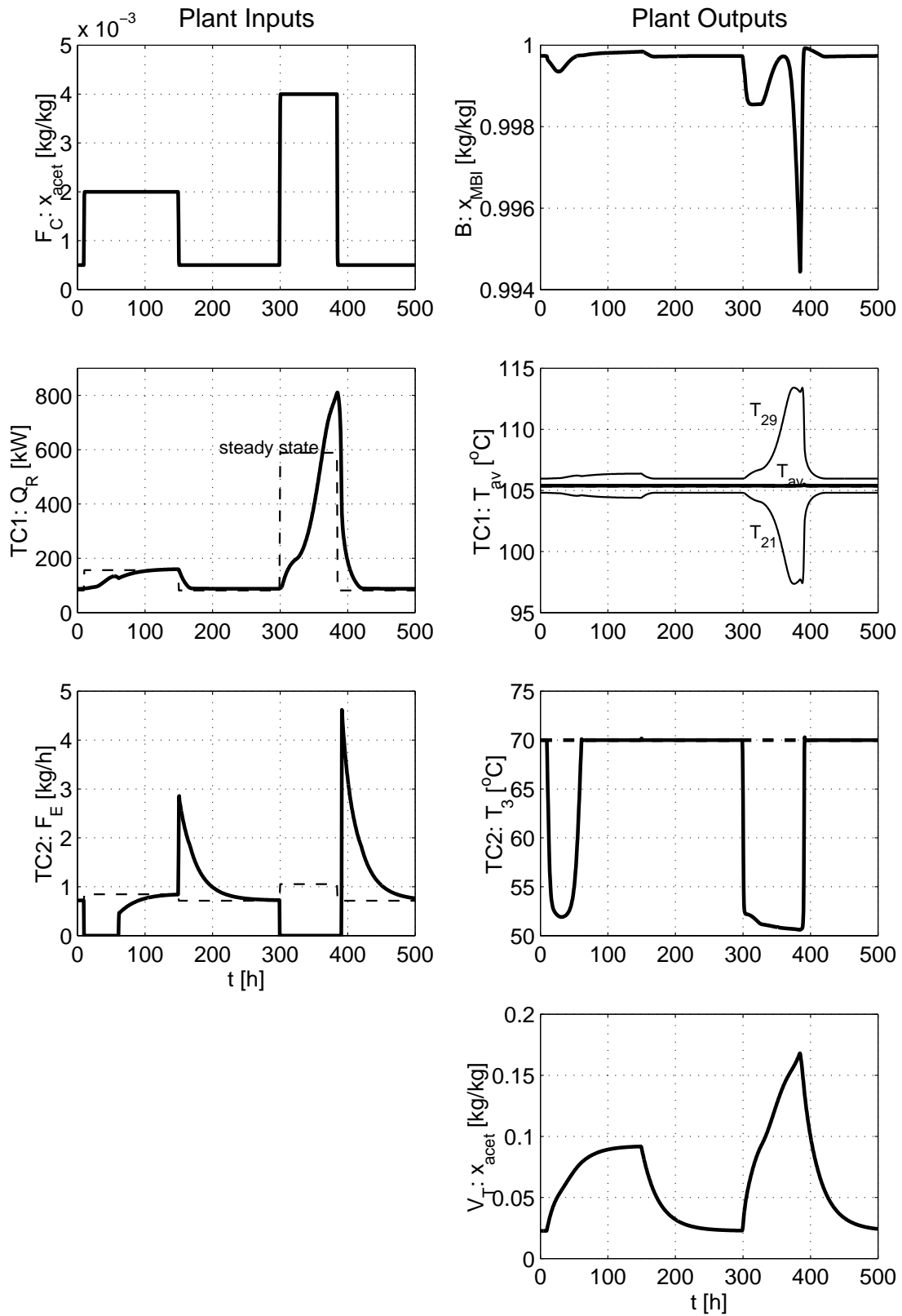


Figure 4.11: System MTBE–acetone–water–MBI. Dynamic simulation of two point control scheme (Figure 3.13) for changes of the acetone content in the ternary crude feed F_C at constant water content (0.02).

4.3.3 Three Point Control

The finite/ ∞ column analysis predicted that an additional controller is necessary to reject disturbances of the impurity acetone. In section 4.3.2, the need for a third controller was shown. Therefore, the three point control scheme as pictured in Figure 3.17 was developed. Again, the linear PI controllers were tuned by trial and error. No lags are modeled in the control loops. Top pressure, condenser duty and all levels were controlled with high gain simulating perfect control. The parameters are also listed in Table 4.5. Figure 4.12 shows that CC3, which works as explained in section 3.4.4, can control the acetone content in the overhead vapor, whereas TC1 and TC2 work as before. As predicted by the finite/ ∞ column, L , Q_R , and the column load do not show the significant increase that was observed in Figure 4.11 for the two point control scheme. The only tradeoff is that more water leaves through the distillate. This increases the wastewater cost. The dynamic response of this process toward changes in acetone is very slow, the column adjusts to the new steady state after roughly 50 hours (2 days), Figure 4.12. Therefore, a composition controller with delay should be sufficient. However, if the process dynamics are much faster for a different mixture, then it might be desirable to switch to a fast temperature sensor.

As explained in section 3.4.4, a new temperature front will appear, if the impurity introduces a new unstable node. Figure 4.13 shows the top temperature as a function of the composition of F_C according to the two specifications defined in section 4.1.2. As expected, the top temperature decreases for increasing acetone contents in F_C at constant T_3 . As set point of TC3, the temperature of the binary MTBE–water azeotrope (51.7°C at 1 bar) is chosen. The set point should not be above 51.7°C , because then changes in the water content could switch on the controller which is undesired. The lower the set point is, the longer it takes until the controller starts working because more acetone has to accumulate before the temperature in the top is low enough to start the control action. Hence, the set point should not be too close to the temperature of the ternary azeotrope ($\approx 49.8^\circ\text{C}$ in this case). With a set point of TC3 equal to 51.7°C and the controller parameters as listed in in Table 4.5, flow rate and water content changes of F_C are rejected as well as with the acetone composition controller CC3.

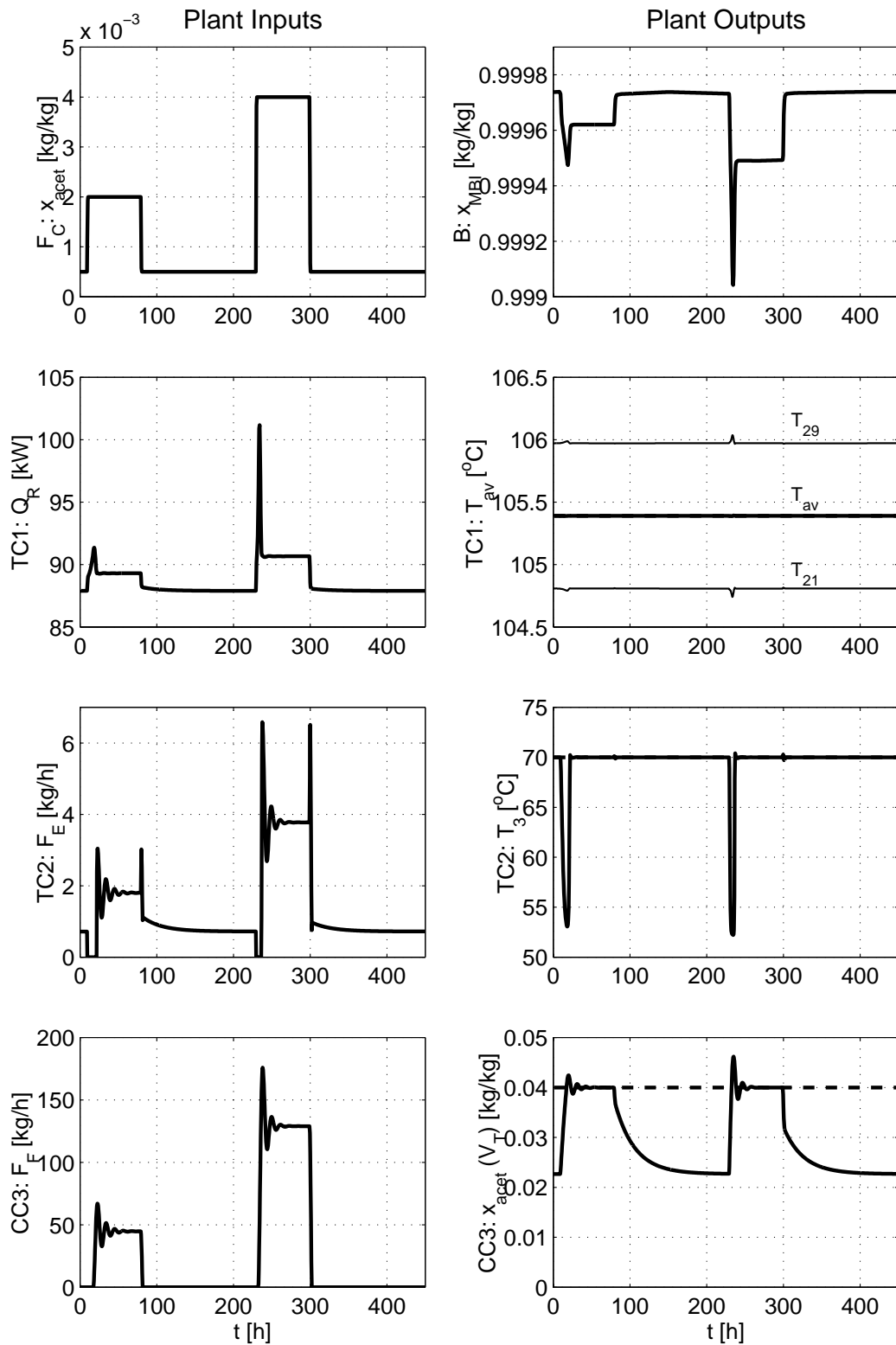


Figure 4.12: System MTBE–acetone–water–MBI. Dynamic simulation of three point control scheme (Figure 3.17) for changes of the acetone content in the crude feed F_C . CC3 controls the acetone content in the overhead vapor V_T .

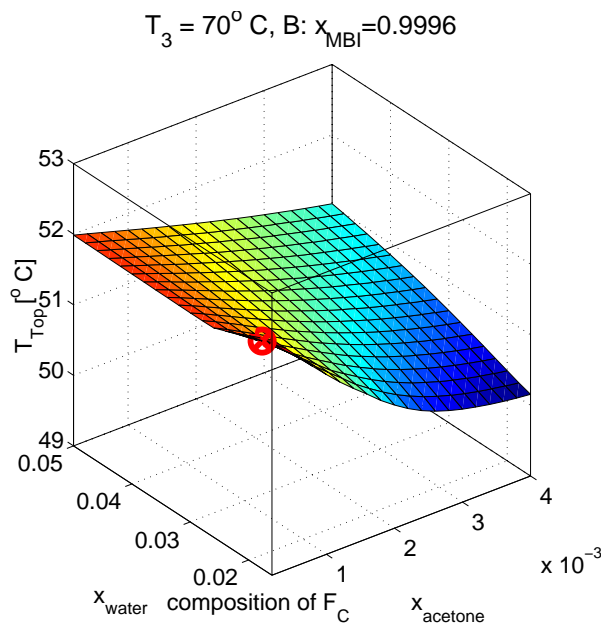


Figure 4.13: Top temperature for different crude feed compositions.

Figure 4.14 illustrates that TC3 can also reject changes of the acetone content in F_C . TC3 works well in simulation, but determining the proper set point may not be feasible under real plant conditions. For example, little fluctuations in the column pressure can lead to erratic behavior of the controller. In that case, one has to return to concentration measurements with possible dead time.

4.3.4 Industrial Plant

The above control schemes were designed using a theoretical approach. They work fine in simulation. A critical aspect in the implementation to a real plant is the design of the decanter. If the decanter is operated with automatic interphase detection so that the column is operated at total reflux if the phase split disappears, the $Q_R F_E$ scheme will work fine despite the fact that F_E is very small (approximately 1 kg/h) compared to the reflux flow rate (approximately 3000 kg/h). With automatic interphase detection, the column is operated similar to a one point Q_R (L/D) scheme for homogeneous columns. Q_R is used to control the bottom purity and (L/D), which is determined by the phase split, is constant. The entrainer makeup flow F_E just prevents the column profile from slowly drifting away,

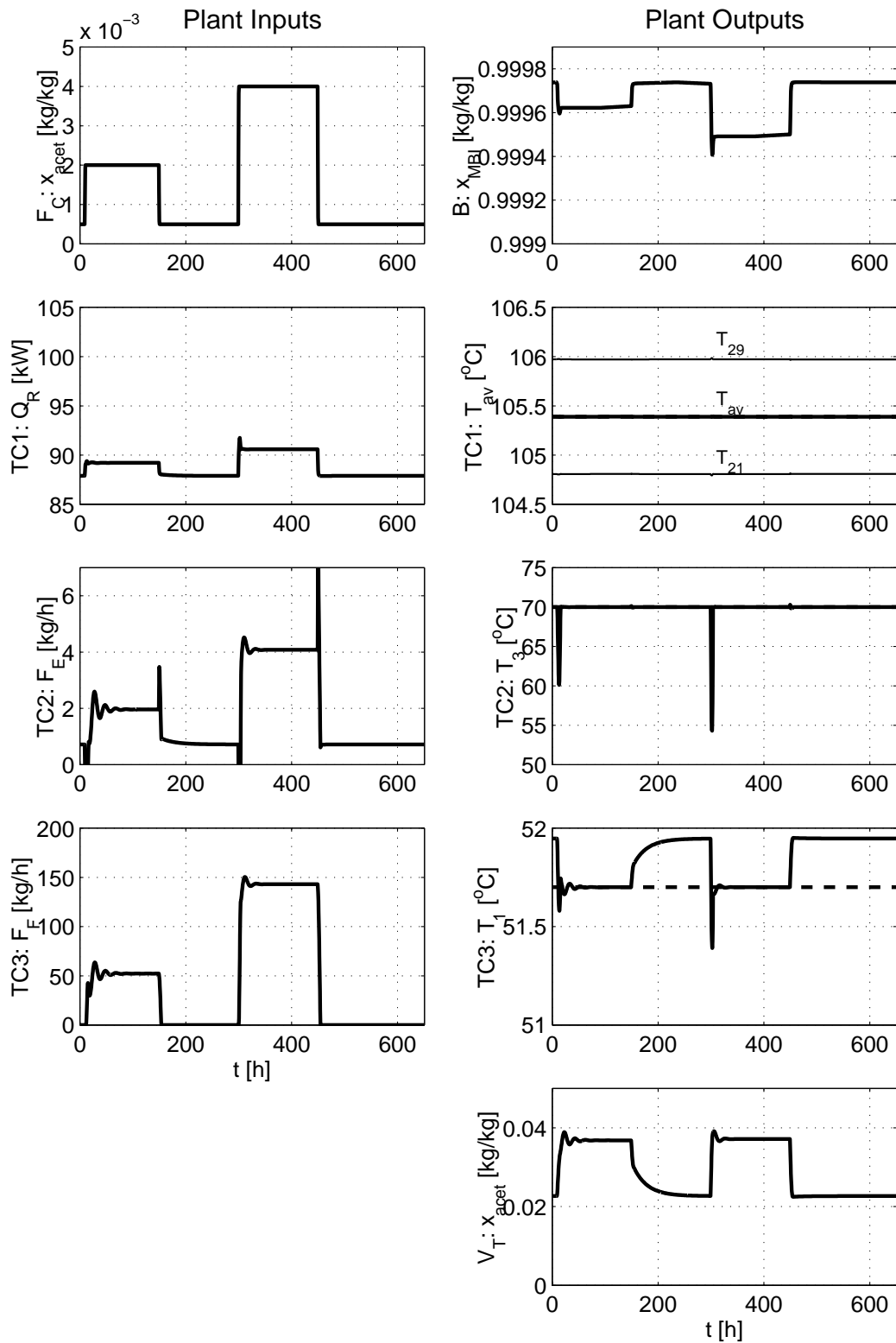


Figure 4.14: System MTBE–acetone–water–MBI. Dynamic simulation of three point control scheme (Figure 3.17) for changes of the acetone content in the crude feed F_C . TC3 controls the top temperature.

Table 4.7: Controller parameters for the controllers TC1 and TC2 of the Q_{RL} scheme.

	K_c	τ_I
TC1	$12 \frac{kW}{K}$	2 min
TC2	$80 \frac{kg/h}{K}$	2 min

once the column is operated close to the desired steady state. During startup, it has to be ensured that there is enough entrainer in the system and the pump/valve of F_E has to be designed such that higher flow rates (in the order of tens of kilograms per hour) are possible. The rest is a tuning issue that has to be done on the real plant. Clearly, the smaller the ratio L/F_E is, the better is the performance of the controller. For other mixtures, such as heterogeneous 222–m, the entrainer loss through the distillate is significantly higher. In this case, the entrainer is recovered from the distillate in a second column and recycled to the first column. An example for this system is the ethanol–water–benzene column (Rovaglio et al., 1993). Here, F_E corresponds to the entrainer recycle and L/F_E is much smaller. The industrial plant is operated as described in section 3.1 and depicted in Figure 3.1. The levels in the decanter are controlled by simple weirs. If the phase split disappears, the decanter is emptied through the exit for the heavier phase, i.e., the distillate. In that case, there is no reflux. Therefore, a buffer tank is used to ensure reflux that is vital for the column operation. The buffer tank increases the inventory time constants especially of acetone and MTBE, the main components of the reflux. The inventory time constant of water is not increased. Dynamic simulations show that changes of the water content are tracked well with the Q_{RL} scheme very similar to the results shown in Figure 4.7 for the Q_{RF_E} scheme. In the industrial setup, the inventory time constant of acetone however increases by a factor 5 compared to the setup without a buffer tank. Hence, a slower process response to acetone composition changes in F_C is expected, as Figure 4.15 illustrates.

The controller parameters for this simulation are given in Table 4.7. No lags are modeled in the control loops. If first–order lags are used, the strong interactions between the two control loops observed in the real plant could be reproduced. However, the focus of these simulations is to illustrate the long term dynamic behavior for a stable tuning. Therefore, no lags were modeled to ease the tuning in this case.

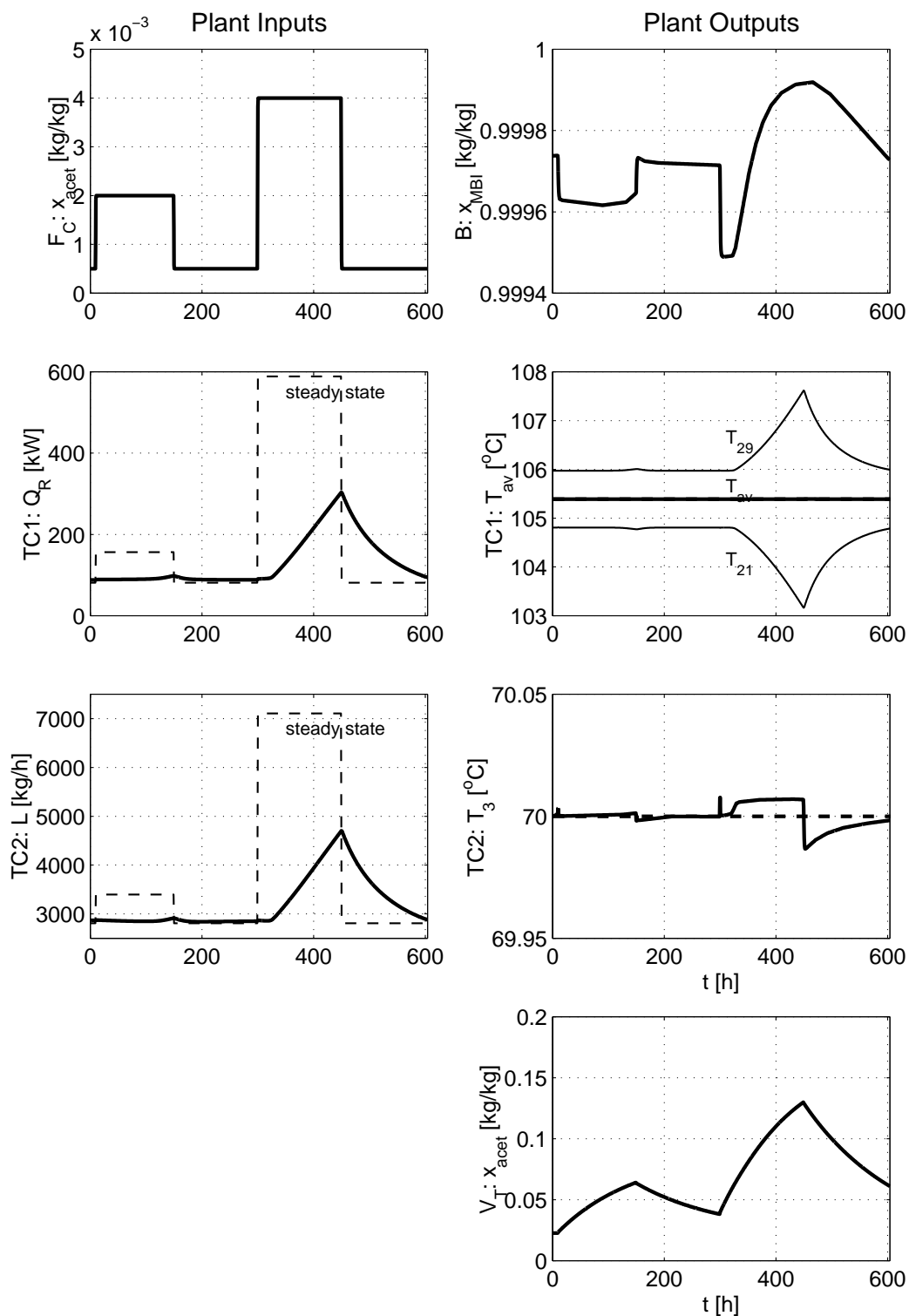


Figure 4.15: System MTBE–acetone–water–MBI. Dynamic simulation of the industrially applied two point control scheme (Figure 3.1) for changes of the acetone content in the ternary crude feed at constant water content (0.02).

As opposed to the setup without a buffer tank, the column does not flood because the load is not increased enough in this time scale as a result of the slow process response. Again, as in section 4.3.2, the increase of the bottom temperature (T_{29}) is a result of the pressure increase caused by the load increase. The buffer tank seems to make the process more robust toward these changes. However, plants are often operated continuously over months. Hence, acetone will eventually trouble the decanter operation as the operation people of our industrial partner observed. They measure the acetone concentration in the buffer tank and flush the decanter with water if necessary. The advantage of the buffer tank is that acetone does not accumulate quickly. Therefore, it suffices to determine the acetone concentration on a daily basis.

This $Q_R L$ scheme however has potentially the same problems as the DB scheme for regular distillation (Finco et al., 1989; Skogestad, Jacobsen and Morari, 1990) with added complexity: For the used decanter policy, Q_R and L cannot be chosen independently (the column has only one degree of freedom), like D and B for regular distillation. The $Q_R L$ scheme lacks integrity, i.e. it cannot be used as one point control in the case of sensor failure and/or valve saturation. In distillation, the steady state effect is large for changes of the external flows, but the dynamic response is slow; changes in the internal flows have smaller effects on composition, but the dynamic response is faster (Skogestad and Morari, 1988). The DB scheme only works, because it is possible to accumulate mass temporarily which makes D and B independent from a dynamic point of view (Skogestad, Jacobsen and Morari, 1990). This is supported by the slow dynamic response of the column toward changes of D or B .

In the heterogeneous column, the two dependent variables L and Q_R have fast dynamic responses. Hence, they are less decoupled than D and B for regular distillation. Clearly, this does not simplify the tuning of the controllers on the real plant. In addition, the LQ_R scheme should not be used for columns with high reflux and high purity (Skogestad, Lundström and Jacobsen, 1990). Currently, the industrial plant only operates satisfactorily because TC2 is a very detuned controller: The reflux is adjusted manually to keep T_3 around 70° C. Exchanging the simple decanter with a decanter with interphase detection would enable an operation of the plant with the $Q_R F_E F_F$ scheme which would improve the plant operation and ease the tuning of the controllers.

Part II

Azeotropic Distillation Column Sequences

Chapter 5

Design and Control of the ∞/∞ Boundary Separation Schemes

The operation of heterogeneous azeotropic distillation columns was analyzed in Part I. For the acetone/water/MBI mixture using MTBE as entrainer, the heterogeneous entrainer MTBE was not recovered because it does not make sense in this case (see appendix A.2.1.3 for a detailed discussion). The energy consumption of the heterogeneous two column sequence is higher than for a homogeneous three column sequence with recycles (boundary separation scheme) for certain feed compositions. Hence, the boundary separation scheme can be economically better, also for other mixtures where the heterogeneous sequence has three columns. To show this, another 020 mixture is chosen: methanol, 2-propanol, and water. The corresponding heterogeneous process uses cyclohexane as entrainer to break the 2-propanol–water azeotrope (Chien et al., 1999; Chien et al., 2000). In chapter 7, the performance of the boundary separation scheme will be compared with the two heterogeneous sequences. But first, operation of the boundary separation scheme is analyzed.

5.1 Problem Statement

Figure 5.1 shows the setup of the boundary separation scheme with two columns with 30 stages (including top and bottom) and one column with 50 stages (including top and

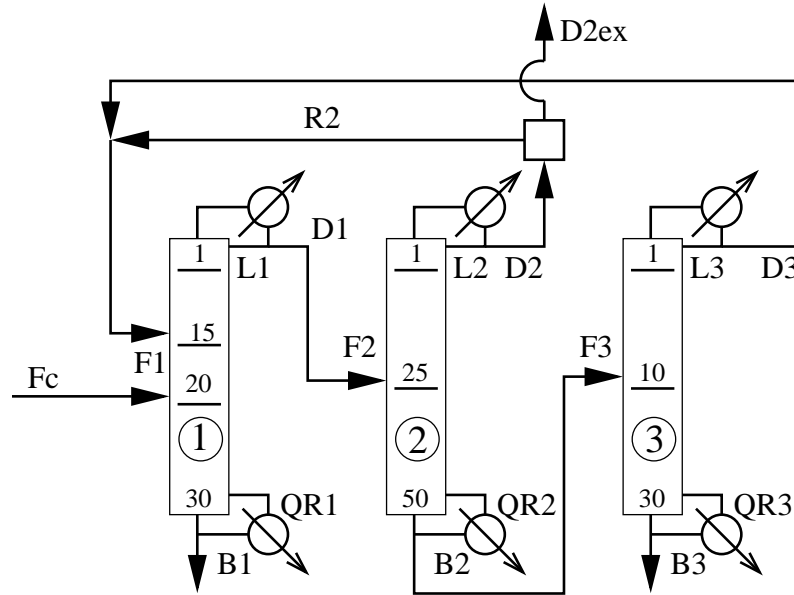


Figure 5.1: Column configuration of the boundary separation scheme.

bottom). Figure 5.2a shows qualitatively the mass balances and column profiles in a residue curve map. The crude feed F_C enters column 1 together with the mix M_1 of two recycles R_2 and D_3 giving F_1 . Here, water is removed via the bottom B_1 . The distillate D_1 , which consists of methanol, 2-propanol, and water, enters the second column. Here, methanol is removed from the sequence via D_2^{ex} and the rest of D_2 is recycled to column 1 as R_2 . In column 3, the remaining two component mixture 2-propanol and water, which lies on the left side of the azeotrope, is separated into pure 2-propanol (B_3) and the 2-propanol-water azeotrope (D_3), which is recycled to column 1.

Figure 5.2b shows a calculated residue curve map for the mixture methanol/2-propanol/water at $p = 1$ bar with $x_{water}^{azeotrope} = 0.13038$ kg/kg. NRTL is used as activity coefficient model using the VLE-IG data set from the AspenPlus database. This set is indicated as NRTL-IG. Later in this thesis, a sensitivity study is done with the different models available in AspenPlus. For each model, there are two different data sets: VLE-IG and VLE-Lit. To differentiate these, the extension IG or Lit is added to the abbreviation of the activity coefficient model. For example, NRTL-IG corresponds to the activity coefficient model NRTL with the VLE-IG parameter set; NRTL-Lit corresponds to the VLE-Lit parameter set.

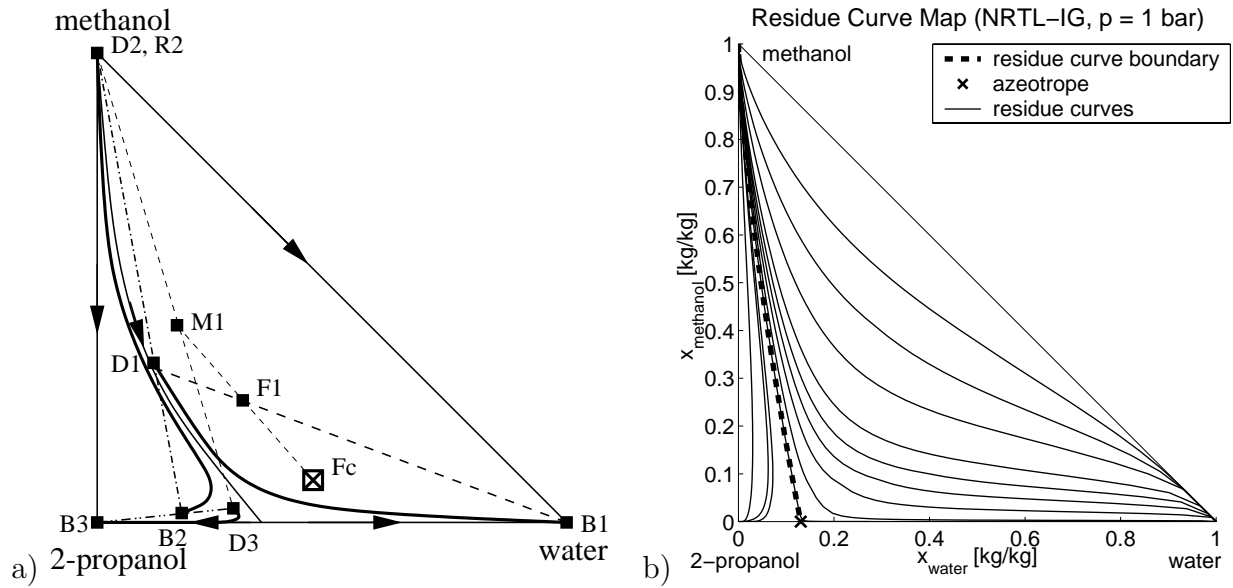


Figure 5.2: a) Qualitative representation of the boundary separation scheme in a residue curve map, b) calculated residue curve map at $p = 1$ bar (NRTL-IG).

If the sequence separates only binary 2-propanol–water feeds, it may be better to introduce the crude feed to column 3 for high 2-propanol contents (Laroche et al., 1992a; Stichlmair and Herguiejuela, 1992). For ternary feeds, it might also be desirable to introduce the crude feed into column 2. The three options are shown in Figure 5.3. To differentiate these three configurations, they are named setup 1, setup 2, and setup 3:

- For setup 1 (Figure 5.3b), the crude feed F_{C1} is introduced to column 1.
- For setup 2 (Figure 5.3c), the crude feed F_{C2} is introduced to column 2. The order of the columns was rearranged such that the crude feed is introduced to the left column.
- For setup 3 (Figure 5.3d), the crude feed F_{C3} is introduced to column 3 and the columns are again rearranged such that the crude feed is introduced to the left column.

For binary crude feeds, setup 1 (Figure 5.3b) and setup 3 (Figure 5.3d) have been discussed in the literature (Laroche et al., 1992a; Stichlmair and Herguiejuela, 1992). Setup 2 (Figure 5.3c) is new.

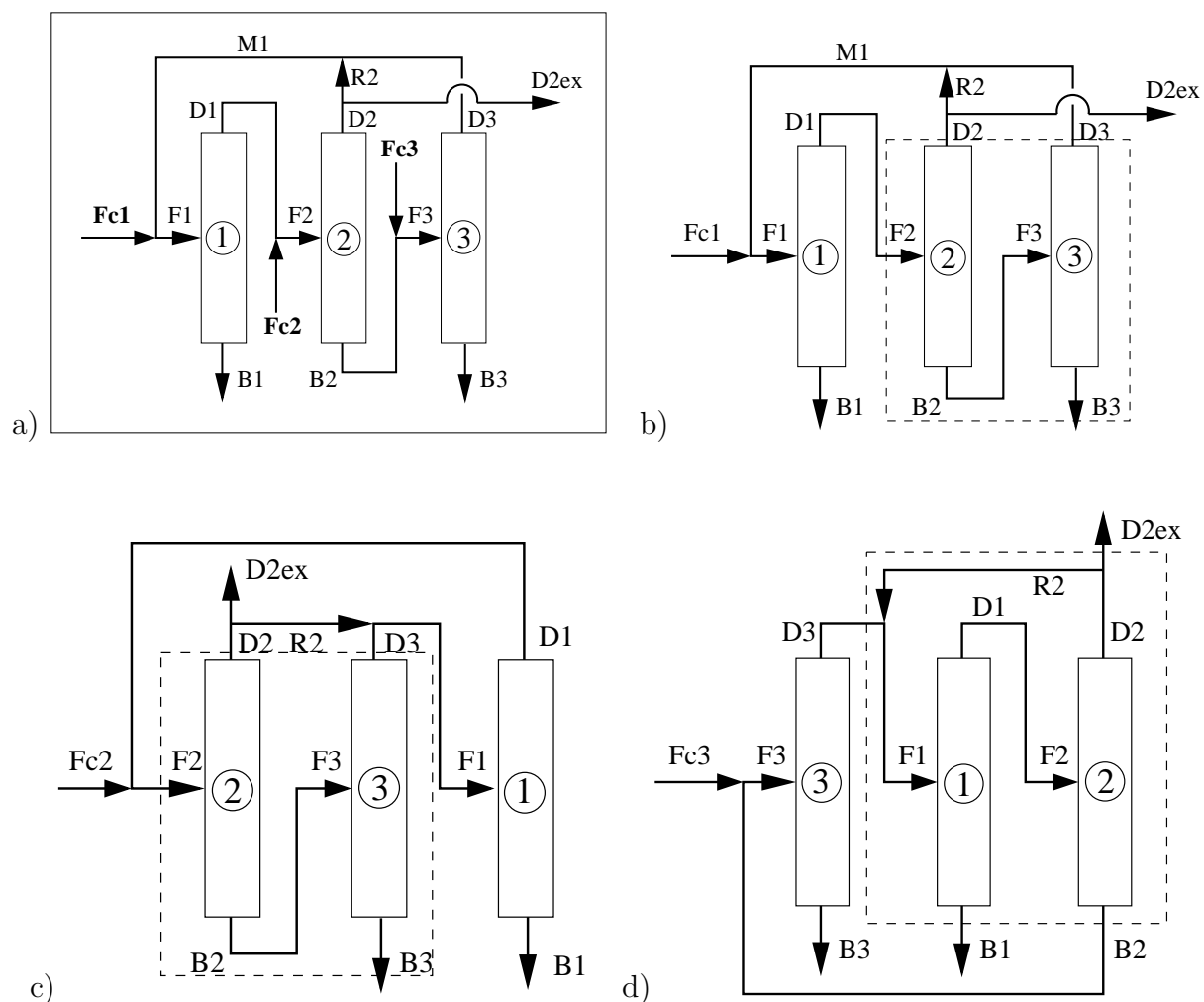


Figure 5.3: a) Boundary separation scheme with three different feed locations: b) setup 1: F_C to column 1, c) setup 2: F_C to column 2, and d) setup 3: F_C to column 3.

The first steps of the self-optimizing control concept that was introduced in section 2.4.2 are now applied to the boundary separation scheme showing the need for model reduction to reduce complexity.

Step 1: Degree of Freedom Analysis. As thoroughly discussed by Skogestad, Lundström and Jacobsen (1990), a homogeneous distillation column without side streams has five degrees of freedom for a fixed design (number of stages, feed stage location and given feed). Normally, the pressure is fixed eliminating one degree of freedom. Of the remaining four variables, two can be chosen independently, the other two are then used to control (stabilize) the levels of the reflux drum and the bottom (these have no steady state effect).

Hence, from a steady state perspective, a homogeneous distillation column has two degrees of freedom for a fixed feed (compare also section 3.2.1). The three column boundary separation schemes has 7 degrees of freedom: 6 degrees of freedom for the three columns and another one for the additional recycle R_2 . The fact that D_3 is recycled does not change the degrees of freedom, neither does the location of F_C .

Step 2: Cost Function and Constraints. For a fixed design, the cost function is the sum of the reboiler duties, which is the main part of the operating costs:

$$J = Q_1^R + Q_2^R + Q_3^R \quad (5.1)$$

Constraints are the product purities:

$$x_{water}^{B_1} \geq 0.9998 \text{ kg/kg} \quad (5.2)$$

$$x_{methanol}^{D_2} \geq 0.9998 \text{ kg/kg} \quad (5.3)$$

$$x_{2-propanol}^{B_3} \geq 0.9998 \text{ kg/kg} \quad (5.4)$$

Step 3: Most Important Disturbances and Uncertainties. Two disturbances are considered:

1. changes in the crude feed condition (flow rate and composition),
2. changes in the interconnecting streams caused by rejection of the crude feed disturbances or pressure fluctuations that give different compositions of the azeotrope which might change x^{D_3} .

The main model uncertainty to be considered is the thermodynamic model for the phase equilibrium calculations. More specific: the curvature of the residue curve boundary, which is critical for the boundary separation scheme, depends on the chosen thermodynamic model and its parameter set.

Step 4: Optimization. The boundary separation scheme has 7 degrees of freedom for fixed column top pressures. The constraints for the product purities $x_{water}^{B_1}$, $x_{methanol}^{D_2}$ and $x_{2-propanol}^{B_3}$ fix three degrees of freedom. Nevertheless, four degrees of freedom remain to

find the optimal operation point. If the sequence is modeled in AspenPlus for example, this can be done with the implemented optimizer. This approach often has two problems:

1. a solution is difficult to find,
2. there is often no guarantee that this solution is the global optimum.

Break: Reduce Complexity. Because of the complexity of the problem, a tool is needed to reduce the complexity for the optimization and to provide process insight that can be used to ease decisions concerning the controller structure. The tool exists. It is the ∞/∞ analysis (Bekiaris et al., 1993) as introduced in section 2.1.2. The steps of the design of a self-optimizing control concept as mentioned in section 2.4.2 are applied to the ∞/∞ sequence, but in a different order.

5.2 Cost Function

The cost function is the sum of the reboiler duties (equation 5.1). The problem of the ∞/∞ analysis is that the reboiler duties are infinite. The reboiler duty of a finite column is proportional to the overhead vapor flow and hence to the sum of reflux and distillate flow:

$$Q_i^R = p_i (L_i + D_i) \quad (5.5)$$

p_i is the proportionality factor that is related to the enthalpy of vaporization of the mixture. If the column is operated with a fixed reflux-to-distillate ratio $r_i = L_i/D_i$, equation 5.5 can be rewritten as:

$$Q_i^R = p_i (r_i + 1) D_i = k_i D_i \quad (5.6)$$

Hence, the reboiler duty is directly proportional to the distillate flow rate for constant p_i and r_i . p_i will be constant if the the enthalpy of vaporization does not the depend on the composition of the vapor flow. In this case, the vapor flow is proportional to the reboiler duty and equation 5.6 is consistent with the approximation given by Doherty and Malone (2001): “For columns with a saturated liquid feed, an approximate expression for the vapor rate leaving the reboiler V is $V = (r + 1) D$ (8.12) where r is the reflux ratio and D is the distillate flow rate.”

Using equation 5.6, the cost function (equation 5.1) can be written as:

$$J = k_1 D_1 + k_2 D_2 + k_3 D_3 \quad (5.7)$$

Assuming $k_1 = k_2 = k_3 = k$, equation 5.7 gets:

$$J = k(D_1 + D_2 + D_3) \quad (5.8)$$

In this case, J is minimal if the sum of the distillate flow rates is minimal:

$$J^D = D_1 + D_2 + D_3 \quad (5.9)$$

The strong assumption that all k_i are equal will be relaxed in section 6.7.4 and chapter 7 when values obtained from rigorous simulations are used.

5.3 Degrees of Freedom and Constraints

The top pressures of the columns are fixed. Understanding the role of the individual flows between the three columns is a necessary prerequisite for proposing the right optimization problem. Therefore, the analysis starts with three columns in a row (sequence A, section 5.3.1). Then, one recycle after the other is closed (sequence B, and C, sections 5.3.2, and 5.3.3, respectively). The recycles change the process properties, especially the feasible feed regions. Therefore, the feasible feed regions are also discussed here. Further, Stichlmair (stated by Laroche et al. (1992b) as personal communication) suggested to use a third recycle. This option is not considered for the design of the control schemes. The reasons are discussed in section 5.7.

5.3.1 Sequence A: Three Columns in a Row

Figure 5.4a shows three columns in a row without any recycles. A distillation column separating a c component mixture has $c + 2$ degrees of freedom. Hence, a three column sequence has $3c + 6$ degrees of freedom. For a given external crude feed F_C , c degrees are fixed: $c - 1$ for the feed composition and one for the feed flow rate. $2c$ degrees are

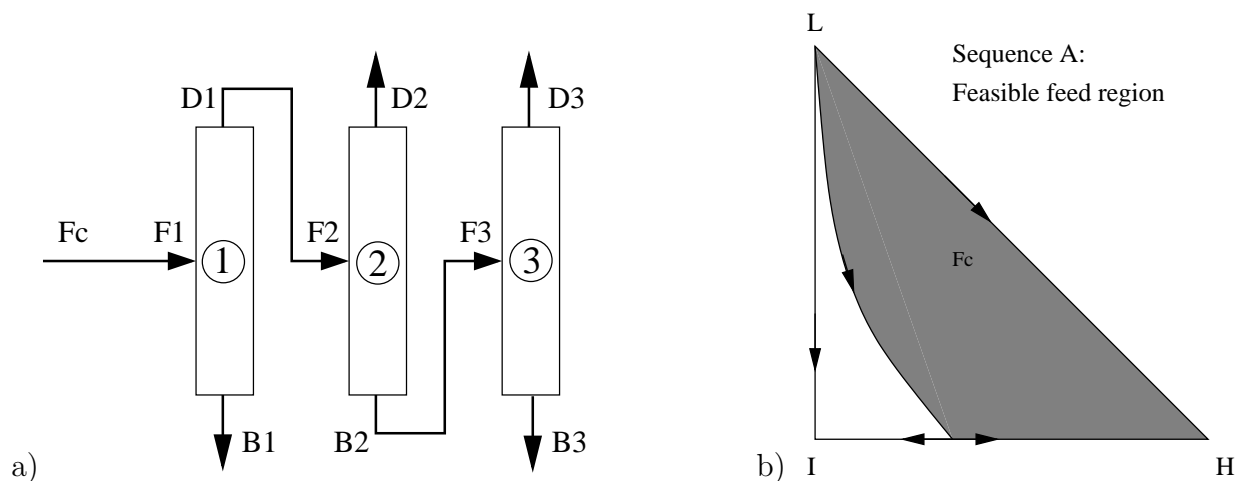


Figure 5.4: Sequence A. a) Column sequence. b) Feasible feed region for a 020 mixture.

Table 5.1: Possible combinations of profile types for sequence A: three columns in a row.

case	1	2	3	4	5	6	7	8	9	10	11	12
column 1	II	II	II	II	II	II	III	III	III	III	III	III
column 2	I	I	I	III	III	III	I	I	I	III	III	III
column 3	I	II	III	I	II	III	I	II	III	I	II	III
feasible?	no	yes	yes	no	yes	yes	no	yes	yes	no	yes	yes
degrees of freedom	-	3	3	-	3	3	-	3	3	-	3	3

fixed by the selected connections ($D_1 = F_2$ and $B_2 = F_3$). For the ∞/∞ analysis, the reflux for each column is infinite fixing three more degrees. Hence, $3c + 3$ degrees are fixed giving 3 degrees of freedom for the sequence. By specifying B_1 , D_2 , and D_3 , all flow rates are determined. Depending on the specific values, the column profiles and product compositions are also determined. In general, each column profile can be of type I, II or III (Bekiaris et al., 1993), which gives $3^3 = 27$ combinations. However, not all of them are feasible/make sense. If the profile of column 1 is a type I profile, the distillate D_1 will consist of pure L. The subsequent columns cannot perform any further, useful separation. Therefore, these cases will be disregarded reducing the possible cases to 18. If the profile of column 2 is of type II, the bottoms B_2 will consist of pure H allowing no further separation in column 3. This reduces the useful combinations to 12 that are listed in Table 5.1.

For the cases 1 and 7, column 3 does not perform any separation that column 2 cannot do.

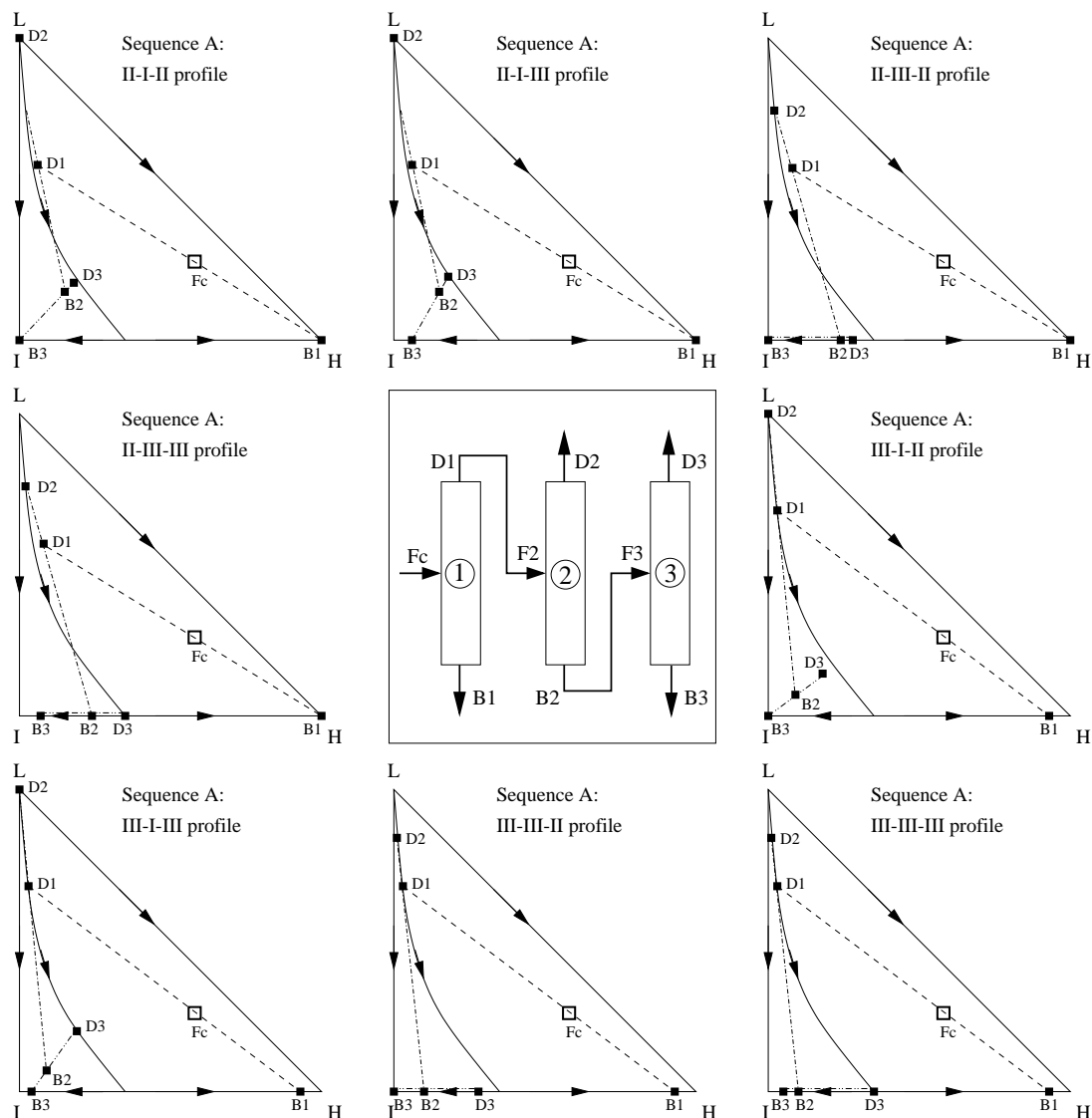


Figure 5.5: Eight cases for sequence A. For simplicity, the column profiles are not shown but only the mass balance lines of the columns. The thick dashed, dashed-dotted, and dashed-double-dotted lines denote columns 1, 2, and 3, respectively.

For the cases 4 and 10, type I for column 3 is infeasible for distillate flows D_3 greater than zero. Hence, eight cases remain for a setup that allows to separate a three component feed into products on both sides of the separatrix. These are shown in Figure 5.5. Here, a II-I-II profile means that column 1 has a profile of type II, column 2 of type I, and column 3 of type II. The feasible feed region of the sequence with x^{B_1} in the convex set is the convex set as shown in Figure 5.4b.

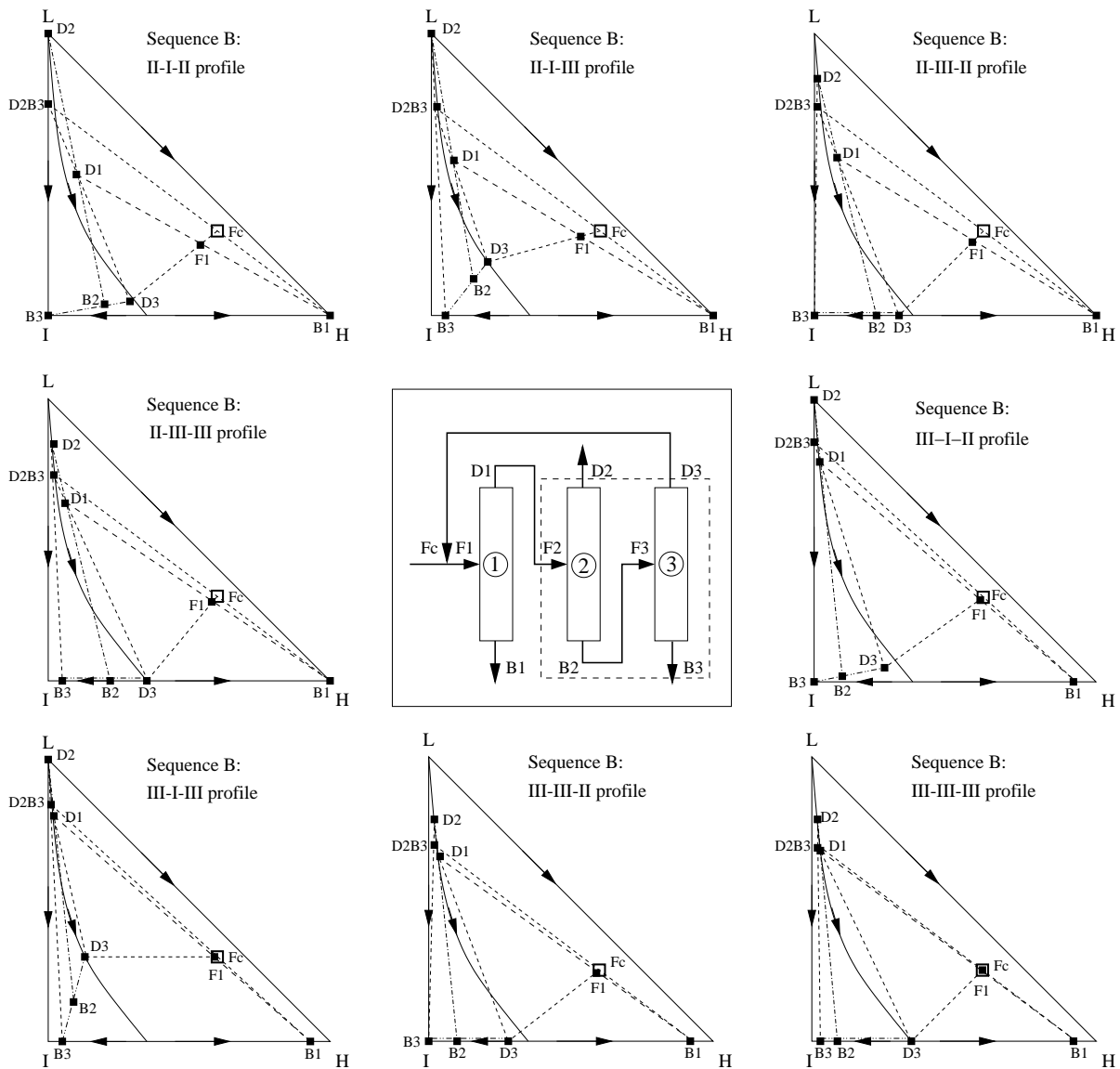


Figure 5.6: Eight cases for sequence B. For simplicity, the column profiles are not shown but only the mass balance lines of the columns. The thick dashed, dashed-dotted, and dashed-double-dotted lines denote columns 1, 2, and 3, respectively.

5.3.2 Sequence B: Three Columns with One Recycle

Figure 5.6 shows in the center the three column sequence with D_3 recycled to the feed of column 1 surrounded by the eight possible cases of profile combinations. In general, closing a recycle does not change the degrees of freedom, but it changes the interval of flow rates for which a specific profile combination is feasible. For a given set of flow rates (e.g. B_1 , D_2 , and D_3), Figure 5.6 shows the mass balance lines of column 1, column 2, and column

Table 5.2: Possible combinations of profile types for sequence B: three columns with one recycle.

case	2	3	5	6	8	9	11	12
column 1	II	II	II	II	III	III	III	III
column 2	I	I	III	III	I	I	III	III
column 3	II	III	II	III	II	III	II	III
degrees of freedom	1	2	2	3	2	2	3	3

3. The mixing of D_3 with F_C is indicated by the thin dashed line. There are two more thin dashed lines that indicate the feasibility of the sequence. The mass balance around column 2 and column 3 has to be fulfilled for a feasible setup:

$$x^{D_1} D_1 = x^{D_3} D_3 + (x^{D_2} D_2 + x^{B_3} B_3) \quad (5.10)$$

With

$$x^{D_2 B_3} = \frac{(x^{D_2} D_2 + x^{B_3} B_3)}{D_2 + B_3} \quad (5.11)$$

follows from equation 5.10 that $x^{D_2 B_3}$ has to be collinear with x^{D_1} and x^{D_3} (thin dashed line). $x^{D_2 B_3}$ follows from the overall mass balance:

$$\begin{aligned} x^{F_C} F_C &= x^{B_1} B_1 + (x^{D_2} D_2 + x^{B_3} B_3) \\ x^{F_C} F_C &= x^{B_1} B_1 + x^{D_2 B_3} (D_2 + B_3) \end{aligned} \quad (5.12)$$

In the residue curve maps (Figure 5.6), $x^{D_2 B_3}$ can be determined by the intersection of the line connecting x^{F_C} and x^{B_1} with the line connecting x^{D_2} and x^{B_3} .

A further analysis shows that some profile combinations reduce the degrees of freedom to one or two, as summarized in Table 5.2. The reason is that some combinations just apply for one particular combination of external flow rates. For the II-I-II profile (case 2), the external flow rates (B_1 , D_2 , and B_3) are given by the composition of the ternary crude feed F_C which fixes two of the three degrees of freedom (the last flow rate, e.g. B_3 results from the overall mass balance). Hence, one degree of freedom remains, which can either be D_1 , B_2 or D_3 . If column 2 has a profile of type I, D_2 is given by the amount of L in the crude feed F_C because L does not leave the process via B_1 or B_3 for any of the other

three possible profile combinations (cases 3, 8, and 9). Hence, only two more flow rates can be freely chosen within certain bounds that are given by the possible product paths of the columns for the select profile combination. The same applies for case 5: L can only leave through D_2 . For the other three cases (6, 11, and 12), three flow rates can be varied within a certain interval.

5.3.2.1 Feasible Feed Region

For sequence B, the feed composition x^{F_C} is restricted to a certain region, where the sequence is able to split F_C into three pure products (II-I-II profile). The feasible feed region is constructed as follows. Figure 5.7a shows the mass balances for a II-I-II profile (B_1 , D_2 are given by x^{F_C} , D_3 is the last degree of freedom). For the location of $x^{D_2B_3}$ and x^{D_3} shown in Figure 5.7a, the mass balance line (equation 5.10) is secant to the residue curve boundary, i.e., it crosses the boundary twice. Increasing the recycle D_3 forces x^{D_1} to move towards the boundary, and at the point where x^{D_1} is at the boundary (Figure 5.7b), increasing D_3 is only possible if x^{D_3} moves towards the I-H azeotrope. In the limiting case of infinite D_3 , the compositions x^{F_1} , x^{D_1} , x^{B_2} , and x^{D_3} all coincide in the I-H azeotrope, as shown in Figure 5.7d.

Figure 5.7c shows the effect on the products if the amount of L in F_C is decreased at constant amount of H. The amount of L in F_C , which equals the amount of L in D_2B_3 , can be decreased until the mass balance line around column 2 and column 3 is tangent to the boundary. Then, x^{D_1} lies on the boundary. The amount of L in D_2B_3 can only be further decreased, if x^{D_3} moves towards the binary azeotrope (Figure 5.7d). Note that during this, the flow rate D_3 has to change (increase). In the limiting case of minimum L content at constant H, D_3 is again infinite and x^{D_1} lies on the binary azeotrope again, as well as x^{F_1} , x^{B_2} , and x^{D_3} . The tangent to the boundary in that point determines the $x^{D_2B_3}$ with a minimum amount of L. This gives the feasible feed region as indicated by the shaded region in Figure 5.7d. A comparison of this region with the feasible region of sequence A shows that the recycle increases the region to part of the non-convex set, but the perfect recovery of the products (all three are obtained pure) decreases the feasible region elsewhere.

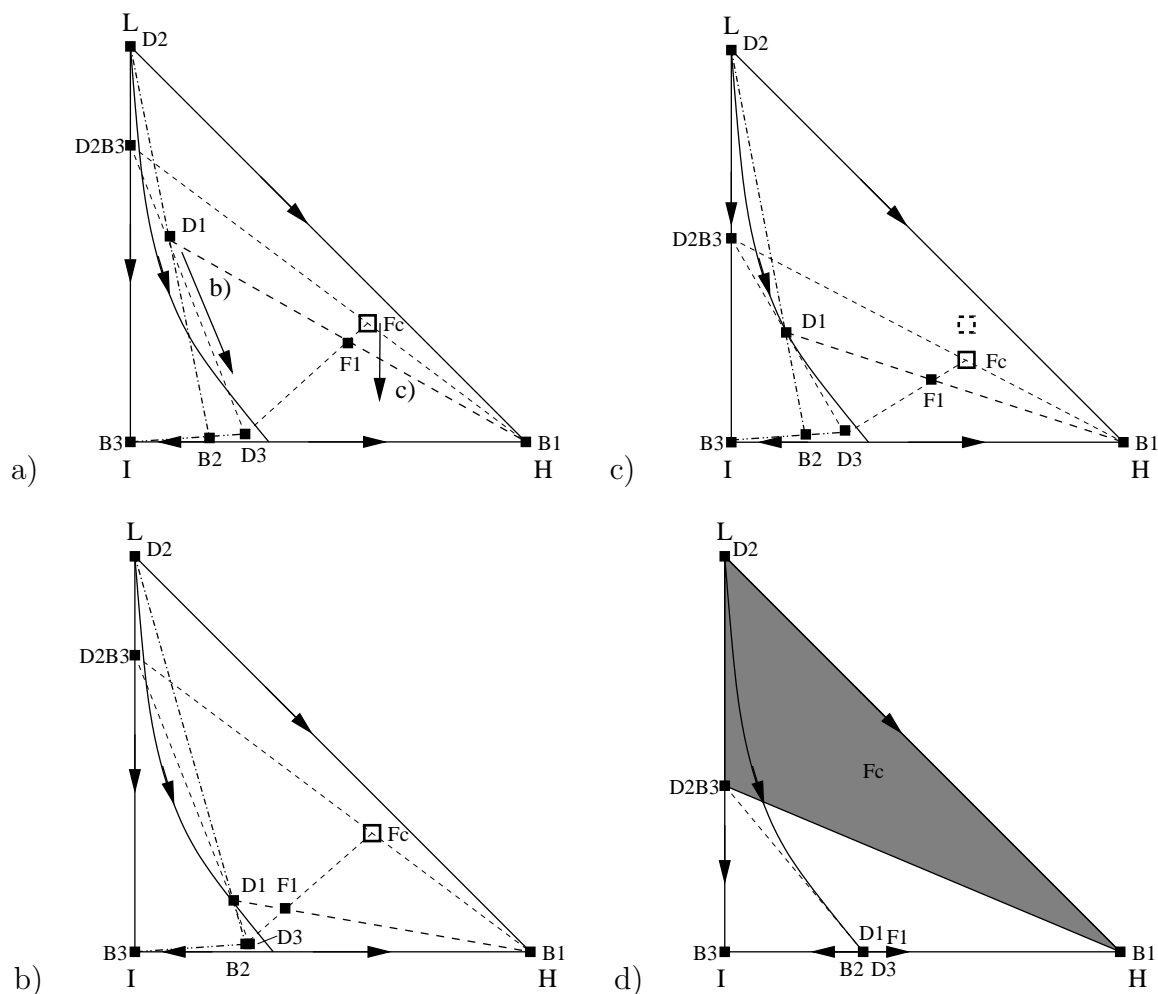


Figure 5.7: Derivation of the feasible feed region for the II-I-II profile of sequence B.

To summarize, the feasible feed region is the triangle spanned by the three compositions x^{D_2} , $x^{D_2B_3}$, and x^{B_1} . $x^{D_2B_3}$ is determined by the crossing of the line connecting D_2 with B_3 and the tangent to the residue curve boundary at the I-H azeotrope (for a monotonic boundary). If a feed is outside the shaded region in Figure 5.7d, a feasible setup can still be found, but at the price of unpure products. For example, the III-I-II profile allows x^{B_1} to move along the I-H edge of the triangle which shifts the feasible region that is spanned by x^{D_2} , $x^{D_2B_3}$, and x^{B_1} to every possible composition of F_C . However, a better strategy is to extend the feasible region to the whole composition space by recycling a part of D_2 (L) to column 1. The mechanism will be discussed in section 5.3.3 where sequence C is introduced. The construction of the feasible feed region is similar to the abstract statements of Serafimov et al. (1992a) that were mentioned in section 2.2.2.

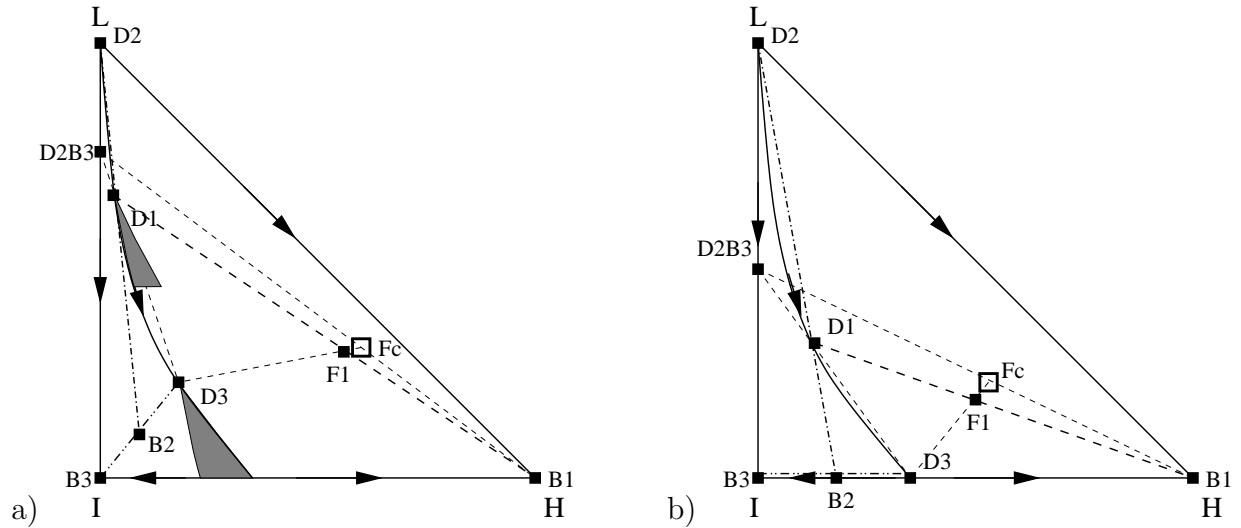


Figure 5.8: Sequence B: II-I-II profile showing a) the solution space for constant D_3 , and b) the solution for the optimal operation point (minimal D_3).

5.3.2.2 Multiplicities

For the II-I-II profile, two kinds of multiplicities are possible for fixed external flow rates (B_1 and D_2) and compositions (x^{B_1} , x^{D_2} , and x^{B_3}):

1. **Input Multiplicities.** For the case shown in Figure 5.7a, the flow D_3 can be continuously varied for a constant x^{D_3} . This gives a set of feasible x^{D_1} , which all lie on the line connecting $x^{D_2 B_3}$ with x^{D_3} given by the mass balance line of the subsystem around column 2 and column 3, equation 5.10. The same external flow rates and compositions can be reached for a continuum of different D_3 .
2. **State Multiplicities.** For a constant D_3 , it is possible to find a feasible set of compositions x^{D_1} , x^{B_2} , and x^{D_3} for a continuous set of x^{D_1} . These sets are illustrated in Figure 5.8a. The size of the sets depends on the value of D_3 . The bigger D_3 , the bigger are these sets. Contrary to that, the size of the sets shrinks to a single point at the minimal recycle D_3 (Figure 5.8b, a different feed F_C was chosen for better illustration).

The input multiplicities are also possible for other profiles such as the III-I-II profile. For constant x^{D_3} , not a continuum, but just two specific points are possible. Figure 5.9a shows

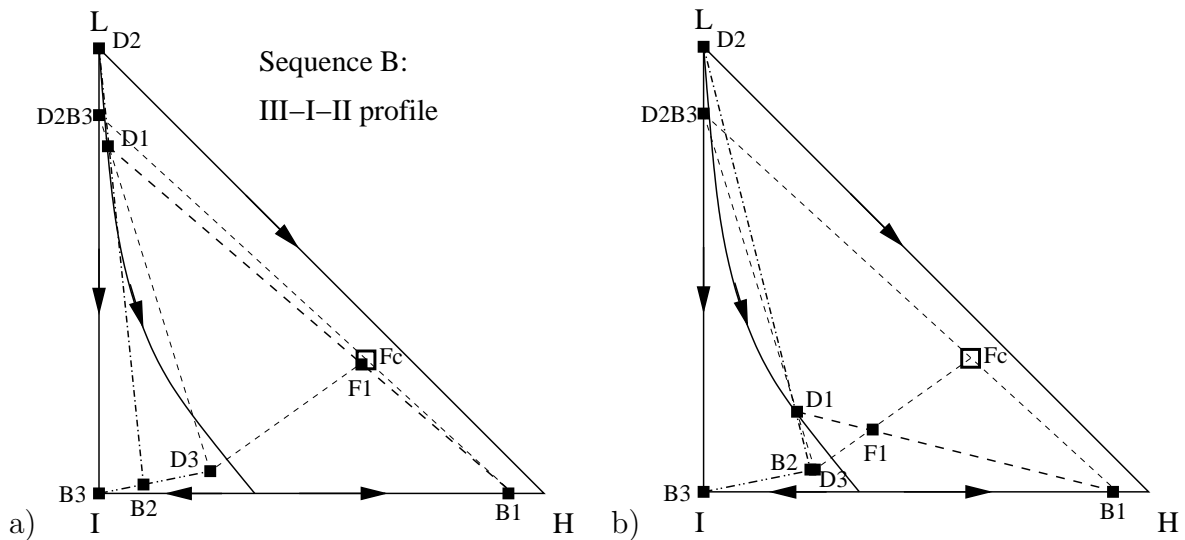


Figure 5.9: Sequence B: III-I-II profile. Two distinct operation points for constant x^{D_3} .

the first possible case and Figure 5.9b shows the second case for the same set of output flows, but for a different recycle flow rate D_3 (input to the overall system). If x^{D_1} lies on the dashed line between the two extremes shown in Figure 5.9, the sequence will also be feasible, but the profile of column 1 is then not a type III profile. It does not contain a pinch and is therefore not a ∞/∞ profile. But such a profile exists for finite columns. Also state multiplicities are possible for III-I-II profiles similar to the state multiplicities for the intermediate entrainer case (Appendix C.2). These kind of multiplicities were also observed for the indirect heterogeneous sequence (Esbjerg et al., 1998).

5.3.3 Sequence C: Three Columns with Two Recycles

As mentioned in section 5.1, three different setups for sequence C are possible (Figure 5.3):

- **Setup 1:** F_C is introduced to column 1.
- **Setup 2:** F_C is introduced to column 2.
- **Setup 3:** F_C is introduced to column 3.

Figure 5.10a shows the three column sequence with the second recycle R_2 (setup 1). This

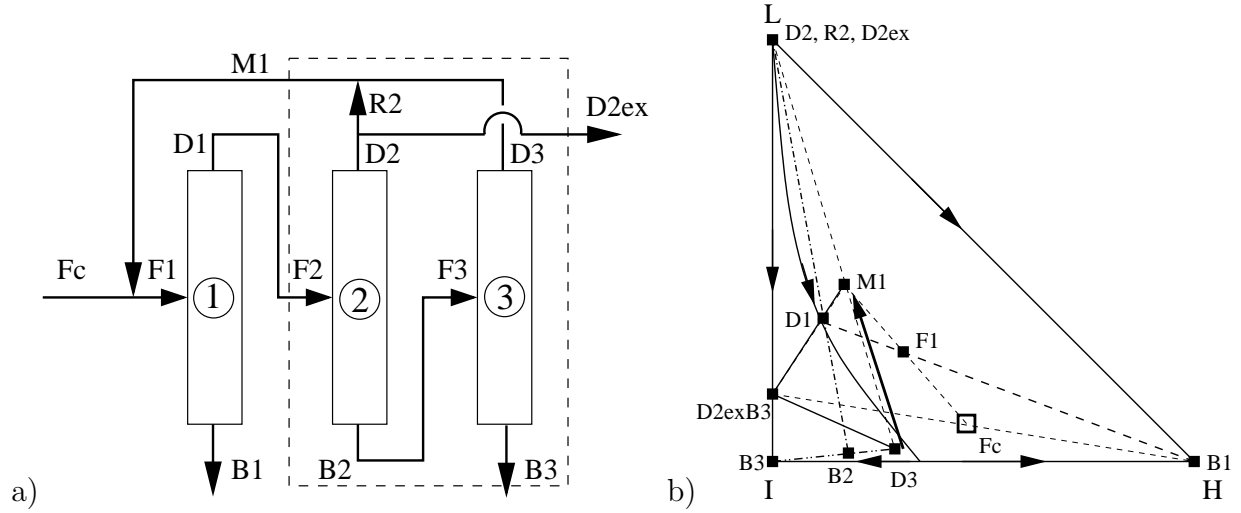


Figure 5.10: Sequence C setup 1. a) Three Columns with two recycles and b) the mass balances for a II-I-II profile.

additional stream introduces an additional degree of freedom. The degrees of freedom for the 8 possible column profiles of sequence B (Table 5.2) are increased by one for sequence C (Table 5.3). The effect of R_2 on the process is illustrated in Figure 5.10b for a II-I-II profile. With the recycle R_2 , the mass balance around column 2 and column 3 changes:

$$\begin{aligned} x^{D_1} D_1 &= (x^{D_2} R_2 + x^{D_3} D_3) + (x^{D_2} D_2^{ex} + x^{B_3} B_3) \\ x^{D_1} D_1 &= x^{M_1} (R_2 + D_3) + x^{D_2^{ex} B_3} (D_2^{ex} + B_3) \end{aligned} \quad (5.13)$$

From equation 5.13 follows that x^{D_1} , $x^{D_2^{ex} B_3}$, and x^{M_1} are collinear. The composition x^{M_1} is determined by the mixing of the two recycle streams R_2 and D_3 . As Figure 5.10b shows, the line connecting $x^{D_2^{ex} B_3}$ with x^{D_3} (x^{M_1} for $R_2 = 0$) is completely in the non-convex set

Table 5.3: Possible combinations of profile types for sequence C: three columns with two recycles.

case	2	3	5	6	8	9	11	12
column 1	II	II	II	II	III	III	III	III
column 2	I	I	III	III	I	I	III	III
column 3	II	III	II	III	II	III	II	III
degrees of freedom	2	3	3	4	3	3	4	4

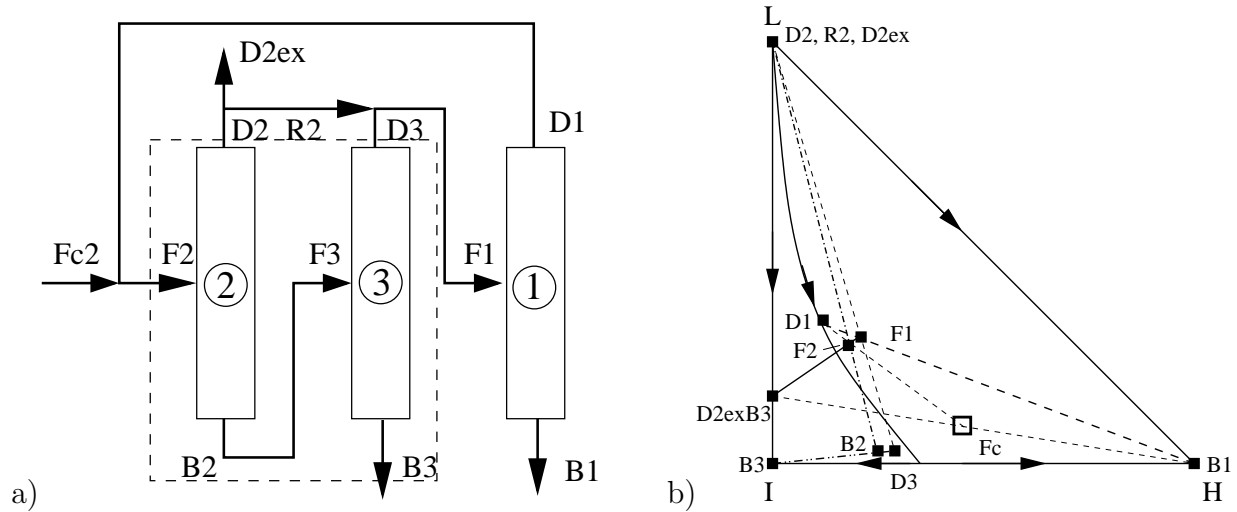


Figure 5.11: Sequence C setup 2. a) Column configuration and b) the mass balances for a II-I-II profile.

for $R_2 = 0$. Since x^{D1} has to lie in the convex set (the residue curve boundary also belongs to the convex set), the feed is infeasible for $R_2 = 0$. For increasing R_2 , x^{M1} moves towards x^{D2} . At some point, x^{M1} enters the convex set. Now, x^{D1} may also lie in the convex set and the sequence is feasible. Since R_2 can be varied between zero and infinity, x^{M1} can move between x^{D2} and x^{D3} . By this, it is possible to find an R_2 such that x^{D1} and x^{M1} are collinear with each possible $x^{D2_{ex}B3}$. Hence, the feasible feed region is now the triangle spanned by x^{B1} , x^{D2} , and x^{B3} . For a II-I-II profile, this corresponds to the whole ternary composition space including the non-convex set. The resulting eight profiles of sequence C are very similar to the profiles of sequence B (Figure 5.6). Therefore, the eight profiles for sequence C are not shown here.

Figure 5.11 shows the configuration of setup 2 and the mass balance for a II-I-II profile. Figure 5.12 shows the same for setup 3. As for setup 1, the feasible feed region of a II-I-II profile is the whole composition triangle. Different to setup 1, setup 2 and setup 3 are infeasible without the recycle R_2 . The reason is that x^{D3} lies in the concave set. Therefore, mixing of $D3$ with $R_2 > 0$ is required to place x^{F1} in the convex set for a feasible column 1 profile. Though all three setups have the same structure, the different positions of the crude feed change the performance of the setups. This is discussed next.

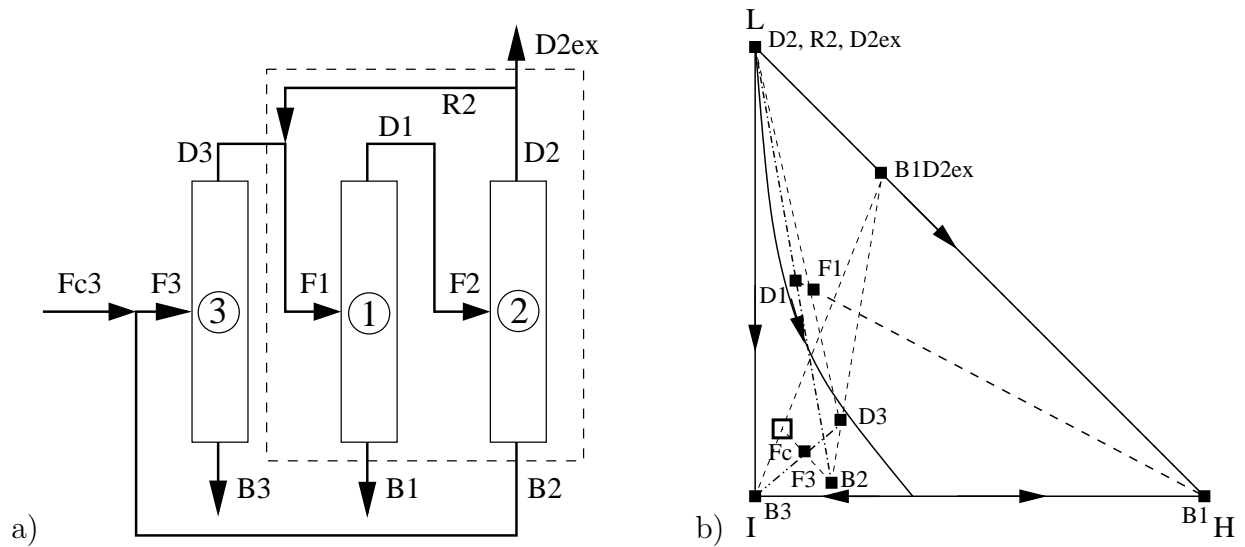


Figure 5.12: Sequence C setup 3. a) Column configuration and b) the mass balances for a II-I-II profile.

5.4 Optimization

With respect to the feasible feed region, only the three setups of sequence C should be further investigated. However, sequence B is a special case of sequence C ($R_2 = 0$) and is therefore also discussed.

5.4.1 Sequence B

The optimal operation point is determined by minimizing J^D , the sum of the distillate flow rates (equation 5.9). For the II-I-II profile, B_1 and D_2 are given by the crude feed:

$$B_1 = x_H^{F_C} F_C \quad \text{and} \quad D_2 = x_L^{F_C} F_C \quad (5.14)$$

In these equations, the subscripts H and L refer to the components H and L , respectively.

The mass balance of column 1 can be written as $D_1 = F_C + D_3 - B_1$ giving:

$$J^D = 2 D_3 + F_C + D_2 - B_1 \quad (5.15)$$

Equation 5.15 shows that D_3 , the last degree of freedom, has to be minimized. Figure 5.7a and Figure 5.7b showed in section 5.3.2.1 that x^{D_1} moves towards x^{D_3} for increasing D_3 .

For the optimal point, the minimum of the recycle D_3 is of interest. For every external feed composition x^{FC} that lies in the feasible region of sequence B, D_3 can be reduced until x^{D_1} hits the boundary close to the composition $x^{D_2B_3}$. As a result of the lever rule, D_3 is minimal when x^{D_3} is at the I-H azeotrope. Hence, every procedure that minimizes the recycle streams for a feasible setup leads to x^{D_3} being at the I-H azeotrope and x^{D_1} lying on the residue curve boundary (Figure 5.8b). For this optimal case, every column profile has two pinches: one of the pure components and the saddle I-H azeotrope. Despite that, this profile is still referred to as a II-I-II profile. The optimal recycle flows D_3 can be calculated using the mass balance around column 2 and column 3 (see appendix C.1.1 for details):

$$D_3(x^{FC}) = \frac{x_H^{D_1}(x^{FC})}{x_H^{D_3} - x_H^{D_1}(x^{FC})} (1 - x_H^{FC}) F_C \quad (5.16)$$

This relation for D_3 is nonlinear in $x^{FC} = [x_H^{FC}; x_L^{FC}]$ because $x_H^{D_1}$ is a function of x^{FC} : x^{D_1} is determined by the intersection of the mass balance line around column 2 and column 3 (equation 5.10) with the residue curve boundary.

The theoretical results are illustrated with a residue curve boundary (RCB) that is given by a simple quadratic expression:

$$x_L^{RCB} = 2 \left(x_H^{RCB} \right)^2 - 3 x_H^{RCB} + 1 \quad (5.17)$$

This specific example does not affect the generality of the results, but enables a good illustration (in chapter 6 and chapter 7, the calculations are done with a real system). Figure 5.13a shows the residue curve boundary (RCB) in these coordinates. The location of the I-H azeotrope is $x^{az} = [x_H^{az}; x_L^{az}] = [0.5; 0]$. To illustrate the curvature of the boundary, a straight line connects L with the I-H azeotrope. The tangent in the azeotrope has the slope -1 which gives $x_L^{D_2B_3} > 0.5$ as the condition for feasible feeds (compare Figure 5.7d in section 5.3.2.1). Figure 5.13b shows the recycle flows calculated with equation 5.16 as a function of x^{FC} . The recycle streams go to infinity when x^{FC} reaches the border of the feasible region.

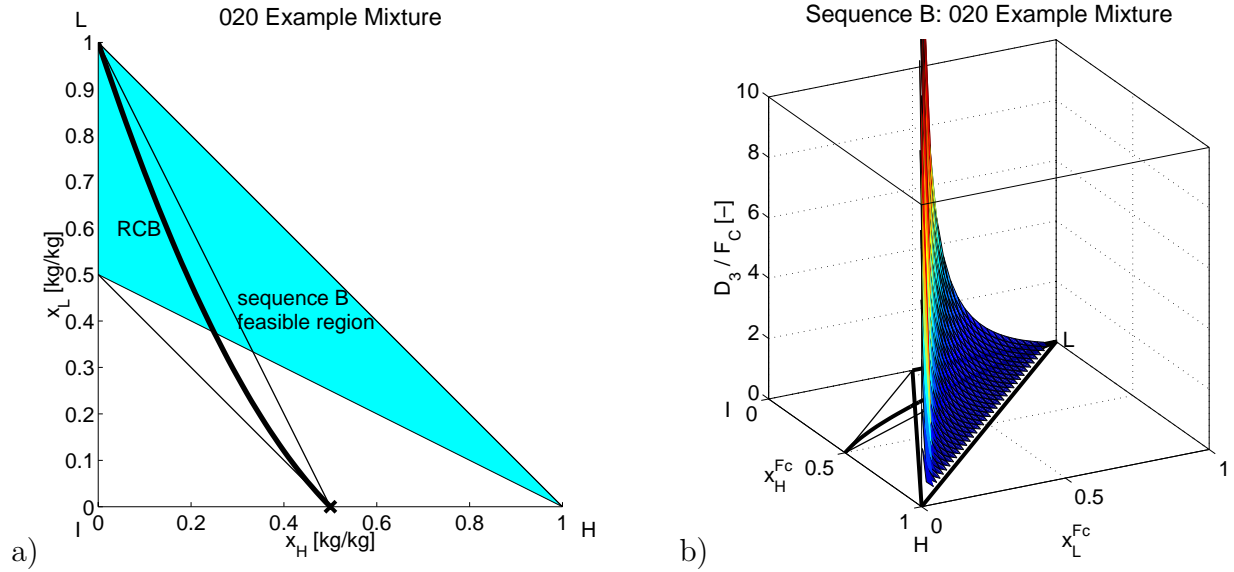


Figure 5.13: 020 mixture: a) Residue curve map with the boundary as defined by equation 5.17, and b) optimal (minimal) D_3 as a function of feed composition.

5.4.2 Sequence C

To find the optimal operation point, the sum of the distillates has to be minimized. The distillate flows can be calculated using the mass balances around the subsystems that are indicated by the dashed lines in Figure 5.10 for setup 1, Figure 5.11 for setup 2, and Figure 5.12 for setup 3. The mass balances can be formulated in the following form:

$$\begin{bmatrix} x_H^{D_1} & -x_H^{D_2} & -x_H^{D_3} \\ x_L^{D_1} & -x_L^{D_2} & -x_L^{D_3} \\ 1 & -1 & -1 \end{bmatrix} \begin{bmatrix} D_1 \\ D_2 \\ D_3 \end{bmatrix} = b(x^{Fc}, F_C) \quad (5.18)$$

The vector b depends on the setup and can be related to the external flows via the overall mass balance:

$$x^{Fc} F_C = x^{B_1} B_1 + x^{D_2} D_2^{ex} + x^{B_3} B_3 \quad (5.19)$$

Hence, the optimization problem can be formulated as follows for the II-I-II profile (x^{D_2} at pure L):

$$J_{min}^D = \min_y (D_1 + D_2 + D_3) \quad (5.20)$$

subject to:

1.

$$\begin{bmatrix} x_H^{D_1} & -0 & -x_H^{D_3} \\ x_L^{D_1} & -1 & -x_L^{D_3} \\ 1 & -1 & -1 \end{bmatrix} \begin{bmatrix} D_1 \\ D_2 \\ D_3 \end{bmatrix} = b(x^{F_C}, F_C) \quad (5.21)$$

2. D_1 , D_2 , and D_3 non negative,3. x^{D_1} lies in the convex set,4. x^{D_3} lies in the non-convex set,5. $x^{B_2} = \frac{x^{D_1} D_1 - x^{D_2} D_2}{D_1 - D_2}$ lies in the non-convex set.

where the vector of unknowns is

$$y = [D_1; D_2; D_3; x_H^{D_1}; x_L^{D_1}; x_H^{D_3}; x_L^{D_3}] \quad (5.22)$$

This can be coded in a commercial solver to determine the optimal x^{D_1} and x^{D_3} for every crude feed composition and every setup. The optimization problem is difficult for the following reasons:

- equation 5.21 is a quadratic constraint,
- constraint 3 is convex quadratic for the example residue curve boundary (equation 5.17),
- constraint 4 is non-convex quadratic for the example residue curve boundary (equation 5.17),
- constraint 5 is non-convex.

Normally, the residue curve boundary is not even quadratic but a nonlinear function, which is given implicitly. Because of these difficulties, the problem is further analyzed for each setup. This leads to a simpler formulation of the problem.

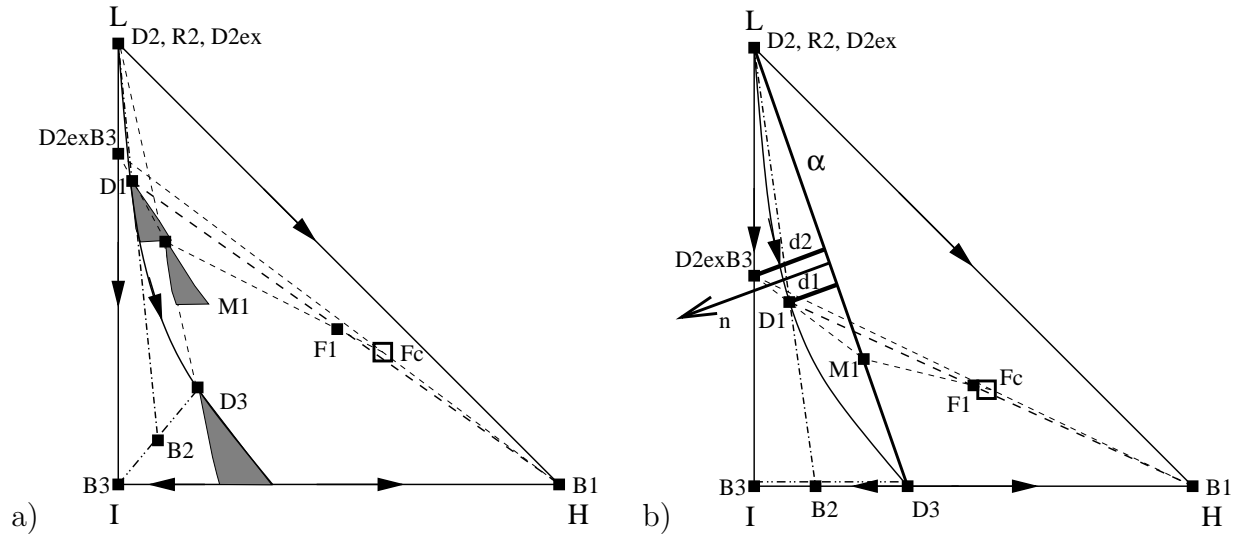


Figure 5.14: Sequence C setup 1: II-I-II profile with fixed R_2 showing a) the solution space for constant D_3 , and b) the solution for the minimal D_3 .

5.4.2.1 Setup 1

For setup 1, the mass balance around column 1 is: $D_1 = F_C + R_2 + D_3 - B_1$; together with $D_2 = R_2 + D_2^{ex}$ follows for the cost function J^D (equation 5.9):

$$J^D = 2(R_2 + D_3) + F_C - B_1 + D_2^{ex} \quad (5.23)$$

For a II-I-II profile, B_1 and D_2^{ex} are given by the overall mass balance (equation 5.19). The sequence has two degrees of freedom. Hence, J^D is minimized over the sum of R_2 and D_3 , the two degrees of freedom.

Monotonic Boundary. The simplification is first illustrated for a monotonic boundary using graphical arguments. First, the role of D_3 is described. For sequence C, the input and state multiplicities that were observed for sequence B are also possible. For any fixed R_2 , D_3 can be fixed in a certain range giving the same external outputs. For each fixed D_3 , a set of solutions is possible (Figure 5.14a, see Appendix B.2.4 for validation). As for sequence B, this set reduces to a single point if D_3 is minimized. At the minimum, x^{D_3} is at the saddle I-H azeotrope (Figure 5.14b, a different feed F_C was chosen for better illustration).

The variation of R_2 changes the location of x^{D_1} , which is given by equation 5.13. From the lever rule follows that $M_1 = R_2 + D_3$ is smallest for a given $x^{D_2^{ex}B_3}$ when x^{D_1} is furthest away from x^{M_1} . This is the case when x^{D_1} lies on the residue curve boundary. Then, the lever rule gives:

$$\frac{R_2 + D_3}{D_2^{ex} + B_3} = \frac{d_2 - d_1}{d_1} = \frac{d_2}{d_1} - 1 \quad (5.24)$$

As shown in Figure 5.14b, the scalars d_1 and d_2 stand for the distance between the two compositions x^{D_1} and $x^{D_2^{ex}B_3}$ and the line α , which connects x^{D_2} with x^{D_3} . The two dimensional vector n , defined as

$$n = \begin{bmatrix} 0 & -1 \\ 1 & 0 \end{bmatrix} \left(\begin{bmatrix} x_H^{D_2} \\ x_L^{D_2} \end{bmatrix} - \begin{bmatrix} x_H^{D_3} \\ x_L^{D_3} \end{bmatrix} \right) \quad (5.25)$$

is perpendicular to the line α . Using this vector, the scalar distances d_1 and d_2 can be calculated as follows:

$$d_1 = n^T \left(\begin{bmatrix} x_H^{D_1} \\ x_L^{D_1} \end{bmatrix} - \begin{bmatrix} x_H^{D_3} \\ x_L^{D_3} \end{bmatrix} \right) \quad (5.26)$$

$$d_2 = n^T \left(\begin{bmatrix} x_H^{D_2^{ex}B_3} \\ x_L^{D_2^{ex}B_3} \end{bmatrix} - \begin{bmatrix} x_H^{D_3} \\ x_L^{D_3} \end{bmatrix} \right) \quad (5.27)$$

For a given feed F_C , the flow rates of D_2^{ex} and B_3 as well as $x^{D_2^{ex}B_3}$ are constant. Since x^{M_1} can only move along the line α , d_2 is constant. Figure 5.14b shows that $d_2 > d_1$. Hence, equation 5.24 gives that $R_2 + D_3$ is minimized if d_1 is maximized. In other words, the optimal location of x^{D_1} on the boundary is where the distance d_1 is maximal. Choosing $x^{D_1, opt}$ such that d_1 is maximal determines x^{M_1} and the recycle flows R_2 and D_3 . Therefore, the optimal operation point of the sequence can be determined by the knowledge of the residue curve map only. Note that $x^{D_1, opt}$ is solely determined by the maximum of d_1 which does not depend on d_2 . d_2 only changes as a function of the crude feed composition x^{F_c} . By this, the recycle flow rates depend on x^{D_1} and x^{F_c} , but $x^{D_1, opt}$ that gives the minimum of $R_2 + D_3$ is independent of x^{F_c} . This property makes x^{D_1} a good candidate for a self-optimizing controlled variable. This will be discussed in section 5.6.

This above optimality condition was also derived by Güttinger and Morari (1996) for binary I-H feeds. Since binary I-H feeds are special cases of ternary feeds, the results for

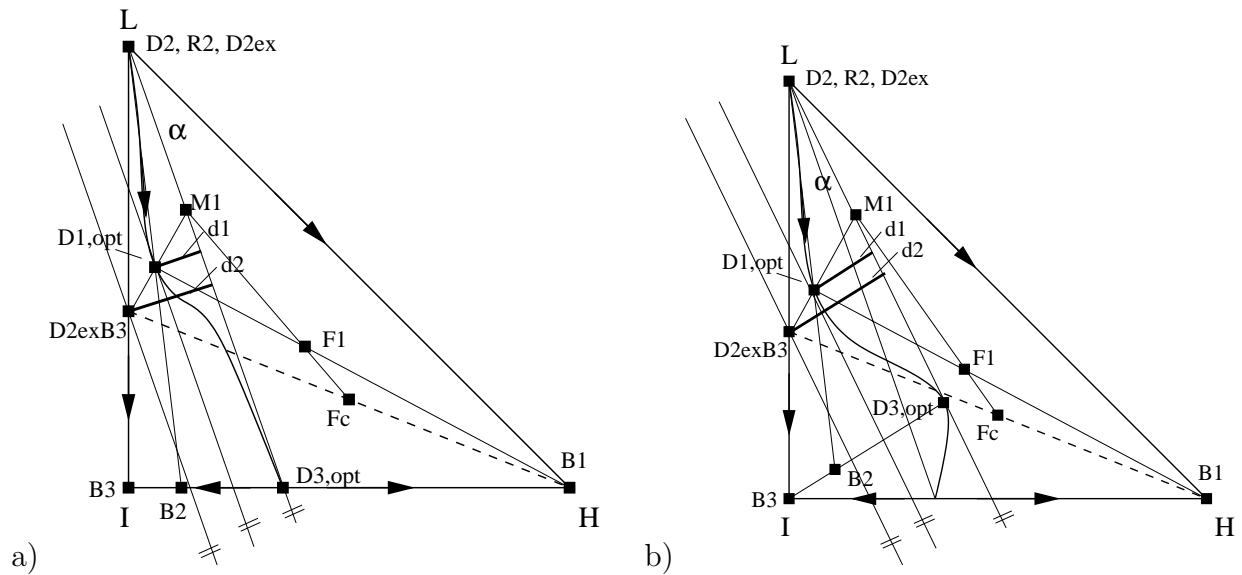


Figure 5.15: Optimal operation point for a residue curve boundary with an inflexion point.

ternary feeds can be easily reduced to the binary case: For binary I-H feeds, no entrainer L leaves the process. Hence, D_2^{ex} is zero and $x^{D_2^{ex}B_3}$ is at the origin (I). Nevertheless, d_2 is independent of the position of x^{M_1} and $R_2 + D_3$ is minimal at the maximum of d_1 .

Another important property of d_1 is that it determines the feasibility of a sequence:

- $d_1 > 0$: the boundary separation scheme is feasible.
- $d_1 \leq 0$: the boundary separation scheme is **infeasible**¹.

Non-monotonic Boundary. In Figure 5.14b, the boundary is monotonous in all three components and has no inflexion point. The procedure of finding the optimal operation point is not restricted to this case. It can also be used for a residue curve boundary with an inflexion point. The only restriction is that the boundary is left of the line α , which connects the I-H azeotrope with the upper pinch L, as shown in Figure 5.15a. If the boundary crosses the straight line (Figure 5.15b), the optimal point for x^{D_1} will still be where d_1 is maximal, but the optimal location of x^{D_3} is not at the I-H azeotrope anymore.

¹For $d_1 = 0$, x^{D_1} lies on the line α in Figure 5.14b giving a x^{B_2} at the I-H azeotrope. This would disable any further separation in column 2 and column 3. For $d_1 < 0$, x^{D_1} lies on the right side of the line α giving an x^{B_2} in the convex set and an x^{B_3} at pure H, and not a pure I as desired.

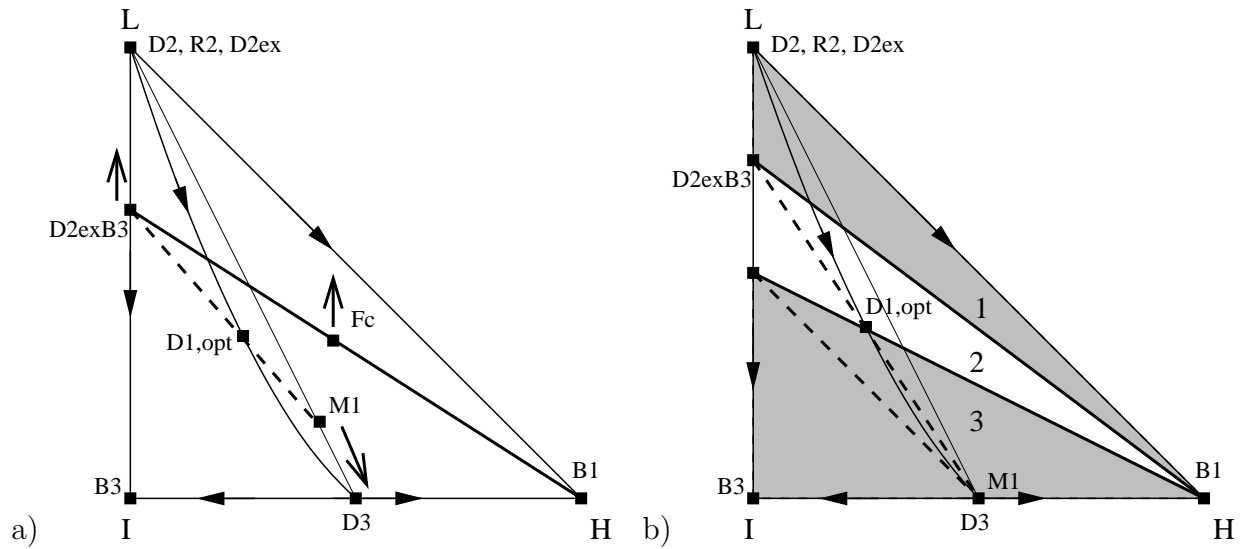


Figure 5.16: a) Derivation of the feasible feed range for a given x^{D_1} ; the dashed line represents equation 5.13. b) The three feed regions: 1) $x^{D_1, opt}$ is infeasible for sequence C, 2) sequence B and $x^{D_1, opt}$ for sequence C are feasible, 3) sequence B is infeasible and $x^{D_1, opt}$ for sequence C is feasible.

Now, the optimal location of x^{D_3} is at the maximum distance from the line α because this places x^{M_1} further away from x^{D_1} , which decreases the sum of the two recycles $R_2 + D_3$.

Feasibility of the Optimal Operation Point. For any given residue curve, x^{D_1} can be varied along the residue curve boundary and the maximum d_1 can be identified. A small problem remains. $x^{D_1, opt}$ is not feasible for all crude feed compositions x^{F_C} . This is explained with Figure 5.16 that shows the products of a II-I-II profile with x^{D_3} being at the I-H azeotrope. The mass balance around column 2 and column 3 (equation 5.13) gives x^{M_1} as a function of x^{D_1} and $x^{D_2^{ex}B_3}$, which is given by x^{F_C} . x^{M_1} is obtained by the mixing of R_2 and D_3 and lies on the line connecting x^{R_2} with x^{D_3} . This determines $R_2 + D_3$ for $x^{D_1, opt}$ (the optimal location in this case). If the L content in F_C increases as indicated by the arrow in Figure 5.16a, $x^{D_2^{ex}B_3}$ has to move towards L. This causes x^{M_1} to move towards x^{D_3} . At a certain L content in F_C , x^{M_1} coincides with x^{D_3} which implies that R_2 is zero. Nevertheless, D_3 still has a finite value (Figure 5.16b). At this point, sequence B and sequence C are identical because the feasible x^{D_1} for sequence B is the same as $x^{D_1, opt}$. If the L content in F_C is further increased, x^{D_1} has to move away from the optimal

point towards L. Hence, the feeds with a higher L content (region 1 in Figure 5.16b) are infeasible for $x^{D_1, opt}$. To summarize:

1. For x^{FC} in region 1, the minimum of the recycles is always at $R_2 = 0$ (which corresponds to sequence B). Despite that, there always exists a feasible x^{D_1} for every $R_2 > 0$ which places x^{M_1} on the line connecting x^{D_2} and x^{D_3} . Since this has implications on the controllability of the process, this is discussed in detail in section 5.6.
2. For x^{FC} in region 2, sequence C is feasible for $x^{D_1, opt}$ ($R_2 > 0$) and for $R_2 = 0$ (sequence B).
3. For x^{FC} region 3, R_2 has to be greater than zero for a feasible setup. Sequence C with $x^{D_1, opt}$ gives minimal J^D .

For the methanol/ethanol/water system, Bauer and Stichlmair (1996) found two different column configurations through their MINLP optimization. Depending on the feed composition, one optimal setup had one recycle, the other one had two recycles. Using the residue curve map, it can be shown that the feed composition for the first configuration lies in region 1 while the feed for the second configuration lies in region 2. Hence, the conclusions of this framework are consistent with the MINLP optimization.

Reformulation of the Optimization Problem. The above analysis simplified the optimization problem (equation 5.20):

- the vector of unknowns (equation 5.22) is reduced from seven elements to five elements: x^{D_3} is fixed at the azeotropic composition,
- constraint 3) is an equality constraint: $x^{D_1} \in$ residue curve boundary,
- constraint 4) is obsolete,
- constraint 5) is also obsolete.

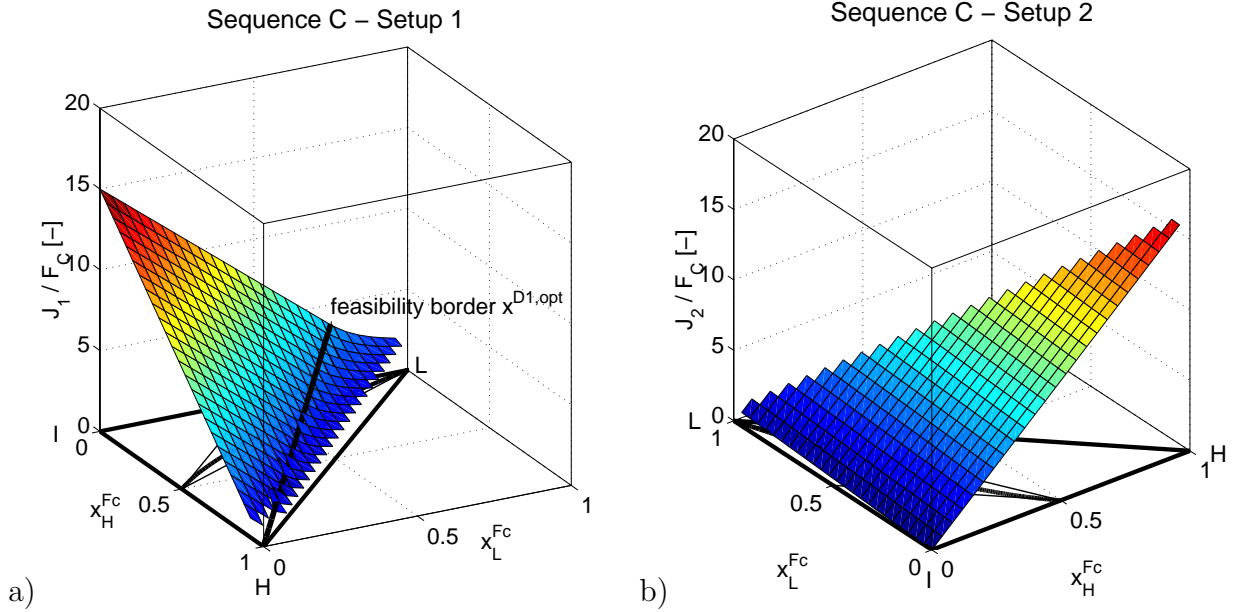


Figure 5.17: Sequence C: Cost function for a) setup 1 (J_1^D) and b) setup 2 (J_2^D) as a function of the crude feed composition.

For setup 1, the vector b in equation 5.18 depends on B_3 , which can be expressed in terms the crude feed using equation 5.19:

$$b = \begin{bmatrix} x_H^{B_3} B_3 \\ x_L^{B_3} B_3 \\ B_3 \end{bmatrix} = \begin{bmatrix} 0 \\ 0 \\ (1 - x_H^{F_C} - x_L^{F_C}) F_C \end{bmatrix} \quad (5.28)$$

For crude feeds in region 1 (Figure 5.16b), the optimum is at $R_2 = 0$ and $x^{D_1,opt}$ depends on x^{F_C} . The optimization of sequence B (section 5.4.1) has to be used.

For crude feeds in region 2 and region 3 in Figure 5.16b, x^{D_1} and x^{D_3} are constant at the optimal point. From equation 5.18 and equation 5.28 follows that all distillate flows are proportional to $(1 - x_H^{F_C} - x_L^{F_C})$ in this case. Hence, the optimal J^D is also proportional to $(1 - x_H^{F_C} - x_L^{F_C})$. In particular for the example residue curve (equation 5.17): $x^{D_1,opt} = [0.25; 0.375]$, and $x^{D_3,opt} = [0.5; 0]$. This gives:

$$J_1^D = 15 (1 - x_H^{F_C} - x_L^{F_C}) F_C \quad (5.29)$$

Figure 5.17a shows J_1^D as a function of x^{F_C} .

5.4.2.2 Setup 2

The optimization procedure is now derived for setup 2. Following the graphical argumentation of setup 1, $x^{D_3, opt}$ is at the azeotrope and $x^{D_1, opt}$ is the same as for setup 1. Different to setup 1, $x^{D_1, opt}$ is feasible for all crude feed compositions for setup 2. The vector b in equation 5.18 depends on F_C and B_3 :

$$b = \begin{bmatrix} x_H^{B_3} B_3 - x_H^{F_C} F_C \\ x_L^{B_3} B_3 - x_L^{F_C} F_C \\ B_3 - F_C \end{bmatrix} = \begin{bmatrix} -x_H^{F_C} F_C \\ -x_L^{F_C} F_C \\ (-x_H^{F_C} - x_L^{F_C}) F_C \end{bmatrix} \quad (5.30)$$

For the example residue curve (equation 5.17), the optimal operation point is at $x^{D_1} = [0.25; 0.375]$ and $x^{D_3} = [0.5; 0]$. From equation 5.18 and equation 5.30 follows:

$$J_2^D = (17 x_H^{F_C} + x_L^{F_C}) F_C \quad (5.31)$$

Figure 5.17b shows J_2^D as a function of x^{F_C} .

5.4.2.3 Setup 3

For setup 3, the optimization problem (equation 5.20) cannot be simplified in the same manner as for setup 1 and setup 2. The main reason is the mass balance around column 1 and column 2:

$$x^{D_3} D_3 = x^{B_2} B_2 + (x^{B_1} B_1 + x^{D_2} D_2^{ex}) \quad (5.32)$$

$$x^{D_3} D_3 = x^{B_2} B_2 + x^{B_1} D_2^{ex} (B_1 + D_2^{ex}) \quad (5.33)$$

x^{D_3} has to be collinear with x^{B_2} and $x^{B_1} D_2^{ex}$. With Figure 5.11a, it can be shown that setup 3 is infeasible every feed F_C that contains L when x^{D_3} is at the I-H azeotrope. Consequently, the optimal operation point is neither at a fixed x^{D_1} nor at a fixed x^{D_3} .

The vector b in equation 5.18 depends on B_1 and D_2^{ex} :

$$b = \begin{bmatrix} -x_H^{B_1} B_1 - x_H^{D_2} D_2^{ex} \\ x_L^{B_1} B_1 - x_L^{D_2} D_2^{ex} \\ -B_1 - D_2^{ex} \end{bmatrix} = \begin{bmatrix} -x_H^{F_C} F_C \\ -x_L^{F_C} F_C \\ (-x_H^{F_C} - x_L^{F_C}) F_C \end{bmatrix} \quad (5.34)$$

The cost function (equation 5.9) can be formulated either as a function of D_1 :

$$J_{3,a}^D = D_1 + (R_2 + D_2^{Ex}) + (D_1 + B_1 - R_2) = 2D_1 + B_1 + D_2^{Ex} \quad (5.35)$$

or as a function of the two recycles R_2 and B_2 :

$$\begin{aligned} J_{3,b}^D &= (R_2 + B_2 + D_2^{Ex}) + (R_2 + D_2^{Ex}) + (F_C + B_2 - B_3) \\ J_{3,b}^D &= 2(R_2 + B_2) + F_C + 2D_2^{Ex} - B_3 \end{aligned} \quad (5.36)$$

The optimal point is where D_1 is minimal (equation 5.35) or where the sum of the two recycles R_2 and B_2 is minimal (equation 5.36). Both cost functions lead to the same optimal operation point.

Using graphical arguments (Figure 5.11a), the optimization problem is simplified. If x^{D_3} moves closer to the I-H azeotrope, D_1/F_1 will be reduced. However, F_1 depends on D_3 , and D_3 is proportional to B_2 . Thus, D_1 might increase though D_1/F_1 is reduced because B_2 has to increase to move D_3 closer to the boundary. From the lever rule follows that B_2 will always be smallest possible if it lies on the binary I-H edge. To identify the optimal operation point, x^{D_1} is varied along the boundary. For each x^{D_1} , the x^{D_3} is determined which gives x^{B_2} on the I-H edge using the mass balance for column 2. The flow rates are determined using equation 5.18 with the b given in equation 5.34. Figure 5.18a shows J_3^D as a function of the feed composition at the optimal point. J_3^D is not a linear function of x^{F_C} . Operation of this setup will be far more difficult because the optimal operation point is not for fixed x^{D_1} and x^{D_3} , as it is for the other two setups. The optimal compositions x^{D_1} and x^{D_3} depend on the feed composition, as shown in Figure 5.18b and Figure 5.18c .

5.4.2.4 Comparison of the Three Setups

The three possible setups of sequence C have been optimized and the dependence of the cost function J^D (equation 5.9) on the crude feed composition has been determined. Figure 5.19 shows the three cost functions J_i^D at the optimal operation points for each crude feed composition as a function of the crude feed composition. The optimal cost function of setup 3 is always greater than the one of setup 2, except for binary I-H feeds where they

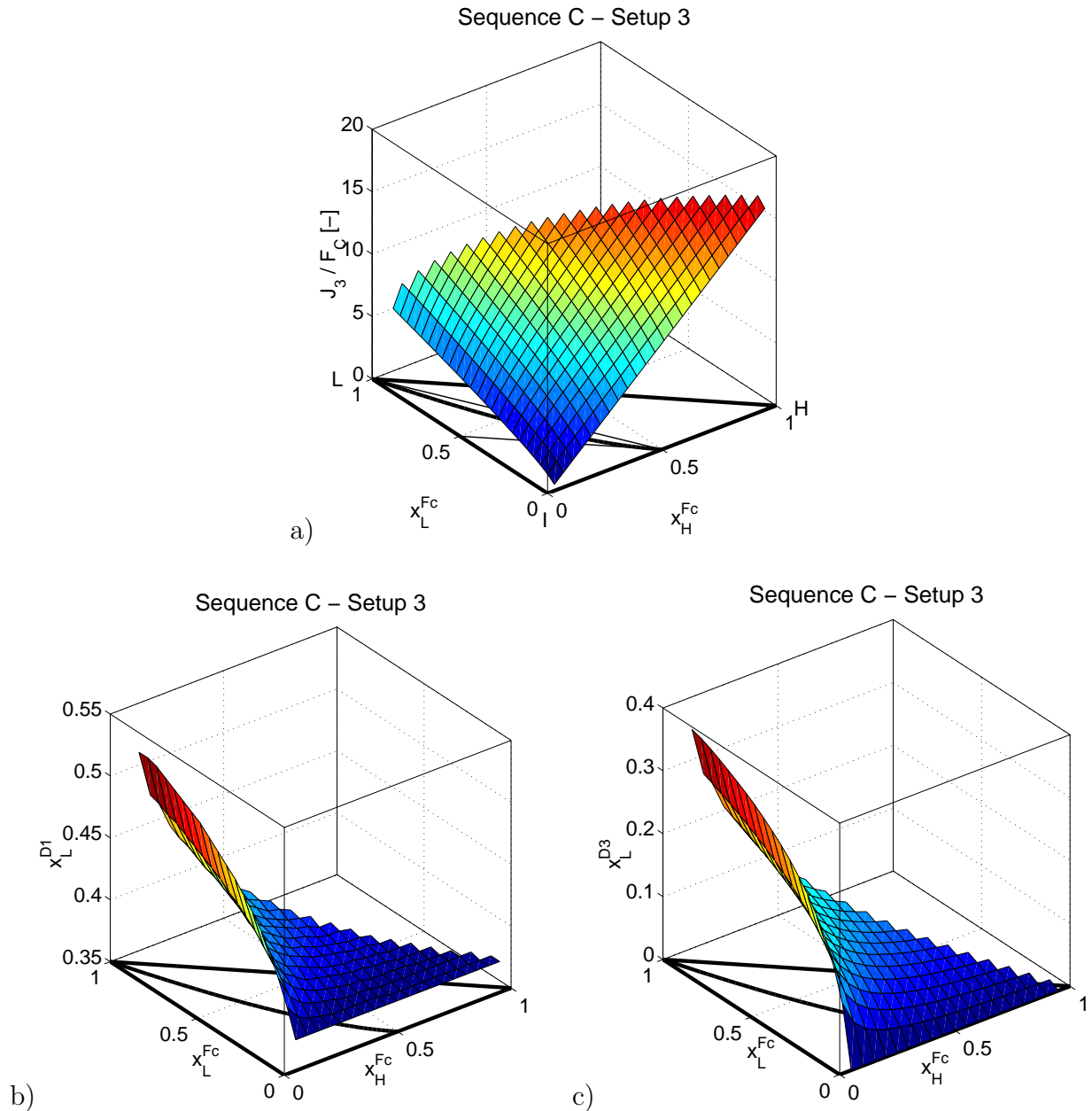


Figure 5.18: Sequence C setup 3: a) cost function J_3^D , b) x_L^{D1} and c) x_L^{D3} as a function of the crude feed composition.

are equal. For binary I-H feeds, D_2^{ex} is zero and x^{D3} being at the I-H azeotrope gives a feasible setup according to the mass balance around column 1 and column 2 (equation 5.32). In this case, the column products and distillate flow rates of setup 3 are equal to the ones of setup 2. For finite columns, the sum of the reboiler duties will be smaller when a binary I-H feed is introduced in column 3 instead of column 2 because the I content of the crude feed does not pass through the reboiler of column 2 if F_C goes directly into column 3.

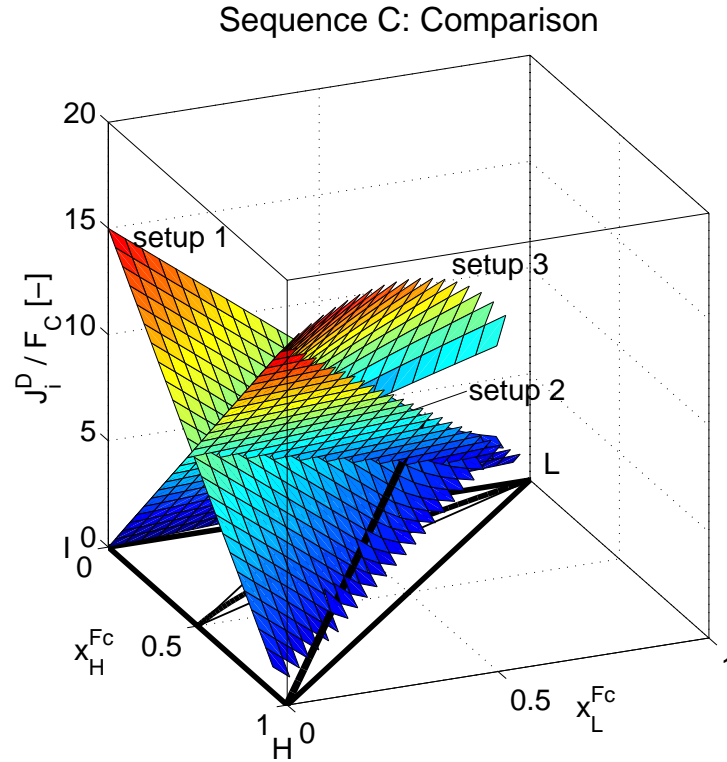


Figure 5.19: Comparison of all three setups of sequence C as shown in Figure 5.17a, Figure 5.17b, and Figure 5.18a for setup 1, setup 2, and setup 3, respectively.

For ternary feeds, setup 3 has the highest operation costs and the most difficult operation behavior. The optimal products x^{D_1} and x^{D_3} are not constant.

Setup 2 has the least energy consumption for high I contents and the best operability because $x^{D_1, opt}$ is feasible for all compositions, while for low I contents, $x^{D_1, opt}$ is not feasible for setup 1. Another reason is that the most important fact for the operation of the scheme is to have x^{D_1} and x^{B_1} on opposite sides of the line connecting x^{D_2} and x^{D_3} . For the residue curve boundary Figure 5.11b, x^{D_1} has to lie left of that line. For setup 2, this is always the case if B_1 is maintained at pure H because by definition x^{F_1} lies on the line connecting x^{D_2} and x^{D_3} . Opposed to that, x^{F_1} will lie on the right side of the line connecting x^{D_2} and x^{D_3} for setup 1 if x^{F_C} lies on the right side of that line, as shown in Figure 5.10b. This is further discussed for a real system in section 6.8.1. Setup 3 has the worst performance of the three schemes and will not be further considered.

5.5 Selection of Controller Pairings

The ∞/∞ sequence has four degrees of freedom and four controlled variables are required for setup 1 and setup 2. Possible candidate controlled variables are only the distillate and bottom flow rates of the columns and the distillate and bottom compositions. Distillate and bottom flow rates should not be controlled variables because they lock the material balance. Hence, only the distillate and bottom compositions remain as candidate controlled variables. For a ∞/∞ column, not all values of the top and bottom composition give a unique ratio D/F . For example, specifying the bottom purity $x_H^{B1} = 1$ will give a type II profile and the ratio D/F is not uniquely defined. Different from that, specifying $x_H^{B1} = 1 - \epsilon$ with ϵ arbitrary small but greater than zero, will give a type III profile with a unique ratio D/F . By this, x^{D1} lies on the boundary. This give the following controller pairings:

1. **Column 1:** D_1 is manipulated to control $x_H^{B1} = 1 - \epsilon$. The column profile is of type III and $x^{D1} \in$ residue curve boundary.
2. **Column 2:** D_2 is manipulated to control $x_L^{D2} = 1 - \epsilon$. The column profile is of type III and x^{B2} lies on the binary I-H edge.
3. **Column 3:** D_3 is manipulated to control $x_I^{B3} = 1 - \epsilon$. The column profile is of type III and x^{D3} is at the binary I-H azeotrope.

This fixes three degrees of freedom. The fourth degree of freedom is fixed by controlling x_L^{D1} . This gives the fourth controller pairing, which is the central controller pairing of the sequence:

4. **Sequence:** R_2 ensures that $x_L^{D1} = x_L^{D1,opt}$ (because of the first controller pairing, $x^{D1} \in$ residue curve boundary).

5.6 Evaluation of the Controlled Variable x^{D_1}

The result of the ∞/∞ analysis is that x^{D_1} is the central variable of the process. The controller of column 1 ensures that x^{D_1} lies on the residue curve boundary. Hence, the L content of x^{D_1} identifies uniquely the location of x^{D_1} . To evaluate the properties of the controlled variable $x_L^{D_1}$, the two disturbances mentioned in section 5.1 are considered:

1. changes in the crude feed composition x^{FC} ,
2. changes in x^{D_3} caused by changes in the interconnecting streams (B_2 and D_3).

5.6.1 Sequence C Setup 1

Manipulation of R_2 can adjust x^{D_1} , but not always reach $x^{D_1, opt}$. Therefore, the influence of R_2 on the sum of the distillate flows J^D is discussed next for fixed, but different crude feeds to analyze the robustness towards disturbance 1). Concerning disturbance 2), the analysis is first done for x^{D_3} at the I-H azeotrope and then repeated if column 3 does not reach the I-H azeotrope in the distillate. The result will be that there is a qualitative change if x^{D_3} is in the non-convex set. Without loss of generality, the calculations are illustrated with the example residue curve boundary (equation 5.17).

5.6.1.1 x^{D_3} at the I-H Azeotrope

Figure 5.20b shows J^D (equation 5.9) as a function of the recycle R_2 for x^{D_3} at the I-H azeotrope for five different crude feed compositions (Figure 5.20a). For the feeds i) to iii), enough “entrainer” L is in the feed such that sequence B ($R_2 = 0$) is also feasible, but not necessarily optimal. For the feeds iv) and v), only sequence C is feasible. In more detail:

- i) x^{FC} is in the infeasible region for $x^{D_1, opt}$. As stated in section 5.4.2.1, the minimum of J^D is at $R_2 = 0$. The slope of the curve is always greater than zero.

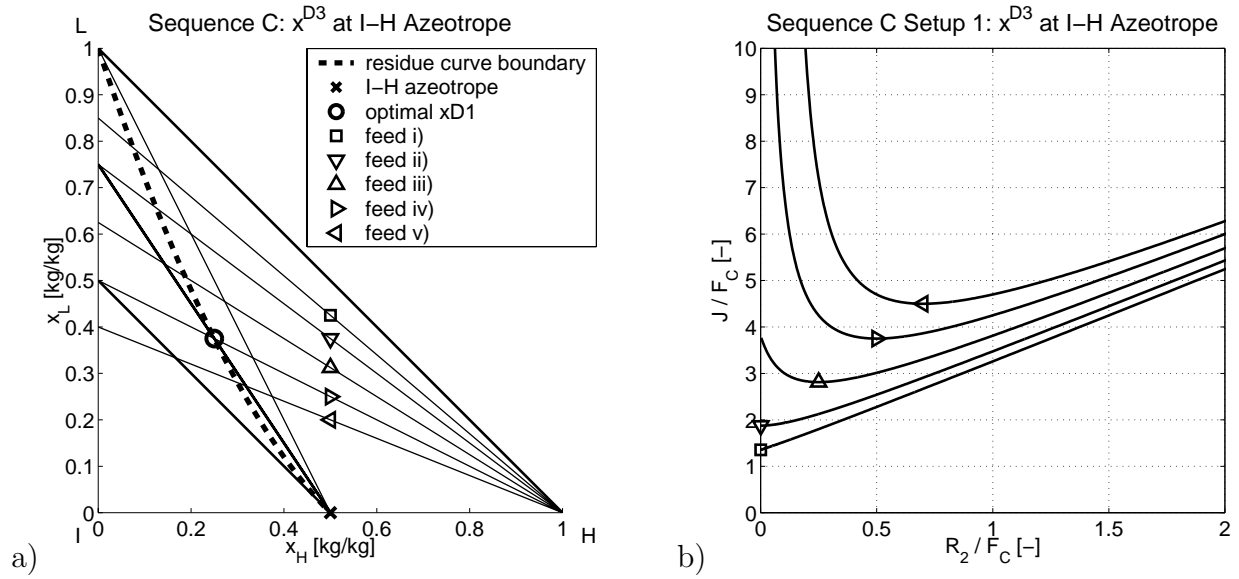


Figure 5.20: Sequence C setup 1 (x^{D3} at I-H azeotrope): a) five different feeds, b) J^D as function of R_2 for five different feed compositions.

- ii) For this feed, $x^{D1, opt}$ is just feasible. Hence, the minimum is also at $R_2 = 0$ with a slope of zero in this point.
- iii) This feed lies in the region where $x^{D1, opt}$ is feasible for sequence C. The minimum of J^D is for $R_2 > 0$.
- iv) For this feed, $x^{D2^{ex}B3}$ lies on the tangent of the residue curve in the I-H azeotrope. For R_2 approaching zero, the sum of the distillates goes to infinity: For $R_2 = 0$, the sequence is infeasible according to definition 4.
- v) For this feed, sequence C is infeasible without any recycle R_2 . J^D goes to infinity as R_2 approaches zero.

In section 5.4.2.1, it was derived that $x^{D1, opt}$ is independent of x^{FC} and that minimizing J^D (equation 5.9) and maximizing d_1 (equation 5.26) are equivalent for all k_i equal. The two plots of Figure 5.21 confirm this. Figure 5.21a shows J^D as a function of the controlled variable x_L^{D1} . For feed i), there is a constraint minimum. For all other feeds, the minimum of J^D is at the same composition x_L^{D1} , but the values of J^D depend on the feed composition x^{FC} , as expected. Figure 5.21b shows d_1 as a function of x_L^{D1} . The optimum is at the same

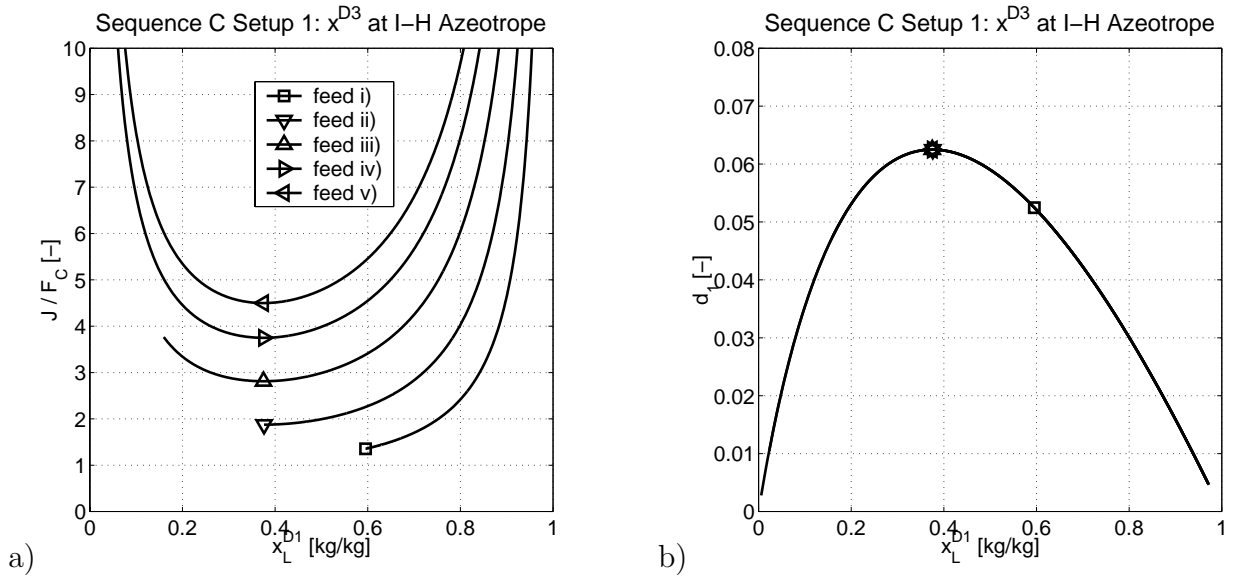


Figure 5.21: Sequence C setup 1 (x^{D3} at I-H azeotrope): a) J^D and b) d_1 as function of controlled variable x_L^{D1} .

location as for J^D . Different from J^D , the optimal value is independent of the crude feed composition. This shows that x_L^{D1} is a good controlled variable (optimal value = 0.375 for the example residue curve).

For the implementation of the controller, the connection between the manipulated and controlled variable has to be analyzed. Figure 5.22a shows the mapping of R_2 on x_L^{D1} . x_L^{D1} is a monotonic function of R_2 . For feed i), $x_L^{D1, opt}$ is not feasible but the minimum of J^D is at $R_2 = 0$. For the feeds ii) to v), $x_L^{D1, opt}$ can be reached. The control law that always reaches the optimal operation point is:

- if $x_L^{D1} > x_L^{D1, opt}$, decrease R_2 until $x_L^{D1, opt}$ is reached or R_2 is zero.
- if $x_L^{D1} < x_L^{D1, opt}$, increase R_2 .

d_1 combines also the information of x^{D2} and x^{D3} with x^{D1} and is an alternative controlled variable. The mapping of R_2 on d_1 is shown in Figure 5.22b. The control law is a bit more difficult: maximize d_1 by manipulating R_2 . Therefore, d_1 should not be used as a controlled variable, but it helps to identify the optimal value of x_L^{D1} : d_1 is a measure for the performance of the sequence that is independent of the crude feed composition x^{FC} .

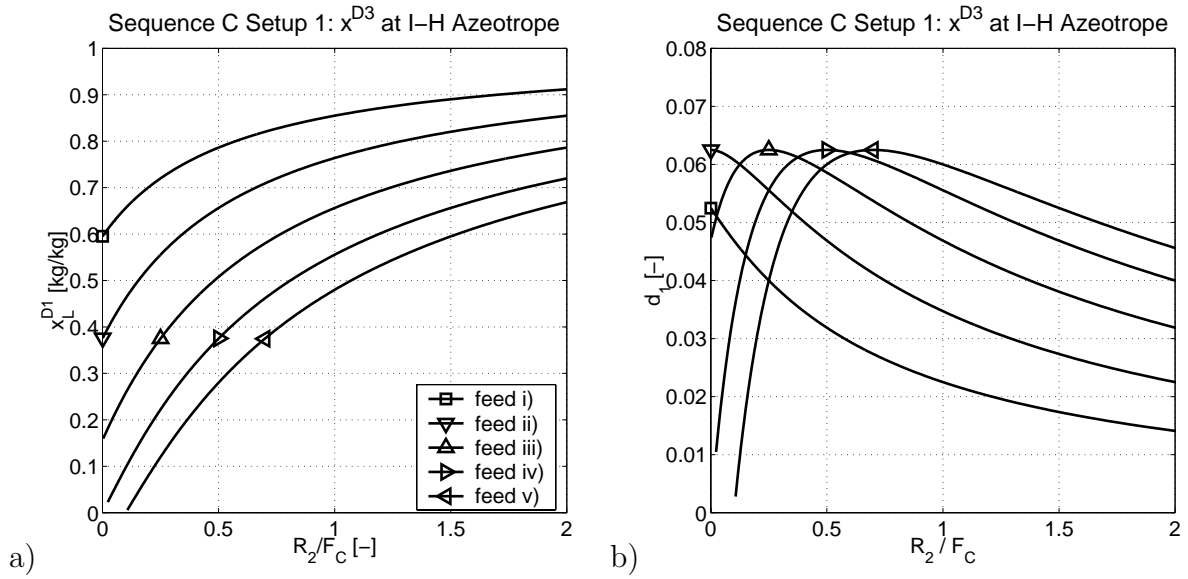


Figure 5.22: Sequence C setup 1 (x^{D3} at I-H azeotrope): a) x_L^{D1} and b) d_1 as function of R_2 .

Qualitatively, all the statements made in this section hold when x^{D3} is not at I-H azeotrope, but on the residue curve boundary. The same also holds when x^{D2} is not at pure L, but on the residue curve boundary. In contrast, there is a qualitative change for x^{D2} or x^{D3} in the non-convex set.

5.6.1.2 x^{D3} in Non-Convex Set

If either x^{D2} or x^{D3} is in the non-convex set, the relations between J^D , R_2 , d_1 and x_L^{D1} will also change qualitatively. If x^{D2} lies in the non-convex set, the profile of column 2 has to be of type II. For the ∞/∞ sequence, this is not possible as discussed in section 5.3.1. But it is possible for finite columns. If x^{D3} lies in the non-convex set, the profile of column 3 will still be a type II profile, which is a feasible ∞/∞ profile. Figure 5.23 shows the same as Figure 5.20 but with $x^{D3} = [0.48; 0]$, i.e., $x^{D3} \in$ non-convex set:

- For feeds I) to III), the same statements hold as for the case that x^{D3} is at the I-H azeotrope.
- For feed IV), the tangent condition to identify the feasible region (section 5.3.2.1)

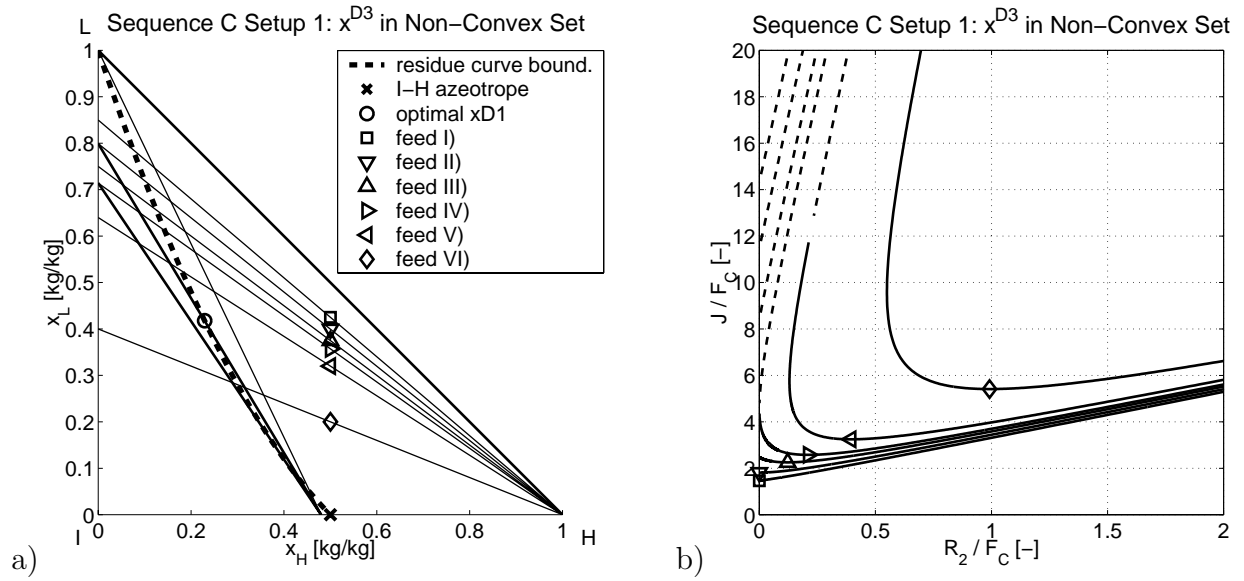


Figure 5.23: Sequence C setup 1 ($x^{D3} = [0.48; 0]$): a) six different feeds, b) J^D as function of R_2 for five different feed compositions.

changes. The mass balance line of column 2 and column 3 is tangent to the residue curve boundary but it does not touch it at the I-H azeotrope, but somewhere else. Therefore, J^D is finite as R_2 goes to zero.

- For feeds V) and VI), a minimum amount of R_2 is required for a feasible operation point of the sequence.
- For all feeds, two solutions exist for a given R_2 and x^{D3} in the non-convex set. The reasons are discussed next.

Second Solution. There are two reasons for the occurrence of the second solution. For the cases indicated with the dashed line, the reason is that x^{M1} can lie in the non-convex set and the mass balance line around column 2 and column 3 crosses the boundary twice (compare Figure 5.9 for $R_2 = 0$). x^{M1} is given as

$$x^{M1} M_1 = x^{D2} R_2 + x^{D3} D_3 \quad (5.37)$$

For $R_2 > 0$ and x^{M1} in the non-convex set, $R_2 + D_3$ has to go to infinity if x^{M1} approaches the residue curve boundary because x^{D1} approaches x^{M1} . For this case, x^{M1} is given by

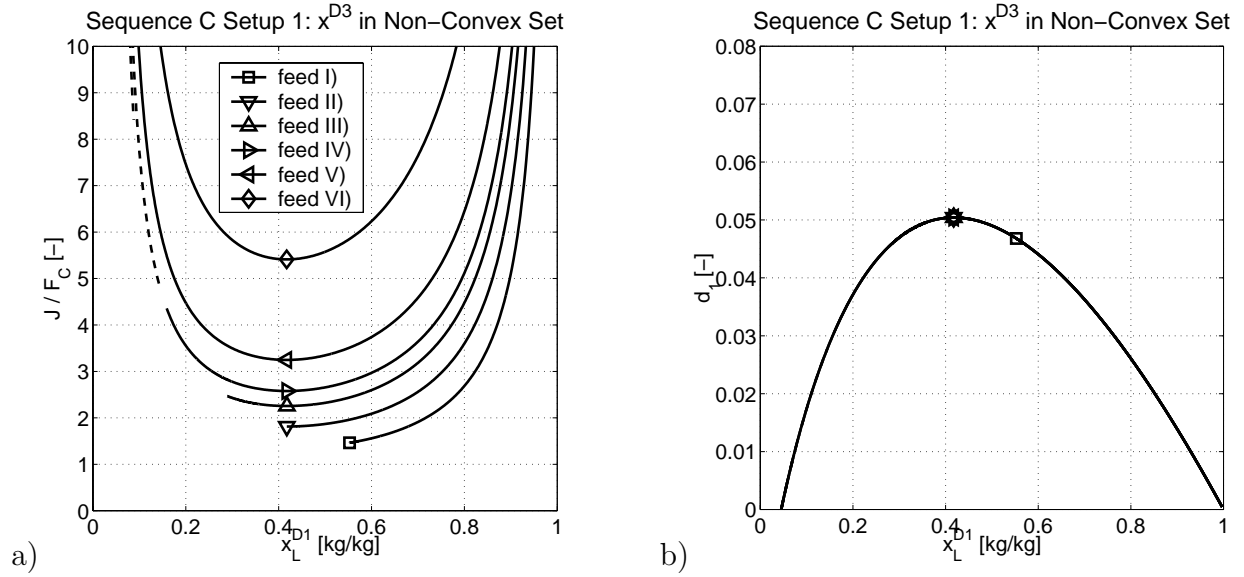


Figure 5.24: Sequence C setup 1 ($x^{D3} = [0.48; 0]$): a) J^D and b) d_1 as function of controlled variable x_L^{D1} .

the overall feed and constant. Equation 5.37 gives that D_3/R_2 is constant for a given x^{M1} . Hence, for R_2 going to infinity, $R_2 + D_3$ has also to go to infinity with the slope $(1 + D_3/R_2)$:

$$M_1 = R_2 + D_3 = R_2 (1 + D_3/R_2) = R_2 (1 + \text{const.}) \quad (5.38)$$

The other reason is: When R_2 is reduced on the lower branch, x^{M1} moves towards x^{D3} and $R_2 + D_3$ goes through a minimum. When x^{M1} goes further towards the boundary, R_2 has to increase again while $R_2 + D_3$ also increases because x^{D1} and x^{M1} move closer to each other. This does not depend on the fact that the mass balance line of column 2 and column 3 may cross the boundary twice at some point, as it does for case V). For case VI), the L content in F_C is too low such that the mass balance of column 2 and column 3 does not cross the residue curve boundary twice.

Controlled Variables. Figure 5.24a shows J^D as a function of the controlled variable x_L^{D1} for x^{D3} in the non-convex set. The difference to the cases with x^{D3} at the I-H azeotrope (Figure 5.21a) are merely that the location of the optimum is shifted: $x^{D1, opt}$ changes as well as the value of the cost function J^D . This is also reflected in d_1 , as shown in Figure 5.24b. The maximum of d_1 is smaller than for x^{D3} at the I-H azeotrope.

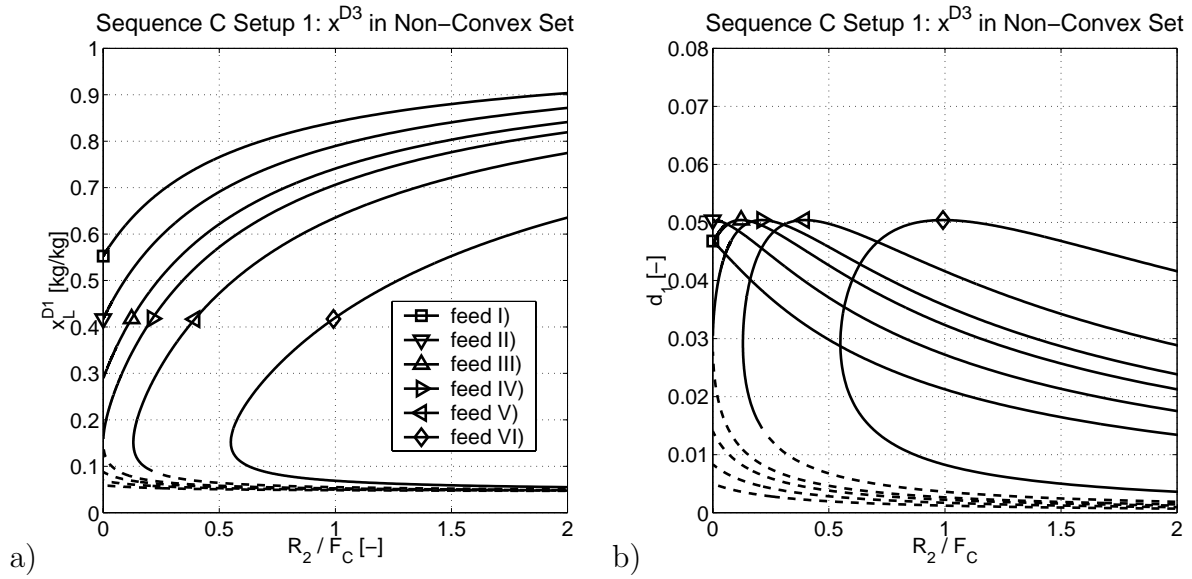


Figure 5.25: Sequence C setup 1 ($x^{D3} = [0.48; 0]$): a) x_L^{D1} and b) d_1 as function of R_2 .

For the implementation of the controller, the change between x^{D3} at the I-H azeotrope and in the non-convex set is drastic caused by the occurrence of the second solution: a fold bifurcation appears. Figure 5.25a shows the mapping of R_2 on x_L^{D1} . For x^{D3} in the non-convex set, there is a big range where x_L^{D1} is a monotonic function of R_2 which can be used for the control algorithm. But at some point, the gain changes sign for R_2 as input and x_L^{D1} as output. This is a fold bifurcation where the stability of the system changes because a pole moves from the left-half plane to the right-half plane. This behavior is introduced by the recycle because the individual columns do not exhibit multiple steady states; hence, they are all stable. Hence, the recycle introduces this behavior. The effect is analog to a multi-variable system with partial feedback control (Jacobsen, 1997; Jacobsen, 1999).

5.6.2 Sequence C Setup 2

The properties of the controlled and manipulated variables change slightly for setup 2. Different from setup 1, the optimal composition of x^{D1} is feasible for all feeds. Equal to setup 1, x_L^{D1} is a monotonic function of R_2 for x^{D3} at the I-H azeotrope, while a second solution appears for the same reason as for setup 1 for x^{D3} in the non-convex set.

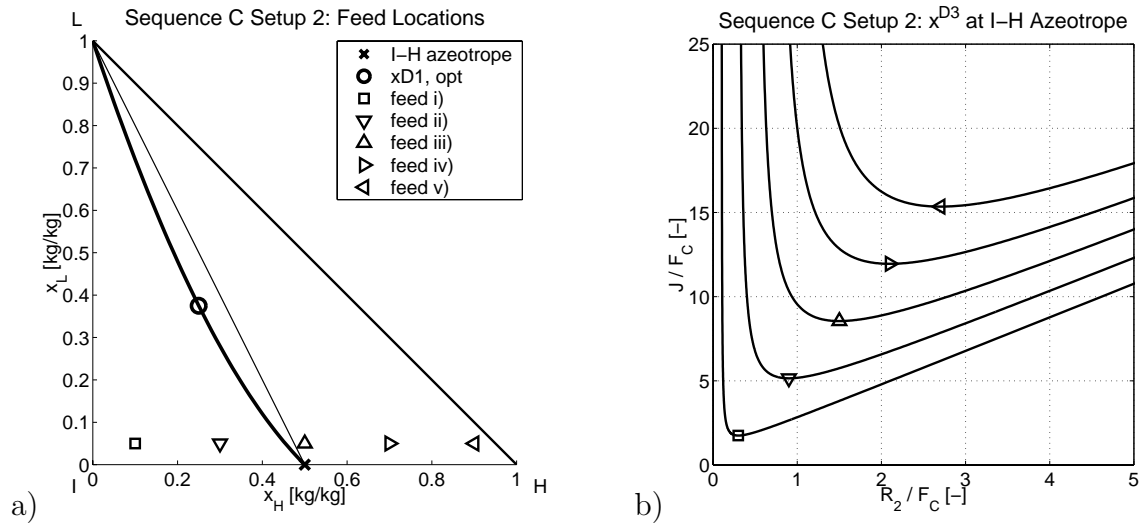


Figure 5.26: Sequence C setup 2 (x^{D3} at I-H azeotrope): a) five different feeds, b) J^D as function of R_2 for five different feed compositions.

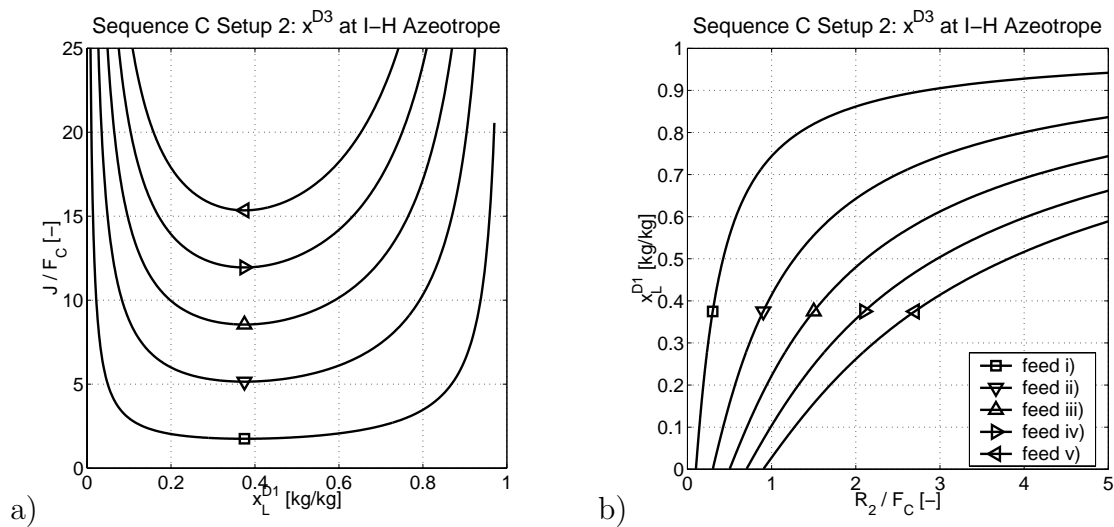


Figure 5.27: Sequence C setup 2 (x^{D3} at I-H azeotrope): a) J^D as function of controlled variable x_L^{D1} , and b) x_L^{D1} as a function of the manipulated variable R_2 .

5.6.2.1 x^{D3} at the I-H Azeotrope

Figure 5.26b shows J^D (equation 5.9) as a function of the recycle R_2 for x^{D3} at the I-H azeotrope for five different crude feed compositions (Figure 5.26a). Figure 5.27a shows J^D as a function of the controlled variable x_L^{D1} . Figure 5.27b shows the relation between the controlled variable x_L^{D1} and the manipulated variable R_2 . As for setup 1, x_L^{D1} is a

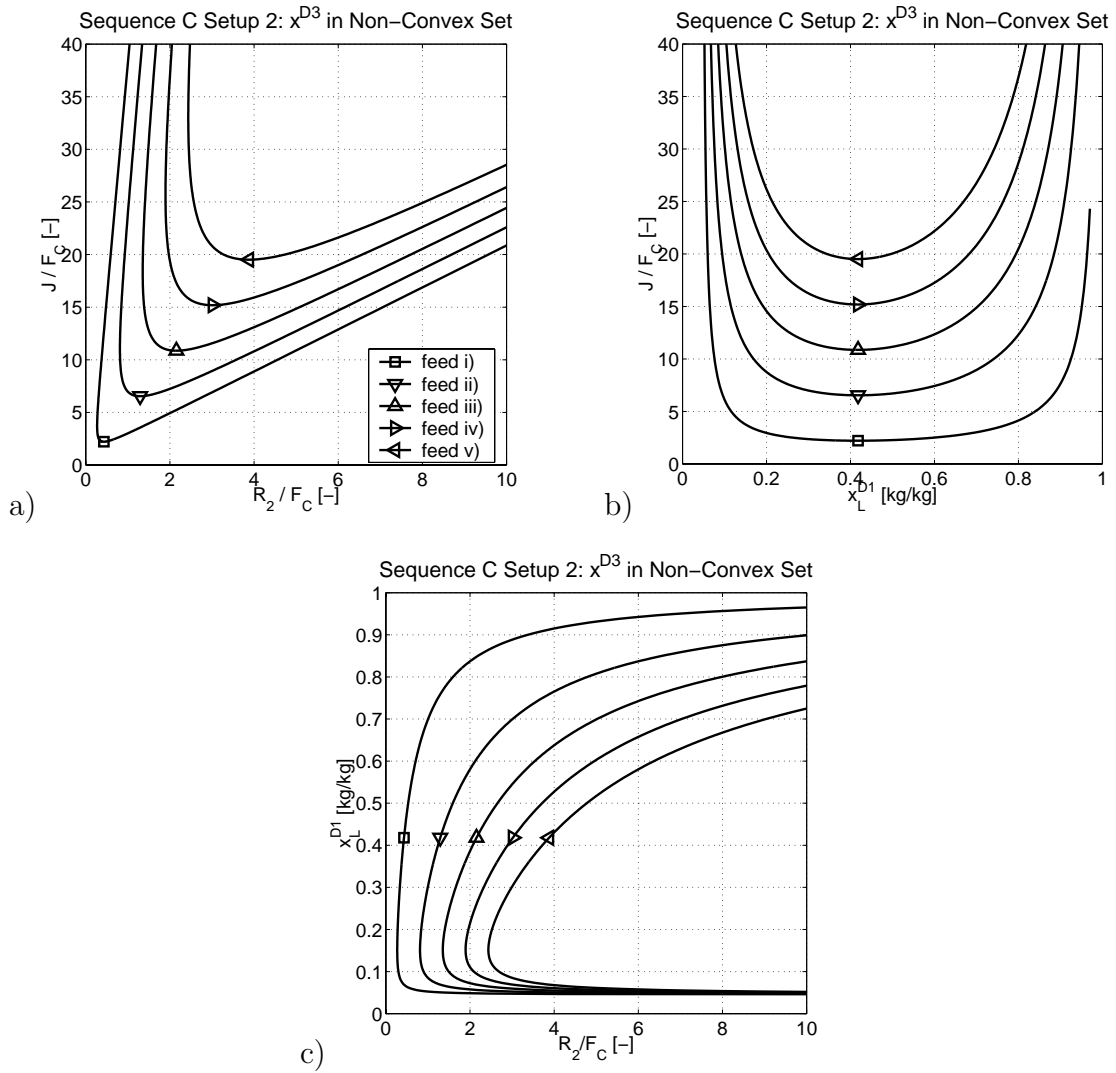


Figure 5.28: Sequence C setup 2 ($x^{D3} = [0.48; 0]$): J^D as function of a) R_2 , and b) x_L^{D1} ; c) x_L^{D1} as a function of R_2 .

monotonic function of R_2 . J^D goes to infinity when x_L^{D1} approaches zero. Interestingly, this is the case when R_2 approaches $x_H^{FC} F_C$. This observation can be proven with $\lim_{x_L^{D1} \rightarrow 0}$ in equation 5.18 and equation 5.30.

5.6.2.2 x^{D3} in Non-Convex Set

Figure 5.28a shows J^D as a function of the manipulated variable R_2 , Figure 5.28b show J^D as a function of the controlled variable x_L^{D1} . As for setup 1, the optimal values are shifted. Figure 5.28c shows the controller pairing with a second solution as for setup 1.

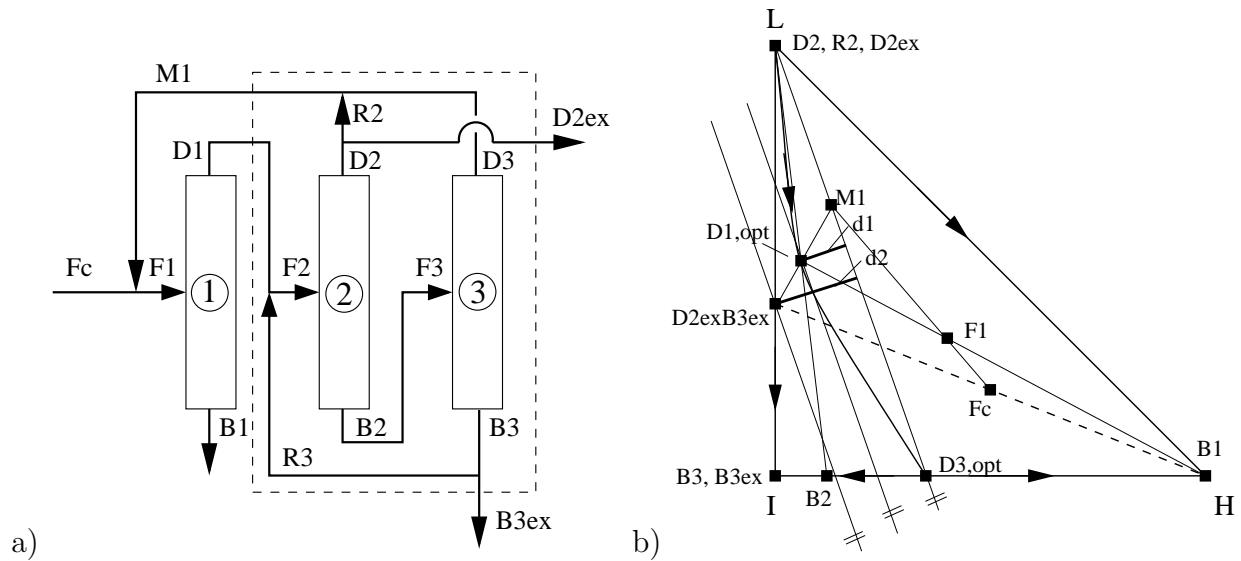


Figure 5.29: Extension: boundary separation scheme with three recycles.

5.7 Boundary Separation Scheme with Three Recycles

Using the ∞/∞ analysis, R_2 was identified as the key variable for operation of sequence C. As discussed in section 5.4.2, R_2 reduces the sum of the distillate flows for feed compositions in region 2 (Figure 5.16). Another option as suggested by Stichlmair (stated by Laroche et al. (1992b) as personal communication) is to use a product recycle R_3 that places F_2 away from the boundary into the non-convex set. Laroche et al. (1992b) state that such a setting might lead to improved economic operation. Figure 5.29a shows this three column system with three recycles. This configuration does not reduce the sum of the distillate flows J^D . In section 5.4.2, it was shown that J^D is minimal if d_1 is maximized. Figure 5.29b shows that d_1 does not depend on R_3 because R_3 lies inside the subsystem shown in Figure 5.29a. Hence, the three distillate flows D_1 , D_2 , and D_3 do also not depend on R_3 and R_3 has no influence on the cost function of the ∞/∞ column. If the columns were operated with constant reflux-to-distillate ratios, the recycle R_3 would change the k_i such that the sum of the reboiler duties will be increased. The minimum of the reboiler duties will then be at $R_3 = 0$.

Moreover, the third recycle suggests that the boundary separation scheme might also be

feasible for a straight boundary because the feed to column 2 is placed into the non-convex set even for a straight boundary². However, the mass balance around the dashed subsystem (Figure 5.29a) shows that this sequence is also infeasible for a straight boundary: Though R_3 places F_2 into the non-convex set, the net flux through the boundary is zero for a straight boundary because x^{D_1} and x^{M_1} have to lie at the same point in that case. Then, $D_1 = R_2 + D_3$. Hence, D_2^{ex} and B_3^{ex} is zero independent of R_3 .

In operation of the sequence, R_3 might be useful. If x^{D_1} moves such that $d_1 < 0$ (caused by e.g. a disturbance), R_3 might be used to place the feed to column 2 such that the disturbance in column 1 is not propagated to column 2 and column 3. This can be implemented with an override controller that ensure that x^{F_2} is at the desired point until x^{D_1} returns to that desired point.

Another idea based on the work of Bausa and Tsatsaronis (2001) is to use a cyclic operation of D_1 or R_3 to reduce the recycle flows by changing the mass balances. However, these changes are symmetrical and hence the average flux over the boundary remains constant.

²Note that for a straight boundary the term non-convex set is not exact anymore. For a straight boundary, the non-convex set is in this case defined as the area spanned by L, I, and the I-H azeotrope.

Chapter 6

Design and Control of the Finite Boundary Separation Scheme

The results of the ∞/∞ analysis are used to propose a self-optimizing design and operation scheme of the boundary separation scheme separating the mixture methanol (L)/2-propanol (I)/water (H). As discussed in chapter 5, Sequence C is the core sequence of the boundary separation scheme. The design procedure is applied to setup 1 with the column design as shown in Figure 5.1 for a base case feed (Table 6.1). The control concept is hierarchical. Based on steady state considerations, the controlled variables are identified as a first layer (section 6.1 – section 6.5). Further, the performance of the controlled variables and the robustness towards implementation and modeling errors are analyzed using steady state simulations (section 6.6 – section 6.7). In a second layer, simple single-loop PID controllers are implemented for the selected controller pairing. These simple decentralized PID controllers keep the process at the chosen operation points (section 6.8).

6.1 Degrees of Freedom

A homogeneous column without side stream has two degrees of freedom at steady state for a fixed design, fixed column pressure and fixed feed condition (Skogestad, Lundström and Jacobsen, 1990). Hence, the sequence has six degrees of freedom for the three columns and

Table 6.1: Base case crude feed F_C for the mixture methanol/2-propanol/water.

flow rate	$x_{methanol}$	$x_{2-propanol}$	x_{water}	pressure	temperature
1 kg/h	0.333 kg/kg	0.333 kg/kg	0.334 kg/kg	1.1 bar	20° C

another one for the additional recycle R_2 giving seven degrees of freedom. As discussed in section 5.3.2, recycling of D_3 does not change the degrees of freedom.

6.2 Cost Function and Constraints

For a fixed design, the cost function to be minimized is the sum of the reboiler duties (equation 5.1). As discussed in section 5.2, the cost function can be rewritten as the sum of the distillate flows with simplifying assumptions. In this case, minimizing the cost function J is equivalent to maximizing d_1 (defined by equation 5.26), which is a second objective function besides the cost function J . The advantage of d_1 is two fold. First, d_1 determines the feasibility of the sequence (section 5.4.2.1). Second, d_1 is an absolute measure of the performance of the scheme which is independent of the crude feed composition x^{F_C} as derived in section 5.6.1.1. The constraints are the product purities (equation 5.2, equation 5.3, and equation 5.4).

6.3 Identification of Important Disturbances

Two main disturbances are considered:

- 1) changes in the crude feed condition (flow rate and composition),
- 2) changes in the interconnecting streams caused by rejection of the crude feed disturbances or pressure fluctuations that give different compositions of the azeotrope which might change x^{D_3} .

The main model uncertainty to be considered is the uncertainty of the curvature of the residue curve boundary.

6.4 Optimization

The sequence has seven degrees of freedom for fixed pressures (1.1 bar, 1 bar and 1 bar for columns 1, 2, and 3, respectively). The optimization of the sequence is simplified using the results of the ∞/∞ analysis. The optimal solution of the ∞/∞ boundary separation scheme gave seven conditions (section 5.4.2):

- 1) x^{B_1} at pure water (compare equation 5.2),
- 2) x^{D_2} is at pure methanol (compare equation 5.3),
- 3) x^{B_3} at pure 2-propanol (compare equation 5.4),
- 4) x^{D_3} at the binary 2-propanol–water azeotrope,
- 5) x^{B_2} on binary 2-propanol–water edge,
- 6) x^{D_1} on the residue curve boundary,
- 7) x^{D_1} such that the sum of the distillates is minimal.

The first three conditions (three constraints on the output purities) are easy to implement. The next two are also easy: x^{D_3} close to the azeotrope and $x_{methanol}^{B_2}$ very small (the exact value has to be found by optimization). Further, R_2 can be varied to find the optimal value of x^{D_1} . For the last degree of freedom, the internal flows of column 1 (L_1) need to be varied such that x^{D_1} lies close to the residue curve boundary.

For the optimization, the specifications L_1 , R_2 , x^{B_2} , and x^{D_3} are varied in pairs. First, the two variables L_1 and R_2 , which directly influence column 1, are varied for fixed x^{B_2} and x^{D_3} . Then x^{B_2} and x^{D_3} , which are strongly coupled via the methanol(L) balance, are varied for constant L_1 and R_2 . With the optimal values of x^{B_2} and x^{D_3} , L_1 and R_2 are varied

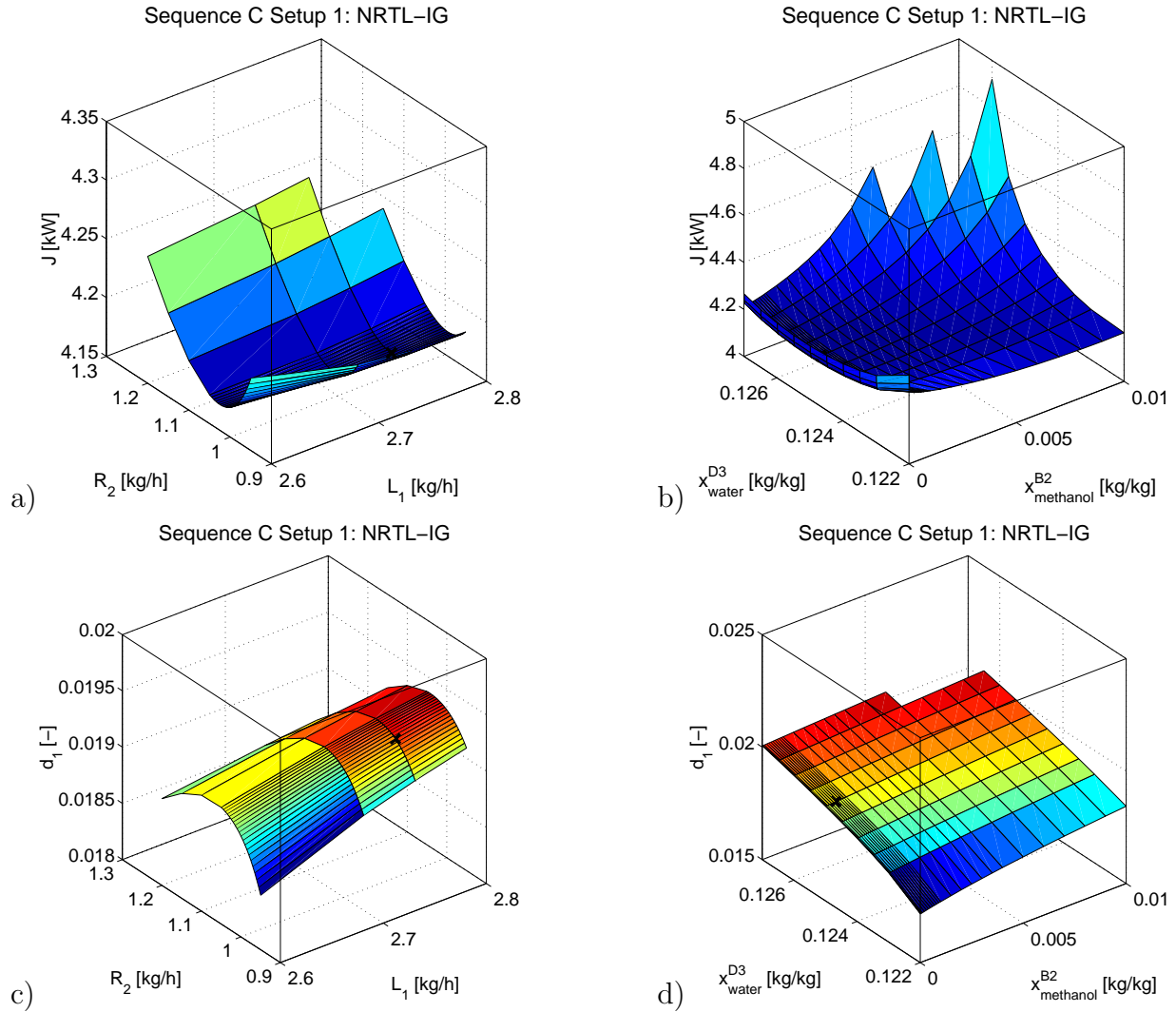


Figure 6.1: Sequence C setup 1: J and d_1 for varying L_1 and R_2 (NRTL-IG parameter set): a) and c), and for varying specifications of x^{B2} and x^{D3} : b) and d).

again to identify the optimal point. Using the new optimal values of L_1 and R_2 , x^{B2} and x^{D3} are varied again. Further iterations showed that the minimum of the objective function does not change anymore. The results are shown in Figure 6.1a and Figure 6.1c. Table 6.2 lists the optimal parameters (the specified variables are the specifications in AspenPlus, and the manipulated variable are the variables that the steady state solver of AspenPlus varies to find the solution). Alternatively, all four variables can be optimized at once with an implemented optimizer in AspenPlus. However, convergence is difficult mainly because of the flat optimum for three of the four variables: L_1 , x^{B2} , and x^{D3} .

Table 6.2: Optimal parameters of sequence C setup 1 for the NRTL-IG parameter set and the base feed (Table 6.1).

specified variable	value	manipulated variable	value
$x_{water}^{B_1}$	0.9998 kg/kg	D_1	2.167 kg/h
L_1	2.7 kg/h	L_1	2.7 kg/h
R_2	1.004 kg/h	R_2	1.004 kg/h
$x_{methanol}^{D_2}$	0.9998 kg/kg	D_2	1.337 kg/h
$x_{methanol}^{B_2}$	0.0005 kg/kg	Q_2^R	2.053 kW
$x_{2-propanol}^{B_3}$	0.9998 kg/kg	B_3	0.333 kg/h
$x_{water}^{D_3}$	0.125 kg/kg	Q_3^R	0.720 kW

Table 6.3: Relation between Q_i^R and D_i at the optimal operation point for NRTL-IG parameter set and the base feed (Table 6.1).

column	Q_i^R	D_i	k_i
1	1.403 kW	2.160 kg/h	0.650 kW/(kg/h)
2	2.047 kW	1.333 kg/h	1.536 kW/(kg/h)
3	0.719 kW	0.494 kg/h	1.455 kW/(kg/h)

Figure 6.1c shows the second objective function, d_1 , as a function of L_1 and R_2 . It shows that the maximum of d_1 is close to the minimum of the sum of reboiler duties. This is, however, not exact. These two extrema only coincide for k_i equal, which is not the case in reality as shown by Table 6.3, and for the distillate composition of the finite column 1 lying on the residue curve boundary, which is also only an approximation. Figure 6.1d shows d_1 as function of $x_{methanol}^{B_2}$ and $x_{water}^{D_3}$. Here, the connection between J and d_1 is not as pronounced as for L_1 and R_2 .

6.5 Selection of Controlled Variables

The finite sequence has seven degrees of freedom. Therefore seven controlled and seven manipulated variables are needed. Candidates for controlled variables are all internal and

external column flow rates (reflux, vapor flow/reboiler duty, distillate, and bottom and R_2), all internal and external compositions (stage compositions and distillate and bottoms compositions) and the stage temperatures. Candidates for manipulated variables are all internal and external column flow rates (reflux, vapor flow/reboiler duty, distillate, and bottom and R_2). Concerning the steady state properties of a column, there is no difference between specifying the distillate flow rate and reboiler duty, specifying reflux and bottom flow rate or specifying any other pairing of the four variables as manipulated variables. They all have the same steady state properties when special cases such as multiplicities caused by the nonlinear mass-to-molar transformation (Jacobsen and Skogestad, 1991; Jacobsen and Skogestad, 1994; Jacobsen and Skogestad, 1995) are excluded. For the design of the first layer, only the steady state properties are of interest. For convenience, the seven manipulated variables of Table 6.2 are chosen at this point as manipulated variables. Concerning the dynamics of the control scheme, the choice of manipulated variables also has an impact. This will be discussed in section 6.8.

The results of the ∞/∞ analysis are used to derive a set of controlled variables. An ∞/∞ column has one degree of freedom and specifying for example the bottom composition at $1 - \epsilon$ gave one particular distillate composition. A distillation column of finite length and finite reflux has two degrees of freedom for a fixed length. This adds one degree of freedom per column to the sequence. Hence, seven controlled variables are needed for the finite sequence. The first five of the seven requirements of the ∞/∞ sequence can be directly transferred into a set of controlled variables: $x_{water}^{B_1}$, $x_{methanol}^{D_2}$, $x_{2-propanol}^{B_3}$, $x_{methanol}^{B_2}$, and $x_{water}^{D_3}$. Only the conditions for x^{D_1} are a bit more difficult to transfer. If x^{D_1} lies on the residue curve boundary, the position of x^{D_1} is uniquely identified by the methanol content of x^{D_1} giving the sixth controlled variable: $x_{methanol}^{D_1}$.

To fulfill the seventh condition, the reflux of the column must be high enough to keep the column profile close to the boundary. Skogestad (2000b) reports that for a distillation column, which separates a binary feed, a constant reflux-to-feed ratio is slightly superior to a constant reflux-to-distillate ratio. However, a result of the recycles in the system is that D_1 and $F_1 = F_C + R_2 + D_3$ are closely related. Hence, a constant reflux-to-distillate ratio is good choice in this case for a self-optimizing controlled variable. This is actually

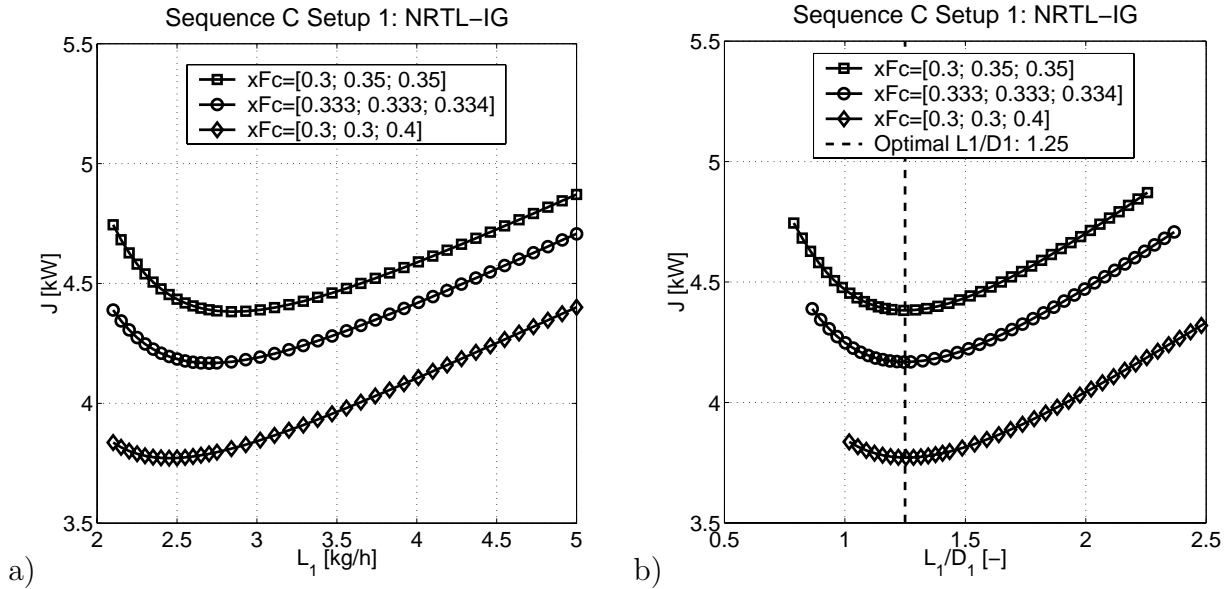


Figure 6.2: Sum of reboiler duties for three different feeds [methanol; 2-propanol; water] as function of a) reflux L_1 and b) reflux ratio L_1/D_1 .

confirmed by the following case study. The reflux L_1 is varied keeping the six controlled variables constant (five at the values given in Table 6.2 and $x_{methanol}^{D_1} = 0.617$ kg/kg). Figure 6.2 shows the sum of reboiler duties as a function of the reflux L_1 for different feed compositions. The optimal reflux L_1 is a function of the water content in the crude feed, but as expected the optimal reflux ratio L_1/D_1 does not depend on the crude feed composition. The optimal reflux-to-distillate ratio is 1.25 for NRTL-IG parameter set. For a more robust convergence behavior of the sequence, 1.3 was chosen in the case studies. Table 6.4 shows the resulting set 1 with the optimal values.

Table 6.4 also lists two more sets of controlled variables. The idea behind set 2 is that the composition of the feed to column 2 (x^{D_1}) is constant at the optimal point, only the flow rate varies. For specified purities of the products of column 2, the split is constant. Hence, the internal flows are proportional to the feed. In this case, the reflux-to-distillate ratio is independent of the crude feed composition. The same applies to column 3. Another option is to keep the reflux at a high but constant value to allow simple one-point control. Therefore, set 3 is also discussed. In practice, the columns are operated with a higher reflux to increase robustness. Therefore, set 2 and set 3 are also analyzed for a reflux increased by 20% (set 2a and set 3a). Internal compositions and stage temperatures are

Table 6.4: Sets of controlled variables for sequence C setup 1 for NRTL-IG.

set 1		set 2 (a)		set 3 (a)	
variable	value	variable	value	variable	value
$x_{water}^{B_1}$	0.9998 kg/kg	$x_{water}^{B_1}$	0.9998 kg/kg	$x_{water}^{B_1}$	0.9998 kg/kg
$x_{methanol}^{D_1}$	0.617 kg/h	$x_{methanol}^{D_1}$	0.617 kg/h	$x_{methanol}^{D_1}$	0.617 kg/h
L_1/D_1	1.3	L_1/D_1	1.3 (1.56)	L_1	2.8 (3.36) kg/h
$x_{methanol}^{D_2}$	0.9998 kg/kg	$x_{methanol}^{D_2}$	0.9998 kg/kg	$x_{methanol}^{D_2}$	0.9998 kg/kg
$x_{methanol}^{B_2}$	0.0005 kg/kg	L_2/D_2	4.05 (4.86)	L_2	5.4 (6.48) kg/h
$x_{2-propanol}^{B_3}$	0.9998 kg/kg	$x_{2-propanol}^{B_3}$	0.9998 kg/kg	$x_{2-propanol}^{B_3}$	0.9998 kg/kg
$x_{water}^{D_3}$	0.125 kg/kg	L_3/D_3	5.10 (6.12)	L_3	2.5 (3) kg/h

Table 6.5: Three crude feeds used in the case studies (p=1.1 bar, T= 20° C).

	flow rate	$x_{methanol}$	$x_{2-propanol}$	x_{water}
feed 1	1 kg/h	0.6 kg/kg	0.066 kg/kg	0.334 kg/kg
feed 2	1 kg/h	0.5 kg/kg	0.166 kg/kg	0.334 kg/kg
feed 3	1 kg/h	0.333 kg/kg	0.333 kg/kg	0.334 kg/kg

not considered here, but in section 6.8.

6.6 Evaluation of the Sets of Controlled Variables

The purpose of this section is two fold. First, the different sets are studied to evaluate them and to lay the basis for the second control layer, which is discussed in section 6.8; and second, the results of chapter 5 are validated with rigorous simulations. Sequence C setup 1 set 1 is studied for three different feeds (Table 6.5) with respect to the key controlled variable $x_{methanol}^{D_1}$. Each of these feeds lies in a region that gives a qualitatively different behavior as derived in section 5.4.2.1. For the methanol–2-propanol–water mixture, the three regions are shown in Figure 6.3. For each of these feeds, the five different sets of controlled variables are compared to each other.

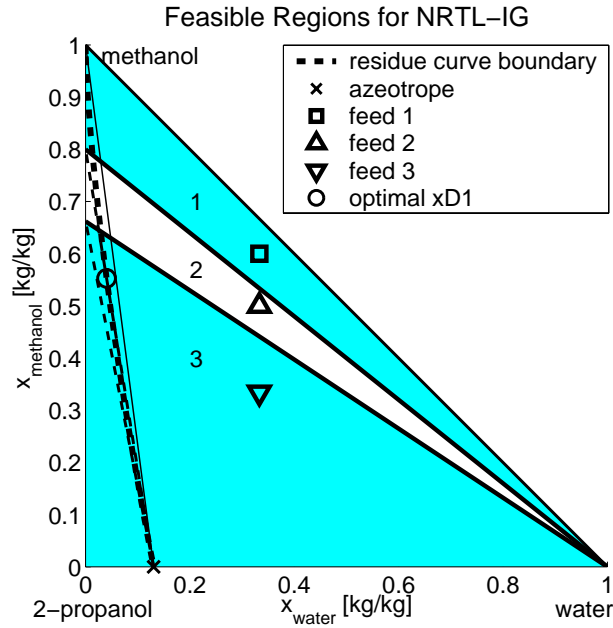


Figure 6.3: Three feed regions of sequence C setup 1 as derived in section 5.4.2.1 for the methanol–2-propanol–water mixture (NRTL-IG). The three feeds are given in Table 6.5.

6.6.1 Set 1

Figure 6.4 shows the cost functions J and the objective function d_1 for the three qualitatively different feeds as a function of the controlled variable $x_{methanol}^{D_1}$ for set 1 (Table 6.4). For feed 2 and feed 3, J has a flat minimum, which is indicated by the symbol. In this case, $x_{methanol}^{D_1}$ is a good controlled variable. For feed 1, $x_{methanol}^{D_1}$ is constrained. This is also easy to implement in this case because R_2 is zero at the minimum value of $x_{methanol}^{D_1}$ (Figure 6.5a). Figure 6.4 confirms the prediction of the ∞/∞ analysis that the optimal value of J depends on the crude feed composition while d_1 is independent of that for compositions in region 2 and region 3. The symbol indicates the location of the minimum of J in Figure 6.4b. The maximum of d_1 is close to that point. This confirms that d_1 is a good and independent measure for the performance of the process.

The mapping of R_2 to $x_{methanol}^{D_1}$ (Figure 6.5a) is further investigated. x^{D_3} lies in the non-convex set. The predictions of the ∞/∞ analysis for this case (section 5.6.1.2) are well confirmed for the finite column for feeds in region 1 and 2 ($R_2 = 0$ is feasible). For feeds in region 3, the ∞/∞ analysis predicted that a fold bifurcation will occur (Figure 5.25b).

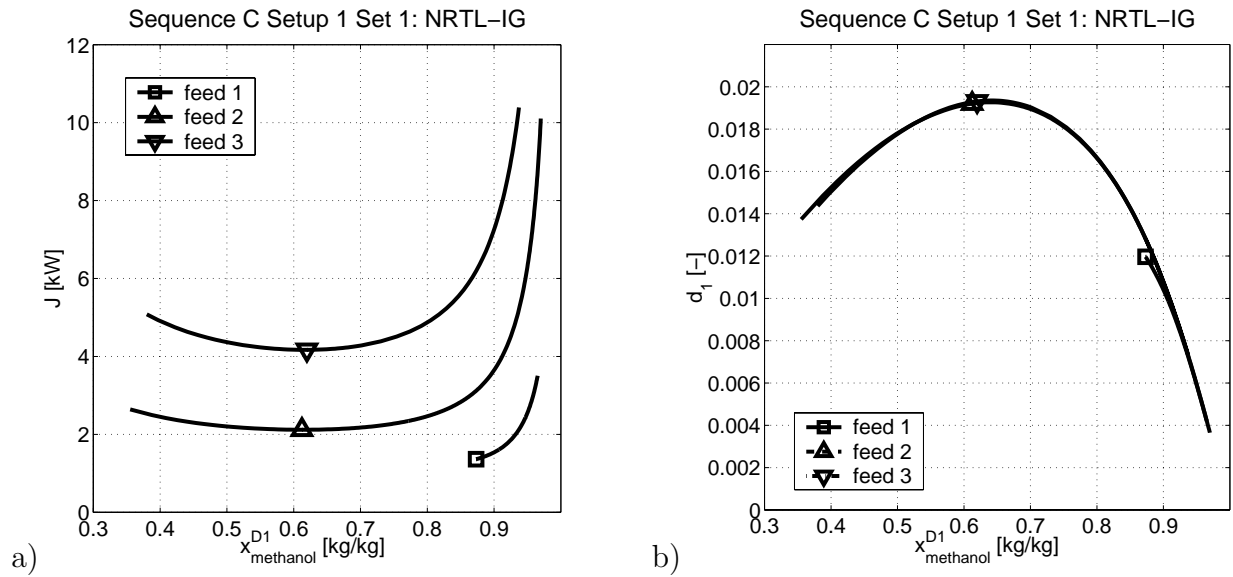


Figure 6.4: Sequence C setup 1 set 1: a) J and b) d_1 as a function of the controlled variable $x_{methanol}^{D1}$.

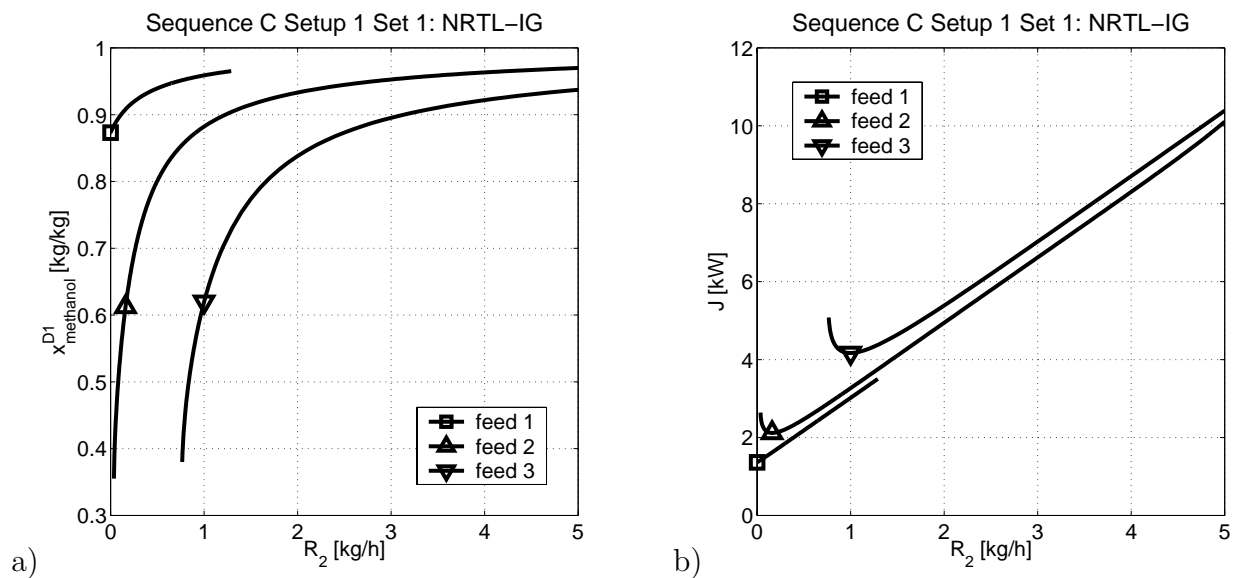


Figure 6.5: Sequence C setup 1 set 1: a) $x_{methanol}^{D1}$ and b) J as a function of R_2 .

For this feed, it was not possible to converge the sequence for $x_{methanol}^{D1} < 0.38$ by varying R_2 . In AspenPlus Version 10.2.1, the sequence is converged sequentially with a block oriented solver. Tear streams are defined: R_2 and D_3 . The blocks (the columns) are solved sequentially for the current values of the tear streams. After one loop has been calculated, the R_2 is adjusted by the solver to match the specified value of $x_{methanol}^{D1}$. This procedure

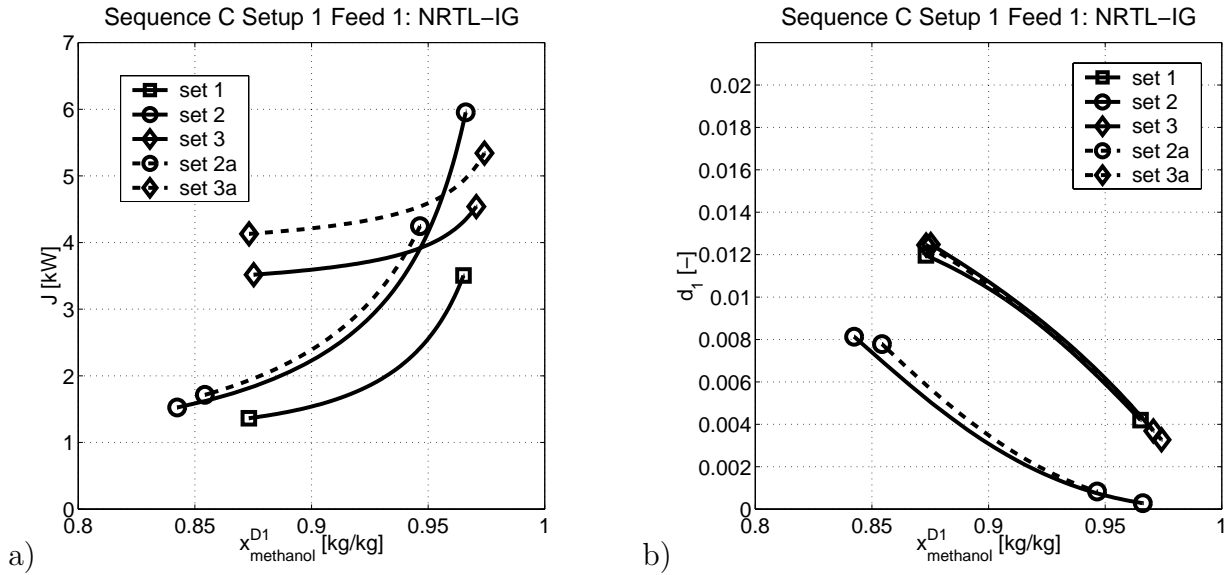


Figure 6.6: Sequence C setup 1 feed 1: Comparison of the different sets of controlled variables for a) J and b) d_1 as a function of $x_{methanol}^{D1}$.

is similar to a discrete time controller, which controls $x_{methanol}^{D1}$ by manipulation of R_2 , with the assumption that the columns are operated with perfect two-point control. The failing of convergence for $x_{methanol}^{D1} < 0.38$ might indicate instability of the sequence for these operation points (see also appendix B.2.3). This is consistent with the prediction of the ∞/∞ analysis. For completeness, Figure 6.5b shows J as a function of R_2 to confirm Figure 5.23b. This analysis is repeated for set 2 and set 3 (appendix B.2.2). It is however more interesting to compare the sets directly for the different feeds.

6.6.2 Feed 1

Figure 6.6 shows J and d_1 for the different sets of controlled variables for feed 1 (Table 6.5). Set 1 is the best alternative with the minimal energy consumption. Set 2 and set 2a have higher energy consumptions and lead to different locations of the optimal point. At these points, the loss of set 2 and set 2a is acceptable. Set 3 and set 3a have an unacceptable performance mostly because the refluxes are not adjusted to this feed.

Figure 6.7 shows the dependence of the controlled variable $x_{methanol}^{D1}$ and of the cost function

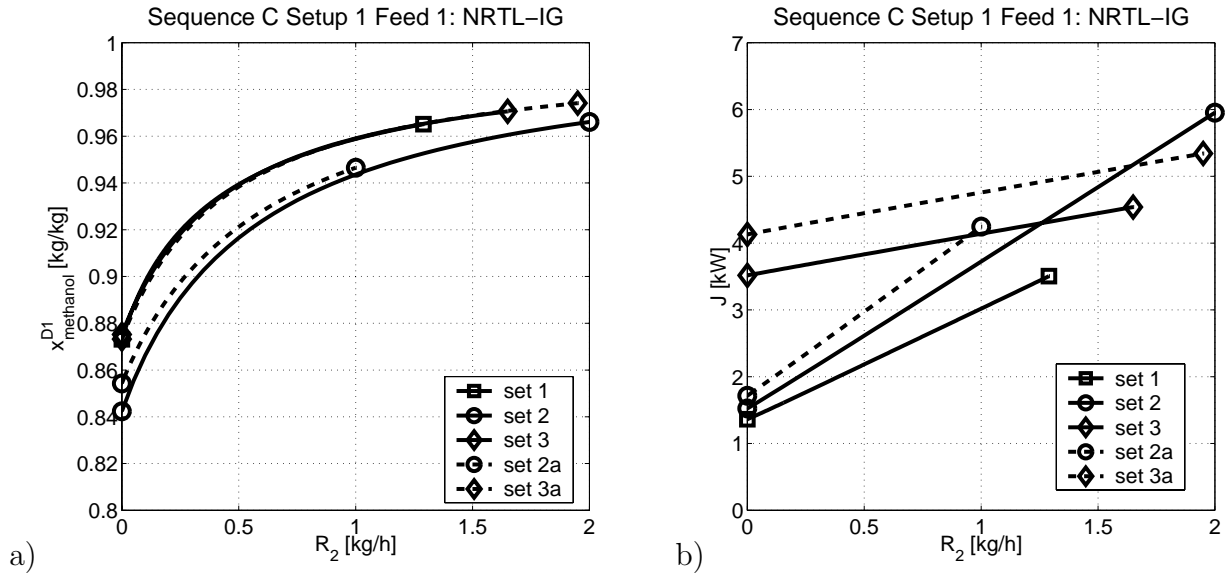


Figure 6.7: Sequence C setup 1 feed 1: Comparison of the different sets of controlled variables for a) $x_{methanol}^{D1}$ and b) J as a function of R_2 .

J on the manipulated variable R_2 for feed 1. Independent of the set, the optimal value is at R_2 equal to zero as predicted by the ∞/∞ analysis.

6.6.3 Feed 2

Figure 6.8 shows J and d_1 for the different sets of controlled variables for feed 2 (Table 6.5). As for feed 1, set 1 is the best alternative and sets 2 and 2a have an acceptable loss. Figure 6.8a shows that J is nearly constant for set 3a and hits the optimal set (set 1) at $x_{methanol}^{D1} = 0.9$. Crossing is not possible because the refluxes would be too small too reach the other process specifications.

Figure 6.9 shows the dependence of the controlled variable $x_{methanol}^{D1}$ and of the cost function J on the manipulated variable R_2 for feed 2. As for feed 1, the predictions of the ∞/∞ analysis are validated. The optimal point is at a positive value of R_2 and R_2 equal to zero is also a possible operation point for all sets except set 2. Here, the refluxes are too small too reach the other process specifications for small values of R_2 .

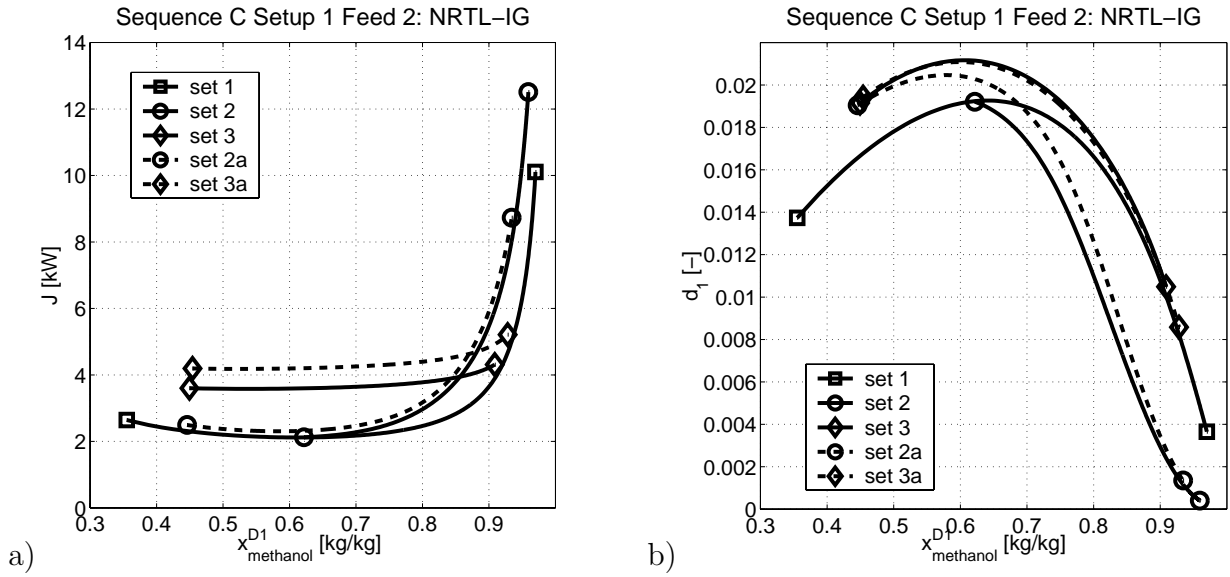


Figure 6.8: Sequence C setup 1 feed 2: Comparison of the different sets of controlled variables for a) J and b) d_1 as a function of $x_{methanol}^{D1}$.

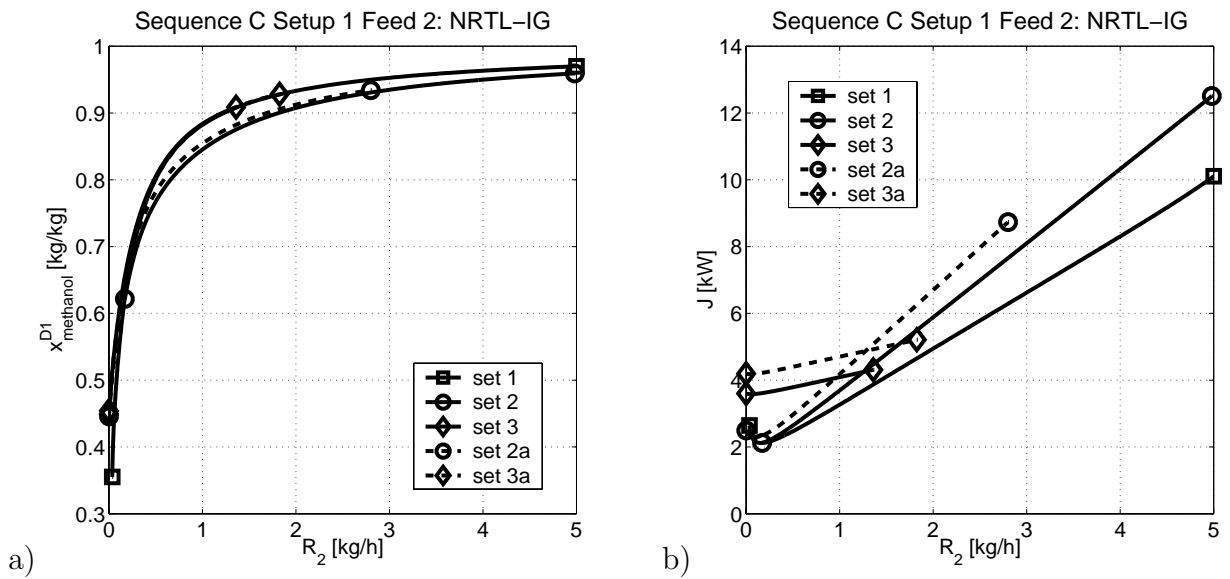


Figure 6.9: Sequence C setup 1 feed 2: Comparison of the different sets of controlled variables for a) $x_{methanol}^{D1}$ and b) J as a function of R_2 .

6.6.4 Feed 3

Figure 6.10 shows J and d_1 for the different sets of controlled variables for feed 3 (Table 6.5). As for feed 1 and feed 2, set 1 is the best alternative and sets 2 and 2a have an acceptable

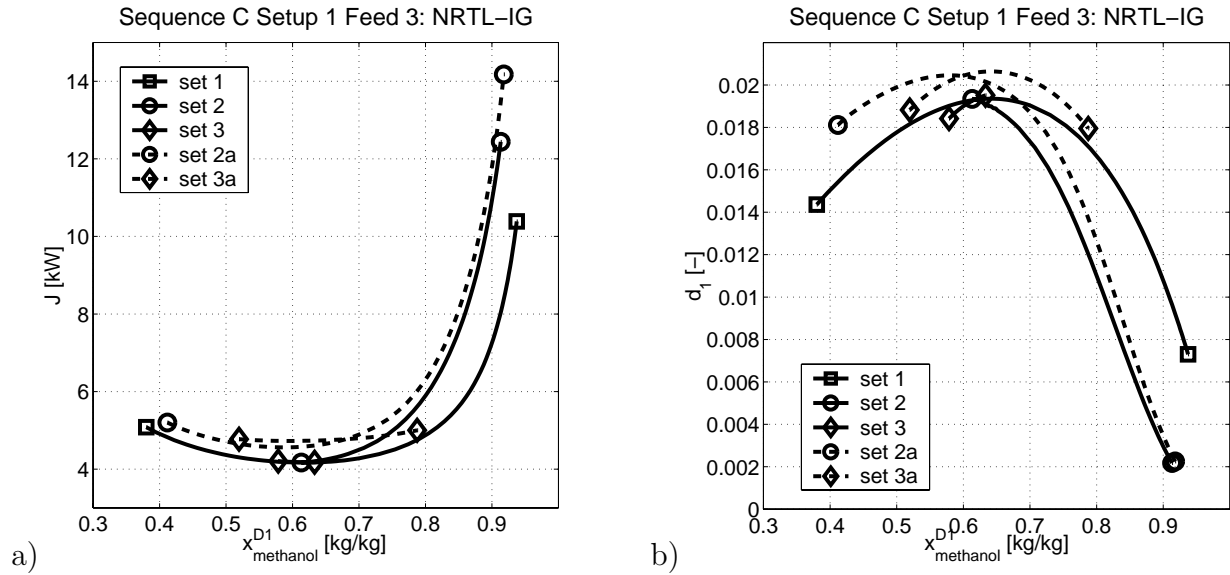


Figure 6.10: Sequence C setup 1 feed 3: Comparison of the different sets of controlled variables for a) J and b) d_1 as a function of $x_{methanol}^{D1}$.

loss. Figure 6.10a shows that J is nearly constant for set 3a and hits the optimal set (set 1) at $x_{methanol}^{D1} = 0.8$. Crossing is not possible because the refluxes would be too small to reach the other process specifications.

Figure 6.11 shows the dependence of the controlled variable $x_{methanol}^{D1}$ and of the cost function J on the manipulated variable R_2 for feed 3. As for feed 1, the predictions of the ∞/∞ analysis are validated. The optimal point is at a positive value of R_2 , but R_2 equal to zero is not a possible operation point.

6.6.5 Feed Variation

Figure 6.12 shows the sum of the reboiler duties for the three sets of controlled variables as a function of the crude feed composition: x_{water}^{FC} is constant at 0.334 kg/kg while $x_{methanol}^{FC}$ is varied between 0.003 kg/kg and 0.653 kg/kg. Set 1 is the best set. The dependence of J on $x_{methanol}^{FC}$ is roughly piecewise linear for set 1. At $x_{methanol}^{FC}$ where the optimum of J is not at $R_2 > 0$, but at $R_2 = 0$, the slope changes. As long as $x_{methanol}^{D1, opt}$ is feasible, set 2 is identical to set 1. Set 3b is for $L_1 = 5.6$ kg/h, $L_2 = 10.8$ kg/h, and $L_3 = 5$ kg/h which is

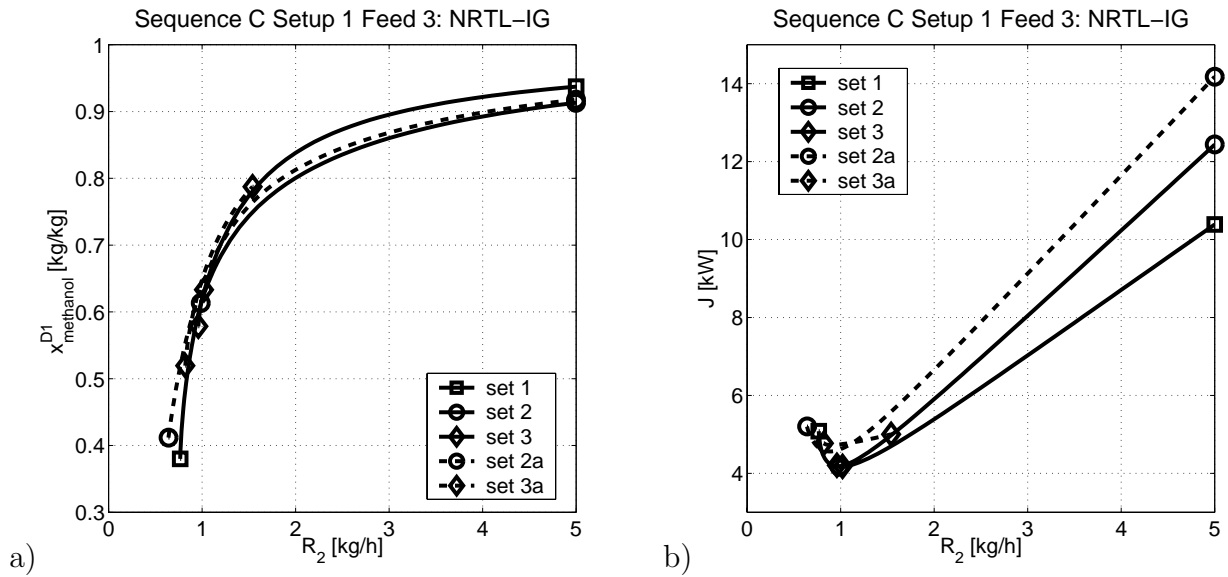


Figure 6.11: Sequence C setup 1 feed 3: Comparison of the different sets of controlled variables for a) x_{methanol}^{D1} and b) J as a function of R_2 .

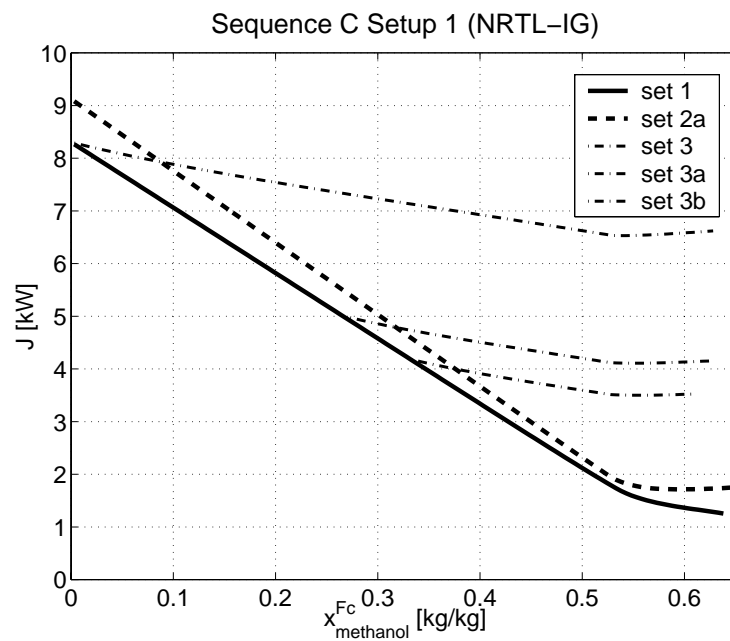


Figure 6.12: Sequence C setup 1: Comparison of the performance of the three different sets including the sets with over-refluxed columns (set 2a and 3a) for different crude feed compositions x^{Fc} (disturbance).

the double of the nominal values given in Table 6.4. It has the highest energy consumption of set 3 but covers the same feed compositions as set 1 and set 2a.

To summarize, set 1 is the best option, but it requires seven composition measurements. Set 2a is a good alternative for this sequence, especially since it is very easy to implement in a real column by a reflux divider. However, there is a catch in set 2 concerning operation: In the calculation of these case studies, it was observed for set 2 that the solution might jump to a different steady state with different compositions x^{B_2} and x^{D_3} for the same set of controlled variables. The most likely reason for this is the continuum of solutions found for the ∞/∞ case (section 5.3.2.2 and section 5.4.2.1). This is further discussed in section B.2.4.

6.7 Model Uncertainties

The main problem of the controlled variable $x_{methanol}^{D_1}$ is that the optimal location depends on the curvature of the boundary which is unknown in reality. The uncertainty is illustrated in Figure 6.13, which shows the residue curve boundary calculated by four different activity coefficient models and two different parameter sets. The influence is first analyzed for the ∞/∞ column sequence (section 6.7.1) and then for set 2a of controlled variables (section 6.7.2). The curvature of the boundary and the location of the azeotrope are also functions of the pressure. Therefore, the influence of the pressure will be analyzed in section 6.7.3. In section 6.7.4, experimental results reported in literature are discussed.

6.7.1 Influence on the ∞/∞ Column Sequence

The advantage of the ∞/∞ analysis is that the influence of the activity coefficient models can be analyzed using only residue curve map information. In section 5.4.2.1, it was derived that the cost function J is proportional to the 2-propanol content in the feed at the optimal point for a wide region of feeds. Choosing $k_1 = k_2 = k_3 = 1 \text{ kW}/(\text{kg/h})$ for simplicity (clearly, k_i depends on the activity coefficient model) gives:

$$J^{min} = (D_1 + D_2 + D_3)^{min} \frac{kW}{kg/h} = J_p^{min} (1 - x_{water}^{FC} - x_{methanol}^{FC}) F_C \quad (6.1)$$

J_p^{min} is a proportionality factor and depends on $x^{D_1, opt}$, which is also a function of k_i , the weighting factors. Table 6.6 lists the different optimal locations of x^{D_1} , J_p^{min} and

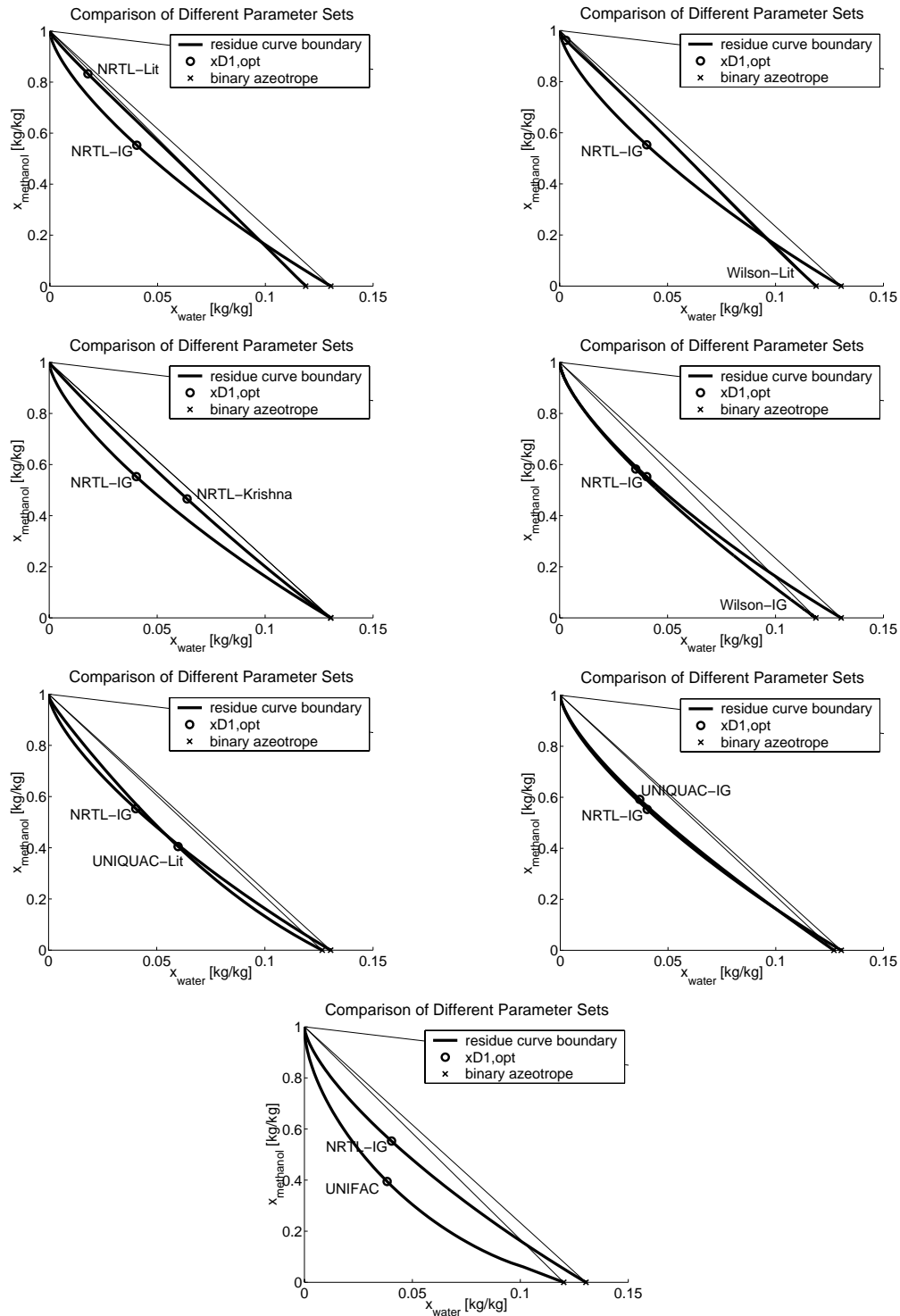


Figure 6.13: Comparison of the different data sets with respect to the residue curve boundary and the resulting $x^{D1,opt}$ (compare also Table 6.6).

d_1^{max} as a function of the activity coefficient models and the different parameter sets. The three VLE-IG sets and UNIQUAC-Lit give essentially the same J_p . Wilson-Lit and

Table 6.6: Optimal location of x^{D_1} as a function of the activity coefficient model and the available parameter sets in AspenPlus (NRTL-Krishna (Springer et al., 2002), $p = 1$ bar).

model	$x_{water}^{azeotrope}$	$x_{water}^{D_1, opt}$	$x_{methanol}^{D_1, opt}$	$J_p^{min} [\frac{kW}{kg/h}]$	d_1^{max}
NRTL-IG	0.1304	0.04032	0.5526	13.5	0.0180
Wilson-IG	0.1187	0.03528	0.5824	15.6	0.0143
UNIQUAC-IG	0.1270	0.03690	0.5916	16.0	0.0150
UNIFAC	0.1201	0.03831	0.3944	5.98	0.0344
UNIQUAC-Lit	0.1265	0.05985	0.4051	15.4	0.0154
Wilson-Lit	0.1188	0.00294	0.9618	148	0.0016
NRTL-Lit	0.1187	0.01768	0.8325	107	0.0022
NRTL-Krishna	0.1304	0.06387	0.4656	43.7	0.0058

NRTL-Lit give a nearly straight boundary with extremely high J_p . UNIFAC gives the best performance of the scheme. However, using UNIFAC-DMD (UNIFAC with Dortmund data base corrections), the curvature of the boundary is the opposite making the system infeasible. For UNIFAC-Lyngby, the boundary is almost straight. In general, predictions of UNIFAC are sometimes not as exact as of the other models because UNIFAC is fitted to many different systems. This often results in less accurate representations compared to parameter sets which were just regressed for the particular binary subsystems. The strength of the UNIFAC method is the prediction of phase equilibrium properties of mixtures for which no binary parameters for the other models are available.

To summarize: the variations of the different sets are significant. However, the proposed control scheme with set 2a is robust towards these uncertainties, which is shown next.

6.7.2 Influence on Set 2a

Set 1 of controlled variables is the best option. However, it is not easy to determine the proper value for x^{D_3} because it depends on the composition of azeotrope, which depends on the chosen activity coefficient parameter set. Concerning this model uncertainty, set 2a is more robust than set 1 because the value for x^{D_3} is not needed. Figure 6.14 shows

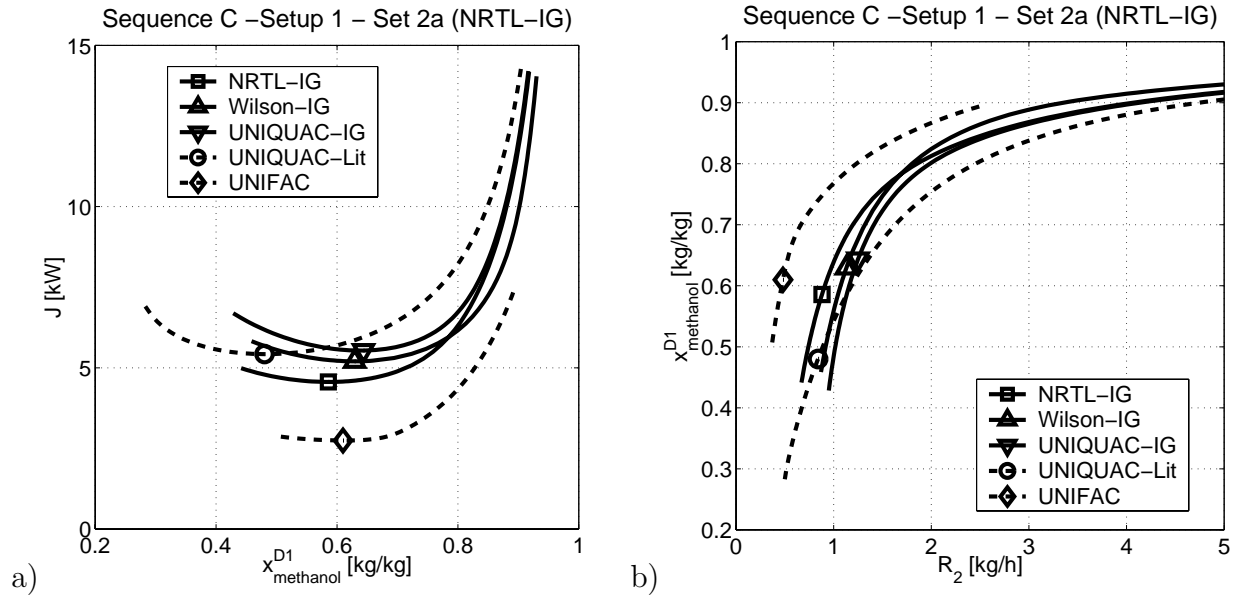


Figure 6.14: Sequence C setup 1 set 2a: a) J as a function of $x_{methanol}^{D1}$ and b) $x_{methanol}^{D1}$ using different activity coefficient models.

the comparison of different activity coefficient models for the base case feed (Table 6.1) using the controlled variables of set 2a (Table 6.4). As predicted by the ∞/∞ system (Table 6.6), UNIFAC gives the best performance. The other four models (NRTL-IG, Wilson-IG, UNIQUAC-IG, and UNIQUAC-Lit) give a similar performance. Table 6.6 indicates that the other sets require higher recycle flows. It was not possible to converge the sequence with the parameters of set 2a. Therefore, they are not shown in Figure 6.14.

6.7.3 Influence of Pressure

The pressure dependence of the binary 2-propanol–water azeotrope is shown in Figure 6.15. The water content increases monotonically for Wilson-IG and NRTL-IG and it decreases for all VLE-LIT data sets. For UNIQUAC-IG, there is maximum, for UNIFAC, there is a minimum. Hence, depending on the set, the water content can either increase or decrease. The influence of pressure is quantified using d_1 (equation 5.26). As derived in Section 5.4.2, the maximum of d_1 corresponds to minimum of the sum of the distillate flow rates. There are two qualitative different behaviors: a) the feed is in region 1 or region 2 ($R_2 = 0$ is feasible) or b) the feed is in region 3 ($R_2 = 0$ is infeasible). Figure 6.16 shows these two for

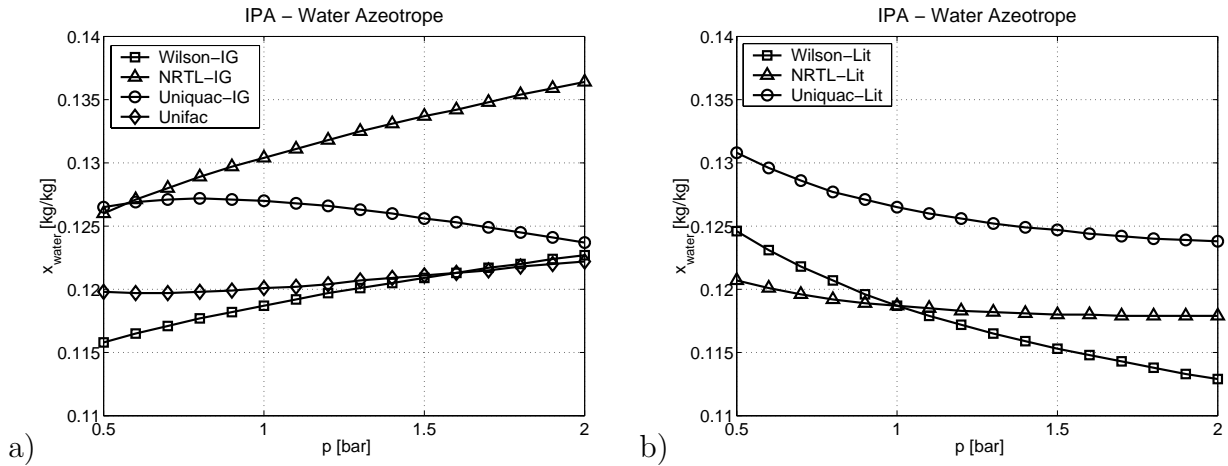


Figure 6.15: Pressure dependence of the 2-propanol(IPA)–water azeotrope. a) database VLE-IG, b) database VLE-Lit

three different compositions of $x_{\text{water}}^{D_3}$: smaller, equal or large than the water content of the 2-propanol–water azeotrope determined by NRTL-IG at 1 bar. The larger $x_{\text{water}}^{D_3}$, the better is the performance of the scheme. If the water content of the azeotrope is monotonically increasing with the pressure (as it is for NRTL-IG), the following predictions for the finite sequence to maximize d_1 can be deduced from Figure 6.16:

- column 1 has to be operated at the lowest possible pressure to move x^{D_1} as close as possible to the methanol–2-propanol edge.
- column 3 has to be operated at the highest possible pressure to obtain a high value of $x_{\text{water}}^{D_3}$.
- The optimal pressure of column 2 is indefinite concerning d_1 .

Figure 6.17 confirms these predictions with rigorous simulations of sequence C setup 1 set 1. While one pressure was varied, the other two pressure remained at the nominal value. A low pressure in column 1 leads to a slightly better performance. Surprisingly, the top pressure of column 2 has a strong influence on J , but the physical cause is not clear. Because of the constant concentrations, d_1 is independent of the top pressures of column 2 and column 3 which is consistent with the ∞/∞ analysis.

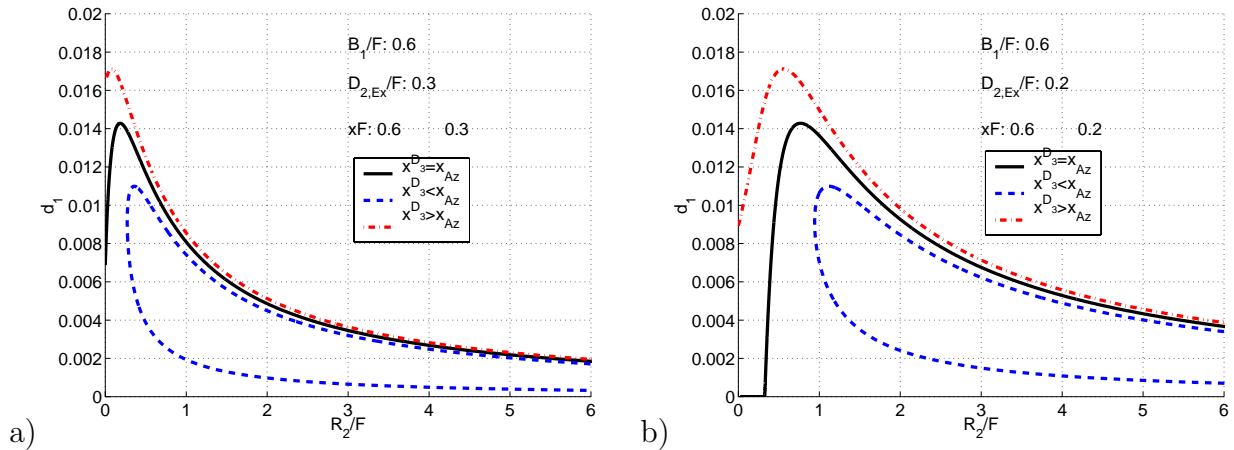


Figure 6.16: Mixture: methanol(L)/2-propanol(I)/water(H). a) feed inside and b) feed outside the feasible region for $R_2 = 0$.

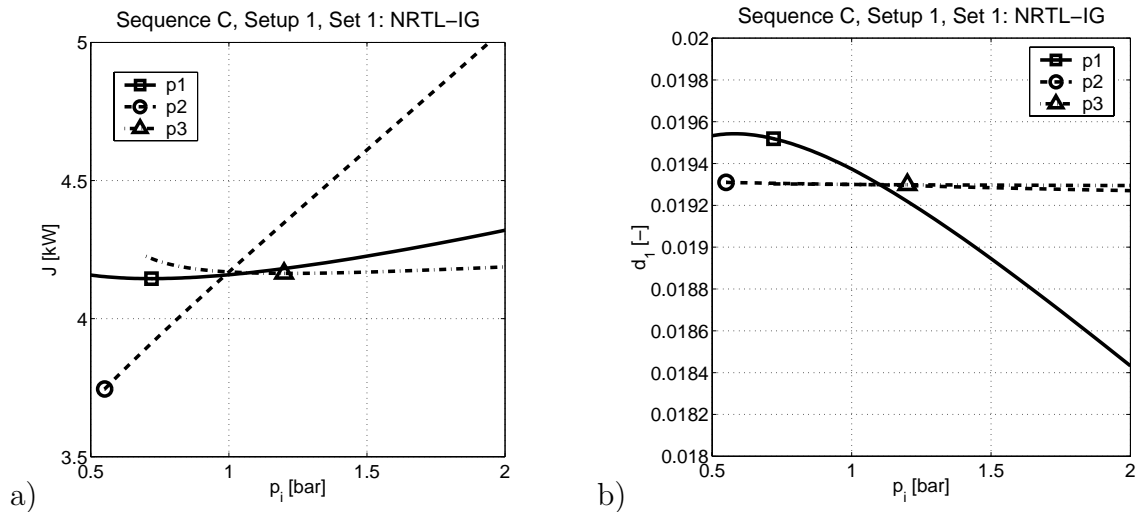


Figure 6.17: Sequence C setup 1 set 1: a) J and b) d_1 as a function of the column top pressures.

The influence of the top pressure of column 3 is less pronounced which is a fact of the constant $x_{water}^{D_3}$ for set 1. Figure 6.18 shows J and d_1 as a function of the top pressure of column 3 for different $x_{water}^{D_3}$. The optimal value of J does not depend strongly on the chosen $x_{water}^{D_3}$, but if the pressure is reduced such that the azeotropic composition reaches the specification of $x_{water}^{D_3}$, J will strongly increase. d_1 is just a function of the concentration and therefore independent of the pressure.

Figure 6.19 shows the same for set 2 and set 2a. The influence of the pressure can be

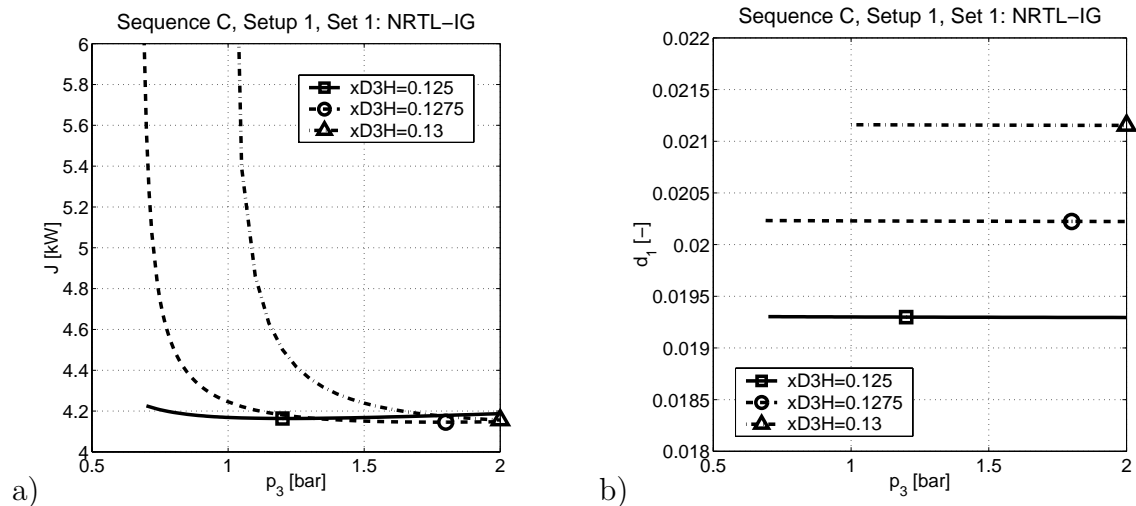


Figure 6.18: Sequence C setup 1 set 1: a) J and b) d_1 as a function of the top pressure of column 3.

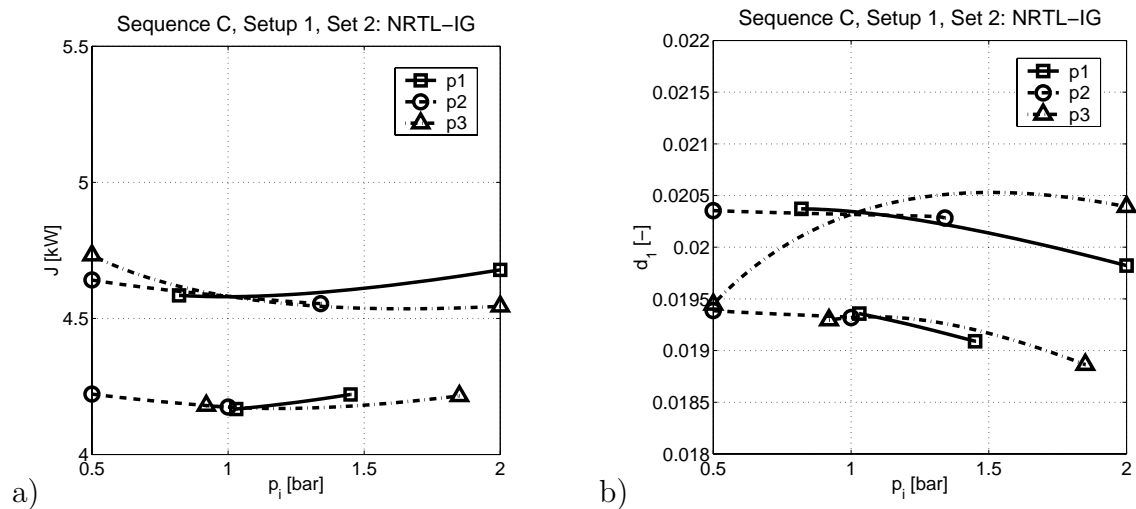


Figure 6.19: Sequence C setup 1 set 2: a) J and b) d_1 as a function of the top pressures.

neglected for this setup because the compositions hardly change and hence the recycles and distillate flow rates remain the same giving nearly constant reboiler duties. Set 3 will give the same result because the changes in the interconnecting flow rates are very small.

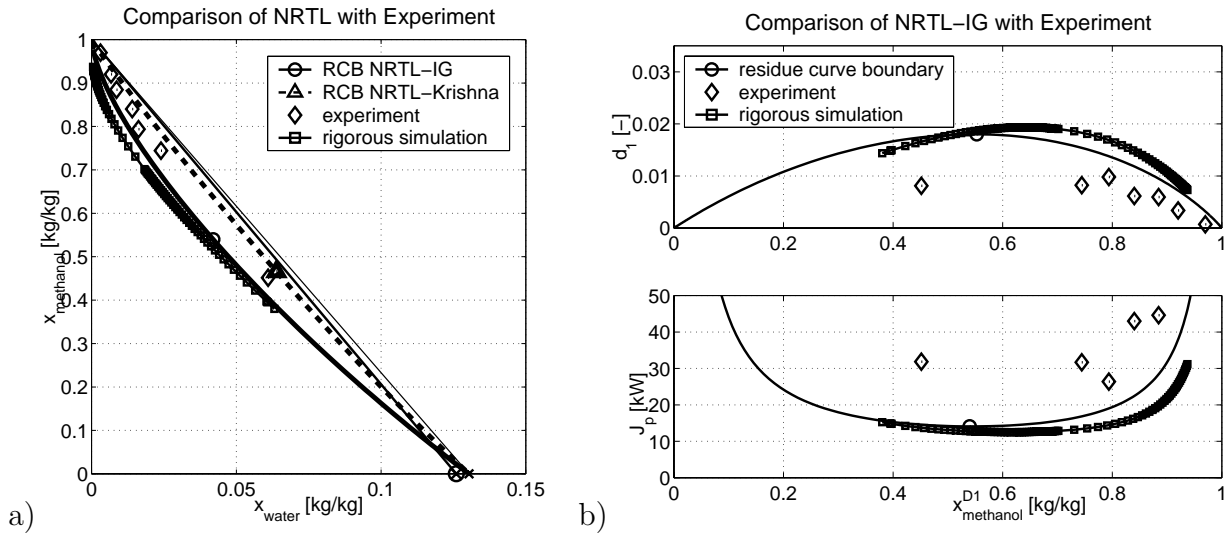


Figure 6.20: Residue curve boundary and $x^{D1,opt}$ for two NRTL parameter sets compared with experimental distillate compositions by Pelkonen et al. (2001) and the azeotrope as reported by Gmehling et al. (1994).

6.7.4 Comparison to Experiments

Pelkonen et al. (1997) studied the distillation of methanol/2-propanol/water with a packed column. The residue curve boundary can be approximated with a packed column operated under total reflux (Laroche et al., 1992a). Figure 6.20a shows the residue curve calculated with NRTL-IG. Pelkonen et al. (2001) list the experimental results of their previous study (Pelkonen et al., 1997). A packed column is operated at 960 mbar under total reflux such that the distillate composition varies along the residue curve boundary of the methanol/2-propanol/water mixture. Different to column 1 of sequence C, the bottom purity is not at pure water. The compositions of the distillate (Figure 6.20a) lie left of the feasibility border line, which connects pure methanol with the 2-propanol–water azeotrope (encircled cross, minimum boiling at $p=1.013 \text{ bar}$, $T = 80.72^\circ\text{C}$, and $x_{\text{water}}^{\text{az}} = 0.126$ (Gmehling et al., 1994)); but they do not cross the NRTL-IG residue curve boundary. Recently, Springer, Baur and Krishna (2002) reported experiments where the distillate composition crossed the residue curve boundary for this mixture. The residue curve boundary using their parameter set (NRTL-Krishna) is also plotted in Figure 6.20. Since they crossed the boundary, they also lie left of the feasibility border line.

Table 6.7: d_1 and J_p for k_i from Table 6.3 for experimental distillate compositions by Pelkonen et al. (2001) and the azeotrope as reported by Gmehling et al. (1994).

experiment	$x_{water}^{azeotrope}$	$x_{water}^{D_1}$	$x_{methanol}^{D_1}$	d_1	J_p [$\frac{kW}{kg/h}$]
MIW 9	0.126	0.0240	0.7443	0.00822	31.7
MIW 10	0.126	0.0162	0.7937	0.00979	26.4
MIW 11	0.126	0.0610	0.4516	0.00810	31.9
MIW 12	0.126	0.0031	0.9698	0.00070	388.
MIW 13	0.126	0.0067	0.9201	0.00337	79.9
MIW 14	0.126	0.0086	0.8846	0.00594	44.6
MIW 15	0.126	0.0140	0.8401	0.00615	43.0

Tray columns can cross the residue curve boundary (Laroche et al., 1992b). Figure 6.20a also shows the distillate composition of sequence C setup 1 set 1 for column 1 with trays calculated with NRTL-IG. The data are from the cases study shown in Figure 6.4. They all lie left of the residue curve boundary, as expected. For the rigorous simulations, d_1 is mostly greater than the one of the residue curve boundary (Figure 6.20b) because of x^{D_1} ; x^{D_3} is different for the two cases which explains that the two curves cross each other despite the fact the x^{D_1} always lies in the non-convex set of the residue curve.

The J_p (equation 6.1) can be obtained with the k_i shown in Table 6.3 for the residue curve boundary. This is shown in the upper plot of Figure 6.20b. For k_i different to each other, the minimum of J_p does not correspond to the maximum of d_1 anymore. For the small differences as reported in Table 6.3, the difference is subtle. Assuming that these factors hold in reality, the experimental data can be compared to the predictions of the ∞/∞ analysis (residue curve boundary information) and the rigorous simulations of the three column sequence using J_p . Using experimental data of Pelkonen et al. (2001), J_p and d_1 can be calculated (Table 6.7). These experimental data give a smaller d_1 than the optimal points for the VLE-IG data and UNIQUAC-Lit (Table 6.6), which are between 0.014 and 0.018. Figure 6.20b shows the comparison of the experimental d_1 and J_p with the residue curve boundary using NRTL-IG. Note that $J_p = J/(1 - x_{water}^{FC} - x_{methanol}^{FC})$ with $x_{L;I,H}^{FC} = [0.333; 0.333; 0.334]$ for the rigorous simulations. These data confirm that the

scheme is feasible in reality.

6.8 Implementation of the Concept in a Process Simulator

The key variable in the self-optimizing control concept of the sequence is the recycle R_2 . In the derivation of the concept, the purities of all three columns were assumed to be perfectly controlled. Table 6.4 listed the analyzed sets of controller pairings. Set 1 is the most sophisticated set because it requires 7 compositions to be measured and controlled. Set 2 reduces the necessary on-line composition measurements to 4 at an acceptable loss in the performance for variations of the crude feed composition x^{FC} . Set 3, which operates with constant reflux, is an unacceptable alternative. Therefore, set 2a will be the basis for the control scheme that should be used for operating the boundary separation scheme: all columns are operated with a constant reflux-to-distillate ratio, and four composition controllers ensure the specified purities. Figure 6.21 shows the proposed control scheme. Three of the four composition controllers are realized as cascaded controllers (TC1, TC2, and TC3) as often done in industrial columns: a temperature front is controlled by manipulating the reboiler duty to stabilize the operation of the individual columns and to ensure the bottom purity. This will be discussed in the sections 6.8.1 to 6.8.3. The setpoints of these three controllers have to be adjusted in the real plant to measurements of the purities to account for model uncertainties. In the simulations that will be shown in this section, the setpoints are constant. The influence of the setpoints will be discussed in section 6.8.4. For the fourth composition controller (R2C), no temperature front could be identified. Hence, it has to be implemented as a real composition controller.

An inspection of Figure 6.21 suggests that D_1 , B_2 and D_3 are uncontrolled flows. This can cause so-called snowball effects. If all flows in a recycle loop are uncontrolled, an infinite number of values is possible that fulfills the mass balances. Hence, a disturbance can lead to a large increase of the recycle streams. To prevent this, one stream in the loop has to be flow controlled (Luyben, 1993c). For the boundary separation scheme, all

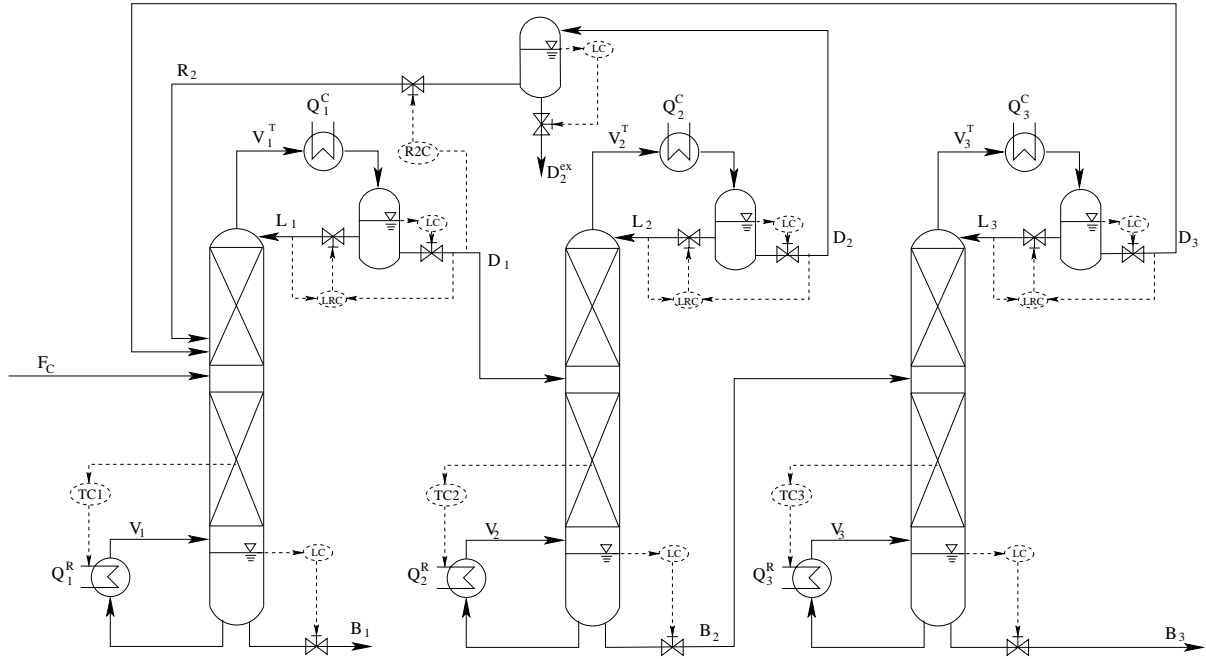


Figure 6.21: Control scheme for the boundary separation scheme.

distillate flows are indirectly controlled via the reboiler duties as a result of the constant reflux-to-distillate ratios. Hence, snowball effects cannot take place.

The goal of this section is to show that the boundary separation scheme can be operated with simple decentralized single-loop controller. The level controllers and the reflux-to-distillate ratio controllers are implemented with high gain simulating perfect control. The four other controllers (TC1, TC2, TC3, and R2C) are linear PID controllers (proportional amplification of the controller error with integral and derivative action) of the following form:

$$K = k_c \left(1 + \frac{1}{\tau_i s} + \frac{\tau_d s}{(0.1\tau_d s + 1)} \right) \quad (6.2)$$

The sensor dynamics are modeled with a first order lag:

$$f = \frac{1}{\tau_f s + 1} \quad (6.3)$$

The controllers are tuned for each column separately using the Ziegler-Nichols method: the gain of a proportional controller is increased until a sustained oscillation is reached giving the ultimate gain (k_u) and the ultimate period (P_u) for the selection of the controller parameters.

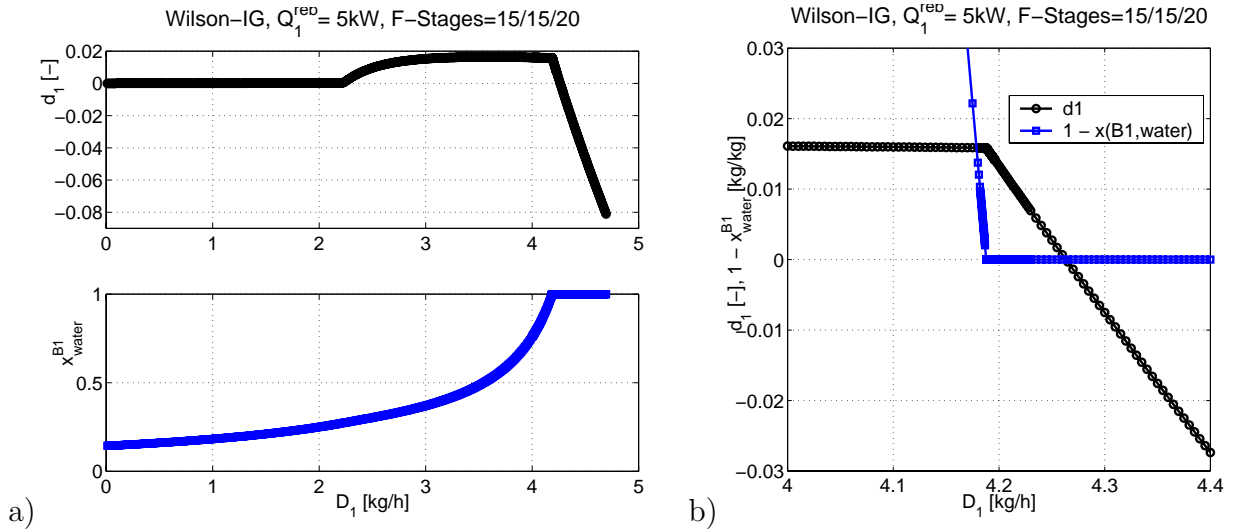


Figure 6.22: a) d_1 and bottom composition x_{water}^{B1} , and b) d_1 and $1 - x_{water}^{B1}$ as a function of D_1 for column 1 (setup 1) with a feed given in Table 6.8.

6.8.1 Control of Column 1

For TC1, a temperature has to be selected. To identify this temperature, the steady-state behavior of column 1 is analyzed first using a case study with Wilson-IG as parameter set. R_2 and D_3 enter column 1 above stage 15 and F_C above stage 20 as indicated by F-Stages=15/15/20 (in Appendix B.2.1, the influence of the feed stage location is discussed in details). Critical for the feasibility of the scheme is that d_1 (equation 5.26) is greater than zero. Figure 6.22a shows d_1 and x_{water}^{B1} as a function of the distillate flow rate D_1 (ranging from zero to F_1) for a feed of setup 1 (Table 6.8). The critical point here is shown by Figure 6.22b, which shows an enlargement of Figure 6.22a. For a feasible sequence ($d_1 > 0$), D_1 has to be smaller than 4.26 kg/h (upper bound). For a purity larger than 0.9998, D_1 has to be larger than 4.188 kg/h. In this region, the pinches of the column change. Since this also has implications on the time constant of the operation point, it is discussed here. The pinches can be identified if the total column holdup (TCH) composition is calculated (equation 6.4), as introduced by Dorn and Morari (2002a):

$$x^{TCH} = \frac{\sum_{k=1}^n x_k M_k}{\sum_{k=1}^n M_k} \quad (6.4)$$

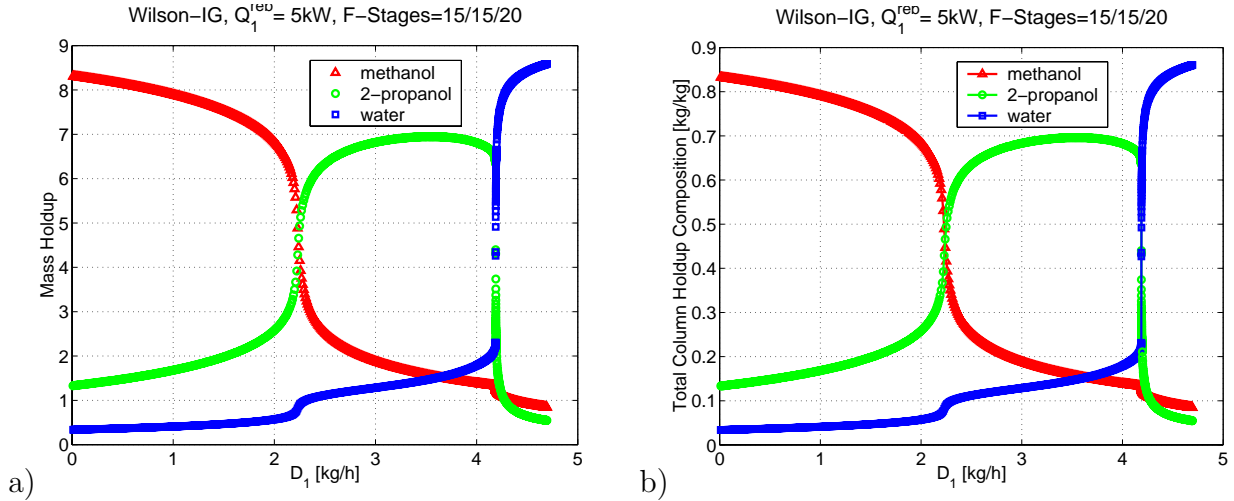


Figure 6.23: a) Holdup of each component and b) total column holdup composition as a function of D_1 .

Table 6.8: Overall feed F_1 to column 1 for setup 1 and setup 2. For setup 1, a binary feed F_C was chosen. For setup 2, F_C was chosen such that x^{F_1} lies on the intersection of the line connecting R_2 and D_3 and the mass balance line of column 1 for $D_1 = 4.196$ kg/h.

stream	Setup 1			Setup 2		
	flow rate [kg/h]	x_{methanol}	x_{water}	flow rate [kg/h]	x_{methanol}	x_{water}
F_C	1.000	0.0000	0.5000	1.000	0.2259	0.0915
R_2	2.224	1.0000	0.0000	2.224	1.0000	0.0000
D_3	1.472	0.0000	0.1187	1.472	0.0000	0.1187
F_1	4.696	0.4737	0.1435	4.696	0.5217	0.0567

x_k is the composition vector at stage k and M_k is the mass holdup of stage k . For the calculations, the holdup of the reflux drum and the bottoms is 1 kg, and the holdup per stage is 0.285 kg. Figure 6.23 shows the total column holdup composition (equation 6.4) as a function of D_1 for a feed F_1 corresponding to setup 1 (Table 6.8). Three different pinches can be identified:

- 1) pinch in column top (pure methanol): $0 < D_1 < 2.24$ kg/h,
- 2) pinch in column middle (2-propanol–water azeotrope): 2.24 kg/h $< D_1 < 4.188$ kg/h,

3) pinch in column bottom (pure water): $4.188 < D_1 < 4.696$ kg/h.

Figure 6.23 confirms that the desired operation range (4.188 kg/h $< D_1 < 4.26$ kg/h) lies exactly at the border between two pinches. If the column is operated such that the pinch is in the bottom, the bottom purity will be very robust towards little fluctuations in D_1 and B_1 because a large amount of water would have to be removed from the column. This gives a large transition time that make the process robust towards little fluctuations (see Appendix B.2.1 for a detailed discussion of the transient behavior of the column). This has also to be considered in the startup of the column.

In contrast, x^{D_1} is very sensitive to increasing distillate flow rates. For setup 1 of Sequence C, this can lead to the fact that d_1 is smaller than zero (compare Figure 6.22). This has to be avoided and column 1 should be operated with the pinch close to the 2-propanol–water azeotrope in the middle of the column because then x^{D_1} will always lie on the boundary for a sufficiently high reflux. For tray columns, it can actually cross the residue curve boundary for lower refluxes which improves the performance of the scheme.

For the desired operation point with the pinch in the middle of the column, the temperature profile will be as shown in Figure 6.24. Because the column is operated close to two different pinches, the numerical determination of the steady-state gain of the temperature vector is tedious. If the derivative is approximated by a perturbation with a finite Δ , the steady-state gain depends strongly on size of the perturbation because of the strong nonlinear behavior of the operation point. Therefore, the stage with the steepest front that indicates the position of the pinch is chosen. For the temperature profile in Figure 6.24, this is temperature on stage 28.

Dynamic Simulations. For column 1, TC1 and R2C have to be tuned. Table 6.9 lists the parameters of the model that is used in the dynamic simulations. The equipment is not optimized to a specific packing, neither is the diameter of the column for the expected throughput. First, TC1 is tuned for constant R_2 . The dynamics of the temperature sensor are modeled with a first order lag (equation 6.3) with $\tau_f = 1$ min. Table 6.10 lists the parameter obtained by the Ziegler-Nichols method. Using TC1, the ultimate gain and

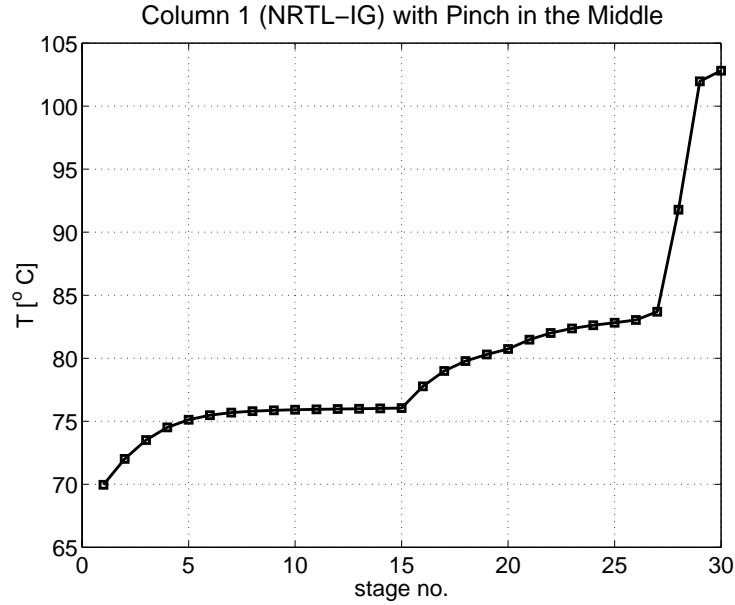


Figure 6.24: Temperature profile for column 1 operated in setup 1 with set 2a of controlled variables.

Table 6.9: Column 1 as modeled in RadFrac (Aspen Dynamics). Heat capacity of the equipment is not considered.

top	$L_1/D_1 = 1.56$, pressure: 1.1 bar, condenser: no subcooling, no holdup holdup of reflux drum: $0.003\ 560\ m^3$
stages	28 theoretical stages, diameter = 0.100 m, simple packing, HETP = 0.05 m, initial liquid volume fraction: 0.05, holdup $\approx 0.000\ 020\ m^3$ /stage pressure stage 2: 1.105 bar, $\Delta p = 15\ mbar$ /column
bottom	one theoretical stage, holdup: $0.003\ 560\ m^3$
feed F_C	above stage 20, flow rate: 1.000 kg/h; $x_{methanol} = 0.333\ kg/kg$ $x_{2-propanol} = 0.333\ kg/kg$, $x_{water} = 0.334\ kg/kg$
feed R_2	above stage 15, flow rate: 0.9463 kg/h; $x_{methanol} = 0.9998\ kg/kg$ $x_{2-propanol} = 0.0002\ kg/kg$, $x_{water} = 0.0000\ kg/kg$
feed D_3	above stage 15, flow rate: 0.4608 kg/h; $x_{methanol} = 0.000\ kg/kg$ $x_{2-propanol} = 0.8733\ kg/kg$, $x_{water} = 0.1267\ kg/kg$

the ultimate period is determined for the composition controller R2C (Table 6.10). The composition measurement dynamics are modeled with a first order lag (equation 6.3) with

Table 6.10: Column 1: parameters of the PID controllers (equation 6.2)

controller	k_u	P_u	k_c	τ_i	τ_d
TC1	0.278 kW/K	2 min	0.167 kW/K	1 min	0.25 min
R2C	8.3 kg/h/(kg/kg)	32 min	5 kg/h/(kg/kg)	16 min	4 min

$\tau_f = 5$ min. For composition measurements, often a pure dead time is the more appropriate sensor dynamics. If the simulations are repeated with a dead time of 5 min, the ultimate gain is 5.4 kg/h/(kg/kg) with an ultimate period of 36 min giving very similar controller settings. Figure 6.25 shows the dynamics of column 1 with these two controllers for step changes in D_3 . The controllers adjust the system well to the new steady state. Only $x_{water}^{B_1}$ might decrease below 0.9998. If a higher setpoint for T_{28} is used (for example 95° C instead of 91.764° C), $x_{water}^{B_1}$ will stay within the specifications. Additional tuning for performance is beyond the scope of this work.

Setup 2. As postulated in section 5.4.2.4, setup 2 has the best operability because feasibility of the sequence is given by definition if column 1 is operated such that x^{B_1} is pure water and D_1 is smaller than F_1 . The reason is that $d_1 > 0$ in this case. This is illustrated with a parameter study as shown in Figure 6.26 for a feed to column 1 as shown in Table 6.8 for setup 2. Figure 6.26 also shows that for this setup only very little water is transferred over the boundary. Independent of that, the optimal operation point is the same as for the feed for setup 1. Note that for the constraint $x_{water}^{B_1} = 0.9998$, which was used in all previous studies, the pinch is always in the middle of column 1.

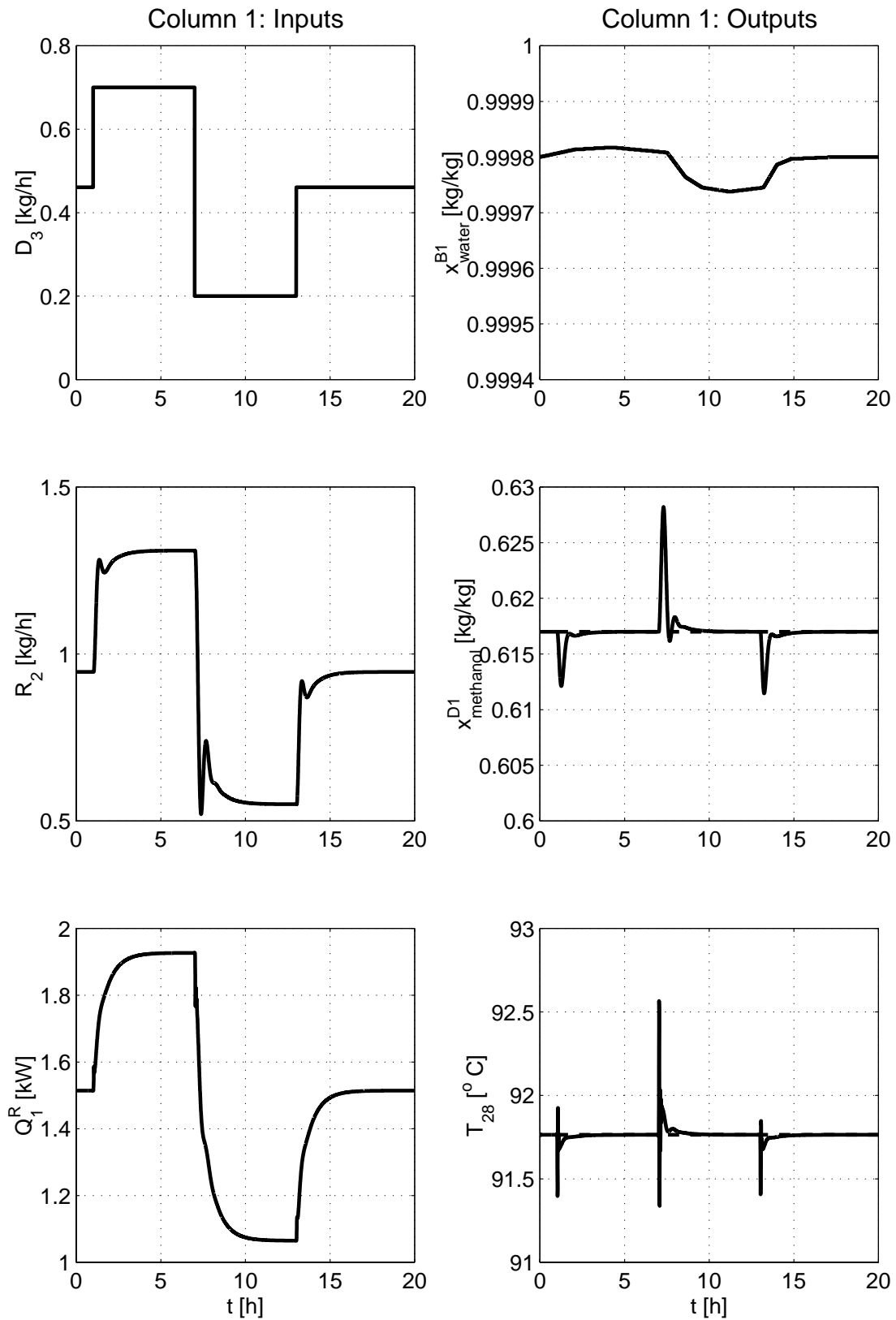


Figure 6.25: Load changes for column 1 with two single loop controllers. R_2 controls x_{methanol}^{D1} and Q_1^R controls T_{28} .

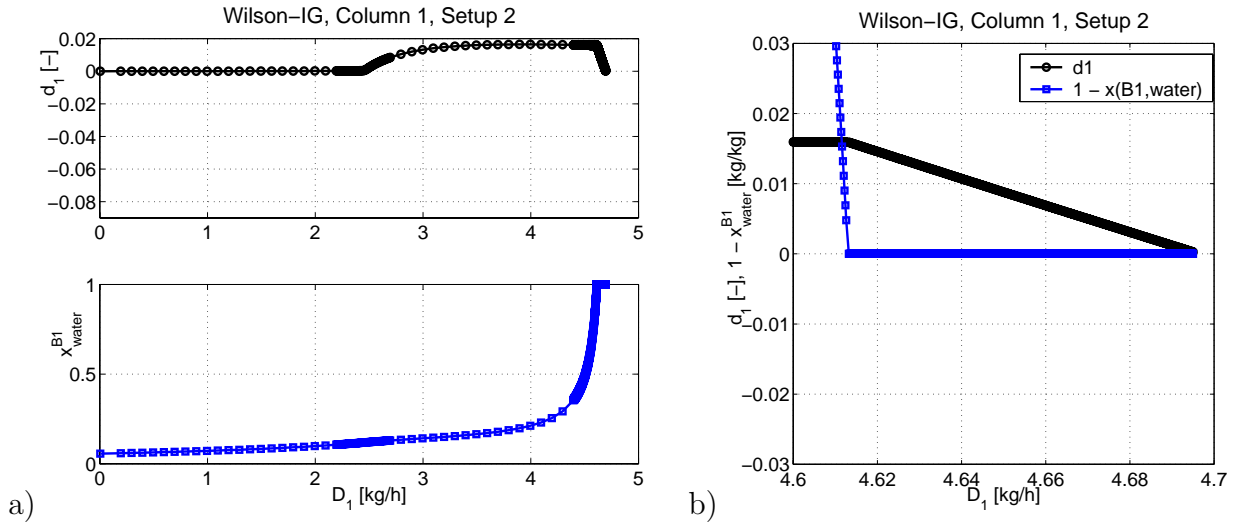


Figure 6.26: a) d_1 and bottom composition x_{water}^{B1} , and b) d_1 and $1 - x_{water}^{B1}$ as a function of D_1 for column 1 (setup 2) with a feed given in Table 6.8.

6.8.2 Control of Column 2

As for column 1, the determination of the sensitivity vector depends on the size of the perturbation around the steady state. Therefore, it is better to select the temperature at the steepest front. For column 2, this is the temperature on stage 28 (Figure 6.27). The dynamics of the temperature sensor are modeled with a first order lag (equation 6.3) with $\tau_f = 1$ min. Table 6.11 lists the parameter obtained by the Ziegler-Nichols method for the column model as listed in Table 6.12. As for column 1, the equipment is not optimized. Figure 6.28 shows the dynamics of the column for a step change in x^{D1} with this controller settings. The changes in x^{D1} were chosen such that the mass balance forces the column profile to cross the distillation boundary. During these transitions, the simple controller can keep the desired purity for x^{D2} while x^{B2} crosses the azeotrope. Figure 6.29 shows the two different steady state column profiles.

Table 6.11: Column 2: parameters of the PID controller (equation 6.2)

controller	k_u	P_u	k_c	τ_i	τ_d
TC2	2.222 kW/K	1.5 min	1.333 kW/K	0.75 min	0.1875 min

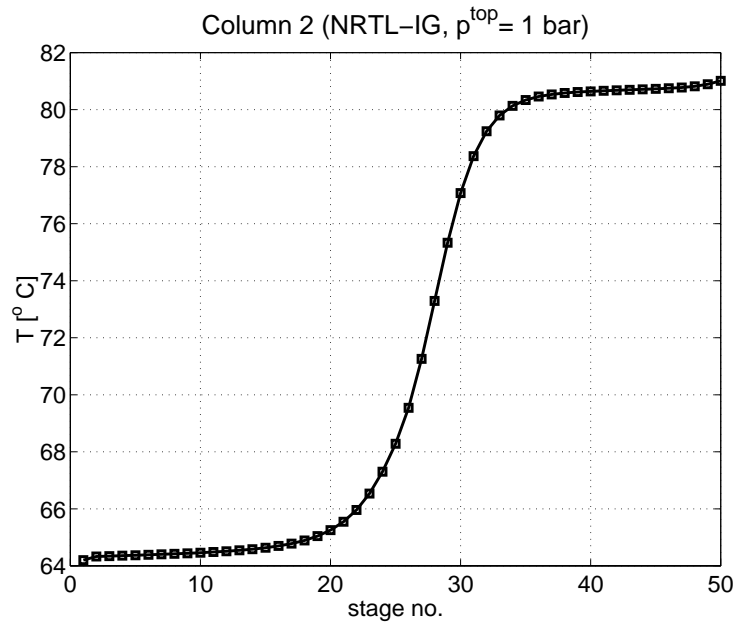


Figure 6.27: Temperature profile for column 2 operated in setup 1 with set 2a of controlled variables.

Table 6.12: Column 2 as modeled in RadFrac (Aspen Dynamics). Heat capacity of the equipment is not considered.

top	$L_2/D_2 = 4.86$, pressure: 1.0 bar, condenser: no subcooling, no holdup holdup of reflux drum: $0.003\ 560\ m^3$
stages	48 theoretical stages, diameter = 0.100 m, simple packing, HETP = 0.05 m, initial liquid volume fraction: 0.05, holdup $\approx 0.000\ 020\ m^3$ /stage pressure stage 2: 1.005 bar, $\Delta p = 25\ mbar$ /column
bottom	one theoretical stage, holdup: $0.003\ 560\ m^3$
feed D_1	above stage 25, flow rate: 2.07312 kg/h; $x_{methanol} = 0.6170\ kg/kg$ $x_{2-propanol} = 0.3548\ kg/kg$, $x_{water} = 0.0282\ kg/kg$

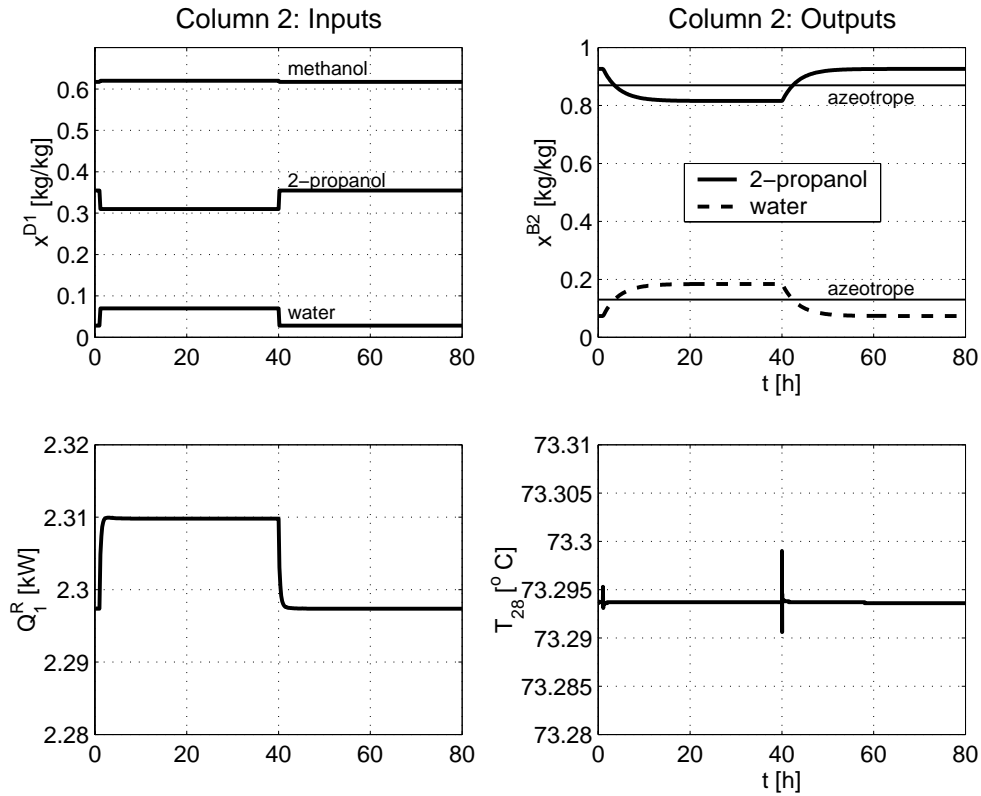


Figure 6.28: Changes in x^{D1} such that the mass balance forces x^{B2} to cross the azeotrope (indicated by the thin solid lines in the upper right plot). The column profiles are shown in Figure 6.29

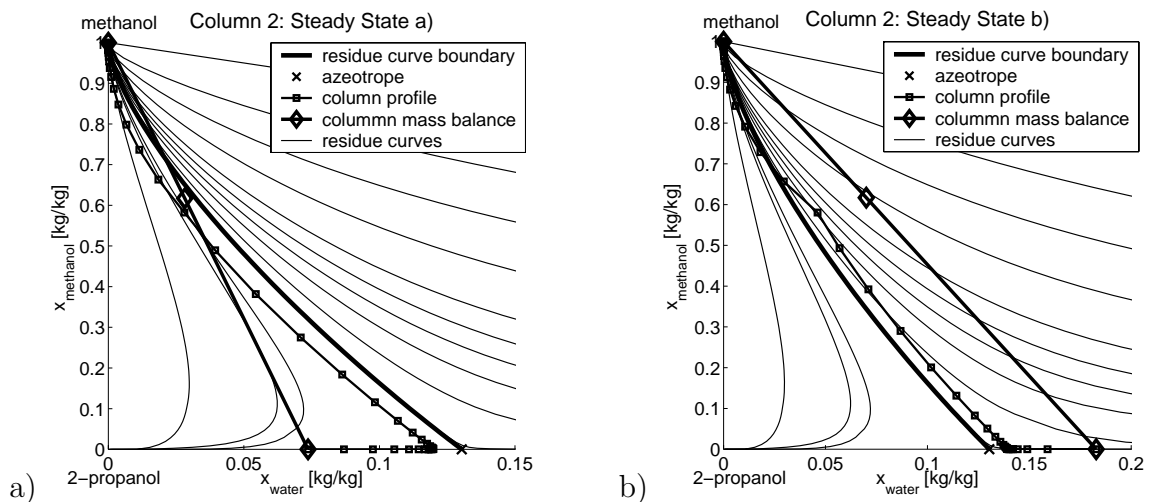


Figure 6.29: Two steady state profiles of column 2 for the transitions shown in Figure 6.28. a) $x_{water}^{D1} = 0.0282$ kg/kg and $x_{methanol}^{D1} = 0.617$ kg/kg, b) $x_{water}^{D1} = 0.07$ kg/kg and $x_{methanol}^{D1} = 0.617$ kg/kg.

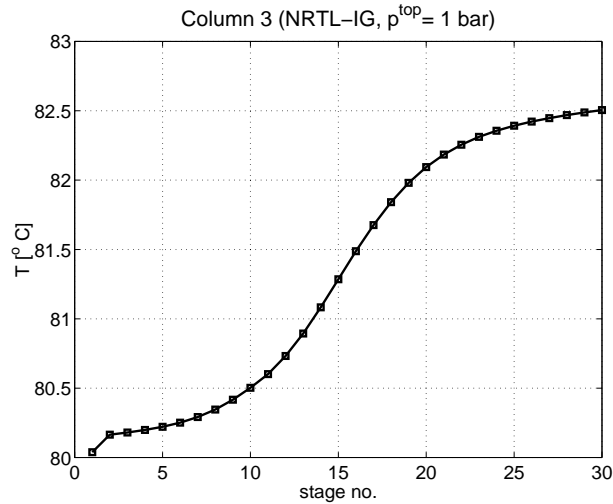


Figure 6.30: Temperature profile for column 3 operated in setup 1 with set 2a of controlled variables.

6.8.3 Control of Column 3

As for column 1 and column 2, the temperature at the steepest front is chosen as controlled variable. For column 3, this is the temperature on stage 16 (Figure 6.30). The temperature profile of column 3 is very flat compared to the profile of the other two columns. The influence of the column load and hence of the column pressure will be significant for the temperature controller. There are two ways to avoid this: pressure compensation or manual adjustment of the temperature set point to reach the desired purity. A further investigation of this is difficult because the predictions of the column hydraulics are often not reliable (Kister, 2002). Therefore, a further investigation of this problem has to be done in connection with a real plant where the predictions can be verified. This was not possible in this project. Assuming that the temperature can be controlled well enough, the simulations will show that column 3 can be operated with this scheme.

The dynamics of the temperature sensor are modeled with a first order lag (equation 6.3) with $\tau_f = 1$ min. Table 6.13 lists the parameters of the model that is used for the dynamic simulations. Again, the dynamic simulations appear for illustration and the equipment is not optimized. For this setup, it was not possible to increase the gain such that a stable oscillation is reached. Though column 3 has the same equipment as column 1, the dynamics

Table 6.13: Column 3 as modeled in RadFrac (Aspen Dynamics). Heat capacity of the equipment is not considered.

top	$L_3/D_3 = 6.12$, pressure: 1.0 bar, condenser: no subcooling, no holdup holdup of reflux drum: $0.003\ 560\ m^3$
stages	28 theoretical stages, diameter = 0.100 m, simple packing, HETP = 0.05 m, initial liquid volume fraction: 0.05, holdup $\approx 0.000\ 020\ m^3$ /stage pressure stage 2: 1.005 bar, $\Delta p = 15\ mbar$ /column
bottom	one theoretical stage, holdup: $0.003\ 560\ m^3$
feed B_2	above stage 15, flow rate: 0.793 779 kg/h; $x_{methanol} = 0.000\ 0001\ kg/kg$ $x_{2-propanol} = 0.926\ 339\ kg/kg$, $x_{water} = 0.073\ 660\ kg/kg$

Table 6.14: Column 3: parameters of the PID controller (equation 6.2)

controller	k_u	P_u	k_c	τ_i	τ_d
TC3	–	–	0.167 kW/K	1 min	0.25 min

are different. Nevertheless, the parameters of column 1 are taken (Table 6.14). Remember: The dynamic simulations appear for illustration. Figure 6.31 shows the dynamics of the column for a step change in x^{B_2} with this control scheme. The changes in x^{B_2} were chosen such that the mass balance forces the column profile to cross the azeotrope. After the step change at 20 hours, the bottom flow goes to zero. The reboiler duty increases to keep T_{16} at the set point. Hence, the bottom level decreases. In this transition, the top composition stays at the azeotrope and the bottom crosses the azeotrope. In that process, there is a point where the whole column has azeotropic composition giving a lower temperature at the same pressure. The set point of the temperature controller is just reached because of the pressure increase during the transition. Approximately 12 hours after the step change, the bottom consists of pure water now, all the 2-propanol was squeezed out via the distillate. Now, the reboiler duty decreases, the bottom level increases and at hour 80, the bottom flow is greater than zero again. At hour 100, the composition is again changed to a value at the other side of the azeotrope and the controller also reaches the steady state with pure 2-propanol in the bottom. In operation of the sequence, these transitions are definitely undesired, but possible.

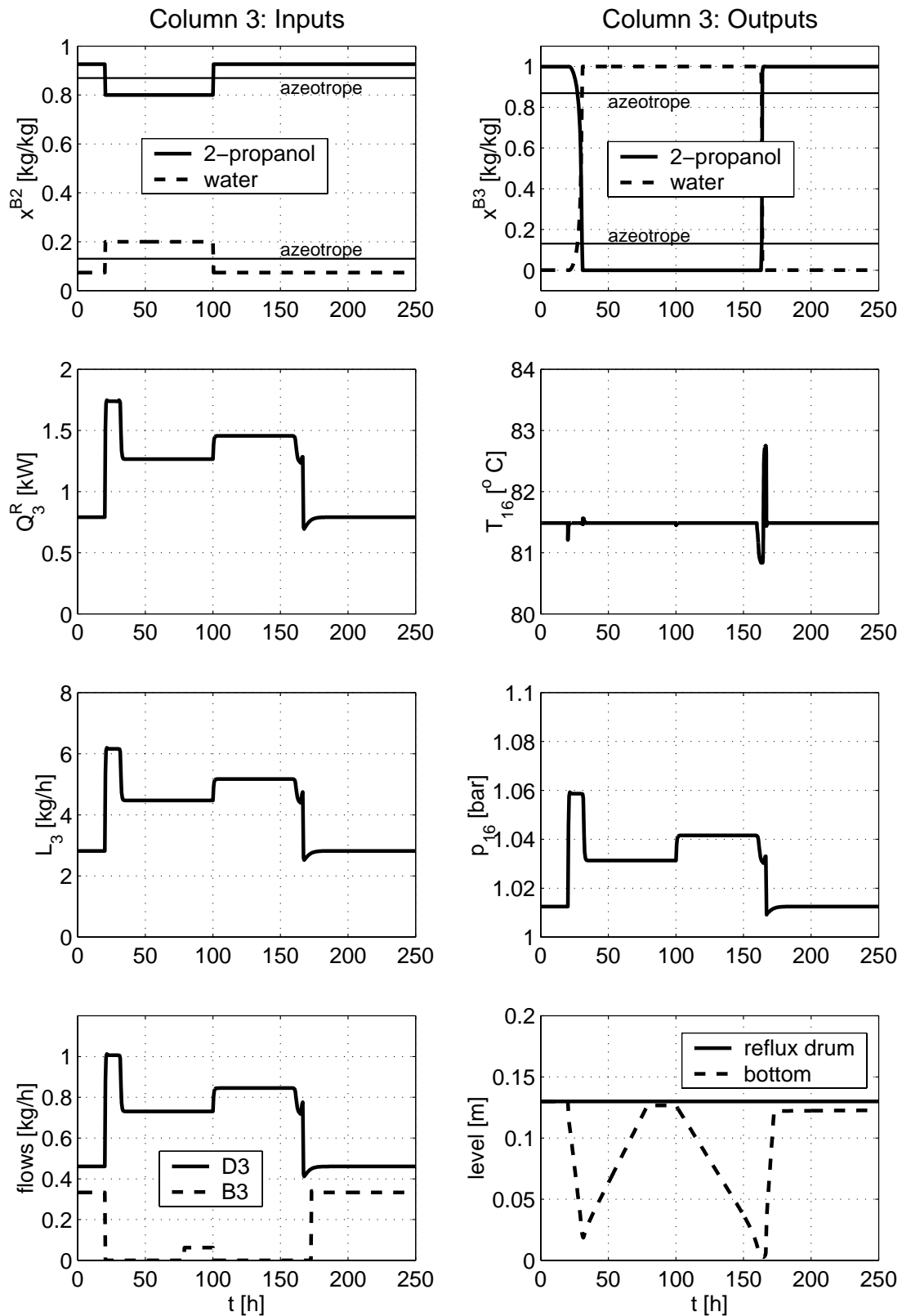


Figure 6.31: Changes in x^{B2} such that the mass balance forces x^{B3} to cross the azeotrope (indicated by the thin solid lines in the upper two plots).

6.8.4 Control of the Three Column Sequence

In the sections 6.8.1 to 6.8.3, it was shown the three columns work fine with constant reflux-to-distillate ratios and controllers that manipulate the reboiler duty to control a temperature front. Figure 6.32 and Figure 6.33 shows the reaction of the full three column sequence to changes in the crude feed composition x^{FC} . The controllers can adjust the process well. All reboiler duties scale linear with the 2-propanol content in the crude feed, as expected. The only drawback is that the purity of x^{B1} cannot be kept within specifications. In this case, the setpoint of TC1 has to be adjusted also to account for changes in x^{FC} .

Figure 6.34a shows the controlled temperatures for the three columns as a function of the methanol mass fraction in the crude feed at a constant water mass fraction of 0.334 for the specifications of set 2a (Table 6.4) as described in section 6.6.5 and illustrated in Figure 6.12. The temperature front in column 1 is very sensitive to the changes in the crude feed composition and hence varies with x^{FC} . For $T_{28} = 91.78^\circ \text{C}$ (the setpoint for the base case feed, Table 6.1), the bottom purity x_{water}^{B1} will be higher than 0.9998 for $x_{methanol}^{FC} < 0.333$ and lower than 0.9998 for $x_{methanol}^{FC} > 0.333$. For $x_{methanol}^{FC} < 0.528$, the controlled temperatures of column 2 and column 3 are constant. The reason is that x^{D1} is constant giving a constant T_{28} for column 2 and a constant x^{B2} . This gives a constant T_{16} for column 3. For $x_{methanol}^{FC} > 0.528$, the optimal operation point is where $R_2 = 0$ and x^{D1} changes. This also changes the temperature fronts in column 2 and column 3 which is reflected by the change of the two temperatures. In a dynamic simulation, these temperatures may also change because of the pressure change caused by the different loads of the columns for varying crude feed composition. This is not reflected here.

Figure 6.34b shows the product purities for set 4a which is as set 2a but with the following temperature fixed (instead of the product purities): $T_{28}^{column1} = 91.78^\circ \text{C}$, $T_{28}^{column2} = 73.28^\circ \text{C}$, and $T_{16}^{column3} = 81.49^\circ \text{C}$. As expected, $x^{B1} > 0.9998$ for $x_{methanol}^{FC} < 0.333$ and lower for higher methanol contents. In region 1 ($R_2 = 0$ is optimal solution), the purities decrease for column 1 and column 3. If the sequence is operated close to that region as defined in section 6.6.1, the temperature set points will have to be adjusted. If a lower purity is

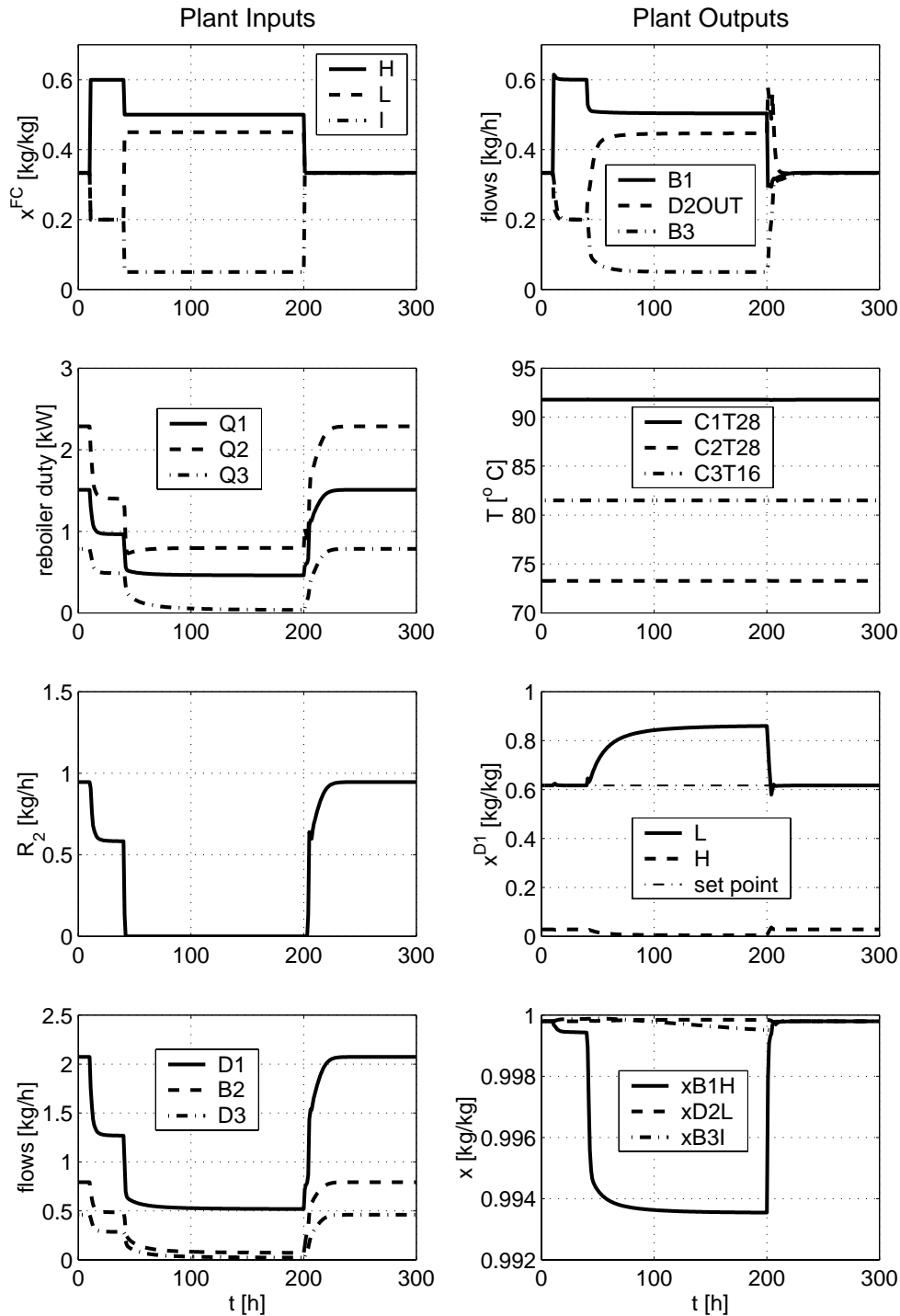


Figure 6.32: Dynamic simulation of the three column sequence for changes in the feed composition x^{FC} (series 1).

accepted, set 4a will operate very robust as shown in Figure 6.32 and Figure 6.33.

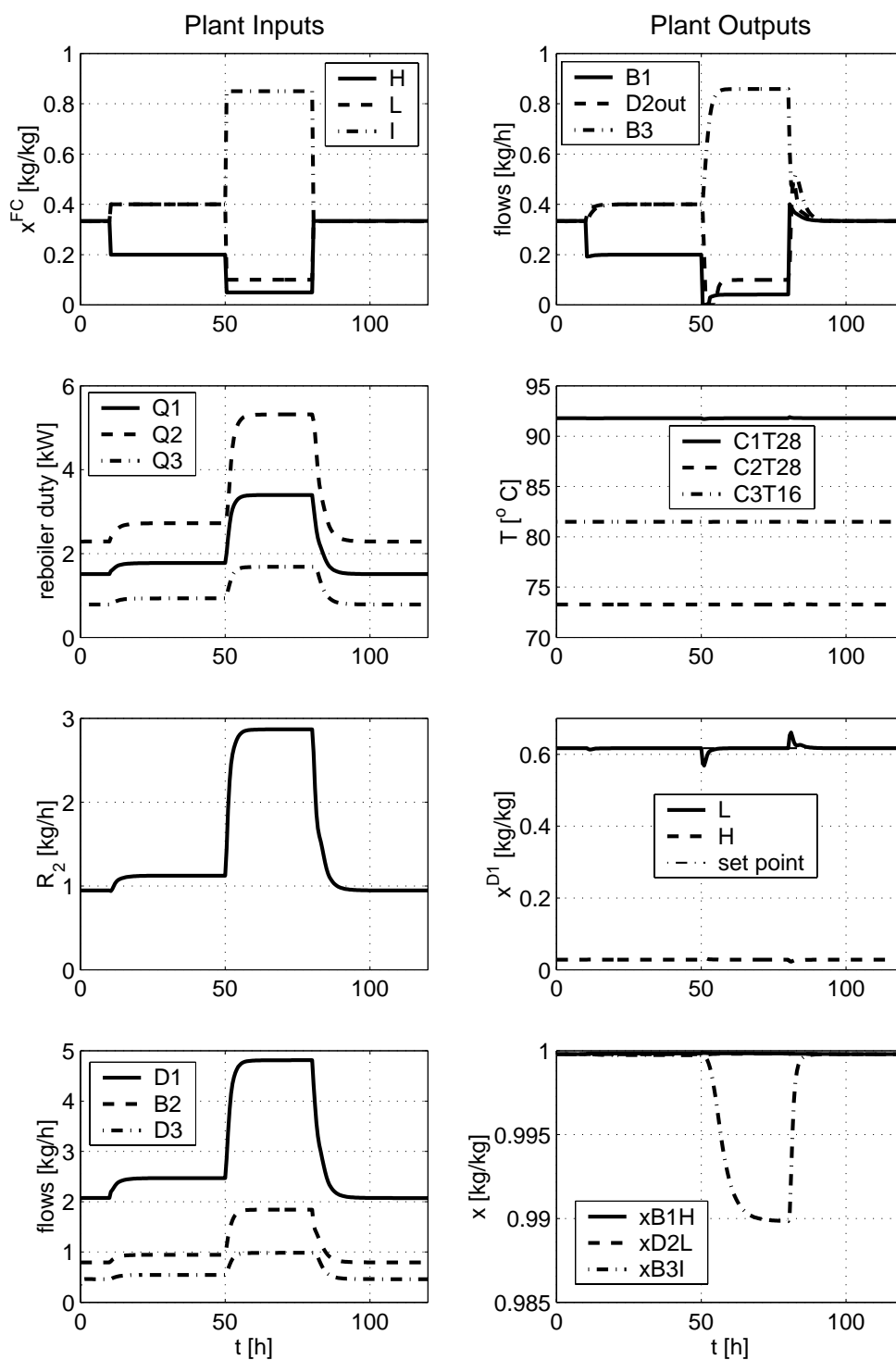


Figure 6.33: Dynamic simulation of the three column sequence for changes in the feed composition x^{FC} (series 2).

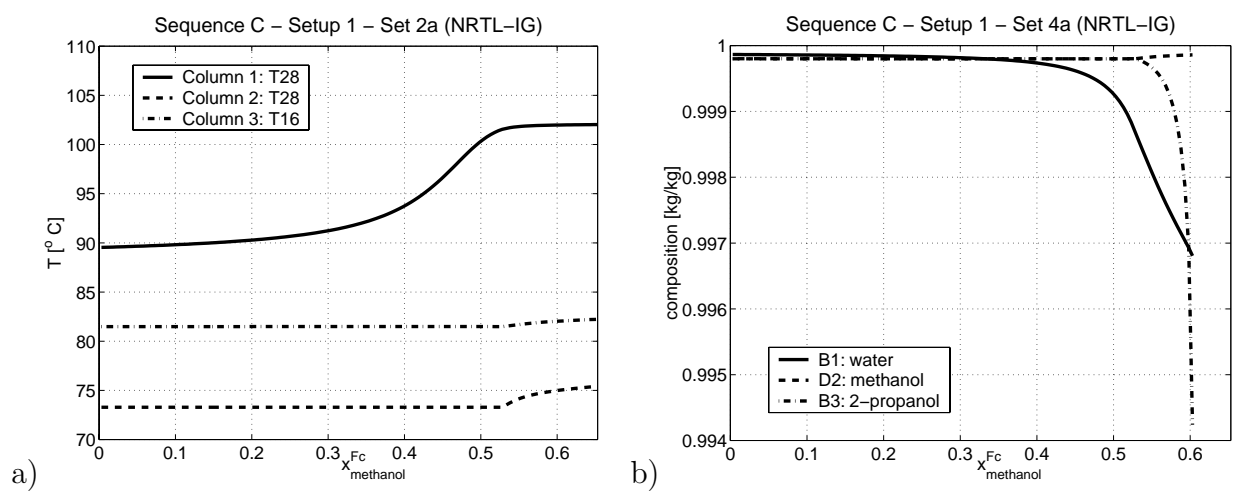


Figure 6.34: Sequence C, setup 1: a) The three controlled temperatures for the set 2a (over-refluxed columns, fixed product compositions) for different $x_{\text{methanol}}^{F_C}$ at $x_{\text{water}}^{F_C} = 0.334$, b) the three product purities for set 4a (over-refluxed columns, fixed temperatures).

Chapter 7

Performance of Homogeneous and Heterogeneous Sequences

In chapter 5, the ∞/∞ boundary separation scheme was analyzed and optimal operation points for the three setups were identified using the approximation that the sum of the reboiler duties is proportional to the sum of the distillate flows. Further, a self-optimizing control concept was elaborated. In chapter 6, the results of the ∞/∞ analysis were validated with simulations of a real process: the separation of methanol, 2-propanol and water. Chapter 6 focussed more on the operation of the process. In this chapter, the performance of setup 1 and setup 2 is compared for the separation of methanol, 2-propanol, and water using a short cut method. Further, the results are compared to heterogeneous distillation column sequences.

A fair economic comparison is based on the total annualized cost that includes capital costs and operating costs. To exclude the influence of the capital costs from this analysis, the same equipment is used for all homogeneous and heterogeneous sequences: a combination of two columns with 30 stages (including top and bottom) and one column with 50 stages (including top and bottom). The difference between the cost of a reflux drum and a decanter is neglected. Concerning the operating costs, the energy consumption is the main cost factor. Therefore, it will be used as cost function to compare the performance of the column sequences. For a fixed column design, the energy consumption depends only on

physical properties of the mixture. In general, it is possible to model all possible column configurations for the desired separation task and to compare the energy consumption. The method proposed here is a short cut method. Using residue curve map information and one rigorous simulation, an estimate for the energy consumption for the whole feed composition range is given. This can be used as a first step to decide which process has some potential for a given feed and which process does not need to be further analyzed.

7.1 Boundary Separation Scheme

The key idea for the optimization of the boundary separation scheme is that the reboiler duty is directly proportional to the distillate rate in a first approximation (equation 5.6, as derived in section 5.2). The optimization problem is in this case:

$$J_{min} = \min_y (k_1 D_1 + k_2 D_2 + k_3 D_3) \quad (7.1)$$

subject to:

1)

$$\begin{bmatrix} x_{water}^{D_1} & -x_{water}^{D_2} & -x_{water}^{D_3} \\ x_{methanol}^{D_1} & -x_{methanol}^{D_2} & -x_{methanol}^{D_3} \\ 1 & -1 & -1 \end{bmatrix} \begin{bmatrix} D_1 \\ D_2 \\ D_3 \end{bmatrix} = b(x^{FC}, F_C) \quad (7.2)$$

- 2) D_1 , D_2 , and D_3 non negative,
- 3) $x^{D_1} \in$ residue curve boundary,
- 4) x^{D_2} at pure methanol,
- 5) x^{D_3} at the 2-propanol–water azeotrope.

where the vector of unknowns is

$$y = [D_1; D_2; D_3; x_{water}^{D_1}; x_{methanol}^{D_1}] \quad (7.3)$$

The optimal operation point of boundary separation scheme for a given feed is found in three steps:

Table 7.1: Optimal parameters for setup 2 for the base feed (Table 6.1) using NRTL-IG.

specified variable	value	manipulated variable	value
$x_{water}^{B_1}$	0.9998 kg/kg	D_1	14.662 kg/h
L_1/D_1	1.2	L_1	17.595 kg/h
$x_{methanol}^{D_1}$	0.5935	R_2	8.7 kg/h
$x_{methanol}^{D_2}$	0.9998 kg/kg	D_2	9.033 kg/h
$x_{methanol}^{B_2}$	0.0005 kg/kg	Q_2^R	14.353 kW
$x_{2-propanol}^{B_3}$	0.9998 kg/kg	B_3	0.333 kg/h
$x_{water}^{D_3}$	0.1272 kg/kg	Q_3^R	4.271 kW

Table 7.2: Relation between Q_i^R and D_i for setup 2 at the optimal operation point for the NRTL-IG parameter set and the base feed (Table 6.1).

column	Q_i^R	D_i	k_i
1	8.720 kW	14.662 kg/h	0.595 kW/(kg/h)
2	14.353 kW	9.033 kg/h	1.589 kW/(kg/h)
3	4.721 kW	6.296 kg/h	0.750 kW/(kg/h)

- 1) the optimal x^{D_1} is found for $k_1 = k_2 = k_3 = 1kW/(kg/h)$ using residue curve map information only,
- 2) the finite sequence is optimized as discussed in section 6.4 which gives the k_i that can be used for the second optimization,
- 3) with these k_i (Table 6.3 in this case), the optimal cost function is determined as a function of the crude feed composition x^{FC} .

This gives for setup 1 for feed in the regions 1 and 2:

$$J_{Setup1} = 12.47 \frac{kW}{kg/h} \left(1 - x_{water}^{FC} - x_{methanol}^{FC}\right) F_C \quad (7.4)$$

For setup 2, the k_i are different. The optimal variables of the full sequence are listed in Table 7.1 for the base case feed. With the resulting k_i (Table 7.2), the cost function for setup 2 is:

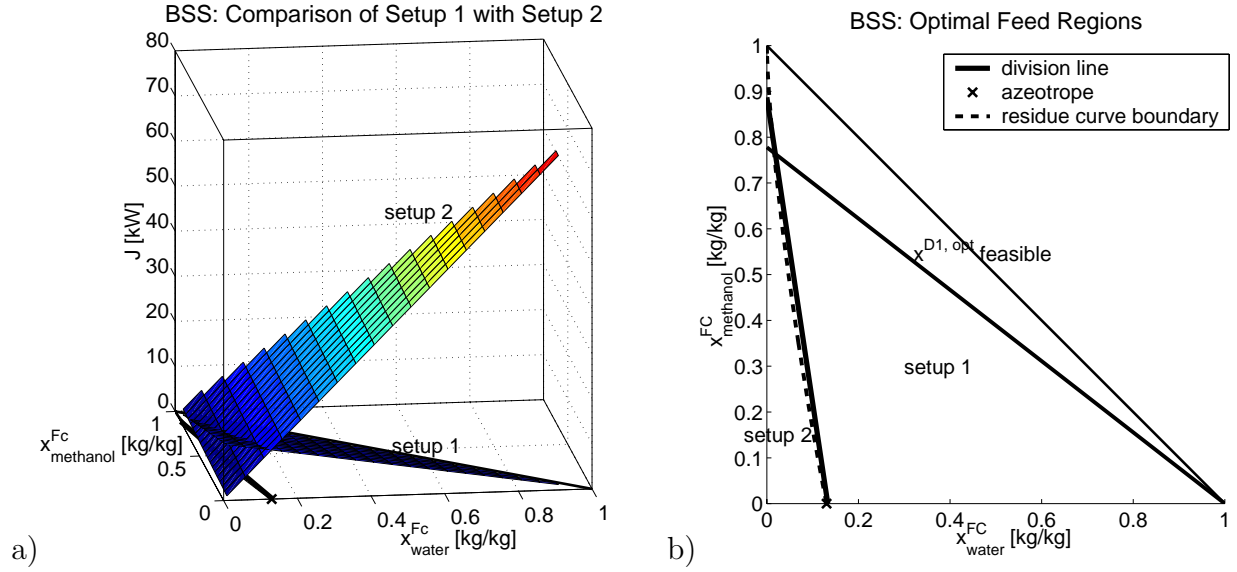


Figure 7.1: a) J_{setup1} and J_{setup2} as a function of the crude feed composition x^{Fc} (flow rate = 1 kg/h). b) Two regions where setup 1 and setup 2 are optimal.

$$J_{\text{Setup2a}} = \left(81.27 \frac{\text{kW}}{\text{kg/h}} x_{\text{water}}^{Fc} + 1.59 \frac{\text{kW}}{\text{kg/h}} x_{\text{methanol}}^{Fc} \right) F_C \quad (7.5)$$

For setup 2, k_1 and k_2 hardly change compared to setup 1, but k_3 is just half of the value for setup 1. The different location of the crude feed changes the mass balance of column 2 such that x^{B2} is closer to the 2-propanol–water azeotrope than for setup 1. This changes the split D_3/B_3 of column 3 which changes k_3 .

Figure 7.1a shows the cost functions J_{setup1} and J_{setup2} as a function of the crude feed composition x^{Fc} . They intersect in a line that can be calculated by setting equation 7.4 equal to equation 7.5:

$$x_{\text{methanol}}^{Fc} = 0.887 - 6.667 x_{\text{water}}^{Fc} \quad (7.6)$$

Figure 7.1b shows the different optimal regions for setup 1 and setup 2. The intersection line lies close to the residue curve boundary. The exact location depends on the curvature, but the intersection line will always cross the x_{water}^{Fc} axis close to the azeotrope. Above the line indicated with $x^{D1, opt}$ feasible, the cost function is not linear for setup 1. If the composition of the crude feed lies close to the line separating setup 1 and setup 2 and close to this feasibility line, both setups have to be investigated in a rigorous simulation to identify the better setup.

Table 7.3: Comparison of the cost function J for the two different setups and different feed compositions (flow rate: 1 kg/h) obtained by predictions of the ∞/∞ analysis and rigorous simulations.

feed		setup 1: J [kW]		setup 2: J [kW]	
$x_{methanol}^{F_C}$	$x_{water}^{F_C}$	predicted	simulated	predicted	simulated
0.333	0.334	4.154	4.169	27.675	27.343
0.333	0.200	5.826	5.802	16.784	17.267
0.333	0.083	7.285	7.219	7.275	8.262
0.333	0.050	7.697	7.617	4.593	5.663

To validate that this procedure is a justified approximation, setup 1 and setup 2 are simulated for different feeds that lie close to that boundary with the specified variables given in Table 6.2 and Table 7.1, respectively. The results are shown in Table 7.3. The difference of the simulation and prediction for the base case feed results from the fact that pure products are used instead of products with 0.9998 purity. For the other crude feed compositions, the accuracy of the prediction is fair enough as a first approximation. The difference is mainly caused by the fact that the approximation (equation 5.6) is not exact for varying crude feeds for column 1 of setup 1 and for column 2 of setup 2.

Figure 7.2 shows the reboiler duties of a finite sequence (setup 1) with specifications of set 1 (Table 6.4) validating the linear relationship. The difference of the reboiler duties between the rigorous simulation and equation 7.4 is less than 0.06 kW for the crude feeds in region 2 and 3 where the linear relationship is valid.

7.2 Heterogeneous Sequences

For the heterogeneous sequences, the methanol has to be removed first giving a setup as shown in Figure 7.3 for direct heterogeneous sequence. The crude feed F_C enters the column 1 where methanol is removed as D_1 . The bottom B_1 containing 2-propanol and water is fed to the recycle system of column 2 and column 3 with the entrainer cyclohexane.

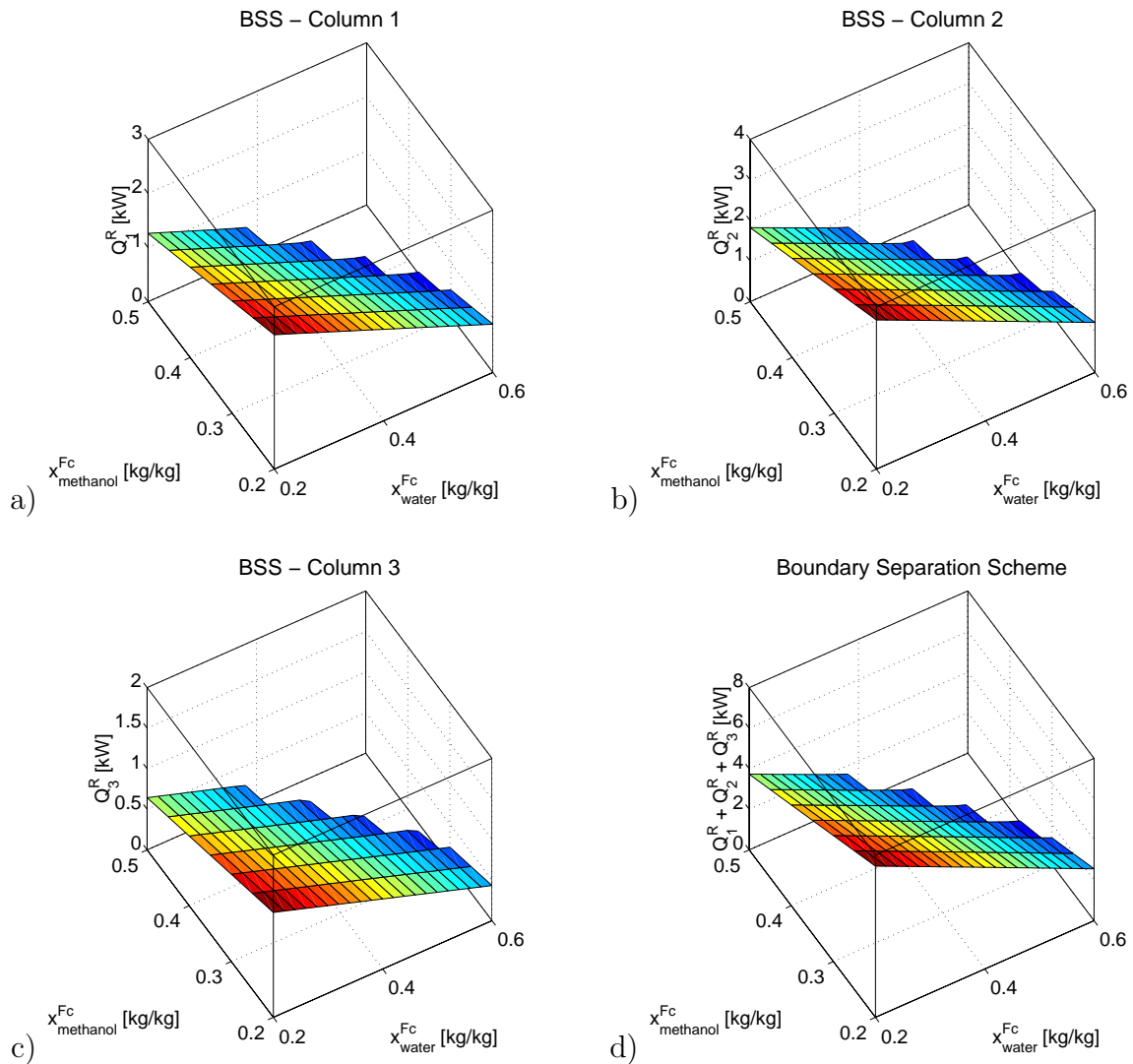


Figure 7.2: Reboiler duties of the boundary separation scheme setup 1 as function of the crude feed composition x^{Fc} for set 1 (Table 6.4).

These heterogeneous sequence can be either a direct sequence as shown in Figure 7.3 or an indirect sequence as will be introduced in section 7.2.3. These two sequences will be discussed later. First, the methanol removal column is analyzed.

7.2.1 Methanol Removal Column

As for the boundary separation scheme, the methanol removal column is the one with the 48 stages. The main interest is the dependence of the reboiler duties on the crude feed

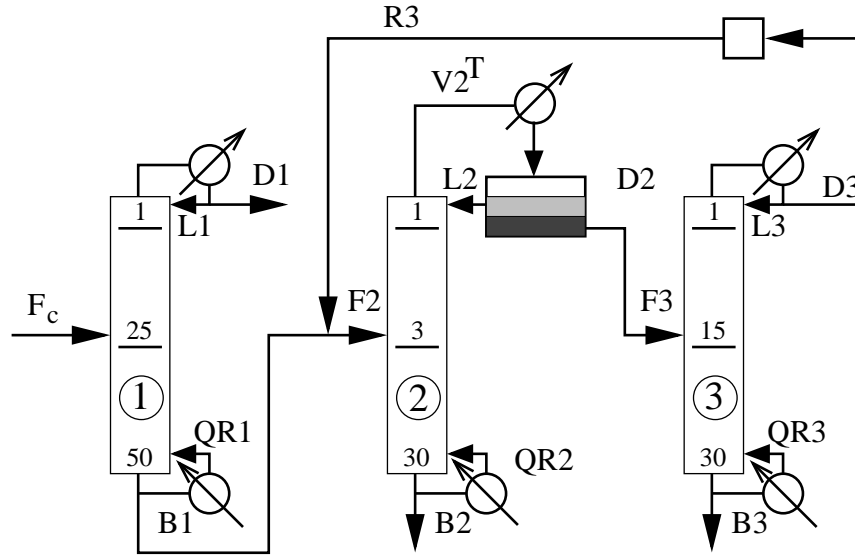


Figure 7.3: Setup of the direct heterogeneous sequence as implemented in AspenPlus for the system methanol / 2-propanol / water using cyclohexane as entrainer.

composition for the two specifications: $x_{methanol}^{D_1} = 0.9998$ and $x_{methanol}^{B_1} = 0.0001$. For these specifications, the distillate flow rate D_1 is proportional to the methanol content. However, Figure 7.4 shows that the reboiler duty is roughly proportional to the methanol content and the water content of the crude feed. This is mainly caused by the higher heat of vaporization of water (2256.7 kJ/kg at $p=1.013$ bar and $T=373.15$ K (VDI-Wärmeatlas, 1994)) compared to the one of 2-propanol (677.8 kJ/kg at $p=1.013$ bar and $T=355.65$ K (VDI-Wärmeatlas, 1994)). The approximation for the reboiler duty (equation 5.6) is good for columns with a constant feed composition and a constant split, as it is the case for the boundary separation scheme or the two columns of the heterogeneous sequence, but not for this case. To use the simple method of comparison as derived for the two setups of the boundary separation scheme (section 7.1), the reboiler duty Q_1^R is given by

$$Q_1^R = (1.221 x_{water}^{F_C} + 0.7936 x_{methanol}^{F_C} + 0.4261) \frac{kW}{kg/h} F_C \quad (7.7)$$

This relation was obtained by linear regression of the data points shown in Figure 7.4. It will be used to compute the sum of the reboiler duties of the complete direct and indirect sequences whose core sequences are analyzed next.

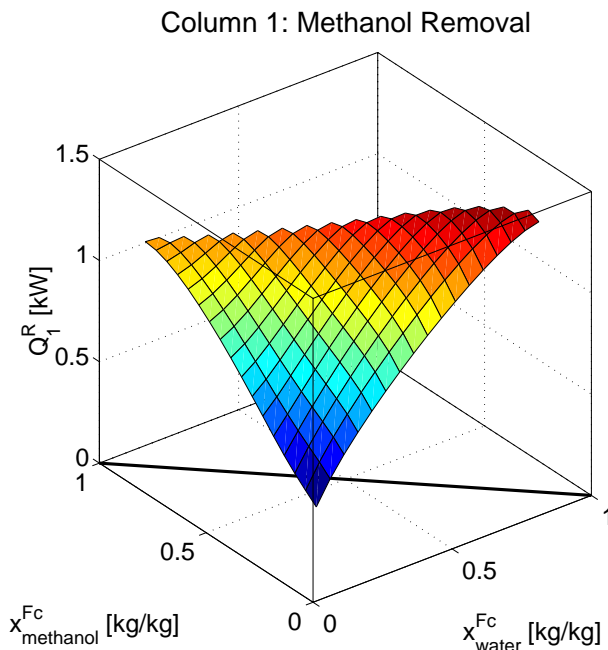


Figure 7.4: Reboiler duty of column 1 as a function of the crude feed composition.

7.2.2 Direct Heterogeneous Sequence

Figure 7.3 showed the setup of the direct heterogeneous sequence. Figure 7.5 shows the column profiles in a qualitative four component residue curve map¹. In column 2, 2-propanol leaves through the bottom B_2 , the overhead vapor V_2^T is condensed and fed to a decanter. The organic phase is taken as reflux and water is processed via D_2 to column 3. In column 3, the entrainer cyclohexane is recovered and recycled to column 2 via D_3 while the water leaves column 3 as bottoms.

The optimization of such a heterogeneous sequence has been discussed in literature for the separation of ethanol and water using benzene as entrainer (Ryan and Doherty, 1989; Doherty and Malone, 2001), which is also a 222-m mixture. Ryan and Doherty (1989) state that the composition of the entrainer recovery column should lie as close as possible to the residue curve boundary that connects the ternary azeotrope with the binary ethanol-water azeotrope (the 2-propanol–water azeotrope for the mixture here). They identify the position of the decanter tie-line as sole optimization factor. For their system, the variation

¹Computed residue curve maps and liquid-liquid equilibria are in Appendix B.1.

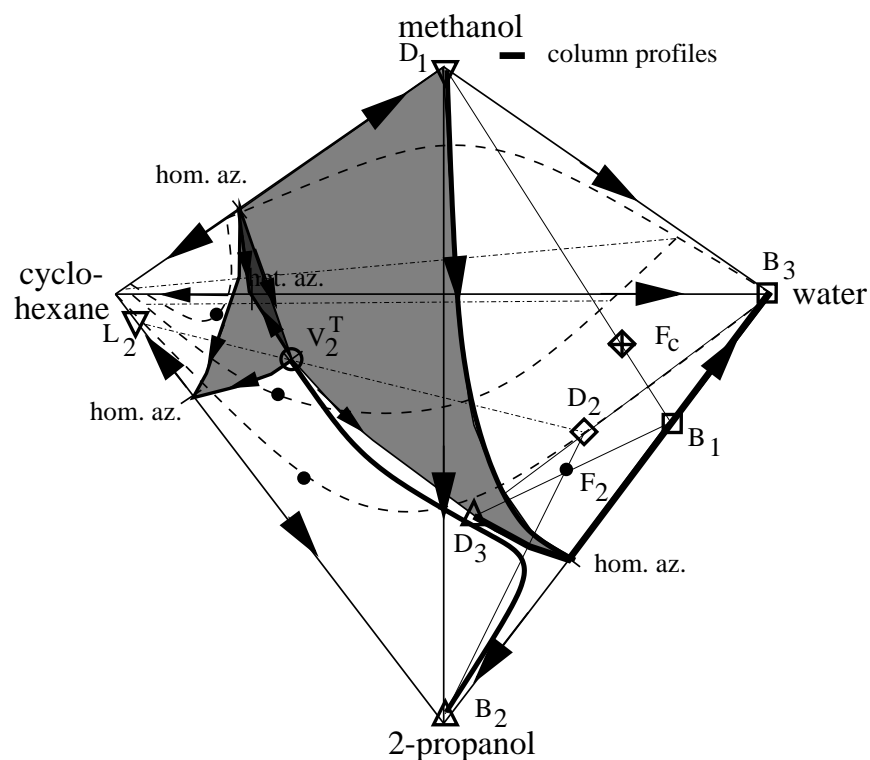


Figure 7.5: Quaternary residue curve map for the system methanol / 2-propanol / water using cyclohexane as entrainer illustrating qualitatively the column profiles and mass balances of the direct heterogeneous sequence (Figure 7.3).

of the decanter tie-line does not have a significant effect on the vapor rate of the azeotropic column, which is the column with decanter, because though the reflux ratio increases, the distillate flow rate decreases as a result of changing levers of the mass balances. Hence, the optimal value of $x^{V_2^T}$ is close to the ternary azeotrope. Doherty and Malone (2001) state that this does not hold in general and therefore these effects should be always analyzed as well. But for the short cut method presented here, this is taken as a good approximation.

Following the results of Ryan and Doherty (1989), the optimal point of the direct heterogeneous sequence for the mixture 2-propanol/water/cyclohexane is for $x^{V_2^T}$ at the ternary azeotrope and x^{D_3} lying at the residue curve boundary connecting the ternary azeotrope with the binary 2-propanol–water azeotrope (this is consistent with minimizing the sum of the distillate flows). Also, the assumption holds that the reboiler duties are proportional to the distillate flow rates.

For an ∞/∞ column sequence, the profile of column 1 is of type I and type III. By this, all methanol leaves through the distillate D_1 and B_1 is a binary mixture of 2-propanol and water. The mass balance gives:

$$x_{methanol}^{B_1} = 0 \quad (7.8)$$

$$x_{2-propanol}^{B_1} = \frac{x_{2-propanol}^{F_C}}{(1 - x_{methanol}^{F_C})} \quad (7.9)$$

$$x_{water}^{B_1} = \frac{x_{water}^{F_C}}{(1 - x_{methanol}^{F_C})} \quad (7.10)$$

$$B_1 = (1 - x_{methanol}^{F_C}) F_C \quad (7.11)$$

The profiles of column 2 and column 3 are of type II with the two different stable nodes 2-propanol and water. The mass balance for column 2 is:

$$x^{D_2} D_2 + x^{B_2} B_2 = x^{D_3} D_3 + x^{B_1} B_1 \quad (7.12)$$

The mass balance can be rewritten as:

$$\begin{bmatrix} x_{water}^{D_2} & x_{water}^{B_2} & -x_{water}^{D_3} \\ x_{cyclohexane}^{D_2} & x_{cyclohexane}^{B_2} & -x_{cyclohexane}^{D_3} \\ 1 & 1 & -1 \end{bmatrix} \begin{bmatrix} D_2 \\ B_2 \\ D_3 \end{bmatrix} = \begin{bmatrix} x_{water}^{F_C} F_C \\ 0 \\ (1 - x_{methanol}^{F_C}) F_C \end{bmatrix} \quad (7.13)$$

This shows that D_2 and D_3 are linear functions of x^{F_C} for fixed product compositions. x^{D_2} and x^{D_3} were identified by rigorous simulations with the specifications given in Table 7.4 (see Appendix B.3 for details).

This gives:

$$\begin{bmatrix} 0.244574 & 0 & -0.11904 \\ 0.0725 & 0 & -0.0845 \\ 1 & 1 & -1 \end{bmatrix} \begin{bmatrix} D_2 \\ B_2 \\ D_3 \end{bmatrix} = \begin{bmatrix} x_{water}^{F_C} F_C \\ 0 \\ (1 - x_{methanol}^{F_C}) F_C \end{bmatrix} \quad (7.14)$$

Further, $k_2 = 0.685$ kW/(kg/h) and $k_3 = 0.459$ kW/(kg/h) for the base case feed (Table 6.1). With equation 7.7 for Q_1^R , the sum of the reboiler duties is:

$$J_{direct} = (0.4261 + 8.790 x_{water}^{F_C} + 0.7936 x_{methanol}^{F_C}) \frac{kW}{kg/h} F_C \quad (7.15)$$

Table 7.4: Specified and manipulated variables (in Aspen Plus simulator) for optimal operation point of the direct heterogeneous sequence for the base feed (Table 6.1) at the ideal case (B_1 without methanol).

specified variable	value	manipulated variable	value
$x_{methanol}^{D_1}$	0.9998 kg/kg	D_1	0.333 kg/h
$x_{methanol}^{B_1}$	0.0001	Q_1^R	1.130 kW
$x_{2-propanol}^{B_2}$	0.9998 kg/kg	B_2	0.333 kg/h
$x_{water}^{B_3}$	0.9998 kg/kg	B_3	0.334 kg/h
L_3/D_3	0.68	L_3	1.37 kg/h
$x_{cyclohexane}^{D_2}$	0.0725	R_3	2.0 kg/h

Note that this is based on the idealized assumption that B_1 is free of methanol. Methanol is a light boiling impurity with the same effects as discussed in section 3.3. The particular effect on the performance of the sequences is discussed in section 7.3 (see also appendix B.3.2 for more details).

7.2.3 Indirect Heterogeneous Sequence

Figure 7.6 shows the setup of the indirect heterogeneous sequence. Figure 7.7 shows the column profiles in a qualitative four component residue curve map. As for the direct sequence, the crude feed F_C enters the column 1 where methanol is removed as D_1 . The bottom B_1 containing the 2-propanol and water is mixed with D_2 , the water-rich phase of the azeotropic column. This mixture is fed to the second column (column 3) where the water is removed via B_3 and 2-propanol leaves together with water and the entrainer cyclohexane through the distillate D_3 . In the last column (column 2), 2-propanol is removed and the waste is recycled to column 3.

As for the direct sequence, a methanol free feed to the heterogeneous sequence is assumed. A mass balance can be derived that shows that the distillate flow rates are linear to the feed composition. This time, it is the mass balance around column 3:

$$x^{D_2} D_2 + x^{B_1} B_1 = x^{D_3} D_3 + x^{B_3} B_3 \quad (7.16)$$

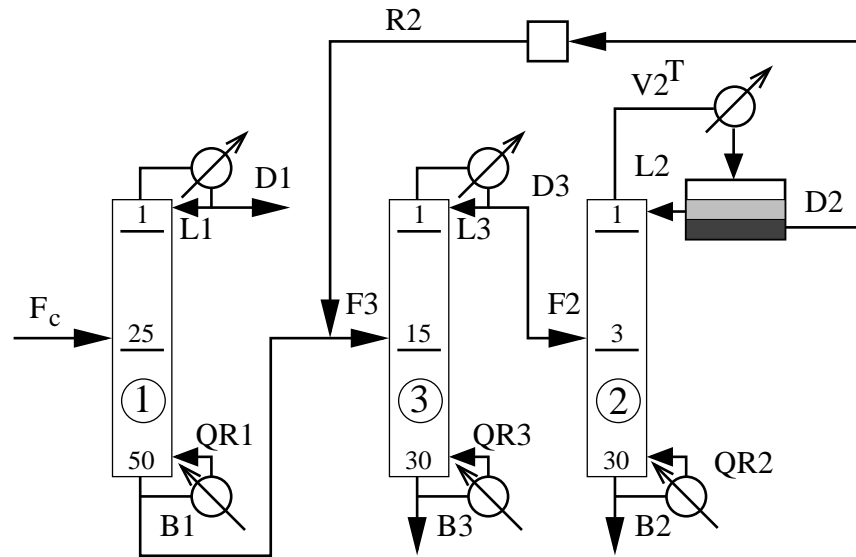


Figure 7.6: Setup of the indirect heterogeneous sequence as implemented in AspenPlus for the system methanol / 2-propanol / water using cyclohexane as entrainer.

Table 7.5: Specified and manipulated variables (in Aspen Plus simulator) for optimal operation point of the indirect heterogeneous sequence for the base feed (Table 6.1) at the ideal case (B_1 without methanol).

specified variable	value	manipulated variable	value
$x_{methanol}^{D_1}$	0.9998 kg/kg	D_1	0.333 kg/h
$x_{methanol}^{B_1}$	0.0001 kg/kg	Q_1^R	1.130 kW
$x_{2-propanol}^{B_2}$	0.9998 kg/kg	B_2	0.333 kg/h
$x_{water}^{B_3}$	0.9998 kg/kg	B_3	0.334 kg/h
-	-	L_3	1.36 kg/h
$x_{cyclohexane}^{D_3}$	0.038 kg/kg	R_2	0.32 kg/h

Equation 7.16 can be rewritten as:

$$\begin{bmatrix} -x_{water}^{D_2} & x_{water}^{D_3} & x_{water}^{B_3} \\ -x_{cyclohexane}^{D_2} & x_{cyclohexane}^{D_3} & x_{cyclohexane}^{B_3} \\ -1 & 1 & 1 \end{bmatrix} \begin{bmatrix} D_2 \\ D_3 \\ B_3 \end{bmatrix} = \begin{bmatrix} x_{water}^{F_C} F_C \\ 0 \\ (1 - x_{methanol}^{F_C}) F_C \end{bmatrix} \quad (7.17)$$

A rigorous AspenPlus simulation (specifications in Table 7.5, see Appendix B.4 for details) for the base case feed (Table 6.1) gives:

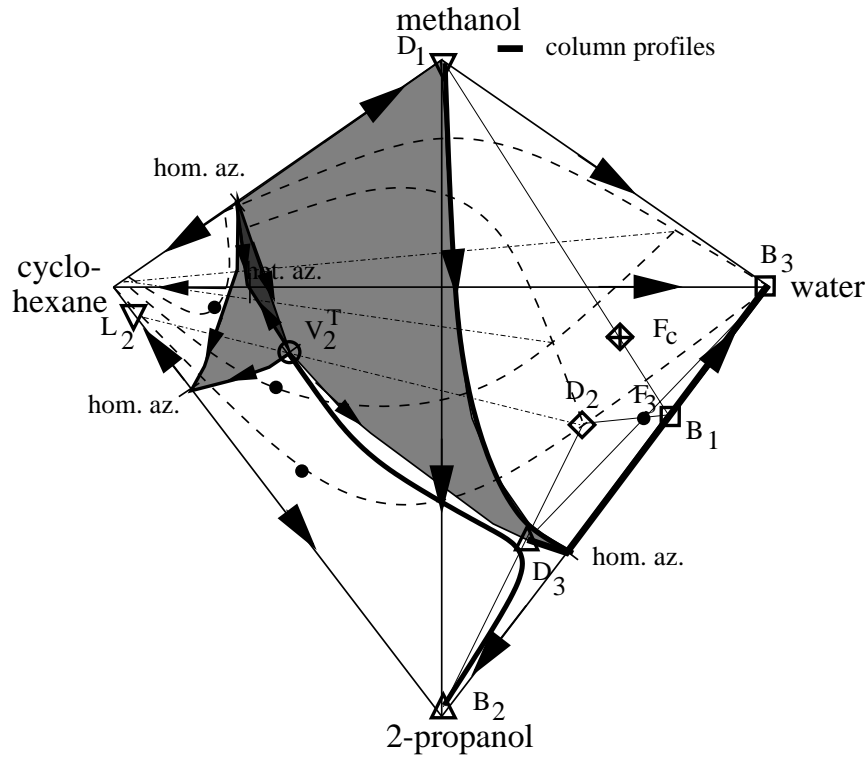


Figure 7.7: Quaternary residue curve map for the system methanol / 2-propanol / water using cyclohexane as entrainer illustrating qualitatively the column profiles and mass balances of the indirect heterogeneous sequence (Figure 7.6).

$$\begin{bmatrix} -0.2348303 & 0.1153446 & 1 \\ -0.0774325 & 0.038 & 0 \\ -1 & 1 & 1 \end{bmatrix} \begin{bmatrix} D_2 \\ D_3 \\ B_3 \end{bmatrix} = \begin{bmatrix} x_{water}^{F_C} F_C \\ 0 \\ (1 - x_{methanol}^{F_C}) F_C \end{bmatrix} \quad (7.18)$$

and $k_2 = 0.673 \text{ kW}/(\text{kg/h})$ and $k_3 = 0.750 \text{ kW}/(\text{kg/h})$. With equation 7.7 for Q_1^R , the sum of the reboiler duties is:

$$\begin{aligned} J_{indirect} &= (0.4261 + 1.221 x_{water}^{F_C} + 0.7936 x_{methanol}^{F_C}) \frac{\text{kW}}{\text{kg/h}} F_C \\ &\quad + 2.122 \frac{\text{kW}}{\text{kg/h}} (1 - x_{water}^{F_C} - x_{methanol}^{F_C}) F_C \\ &= (2.5481 - 0.901 x_{water}^{F_C} - 1.328 x_{methanol}^{F_C}) \frac{\text{kW}}{\text{kg/h}} F_C \end{aligned} \quad (7.19)$$

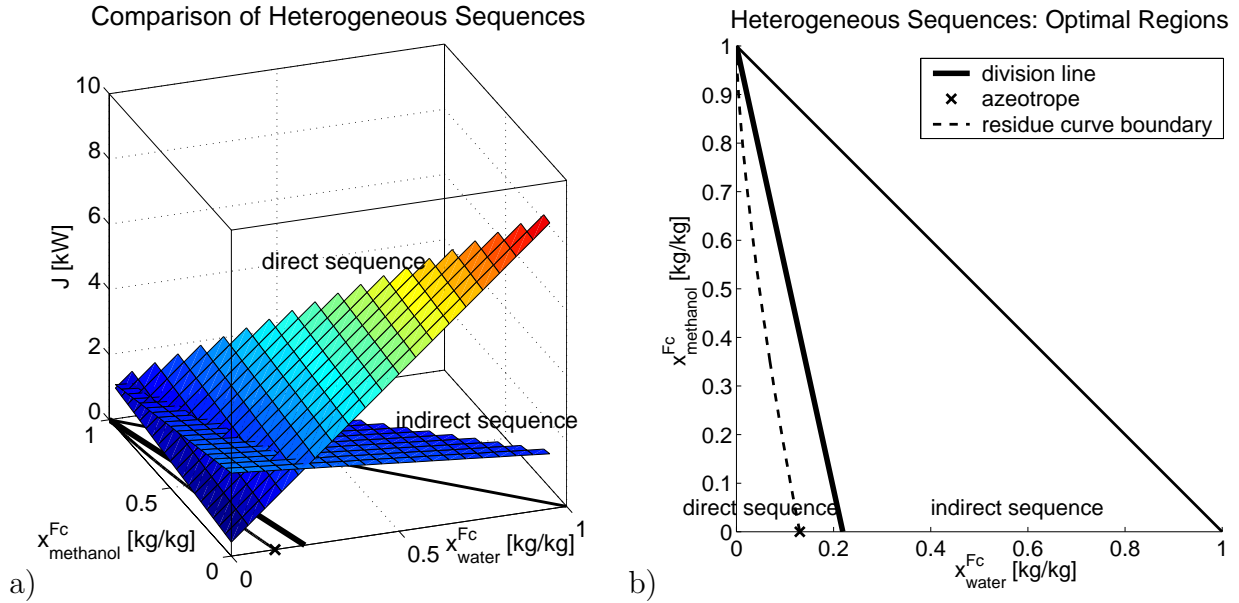


Figure 7.8: a) The two cost functions for the direct and indirect heterogeneous sequence as a function of the crude feed composition x^{Fc} . b) The two crude feed regions where the direct sequence and the indirect sequence are optimal.

7.2.4 Comparison of the Direct with the Indirect Sequence

Figure 7.8a shows the cost functions of the direct and the indirect sequence as a function of the crude feed composition x^{Fc} . They intersect in a line that can be calculated by setting equation 7.15 equal to equation 7.19:

$$x_{\text{methanol}}^{Fc} = 1 - 4.567x_{\text{water}}^{Fc} \quad (7.20)$$

Figure 7.8b shows the different optimal regions for the direct sequence and the indirect sequence. Compared to the boundary separation scheme, the intersection line does not lie close to the residue curve boundary. Though the line is correlated to the location of the binary azeotrope, the exact run depends on the location of the ternary azeotrope and the location of the corresponding tie line. Hence, it depends on the chosen heterogeneous entrainer.

The location of the intersection line and the linear dependence of the reboiler duties of the two heterogeneous sequences is validated with rigorous simulations. The process specifications were given in Table 7.4 and in Table 7.5. Figure 7.9 shows the sum of Q_2^R and Q_3^R of the two sequences for $x_{\text{methanol}}^{Fc} = 0.333$ kg/kg and varying x_{water}^{Fc} such that $x_{\text{water}}^{B_1}$ changes.

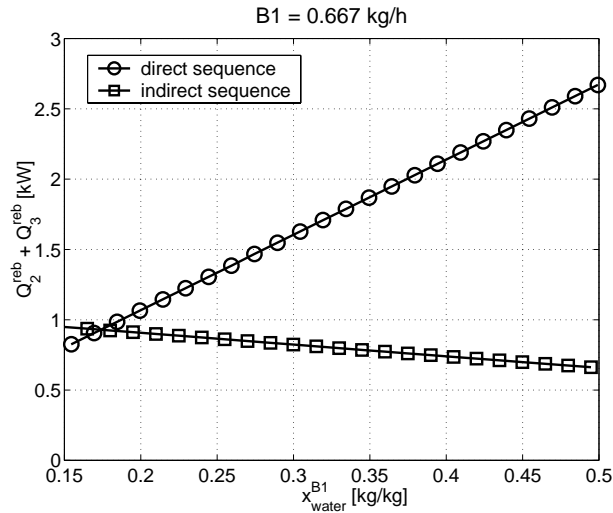


Figure 7.9: Comparison of the reboiler duties for a methanol-free feed $B_1 = 0.667 \text{ kg/h}$ and varying water contents. The direct sequence with specifications of Table 7.4 and indirect sequences with specification as in Table 7.5.

They intersect at $x_{water}^{F_C} = 0.17 \text{ kg/kg}$ which corresponds well to the value obtained by equation 7.20: 0.146 that was obtained by an linearized approximation of Q_1^R .

7.3 Comparison of the Homogeneous Sequences with the Heterogeneous Sequences

For the four sequences, the cost functions are plotted in Figure 7.10a as a function of the crude feed composition. The cost function for setup 2 of the boundary separation scheme is larger than the cost functions of the other scheme. An exception is a very small region close to the binary methanol–2-propanol edge. In Figure 7.10b, the cost functions of setup 1 of the boundary separation scheme and of the two heterogeneous sequences are shown. These three planes intersect in one point and thrice with each other. The projection of these intersections is plotted on the ground of the cube. For a clearer picture, these line are also plotted in the residue curve map in Figure 7.11a. To see these regions even more clearly, Figure 7.11b shows a qualitative division of the component space with shaded regions indicating for which sequence the cost function is minimal.

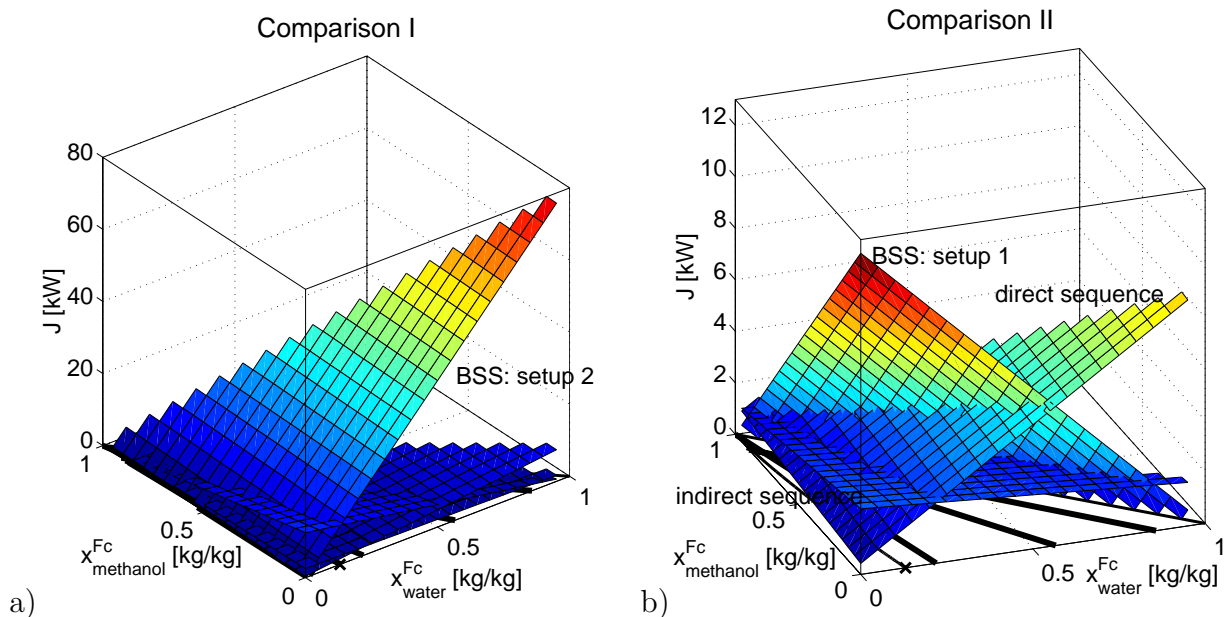


Figure 7.10: Comparison of the cost functions of a) setup 1 and setup 2 of the boundary separation scheme with the two heterogeneous sequences, and b) setup 1 of the boundary separation scheme with the two heterogeneous sequences.

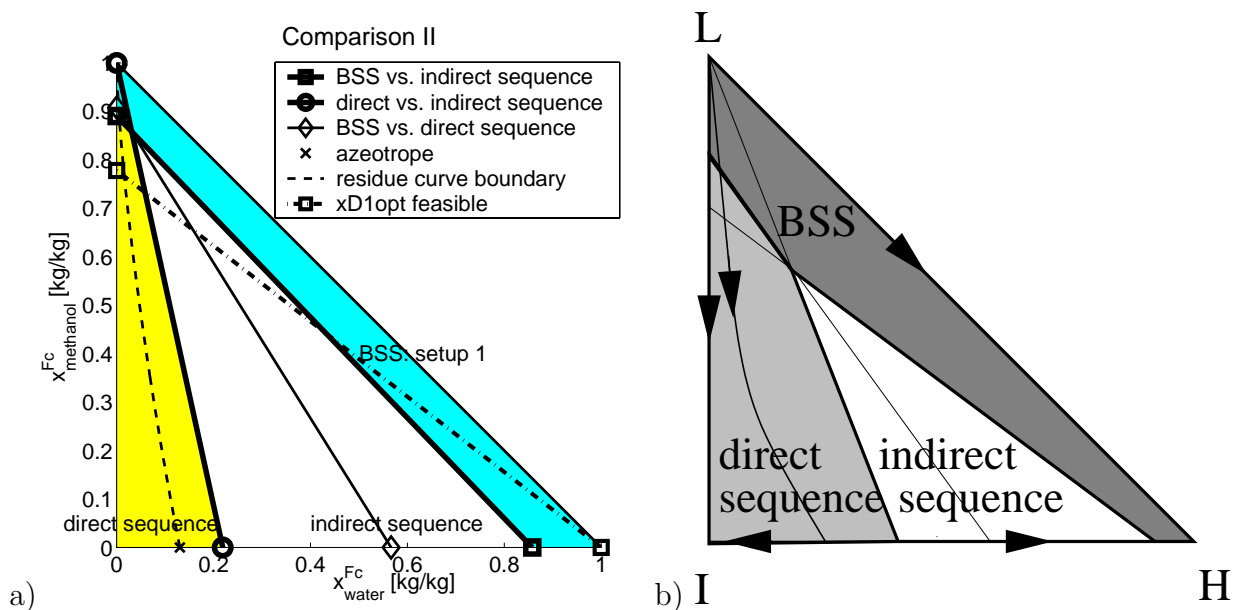


Figure 7.11: a) Projection of the intersections of the different cost functions shown in Figure 7.10b, b) qualitative figure for illustration.

Figure 7.11a shows that the indirect heterogeneous sequence is the one which is optimal over the broadest range of crude feeds. The direct sequence is best for low water contents,

Table 7.6: Distillate compositions of the heterogeneous sequences for accumulated methanol in the recycle loop.

	flow	$x_{methanol}$	$x_{cyclohexane}$	$x_{2-propanol}$	x_{water}
direct	D_2	0.0985631	0.0982354	0.6029861	0.2002153
sequence	D_3	0.1103395	0.1103391	0.6772571	0.1020643
indirect	D_2	0.2004302	0.2005077	0.4910242	0.1080378
sequence	D_3	0.1502711	0.1503292	0.6183491	0.0910506

the boundary separation scheme setup 1 is best for low 2-propanol contents. A crucial part is the line shown in Figure 7.11a that indicates whether $x^{D_1, opt}$ is feasible for a given x^{FC} , or not. For x^{FC} above this line, $x^{D_1, opt}$ is infeasible and the cost function of setup 1 is nonlinear. This nonlinearity causes a flatter slope than the linear correlation. The boundary separation scheme and the indirect heterogeneous sequence will have a similar performance then. However, there is a catch for the heterogeneous sequences: the impurity methanol which was not taken into account in this analysis.

If methanol is taken into account, the whole picture will change. Methanol is the lightest boiling component and has homogeneous minimum-boiling azeotrope with cyclohexane, which is the unstable node of the four component mixture (compare to Figure 7.5). According to the analysis in section 3.3, this causes trouble in the decanter operation because methanol will collect in the decanter and the phase split will disappear for high methanol contents in the decanter. In this case, a purge stream would be necessary (see appendix B.3.2 and appendix B.4.2 for details). Table 7.6 shows the compositions of the direct and indirect sequences for accumulated methanol. These compositions give $k_2 = 0.630$ kW/(kg/h) and $k_3 = 0.416$ kW/(kg/h) for the direct sequence. Together with equation 7.13, the sum of the two reboiler duties of column 2 and column 3 is:

$$Q_2^R + Q_3^R = 9.1486 \frac{kW}{kg/h} x_H^{FC} F_C \quad (7.21)$$

With equation 7.7 for Q_1^R , the sum of the reboiler duties is for the direct sequence:

$$J_{direct, high\ methanol} = (0.4261 + 10.3696 x_{water}^{FC} + 0.7936 x_{methanol}^{FC}) \frac{kW}{kg/h} F_C \quad (7.22)$$

For the indirect sequence, $k_2=0.522$ kW/(kg/h) and $k_3=0.506$ kW/(kg/h). With equa-

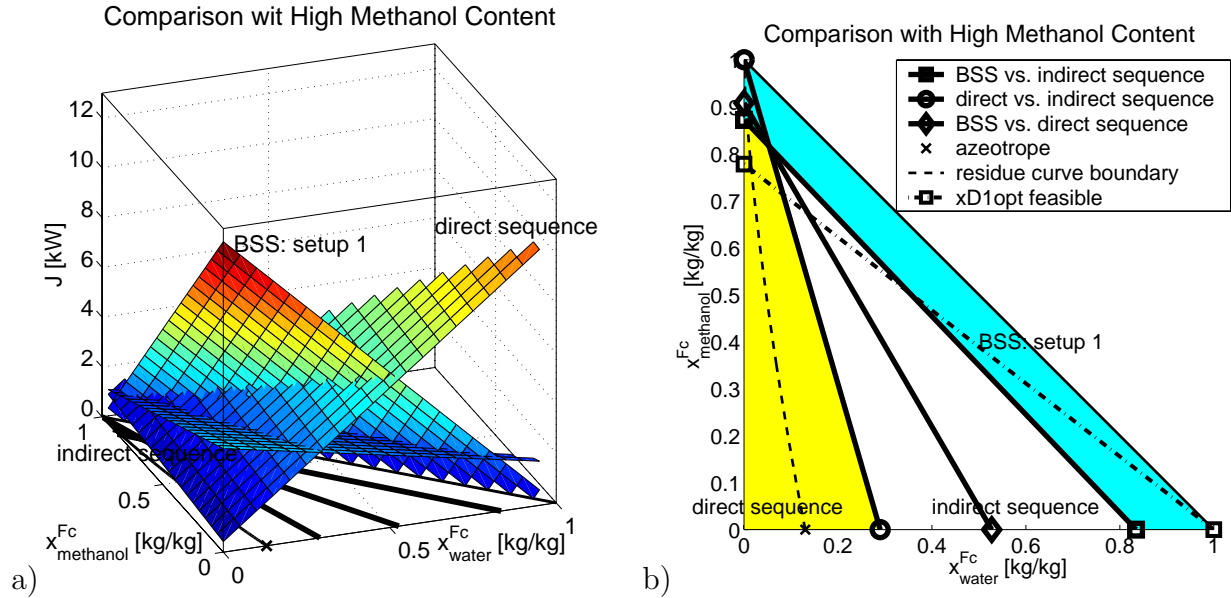


Figure 7.12: a) Comparison of the cost functions setup 1 of the boundary separation scheme with the two heterogeneous sequences for high methanol contents; b) the different optimal regions of the sequences.

tion 7.17, the sum of the two reboiler duties of column 2 and column 3 is:

$$Q_2^R + Q_3^R = 3.7358 \frac{kW}{kg/h} (1 - x_H^{Fc} - x_L^{Fc}) F_C. \quad (7.23)$$

With equation 7.7 for Q_1^R , the sum of the reboiler duties is for the indirect sequence:

$$J_{\text{indirect, high methanol}} = (4.1619 - 2.5148 x_{\text{water}}^{Fc} - 2.9422 x_{\text{methanol}}^{Fc}) \frac{kW}{kg/h} F_C \quad (7.24)$$

Figure 7.12a shows the new cost functions in comparison with the boundary separation scheme. Figure 7.12b shows that the region, where the boundary separation scheme is optimal, is larger. Contrary to the heterogeneous sequence, the boundary separation scheme does not have any problems like the pollution of the heterogeneous sequences with methanol which troubles the decanter operation. Hence, the boundary separation scheme is a real alternative for low 2-propanol contents.

Chapter 8

Conclusions

In this work, the ∞/∞ analysis (Bekiaris et al., 1993; Bekiaris et al., 1996) was used to understand and to propose control concepts for homogeneous and heterogeneous azeotropic distillation column sequences.

First (Part I), operation and control of a heterogeneous distillation column in presence of impurities was analyzed. These columns are operated such that the nominal top composition is close to the unstable node that is a heterogeneous azeotrope. For a fixed overall feed, these columns have one degree of freedom. To control two variables, a second manipulated variable was introduced: the entrainer makeup flow. Using a theoretical approach (the finite/ ∞ column), the influence of impurities on the process behavior was analyzed based on residue curve maps of the mixture. Impurities have an unpleasant effect on process operation if they change the locus of the unstable node. In that case, a two point control scheme is not able to robustly control the process, a third control loop has to be introduced which changes the overall feed of the process such that the plant is able to operate in the desired operation region.

The theoretical results were validated using simulations of a real industrial process. The reboiler duty/entrainer makeup flow/(decanter flush) schemes are expected to work well and to be easy to tune under real plant conditions if the decanter is designed in a way that it always returns reflux to the column. The larger the entrainer loss through the distillate is, the better is the performance of the controller that manipulates the makeup flow. If the

decanter design does not ensure reflux, the reboiler duty/reflux/(decanter flush) scheme has to be used which is not recommended: reboiler duty and reflux are not independent at steady state (the column has only one degree of freedom). Hence, the reboiler duty/reflux scheme has potentially the same problems as the DB scheme for regular distillation with added complexity. Currently, the industrial plant only operates satisfactorily because the reflux controller is very detuned: the reflux is adjusted manually to keep a temperature inside the column around the desired value. These results showed that plant design plays a major role for operation performance.

Second (Part II), operation and control of column sequences were analyzed. A sequence of three homogeneous azeotropic distillation columns with two recycles (boundary separation scheme) separates a three component 020 mixture into pure components. The intermediate and the heavy boiler form a minimum boiling azeotrope that is broken by the light boiler that acts as entrainer. The results are illustrated with simulations of three column sequence for the mixture of methanol, which acts as entrainer, 2-propanol and water. The process has seven degrees of freedom.

Studying a case with reduced complexity (columns of infinite length operated at infinite reflux), one of the two recycles (the recycle of the entrainer) was identified as the key manipulated variable to ensure the feasibility and optimality of the process. The key aspect is that the mass balance of column 1 has to be manipulated such that the distillate composition is at the optimal point. A sensitivity analysis shows that a control scheme that keeps the column compositions at the specified values is self-optimizing with respect to the energy consumption and robust towards model uncertainties.

Because of the recycle structure, the boundary separation scheme should be operated with constant reflux-to-distillate ratios. Dynamic simulations confirm that the boundary separation scheme can be operated with the $(L/D) Q^R$ scheme for each column and an additional control loop that controls the entrainer content in the sequence, in particular the entrainer fraction of the distillate of column 1 by manipulating the entrainer recycle flow. The importance of the entrainer holdup of the sequence will become even more pronounced if the boundary separation scheme is operated with a binary external feed of the azeotropic mixture because then, the entrainer can neither leave nor enter the system.

A buffer tank would be needed to allow the entrainer holdup to change.

Dynamic simulations showed that column profiles can cross residue curve boundaries, distillation boundaries and even azeotropes if the feed composition is changed such that a column profile is only feasible in the other distillation region. The operation concept of the boundary separation scheme can be transferred to heterogeneous distillation column sequences of a heterogeneous 222-m mixture: the entrainer recycle has to be manipulated such that the distillate of the heterogeneous column lies on the tie line which lies close to or at the ternary heterogeneous azeotrope. This is consistent with the results of Rovaglio et al. (1993) who also recognized the importance of the entrainer holdup in the system.

A short cut method was developed to compare the performance of homogeneous and heterogeneous sequences based on the sum of the reboiler duties for identical equipment. In general, the homogeneous boundary separation scheme has a lower energy consumption for low contents of the intermediate boiler of 020 mixtures compared to heterogeneous sequences with the same equipment. For methanol–2-propanol–water mixtures, the boundary separation scheme is the best alternative up to 15 mass-% 2-propanol in the crude feed compared to heterogeneous sequences that use cyclohexane as heterogeneous entrainer.

Bibliography

Andersen, H., Laroche, L. and Morari, M.: 1991, Dynamics of Homogeneous Azeotropic Distillation Columns, *Ind. Eng. Chem. Res.* **30**, 1846–1855.

Andersen, H., Laroche, L. and Morari, M.: 1995, Effect of Design on the Operation of Homogeneous Azeotropic Distillation, *Comput. Chem. Eng.* **19**(1), 105–122.

Asp: 1999a, *Aspen Dynamics Release 10 User Guide*.

Asp: 1999b, *Aspen Plus Release 10 Reference Manual: Physical Property Methods and Models*.

Bai, R., Yang, H., Hu, X., Wan, X. and Deng, J.: 2001, Study on separation flowsheet of methanol-ethanol-water ternary system by distillation, *Huaxue-Gongcheng-Chemical-Engineering* **29**(3), 8–10.

Bauer, M. and Stichlmair, J.: 1996, Superstructures for the Mixed Integer Optimization of Nonideal and Azeotropic Distillation Prozesses, *Comput. Chem. Eng.* **20**(Suppl.), S25–S30.

Bauer, M. and Stichlmair, J.: 1998, Design and economic optimization of azeotropic distillation processes using mixed-integer nonlinear programming, *Comput. Chem. Eng.* **22**(9), 1271–1286.

Bausa, J. and Tsatsaronis, G.: 2001, Reducing the energy demand of continuous distillation processes by optimal controlled forced periodic operation, *Comput. Chem. Eng.* **25**(2-3), 359–370.

- Bekiaris, N., Meski, G. and Morari, M.: 1996, Multiple Steady States in Heterogeneous Azeotropic Distillation, *Ind. Eng. Chem. Res.* **35**(1), 207–227.
- Bekiaris, N., Meski, G., Radu, C. and Morari, M.: 1993, Multiple Steady States in Homogeneous Azeotropic Distillation, *Ind. Eng. Chem. Res.* **32**(9), 2023–2038.
- Bozenhardt, H.: 1988, Modern control tricks solve distillation problems, *Hydrocarbon Process.* **67**(6), 47–50.
- Chien, I.-L., Wang, C. and Wong, D.: 1999, Dynamics and Control of a Heterogeneous Azeotropic Distillation Column: Conventional Control Approach, *Ind. Eng. Chem. Res.* **38**(2), 468–478.
- Chien, I.-L., Wang, C., Wong, D., Lee, C.-H., Cheng, S.-H., Shih, R., Liu, W. and Tsai, C.: 2000, Experimental Investigation of Conventional Control Strategies for a Heterogeneous Azeotropic Distillation Column, *J. Proc. Cont.* **10**(4), 333–340.
- Corrêa, R. and Jørgensen, S.: 1992, Static and Dynamic Behavior of Heterogeneous Azeotropic Distillation Columns, *Distillation and Absorption '92, IChemE Symposium Series No. 128*, Vol. 2, The Institution of Chemical Engineers, Rugby, UK, pp. B277–B296.
- De Malde, M., Cio, A. D. and Massi, M. M.: 1964, New SNAM process for isoprene, *Hydrocarbon Process. & Petroleum Refiner* **43**(7), 149.
- Doherty, M. and Caldarola, G.: 1985, Design and Synthesis of Homogeneous Azeotropic Distillations 3: The Sequencing of Columns for Azeotropic and Extractive Distillations, *Ind. Eng. Chem. Fundam.* **24**(4), 474–485.
- Doherty, M. and Malone, M.: 2001, *Conceptual Design of Distillation Systems*, McGraw Hill, Boston.
- Doherty, M. and Perkins, J.: 1978, On the Dynamics of Distillation Processes I: The Simple Distillation of Multicomponent Non-Reacting, Homogeneous Liquid Mixtures, *Chem. Eng. Sci.* **33**, 281–301.

- Dorn, C.: 2000, *Nonlinear Dynamics in Homogeneous Azeotropic Distillation*, PhD Thesis, ETH No. 13947, ETH Zürich, Switzerland. available via <http://www.control.ethz.ch/~disti>.
- Dorn, C., Güttinger, T., Wells, J., Morari, M., Kienle, A., Klein, E. and Gilles, E.: 1998, Stabilization of an Azeotropic Distillation Column, *Ind. Eng. Chem. Res.* **37**(2), 506–515.
- Dorn, C. and Morari, M.: 2002a, Qualitative Analysis for Homogeneous Azeotropic Distillation 1 — Local Stability, *Ind. Eng. Chem. Res.* **41**(16), 3930–3942.
- Dorn, C. and Morari, M.: 2002b, Qualitative Analysis for Homogeneous Azeotropic Distillation 2 — Bifurcation Analysis, *Ind. Eng. Chem. Res.* **41**(16), 3943–3962.
- Esbjerg, K., Andersen, T., Müller, D., Marquardt, W. and Jørgensen, S.: 1998, Multiple Steady States in Heterogeneous Azeotropic Distillation Sequences, *Ind. Eng. Chem. Res.* **37**(11), 4434–4452.
- Finco, M., Luyben, W. and Polleck, R.: 1989, Control of Distillation Columns with Low Relative Volatilities, *Ind. Eng. Chem. Res.* **28**(1), 75–83.
- Foss, A.: 1973, Critique of Chemical Process Control Theory, *AIChE J.* **19**(2), 209–214.
- Foucher, E., Doherty, M. and Malone, M.: 1991, Automatic Screening of Entrainers for Homogeneous Azeotropic Distillation, *Ind. Eng. Chem. Res.* **30**, 760–772.
- Frey, T., Bauer, M. and Stichlmair, J.: 1997, MINLP–Optimization of Complex Column Configuration for Azeotropic Mixtures, *Comput. Chem. Eng.* **21**(Suppl.), S217–S222.
- Gmehling, J., Menke, J., Krafczyk, J. and Fischer, K.: 1994, *Azeotropic Data*, VCH, Weinheim, Germany.
- Güttinger, T.: 1998, *Multiple Steady States in Azeotropic and Reactive Distillation*, PhD Thesis, ETH No. 12720, ETH Zürich, Switzerland. available via <http://www.control.ethz.ch/~disti>.
- Güttinger, T. and Morari, M.: 1996, Multiple Steady States in Homogeneous Separation Sequences, *Ind. Eng. Chem. Res.* **35**(12), 4597–4611.

- Hunek, J., Gal, S., Posel, F. and Glavič, P.: 1989, Separation of an Azeotropic Mixture by Reverse Extractive Distillation, *AIChE J.* **35**(7), 1207–1210.
- Jacobsen, E.: 1997, Effect of Recycle on the Plant Zero Dynamics, *Comput. Chem. Eng.* **21**(Suppl.), S279–S284.
- Jacobsen, E.: 1999, On the Dynamics of Integrated Plants – Non–Minimum Phase Behavior, *J. Proc. Cont.* **9**, 439–451.
- Jacobsen, E. and Skogestad, S.: 1991, Multiple Steady States in Ideal Two–Product Distillation, *AIChE Journal* **37**(4), 499–511.
- Jacobsen, E. and Skogestad, S.: 1994, Instability of Distillation Columns, *AIChE Journal* **40**(9), 1466–1479.
- Jacobsen, E. and Skogestad, S.: 1995, Multiple Steady States and Instability in Distillation. Implications for Operation and Control, *Ind. Eng. Chem. Res.* **34**(12), 4395–4405.
- Kister, H.: 2002, Can We Believe the Simulation Results?, *Chem. Eng. Prog.* **98**(10), 52–58.
- Knight, J. and Doherty, M.: 1989, Optimal Design and Synthesis of Homogeneous Azeotropic Distillation Sequences, *Ind. Eng. Chem. Res.* **28**(5), 564–572.
- Kovach III, J. and Seider, W.: 1987, Heterogeneous Azeotropic Distillation: Experimental and Simulation Results, *AIChE J.* **33**(8), 1300–1314.
- Kubierschky, K.: 1915, German Patent 287,897.
- Kürüm, S.: 1996, *Waste Minimisation in Chemical Process Industries with Economic Improvements via Simulation of Process Models*, PhD thesis, Swiss Federal Institute of Technology Zürich, Laboratorium für technische Chemie, ETH Zentrum, CH-8092 Zürich, Switzerland.
- Laroche, L., Bekiaris, N., Andersen, H. and Morari, M.: 1991, Homogeneous Azeotropic Distillation: Comparing Entrainers, *Can. J. of Chem. Eng.* **69**(12), 1302–1319.
- Laroche, L., Bekiaris, N., Andersen, H. and Morari, M.: 1992a, Homogeneous Azeotropic Distillation: Separability and Flowsheet Synthesis, *Ind. Eng. Chem. Res.* **31**(9), 2190–2209.

- Laroche, L., Bekiaris, N., Andersen, H. and Morari, M.: 1992b, The Curious Behavior of Homogeneous Azeotropic Distillation — Implications for Entrainer Selection, *AIChE Journal* **38**(9), 1309–1328.
- Larsson, T., Hestetun, K., Hovland, E. and Skogestad, S.: 2001, Self-Optimizing Control of a Large-Scale Plant: The Tennessee Eastman Process, *Ind. Eng. Chem. Res.* **40**(22), 4889–4901.
- Luyben, W.: 1993a, Dynamics and Control of Recycle Systems. 1. Simple Open-Loop and Closed-Loop Systems, *Ind. Eng. Chem. Res.* **32**(3), 466–475.
- Luyben, W.: 1993b, Dynamics and Control of Recycle Systems. 2. Comparison of Alternative Process Designs, *Ind. Eng. Chem. Res.* **32**(3), 476–486.
- Luyben, W.: 1993c, Dynamics and Control of Recycle Systems. 3. Alternative Process Designs in a Ternary System, *Ind. Eng. Chem. Res.* **32**(6), 1142–1153.
- Luyben, W.: 1993d, Dynamics and Control of Recycle Systems. 4. Ternary Systems with One or Two Recycle Streams, *Ind. Eng. Chem. Res.* **32**(6), 1154–1162.
- Matsuyama, H. and Nishimura, H.: 1977, Topological and Thermodynamic Classification of Ternary Vapor–Liquid Equilibria, *J. Chem. Eng. Jpn.* **10**(3), 181–187.
- Moore, C.: 1992, Selection of Controlled and Manipulated Variables, in W. L. Luyben (ed.), *Practical Distillation Control*, Van Nostrand Reinhold, New York, chapter 8, pp. 140–177.
- Morari, M., Arkun, Y. and Stephanopoulos, G.: 1980, Studies in the Synthesis of Control Structures for Chemical Processes. Part I: Formulation of the Problem. Process Decomposition and the Classification of the Control Task. Analysis of the Optimizing Control Structures., *AIChE J.* **26**(2), 220–232.
- Pearson, R.: 1999, *Discrete-Time Dynamic Models*, Oxford University Press, New York.
- Pearson, R. and Pottmann, M.: 2000, Gray-box identification of block-oriented nonlinear models, *J. Proc. Cont.* **10**(4), 301–315.

- Pelkonen, S., Górak, A., Ohligschläger, A. and Kaesemann, R.: 2001, Experimental Study on Multicomponent Distillation in Packed Columns, *Chem. Eng. Process.* **40**(3), 235–243.
- Pelkonen, S., Kaesemann, R. and Górak, A.: 1997, Distillation Lines for Multicomponent Separation in Packed Columns: Theory and Comparison with Experiment, *Ind. Eng. Chem. Res.* **36**(12), 5392–5398.
- Petlyuk, F. and Avet'yan, V.: 1971, Investigation of the Rectification of Three-Component Mixtures with Infinite Reflux, *Theor. Found. Chem. Eng.* **5**(4), 499–507.
- Pham, H. and Doherty, M.: 1990a, Design and Synthesis of Heterogeneous Azeotropic Distillations I: Heterogeneous Phase Diagrams, *Chem. Eng. Sci.* **45**(7), 1823–1836.
- Pham, H. and Doherty, M.: 1990b, Design and Synthesis of Heterogeneous Azeotropic Distillations II: Residue Curve Maps, *Chem. Eng. Sci.* **45**(7), 1837–1843.
- Prokopakis, G. and Seider, W.: 1983a, Dynamic Simulation of Azeotropic Distillation Towers, *AIChE J.* **29**(6), 1017–1029.
- Prokopakis, G. and Seider, W.: 1983b, Feasible Specifications in Azeotropic Distillation, *AIChE J.* **29**(1), 49–60.
- Rovaglio, M., Faravelli, T., Biardi, G., Gaffuri, P. and Soccol, S.: 1992, Precise Composition Control of Heterogeneous Azeotropic Distillation Towers, *Comput. Chem. Eng.* **16**(Suppl.), S535–S547.
- Rovaglio, M., Faravelli, T., Biardi, G., Gaffuri, P. and Soccol, S.: 1993, The Key Role of Entrainer Inventory for Operation and Control of Heterogeneous Azeotropic Distillation Towers, *Comput. Chem. Eng.* **15**(5/6), 535–547.
- Ryan, P. and Doherty, M.: 1989, Design/Optimization of Ternary Heterogeneous Azeotropic Distillation Sequences, *AIChE J.* **35**(10), 1592–1601.
- Seader, J. and Henley, E.: 1997, *Separation Process Principles*, John Wiley & Sons, Inc., New York.

- Serafimov, L., Frolkova, A. and Pavlenko, T.: 1992a, Determination of existence conditions for steady-state operating protocols in systems with recycle for separating ternary mixtures, *Teor. Osn. Khim. Tekhnol* **26**(2), 281.
- Serafimov, L., Frolkova, A. and Pavlenko, T.: 1992b, Influence of Phase Diagram Structure and Initial Mixture Composition on Serviceability of Separation Systems with Recycle, *Teor. Osn. Khim. Tekhnol* **26**(3), 425–428.
- Skogestad, S.: 1997, Dynamics and Control of Distillation Columns: A Tutorial Introduction, in R. Darton (ed.), *Distillation and Absorption '97*, Vol. one of *ICHEME Symposium Series No. 142*, IChemE, Rugby, UK, pp. 23–58.
- Skogestad, S.: 2000a, Plantwide Control: The Search for the Self-Optimizing Control Structure, *J. Proc. Cont.* **10**, 487–507.
- Skogestad, S.: 2000b, Self-optimizing control: A distillation case study, *Preprints of AD-CHEM 2000: International Symposium on Advanced Control of Chemical Processes*, Vol. II, IFAC, Oxford, UK, pp. 1013–1018.
- Skogestad, S.: 2000c, Self-Optimizing Control: The Missing Link between Steady-State Optimization and Control, *Comput. Chem. Eng.* **24**(2-7), 569–575.
- Skogestad, S., Jacobsen, E. and Morari, M.: 1990, Inadequacy of steady-state analysis for feedback control: Distillate-bottom control of distillation columns, *Ind. Eng. Chem. Res.* **29**(12), 2339–2346.
- Skogestad, S., Lundström, P. and Jacobsen, E.: 1990, Selecting the Best Distillation Control Configuration, *AIChE J.* **36**(5), 753–764.
- Skogestad, S. and Morari, M.: 1987, The dominant time constant for distillation columns, *Comput. Chem. Eng.* **11**(6), 607–617.
- Skogestad, S. and Morari, M.: 1988, Understanding the Dynamic Behavior of Distillation Columns, *Ind. Eng. Chem. Res.* **27**(10), 1848–1862.
- Skogestad, S. and Postlethwaite, I.: 1996, *Multivariable Feedback Control - Analysis and Design*, First edn, John Wiley & Sons Ltd., Chichester, England.

- Springer, P., Baur, R. and Krishna, R.: 2002, Influence of Interphase Mass Transfer on the Composition Trajectories and Crossing of Boundaries in Ternary Azeotropic Distillation, *Sep. Pur. Technology* **29**(1), 1–13.
- Springer, P., Buttinger, B., Baur, R. and Krishna, R.: 2002, Crossing of the Distillation Boundary in Homogeneous Azeotropic Distillation: Influence of Interphase Mass Transfer, *Ind. Eng. Chem. Res.* **41**(6), 1621–1631.
- Stichlmair, J.: 1988, Zerlegung von Dreistoffgemischen durch Rektifikation, *Chem. Ing. Tech.* **60**(10), 747–754.
- Stichlmair, J. and Fair, J.: 1998, *Distillation: Principles and Practice*, Wiley-VCH, New York.
- Stichlmair, J., Fair, J. and Bravo, J.: 1989, Separation of Azeotropic Mixtures via Enhanced Distillation, *Chem. Eng. Prog.* **85**(1), 63–69.
- Stichlmair, J. and Herguiejuela, J.-R.: 1992, Separation Regions and Processes of Zeotropic and Azeotropic Distillation, *AIChE J.* **38**(10), 1523–1535.
- Tedeschi, R. J., Weeks, A. and Russel, J.: 1963, U.S. Patent No. 3,082,260.
- Thong, D.-C. and Jobson, M.: 2001a, Multicomponent homogeneous azeotropic distillation 1. Assessing product feasibility, *Chem. Eng. Sci.* **56**(14), 4369–4391.
- Thong, D.-C. and Jobson, M.: 2001b, Multicomponent homogeneous azeotropic distillation 2. Column design, *Chem. Eng. Sci.* **56**(14), 4393–4416.
- Thong, D.-C. and Jobson, M.: 2001c, Multicomponent homogeneous azeotropic distillation 3. Column sequence synthesis, *Chem. Eng. Sci.* **56**(14), 4417–4432.
- Tonelli, S., Brignole, N. and Brignole, E.: 1997, Modelling and Control of an Industrial Azeotropic Train, *Comput. Chem. Eng.* **21**(Suppl.), S559–S564.
- Tyner, K. and Westerberg, A.: 2001a, Multiperiod design of azeotropic separation systems. I. An agent based solution, *Comput. Chem. Eng.* **25**(9-10), 1267–1284.
- Tyner, K. and Westerberg, A.: 2001b, Multiperiod design of azeotropic separation systems. II. approximate models, *Comput. Chem. Eng.* **25**(11-12), 1569–1583.

- Tyr us, B.: 1992, Selection of Controller Structure, *in* W. L. Luyben (ed.), *Practical Distillation Control*, Van Nostrand Reinhold, New York, chapter 9, pp. 178–191.
- Ulrich, J. and Morari, M.: 2000, Design and Operation of a Heterogeneous Dehydration Column, *Technical Report AUT00-05*, Automatic Control Laboratory, ETH Zentrum, CH-8092 Z rich, Switzerland. available via <http://www.control.ethz.ch/~disti>.
- Ulrich, J. and Morari, M.: 2002, Influence of the Impurities on the Control of Heterogeneous Azeotropic Distillation Columns, *Ind. Eng. Chem. Res.* **41**(2), 230–250.
- Vadapalli, A. and Seader, J.: 2001, A generalized framework for computing bifurcation diagrams using process simulation programs, *Comput. Chem. Eng.* **25**, 445–464.
- Van Dongen, D. and Doherty, M.: 1985, Design and Synthesis of Homogeneous Azeotropic Distillations 1: Problem Formulation for a Single Column, *Ind. Eng. Chem. Fundam.* **24**(4), 454–463.
- VDI-W rmeatlas: 1994, *Berechnungsbl tter f r den W rme bergang*, 7. edn, VDI-Verlag GmbH, D sseldorf (Germany).
- Wahnschafft, O. M., Koehler, J., Blass, E. and Westerberg, A.: 1992, The Product Composition Regions of Single-Feed Azeotropic Distillation Columns., *Ind. Eng. Chem. Res.* **31**(10), 2345–2362.
- Wahnschafft, O. M., Koehler, J. and Westerberg, A.: 1994, Homogeneous Azeotropic Distillation: Analysis of Separation Feasibility and Consequences for Entrainer Selection and Column Design, *Comput. Chem. Eng.* **18**(Suppl.), S31–S35.
- Wahnschafft, O. M., Le Rudulier, J. and Westerberg, A.: 1993, A Problem Decomposition Approach for the Synthesis of Complex Separation Processes with Recycles, *Ind. Eng. Chem. Res.* **32**(6), 1121–1141.
- Wahnschafft, O. M. and Westerberg, A.: 1993, The Product Composition Regions of Azeotropic Distillation Columns. 2. Separability in Two-Feed Columns and Entrainer Selection, *Ind. Eng. Chem. Res.* **32**(6), 1108–1120.

- Wang, C., Wong, D., Chien, I.-L., Shih, R., Liu, W. and Tsai, C.: 1998, Critical Reflux, Parametric Sensitivity, and Hysteresis in Azeotropic Distillation of Isopropyl Alcohol + Water + Cyclohexane, *Ind. Eng. Chem. Res.* **37**(7), 2835–2843.
- Yeomans, H. and Grossmann, I.: 2000, Optimal Design of Complex Distillation Columns Using Rigorous Tray-by-Tray Disjunctive Programming Models, *Ind. Eng. Chem. Res.* **39**(11), 4326–4335.
- Zheng, A., Grassi, V. and Meski, G.: 1998, On Control of Distillation Columns with Input Multiplicity, *Ind. Eng. Chem. Res.* **37**(5), 1836–1840.

Appendix A

System Acetone/Water/MBI/MTBE

A.1 Thermodynamic Data

A.1.1 Pure Component Data of MBI

The pure component properties of MBI which are used in the Aspen models are listed in Table A.1. The parameters for the calculation of ideal gas heat capacities of MBI according to the CPIG model (J/(mol K)) from Aspen Plus(Asp, 1999b) are: $c_1 = -4.5469$, $c_2 = 0.5891$, $c_3 = -4.350 \cdot 10^{-4}$, $c_4 = 1.1627 \cdot 10^{-7}$, all others equal to zero (applicable between 233.15 K and 423.15K). The heat of vaporization of MBI was calculated using the DHVLWT Watson model (Asp, 1999b) with the parameters: $\Delta h_1^{o,vap} = 39652.3$ kJ/mol, $T_1 = 376.75K$, $a=0.38$, $b=0.0$ and $T_{min} = 273.15K$. All data were supplied by our industrial partner.

A.1.2 Vapor–Liquid Equilibrium

The liquid activity coefficients were computed using the Wilson model as is implemented in (Asp, 1999b). The corresponding parameters are shown in Tables A.2. Pure component vapor pressures for all components except MBI were computed by the extended Antoine equation with data from the pure component database of Aspen Plus(Asp, 1999b). The

Table A.1: Pure component data of Methyl–Isobutanol (MBI) used in the Aspen models.

molar weight	84.11 kg/kmol
critical temperature	553.40 K
critical pressure	44.80 atm
critical volume	0.2810 m^3 /kmol
critical compressibility	0.2772
acentric factor ω	0.4950
normal boiling point T_b	376.75 K
heat of vaporization at T_b	39652.3 kJ/kmol
std heat of formation	-42579.8 kJ/kmol
std liquid volume	0.10536 m^3 /kmol

vapor pressure of MBI was computed using the Antoine equation:

$$\ln(p_{MBI}^*/Pa) = 20.2222 - \frac{2248.57}{T/K - 119.07} \quad (A.1)$$

Table A.2: Binary interaction parameters for the Wilson activity coefficient model of AspenPlus.

i	j	a_{ij} [-]	a_{ji} [-]	b_{ij} [K]	b_{ji} [K]
MTBE	acetone	-0.47470	0.47470	149.4123	-424.2339
MTBE	water	0.0	0.0	-1466.970	-990.9910
MTBE	MBI	-0.20470	0.20470	292.6348	-945.9042
acetone	water	-1.40433	1.40433	-147.2720	-727.2830
acetone	MBI	0.26990	-0.26990	-542.8400	443.8501
water	MBI	1.68927	-1.68927	-767.8190	-406.4250

Calculated VLE diagrams using Wilson and also a set of NRTL parameters regressed to the data can be found in the KTI Report(Ulrich and Morari, 2000).

A.1.3 Liquid–Liquid Equilibrium

The UNIQUAC model as implemented in Aspen Plus(Asp, 1999b) was used to model the LLE in the decanter, with the corresponding parameters shown in Table A.3 and Table A.4. Calculated LLE diagrams can be found in the KTI Report(Ulrich and Morari, 2000).

Table A.3: Unary parameters for the UNIQUAC activity coefficient model of AspenPlus.

component	r_i [-]	q_i [-]	q'_i [-]
MTBE	4.0678	3.632	3.632
water	0.9200	1.400	1.400
MBI	3.8444	3.288	3.288
acetone	2.5735	2.336	2.336

Table A.4: Binary interaction parameters for the UNIQUAC activity coefficient model of AspenPlus.

i	j	b_{ij} [K]	b_{ji} [K]
MTBE	acetone	222.6548	-441.9943
MTBE	water	-603.8441	-108.7237
MTBE	MBI	-355.5420	257.0064
acetone	water	-424.6196	151.3670
acetone	MBI	-2110.694	461.5270
water	MBI	-54.9242	-30.7382

A.2 Optimization of the Column Sequences

A.2.1 Heterogeneous Sequence

Figure A.1 shows the setup of the heterogeneous sequence as currently operated in industry including a schematic representation of the column profile in the four component residue curve map. The crude feed F_C enters the first column where acetone is removed as D_1 .

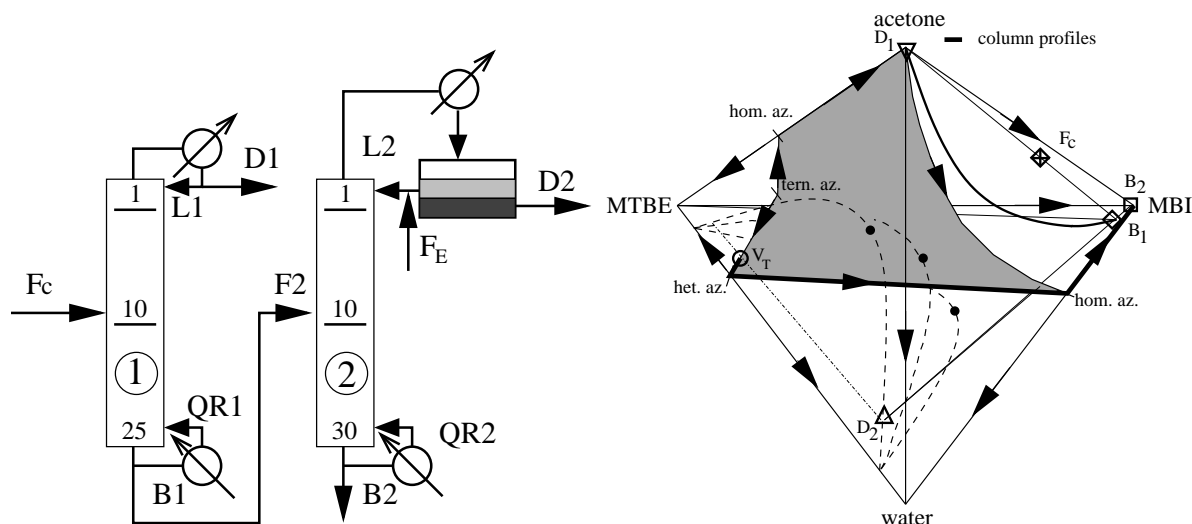


Figure A.1: Heterogeneous two-column sequence for the system acetone/water/MBI using MTBE as entrainer.

The bottom B_1 containing the product MBI and water is fed to the second column where the entrainer MTBE is added (F_E). The water is removed via D_2 and MBI leaves through the bottom B_2 . The specifications for the process are listed in Table A.5.

Table A.5: Specified and manipulated variables (in Aspen Plus simulator) for the heterogeneous two-column sequence for the base feed (Table 1.1).

specified variable	value	manipulated variable	value
$x_{acetone}^{D_1}$	0.99 kg/kg	D_1	599.2 kg/h
$x_{acetone}^{B_1}$	0.0005 kg/kg	L_1	2385.7 kg/h
$x_{MBI}^{D_2}$	0.00075 kg/kg	B_2	1562.6 kg/h
$x_{MBI}^{B_2}$	0.9996 kg/kg	MTBE	0.849 kg/h

A.2.1.1 Design of the Acetone Column

Since the setup of the industrial acetone column is not known, a column with 25 ideal stages was chosen. To identify the optimal feed location for the acetone column, the feed stage was varied for the given specifications. The resulting reboiler duties are shown in

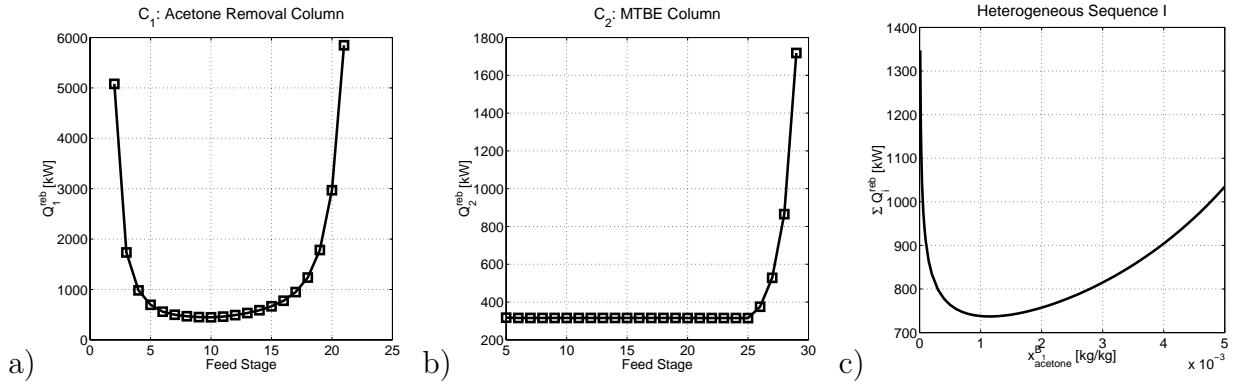


Figure A.2: a) and b) Reboiler duties as function of the feed stage for the specifications given in Table A.5. c) Sum of reboiler duties for different $x_{acet}^{B_1}$.

Figure A.2a. The optimal location of the feed stage is stage 10. The analysis of the second column was the original motivation for this research project and is part I of this thesis. It has 30 stages and the feed is at stage 10 which is a reasonable choice according to the sensitivity study shown in Figure A.2b. The setup of the column was described in detail in section 4.1.1. The specification for $x_{acet}^{B_1}$ is chosen to ensure a high acetone recovery. However, the analysis of the heterogeneous column (part I of this thesis) revealed that $x_{acet}^{B_1}$ plays a critical role for the MTBE column. The impact on the reboiler duties is illustrated by Figure A.2c. The minimum is around 0.0011. Case studies with different crude feed compositions showed that it slightly depends on the crude feed composition (Figure A.3). Though the minimum is at $x_{acet}^{B_1}=0.0011$, the original specification as used by Ulrich and Morari (2002) is chosen to keep the results consistent with the paper. For $x_{acet}^{B_1}=0.0005$, the sum of reboiler duties is 764 kW, which is just 3.6% more than the minimum value.

A.2.1.2 Sensitivity on x^{FC}

Figure A.4 shows the sensitivity of the reboiler duties for varying crude feed composition x^{FC} for the specifications of Table A.5.

Q_1^R is nearly independent of the crude feed composition. Normally, some correlation to the acetone content is expected because this determines the rate of acetone that has to

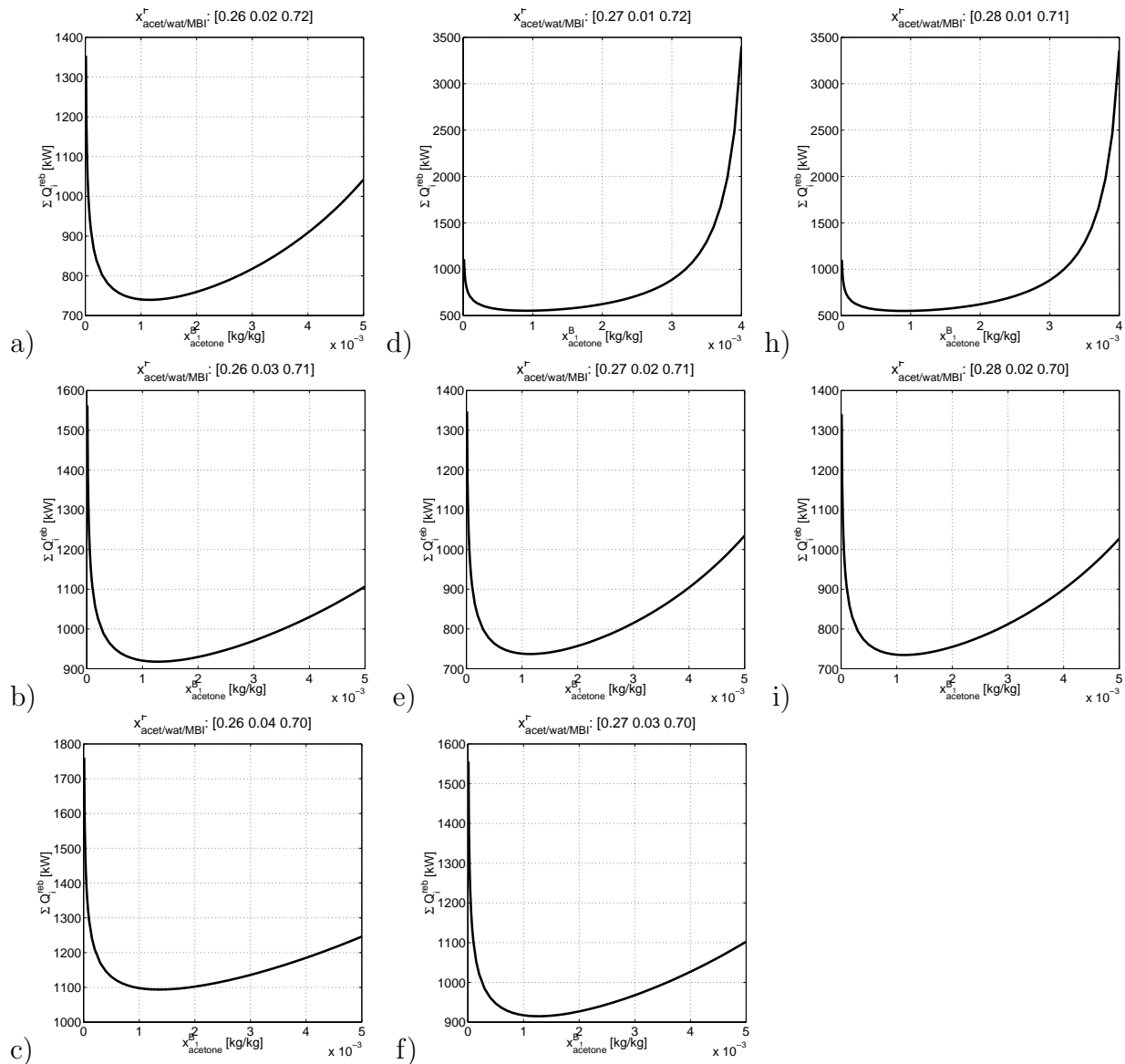


Figure A.3: Sum of reboiler duties as function of $x_{acetone}^{B_1}$ for different crude feed compositions.

be vaporized to reach the top to be removed as distillate. The reason for constant Q_1^R is the specification of the acetone mass fraction in the bottom. To reach this small amount, a high reboiler duty is necessary that is independent of the distillate flow. For $x_{acetone}^{B_1} = 0.005$ kg/kg, the reboiler duty is a function of the acetone mass fraction in the crude feed (ranging between 250 kW for low acetone mass fraction to 500 kW for high acetone mass fractions).

Q_2^R is roughly proportional to the water content but independent of the acetone content in the crude feed. The reason is that Q_2^R only depends on the water flow rate in B_1 if the mass

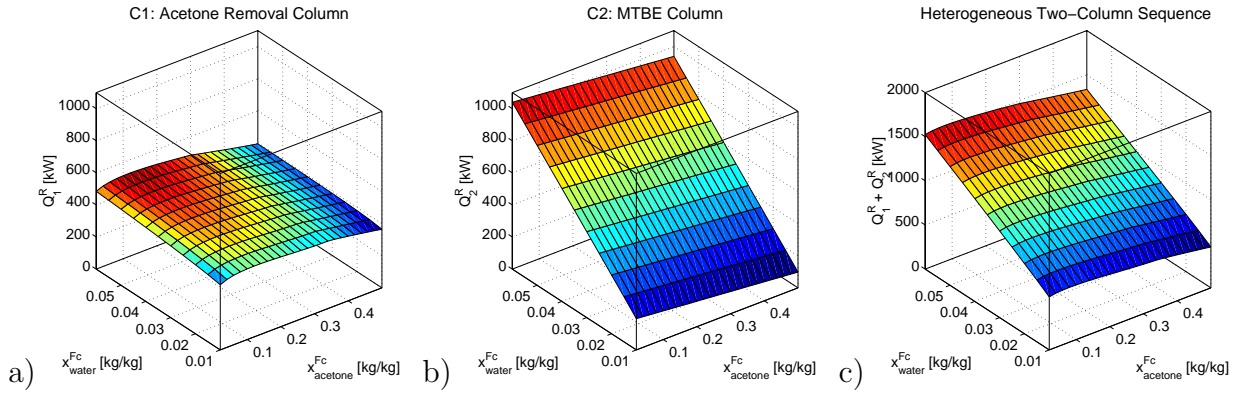


Figure A.4: Reboiler duties of the heterogeneous two-column sequence as function of the crude feed compositions for the specifications given in Table A.5.

fraction of acetone ($x_{acetone}^{B_1}$) remains constant at 0.0005 (see section 3.2.3 and section 4.2.1 for details). For varying crude feed compositions x^{Fc} , $x_{water}^{B_1}$ varies at constant $x_{acetone}^{B_1}$. The analysis of the heterogeneous column will show that Q_2^R is very sensitive with respect to the acetone contents in B_1 (section 4.3). But for the specifications of Table A.5, Q_2^R only depends on the water content in the crude feed.

Because Q_1^R is nearly independent of the crude feed composition, the sum of the two reboiler duties is governed Q_2^R and hence roughly proportional to the water content. For the base case feed (Table 1.1), $Q_1^R = 447.9$ kW and $Q_2^R = 315.9$ kW giving 763.8 kW overall consumption.

A.2.1.3 Three Column Sequence

For a fair comparison to the boundary separation scheme, a third column was introduced in section A.2.1. Apart from the fact that the economical impact is negligible, there are also other problems. The specification of D_3 cannot be reached for high water contents in the crude feed (above 0.03) because for constant $x_{acetone}^{B_1}$, the amount of acetone in D_2 decreases for increasing water contents in B_1 . This is clarified by Figure A.5, which shows the residue map for the four component system with the three column profiles. The movement of D_2 towards the binary MTBE-water edge at fixed B_3 forces D_3 to move towards the residue curve boundary connecting the binary MTBE-acetone azeotrope with

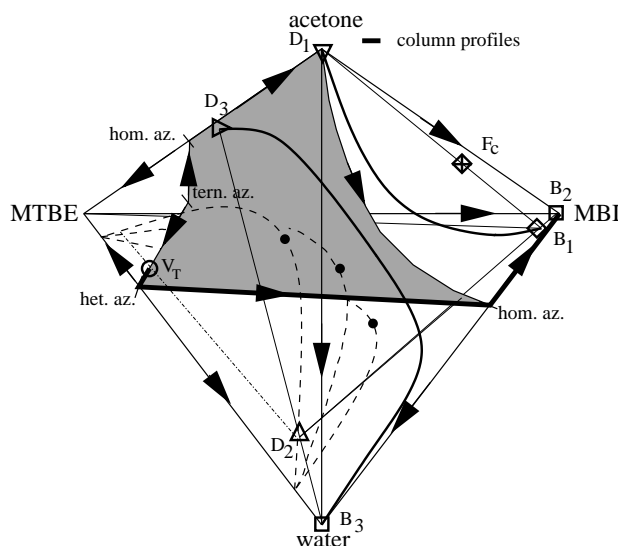


Figure A.5: Heterogeneous three-column sequence for MTBE/acetone/water/MBI.

the ternary azeotrope. At this point, the specification for D_3 would have to be loosened. The flow rate of D_3 is in the order of 2 kg/h which is less than one promille of the crude feed. Hence, the material should be disposed (e.g. burned).

For the following reasons, D_3 should not be recycled. If it is recycled to the first column to recycle the acetone, then MTBE will leave column 1 through the distillate. This is totally undesired because the acetone is recycled to the reactor. By this, MTBE will not leave the process (assuming it is inert for the reaction) and accumulate. Hence, a purge is needed and therefore it is best to “purge” D_3 . If D_3 is recycled to column 2 or the decanter of column 2, then acetone does not leave the process. Hence, a purge of D_3 has to be introduced. The result of recycling some of D_3 would be that the acetone content is increased in the decanter (and hence in D_2). This would move D_3 towards acetone and reduce the MTBE loss through the purge. However, this is not good because a high acetone content in the decanter can result in the loss of the phase split. This is highly undesired (the influence of acetone on the operation of the heterogeneous column is one of the core results of the thesis and extensively discussed in part I). Therefore, it is best to purge all D_3 . Actually, for this specific case, it seems to be best to purge D_2 directly as is currently done in industries.

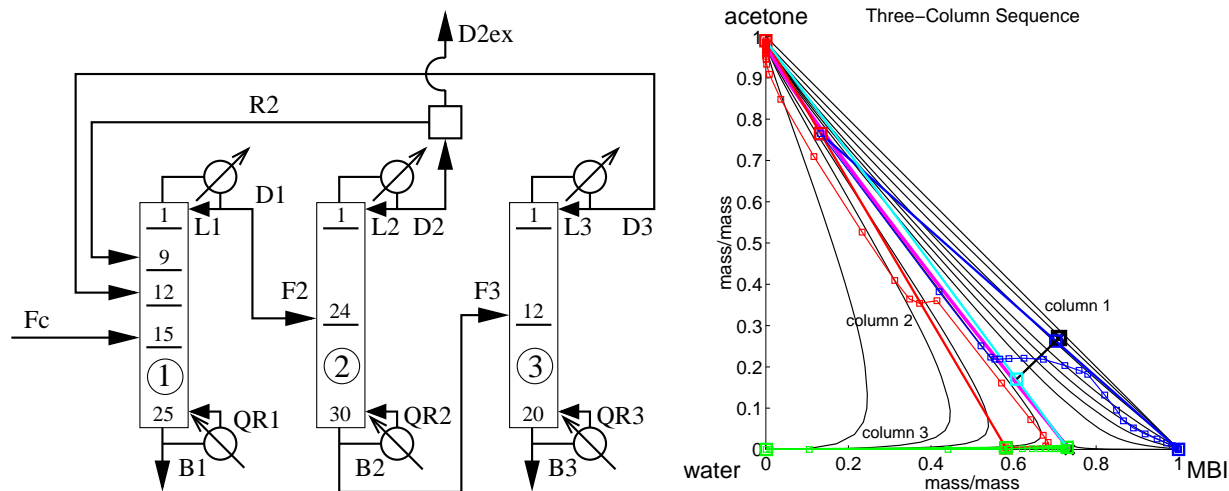


Figure A.6: Boundary separation scheme for acetone/water/MBI ($p=1$ bar).

A.2.2 Boundary Separation Scheme

Figure A.6 shows the setup of the boundary separation scheme for a ternary feed and the resulting column profiles. The crude feed enters column 1 together with two recycles R_2 and D_3 . In column 1, the MBI is removed from the process at the bottom as B_1 . The distillate, which consists of acetone, water, and MBI enters column 2. Acetone is removed from the sequence via D_2^{ex} and the rest of D_2 is recycled to column 1 as R_2 . In column 3, the remaining two component mixture water and MBI (B_2), which lies on the left side of the azeotrope, is separated into pure water (B_3) and the water-MBI azeotrope (D_3), which is recycled to column 1. Table A.6 lists the specifications for these variables at the optimal operation point.

A key point is that R_2 has to be adjusted for the different crude feeds to keep the composition of x^{D_1} constant (section 5.4.2). Figure A.7 shows the reboiler duties for different crude feed compositions at the optimal operation point. They are all proportional to the water content in the crude feed. In section 5.4.2.1, it was derived that the reboiler duties for this particular setup of the boundary separation scheme are all proportional to the mass fraction of the intermediate boiler. For the system acetone/water/MBI, water is the intermediate boiler. For the base case feed (Table 1.1), the sum of the reboiler duties is 558.3 kW. This is 73 % of the reboiler duties for the heterogeneous scheme.

Table A.6: Specified and manipulated variables (in Aspen Plus simulator) for the homogeneous three-column sequence for the base feed (Table 1.1).

specified variable	value	manipulated variable	value
$x_{MBI}^{B_1}$	0.9996 kg/kg	D_1	812.2 kg/h
L_1/D_1	0.80	L_1	649.8 kg/h
$x_{acetone}^{D_1}$	0.765 kg/kg	R_2	27.4 kg/h
$x_{acetone}^{D_2}$	0.99 kg/kg	D_2	626.9 kg/h
$x_{acetone}^{B_2}$	0.004 kg/kg	Q_2^R	197.9 kW
$x_{water}^{B_3}$	0.99925 kg/kg	B_3	37.97 kg/h
L_3/D_3	0.5	Q_3^R	57.3 kW

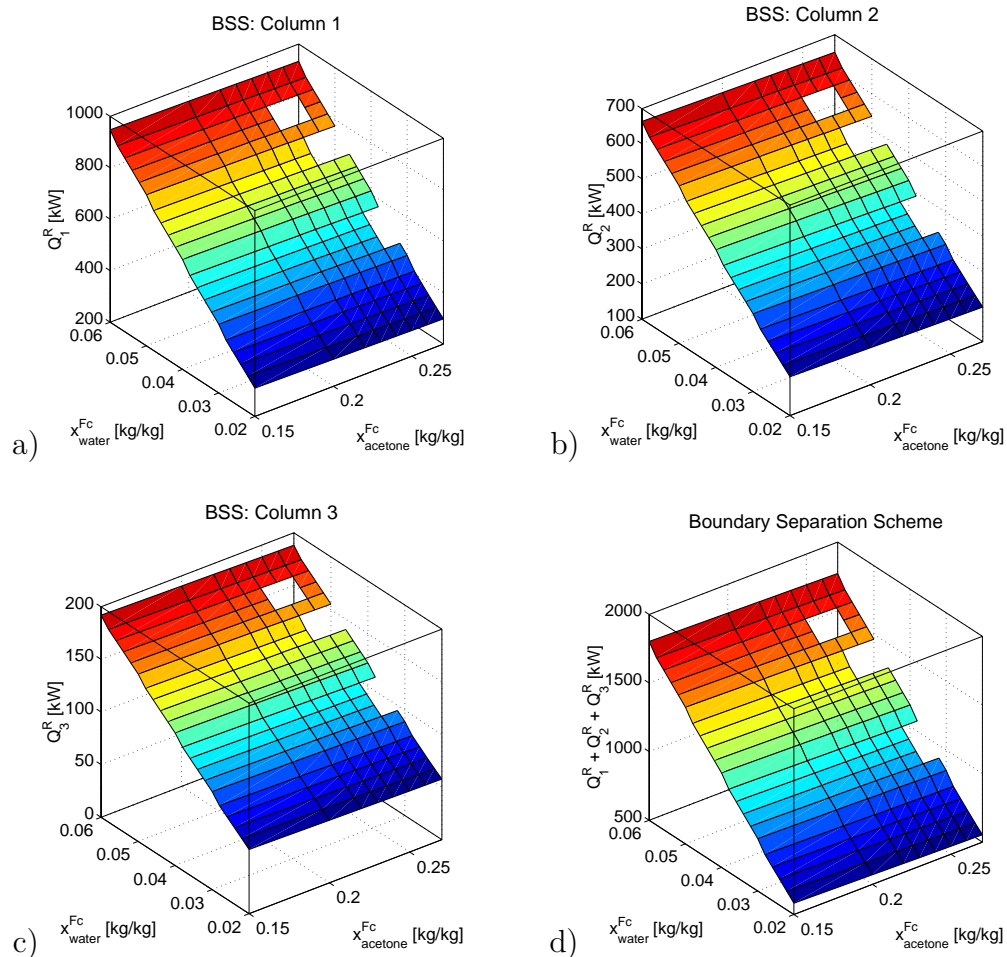


Figure A.7: Reboiler duties of a) column 1, b) column 2, c) column 3 and d) sum of all three column for the boundary separation scheme with specifications of Table A.6.

Appendix B

System Methanol/2-Propanol/ Water/Cyclohexane

B.1 Residue Curve Maps

For the binaries cyclohexane/2-propanol, cyclohexane/water and 2-propanol/water, NRTL parameters of Wang et al. (1998) were used. For the other binaries, NRTL-IG was used.

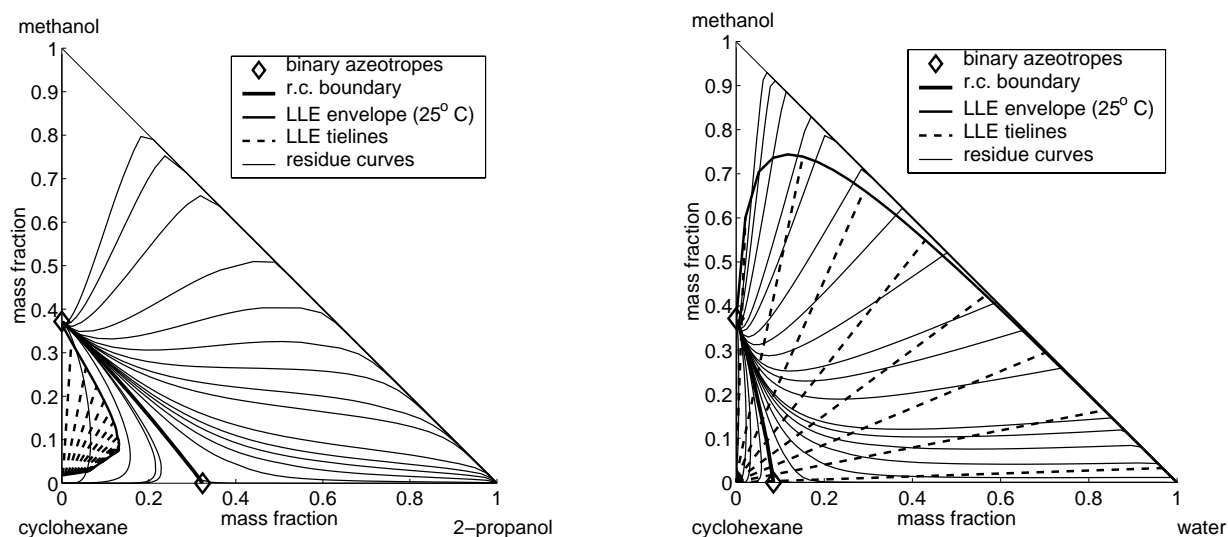


Figure B.1: Ternary residue curve maps (I) for the system methanol/cyclohexane/2-propanol/water ($p = 1$ bar, NRTL-IG).

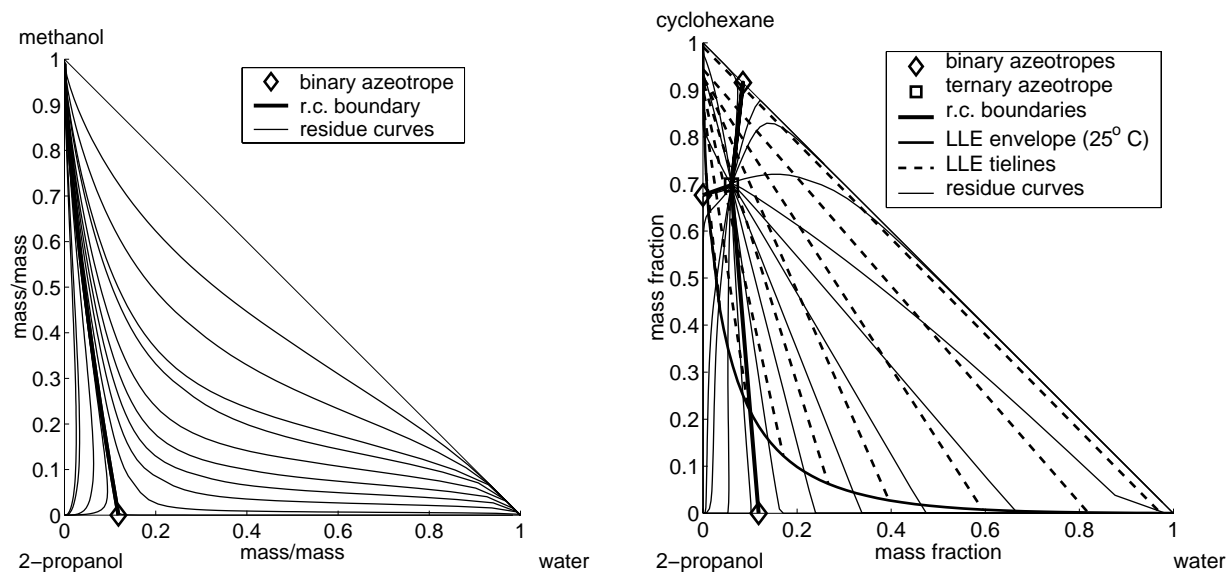


Figure B.2: Ternary residue curve maps (II) for the system methanol/cyclohexane/2-propanol/water ($p = 1$ bar).

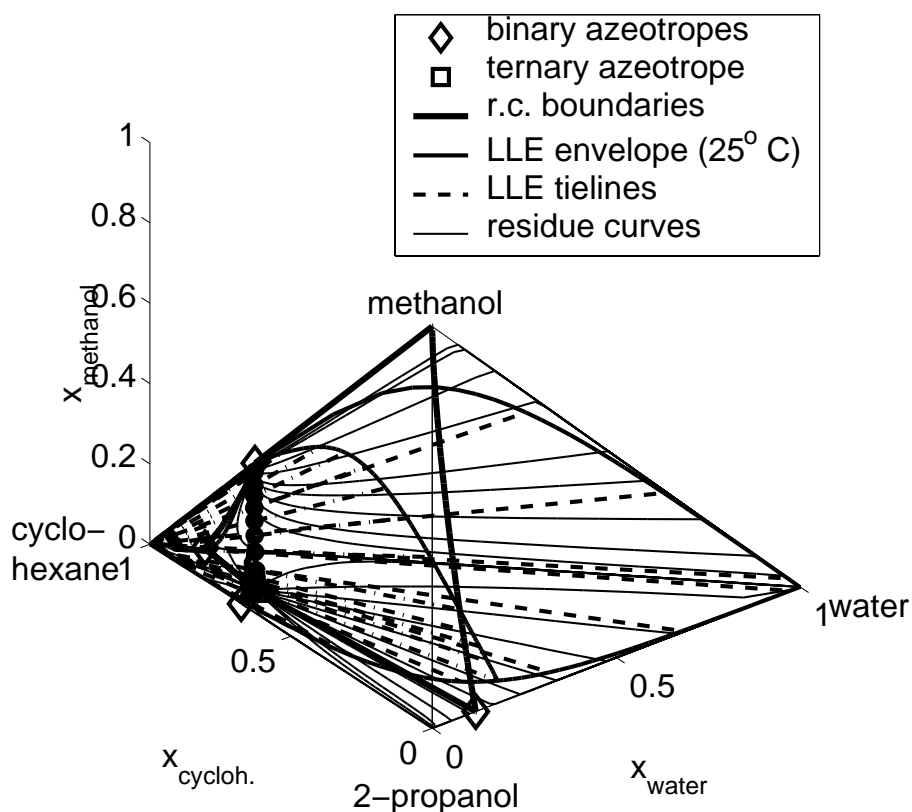


Figure B.3: Quaternary residue curve maps of the system methanol/cyclohexane/2-propanol/water ($p = 1$ bar).

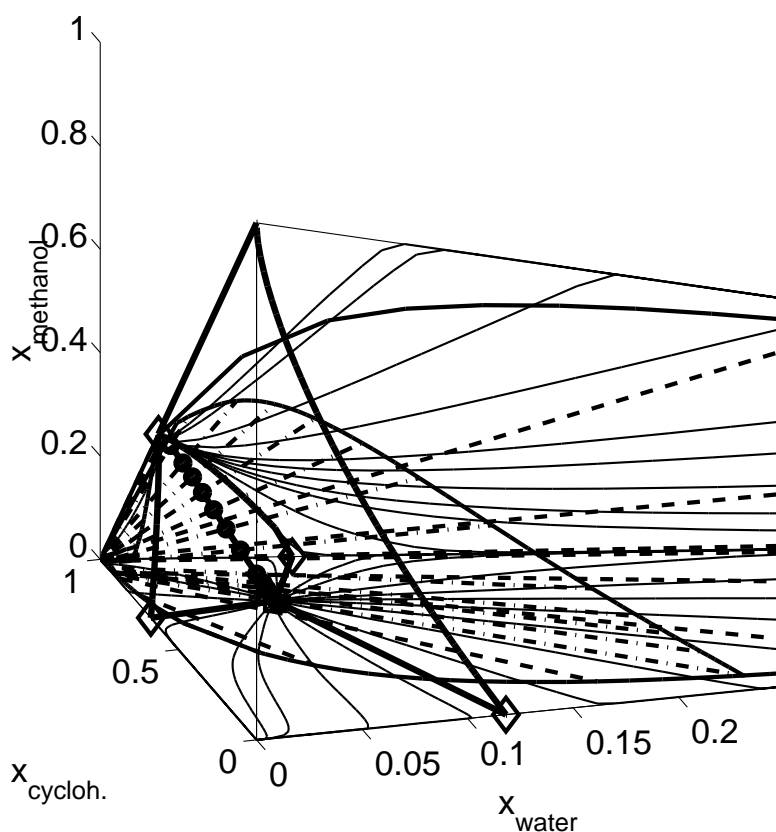


Figure B.4: Enlargement of Figure B.3

B.2 Boundary Separation Scheme

B.2.1 Analysis of Column 1

The number of stages, the locations of the feed trays and the operation parameters have to be chosen. The number of stages was fixed to 30 (including top and bottom). using the Wilson-IG activity coefficient parameter sets

In numerous case studies, the following observations were made for simulations using the Wilson-IG activity coefficient parameter sets with a feed as given in Table 6.8 for setup 1:

- If pinch is in the bottom (pure water) and the reboiler duty is above 5 kW, the location of the feed stages does not change the distillate composition for $D_1 = 4.196$ kg/h and the pinch remains at pure water for varying reboiler duties.

- If distillate flow is varied at constant reboiler duty, the range where the pinch remains in the bottom (pure water) depends on the location of the feed trays.
- For varying distillate flow rates, all three possible pinches (pure water in the bottom, the 2-propanol-water azeotrope in the middle and pure methanol on top) are observed. The ranges depend on the location of the feed trays.
- When the feed stage of the recycles is varied, the upper bound for D_1 does not change. The lower bound for D_1 moves towards the upper bound if the recycle is introduced on stages closer to the top. For example, the lower bound is 4.194 kg/h when R_2 and D_3 enter the column above stage 5.

The distillation column is robust towards little fluctuations in the external flow rates if the transient times for changing from one pinch to another are large. A measure for the transient time between two steady states is the inventory time constant τ which is defined as the change in holdup of one component divided by the imbalance of supply of this component (Skogestad and Morari, 1987). For a step change in D_1 ,

$$\tau = \frac{|TCH(D_1^* + \Delta D_1) - TCH(D_1^*)|}{|\Delta D_1 x^{D_1}(D_1^*) - \Delta D_1 x^{B_1}(D_1^*)|} \quad (\text{B.1})$$

where D_1^* denotes the reference steady state.

If the external flow rate (either D_1 or B_1) is changed such that the new steady state has a different pinch than before, the transient times to reach this new steady state increase drastically. This is illustrated with Figure B.5a and Figure B.5b showing the inventory time constants for different ΔD_1 for $D_1^* = 4.196$ kg/h (the holdup of reflux drum and bottoms: 1 kg, holdup/stage: 0.285 kg). For this D_1^* , the pinch is in the bottom. For small perturbations, $\tau_{2\text{-propanol}}$ is the dominant inventory time constant. Note the peak at $\Delta D_1 = -0.009$ kg/h ($D_1 = 4.187$ kg/h) which indicates that the pinch changes to the 2-propanol–water azeotrope. For $\Delta D_1 = -0.005$ kg/h, $\tau_{2\text{-propanol}}$ is around 240 hours and for $\Delta D_1 = -0.025$ kg/h, $\tau_{2\text{-propanol}}$ is around 400 hours. The transient time for the small step is expected to be about twice as long than for the big step. The transient times estimated with the inventory time constants do not depend on the choice of the manipulated variable (D_1 or B_1). Different to that, the real transient times depend on the manipulated variable because a step change in B_1 is observed in D_1 with a lag, the hydraulic lag of the column.

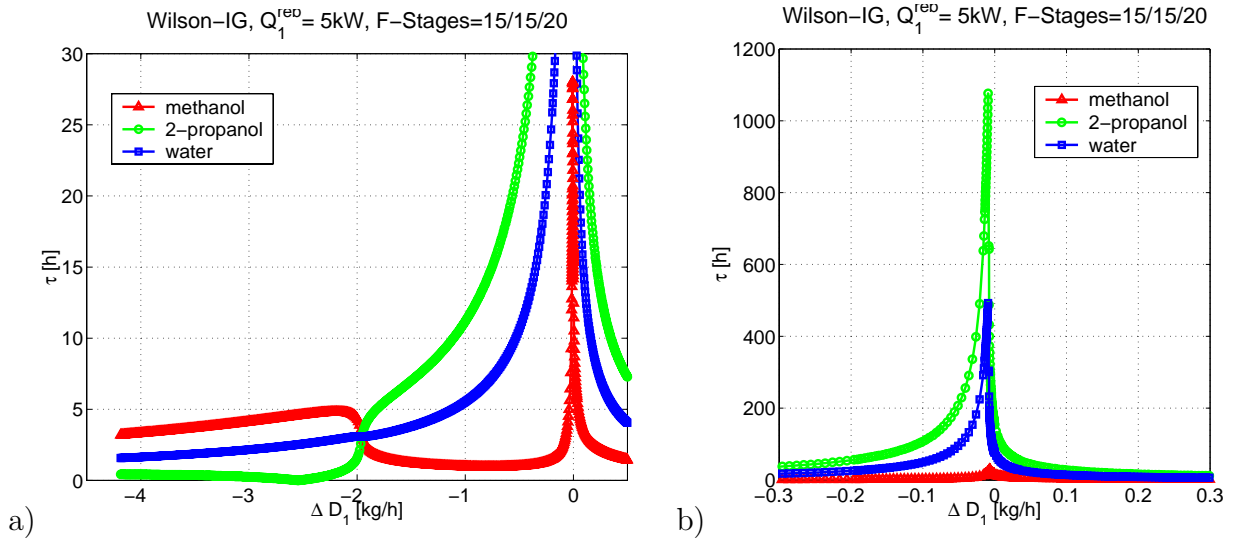


Figure B.5: d_1 and bottom composition $x_{water}^{B_1}$ and $1 - x_{water}^{B_1}$, respectively, as a function of D_1 for column 1 with $F_1 = 4.696$ kg/h.

Dynamic simulations show that these simple rules do not apply because of the strong nonlinearities that occur when the column is operated with a pinch in the bottom. Figure B.6a shows the step answer of the top and bottom composition for $\Delta B_1 = 0.005$ kg/h; and Figure B.6b shows the step answer for $\Delta B_1 = 0.025$ kg/h (holdups: top=6.7 kg, stage=0.285 kg, and bottom=8.1 kg) for constant reflux $L_1 = 13.6$ kg/h. The step in B_1 is applied at 10 hours. For the small step (Figure B.6a), the pinch remains in the bottom: x^{B_1} does not change. x^{D_1} immediately reacts on the step change and slowly adjusts to the new steady state, which the column reached after roughly 1000 hours ($x_{water}^{D_1}(1000h) = 1.00016x_{water}^{D_1}(steady\ state)$).

For the large step ((Figure B.6b), there is a dead time of approximately 300 hours in the step answer for the bottoms composition x^{B_1} while x^{D_1} reacts with approximately the same time constant to the new steady state.

Figure B.7a and Figure B.7b show the 30 temperatures as a function of time for the two different steps. Figure B.7a shows that the pinch remains in the bottom while Figure B.7b shows that the pinch changes. Hence, temperature control should be used to keep the column at the desired pinch.

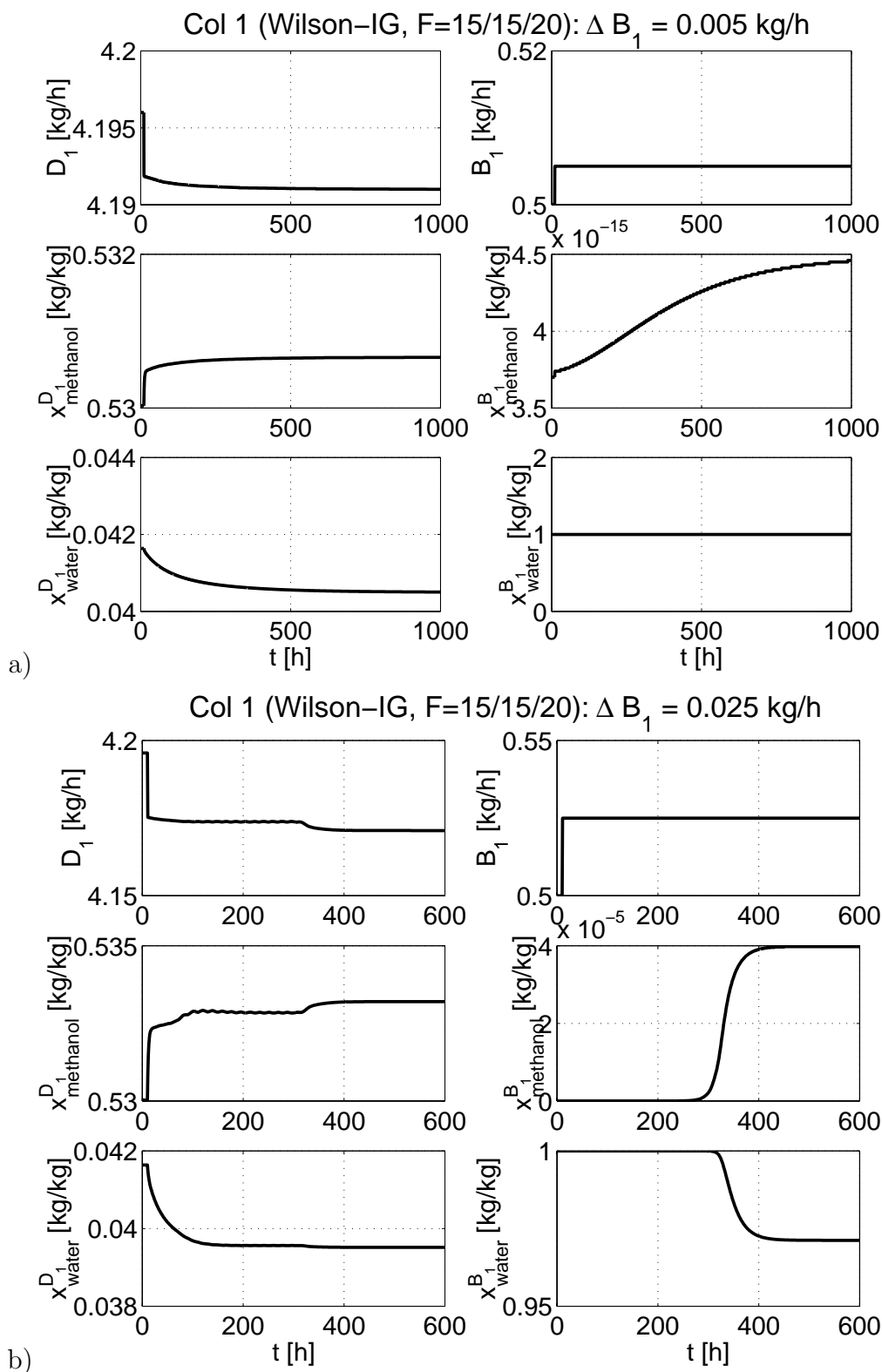


Figure B.6: Step answers of the product compositions of column 1 for two different step changes a) $\Delta B_1 = 0.005$ kg/h and b) $\Delta B_1 = 0.025$ kg/h for $L_1 = 13.6$ kg/h.

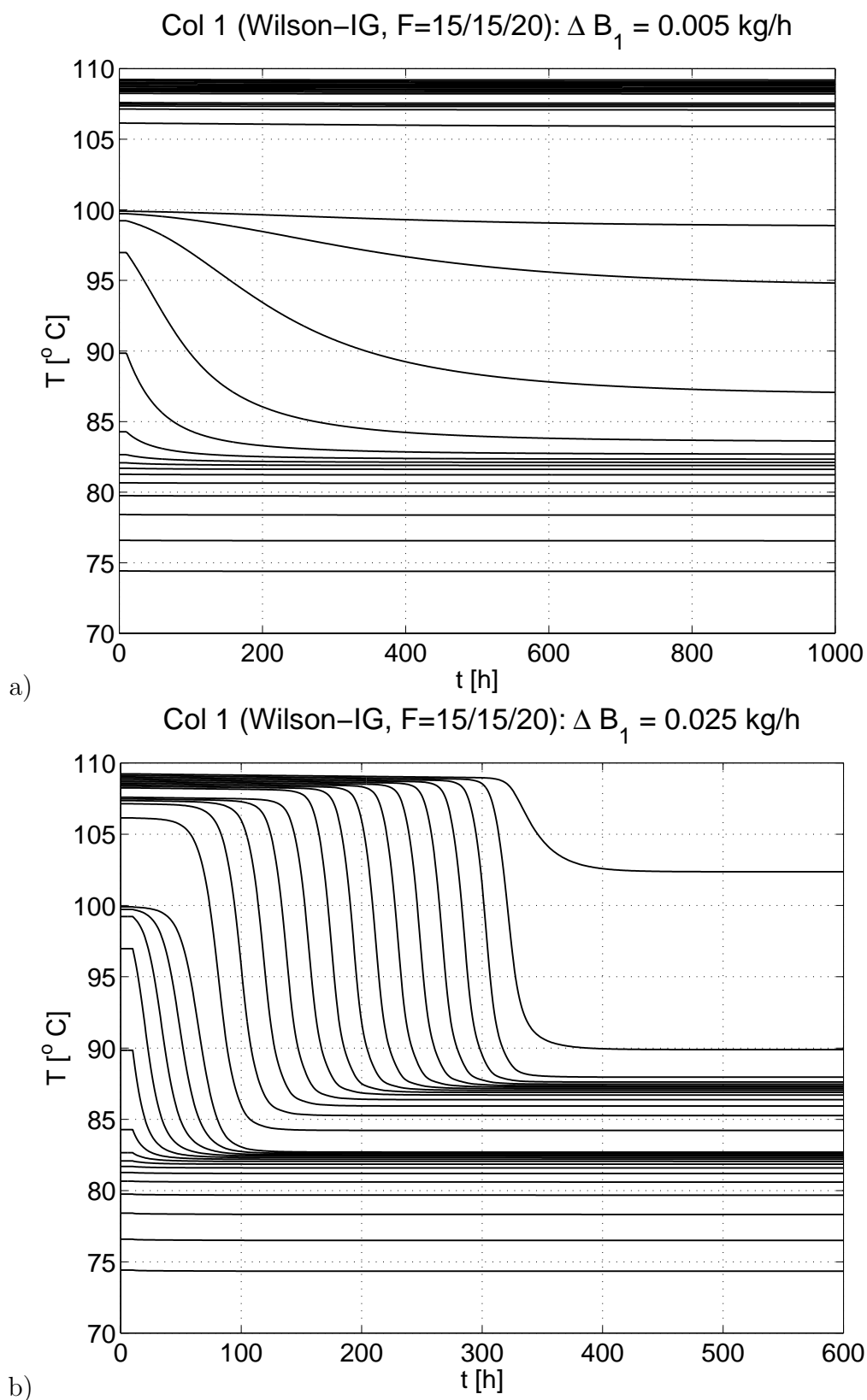


Figure B.7: Step answers of the 30 temperatures of column 1 for two different step changes a) $\Delta B_1 = 0.005$ kg/h and b) $\Delta B_1 = 0.025$ kg/h for $L_1 = 13.6$ kg/h.

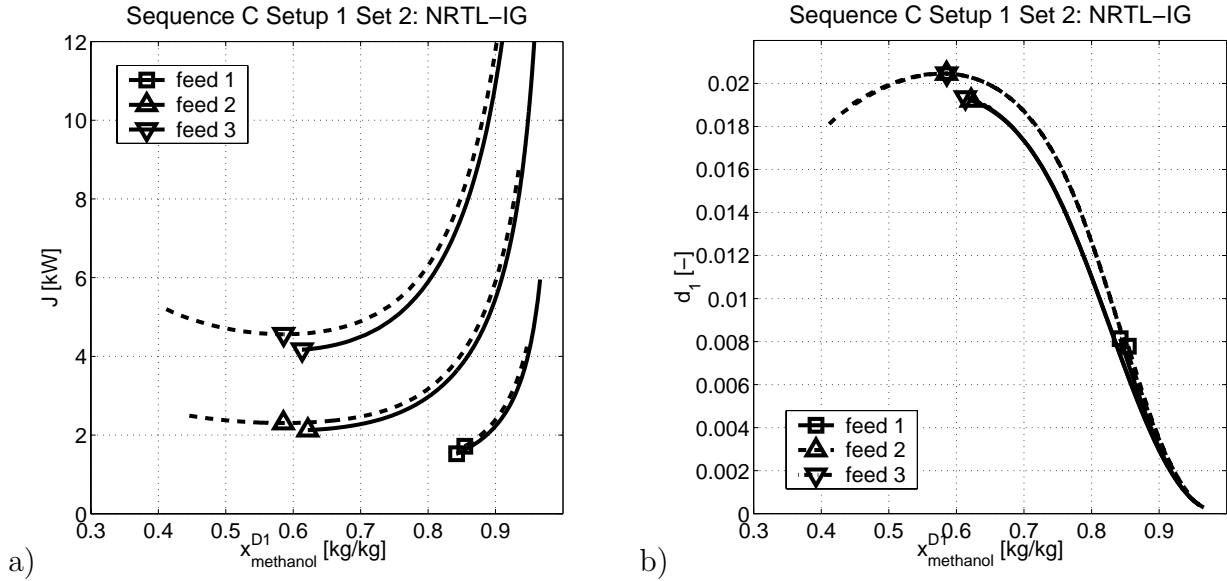


Figure B.8: Sequence C setup 1 set 2: The two objective functions a) J and b) d_1 as a function of the controlled variable $x_{methanol}^{D1}$ for set 2 (solid lines) and set 2a (dashed lines).

B.2.2 Further Sets of Controlled Variables

B.2.2.1 Set 2

Figure B.8a shows the objective function J as a function of the controlled variable $x_{methanol}^{D1}$ for set 2 (Table 6.4). The solid lines stand for set 2. There are convergence difficulties for $x_{methanol}^{D1} < 0.617$. Analyzing the data for set 1, the reflux-to-distillate ratios of column 2 and column 3 vary as a function of R_2 , or $x_{methanol}^{D1}$ respectively. For $x_{methanol}^{D1} < x_{methanol}^{D1, opt}$, column 2 will have a higher reflux-to-distillate ratio than at the optimal point for set 1. Hence, the reflux in column 2 is below the required value which could explain the convergence difficulties. The calculations are repeated with 20% higher reflux-to-distillate ratios: set 2a (dashed lines). The location of the optimum is slightly shifted. Further, the higher reflux-to-distillate ratios sharpen the separation of the columns. This leads to a higher value of d_1 (Figure B.8b) at the cost of a higher energy consumption. Hence, d_1 is not the best measure for the performance of set 2. Figure B.9 shows the relations between R_2 and $x_{methanol}^{D1}$ and J hardly change.

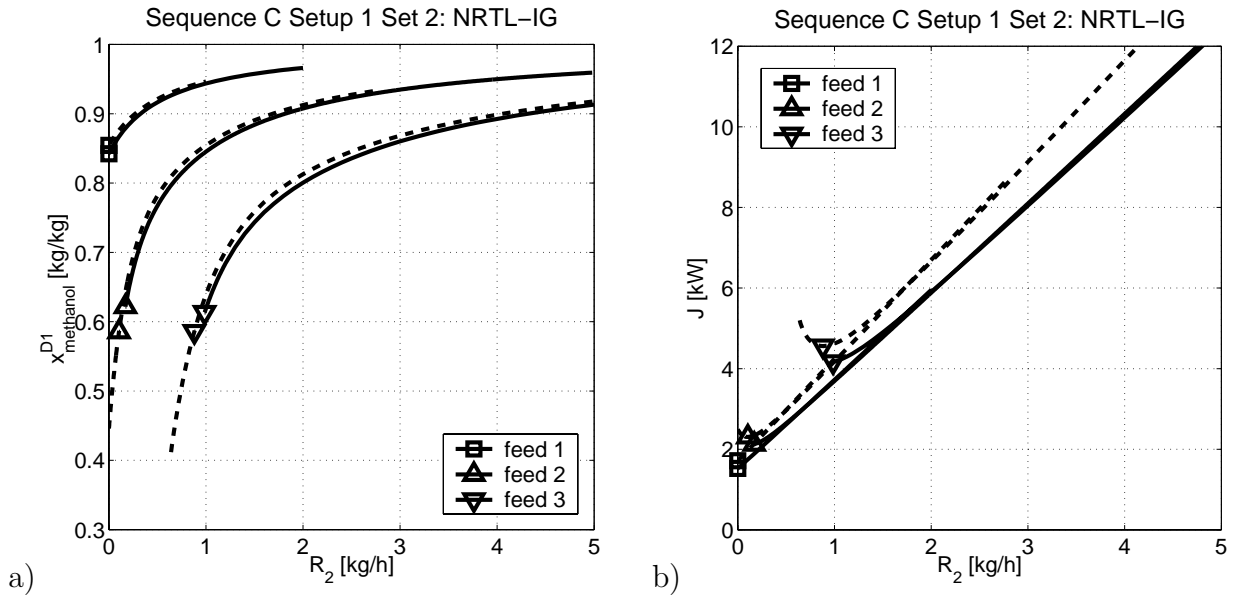


Figure B.9: Sequence C setup 1 set 2 (solid lines) and set 2a (dashed lines): a) $x_{methanol}^{D1}$ and b) J as a function of R_2 .

B.2.2.2 Set 3

Figure B.10a shows the objective function J as a function of the controlled variable $x_{methanol}^{D1}$ with solid lines for set 3 (Table 6.4). In this case, the values are taken for feed 3 which requires the highest refluxes of the three feeds. For constant refluxes, the energy consumption will be more or less independent of the feed composition and the recycles as long as the reflux is above the minimum reflux. For feed 1 and feed 2, J is substantially higher (always above 3.5 kW) than for set 1 and set 2 where it was below 2 kW close to the optimal point (Figure 6.4a and Figure B.8a). For feed 3, column 1 will be below minimum reflux for high values of the recycles R_2 and opposed to that, column 3 will be below minimum reflux for low R_2 because this increases D_3 . The result is that for feed 3), R_2 can just be varied in a small range. As for setup 2, a 20% higher reflux increased the robustness of the convergence. Set 3a is shown with dashed lines in Figure B.10. Figures B.10b, B.10c, and B.10d show the other relations.

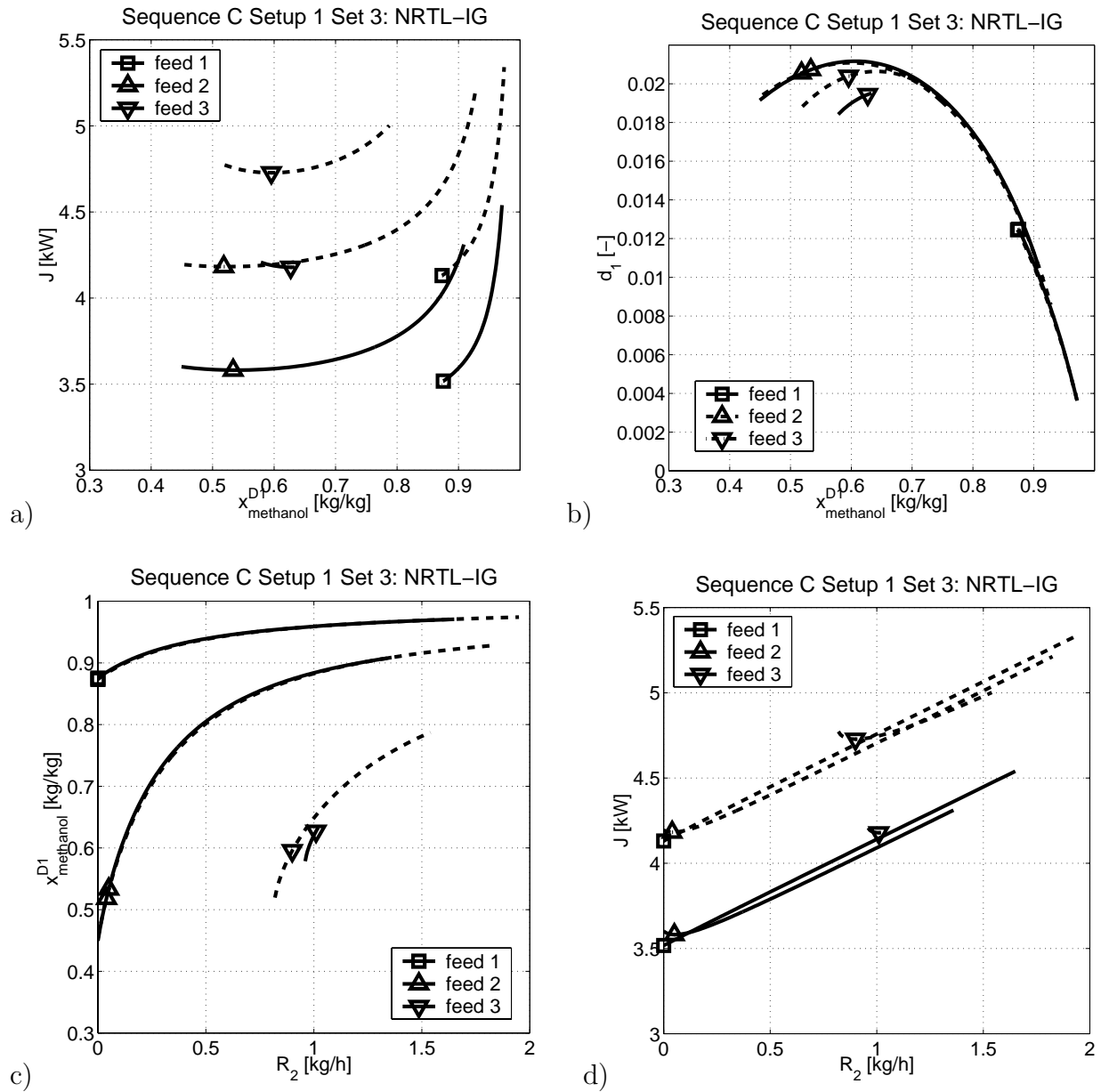


Figure B.10: Sequence C setup 1 set 3: The two objective functions a) J and b) d_1 as a function of the controlled variable x_{methanol}^{D1} ; and c) x_{methanol}^{D1} and d) J as a function of R_2 .

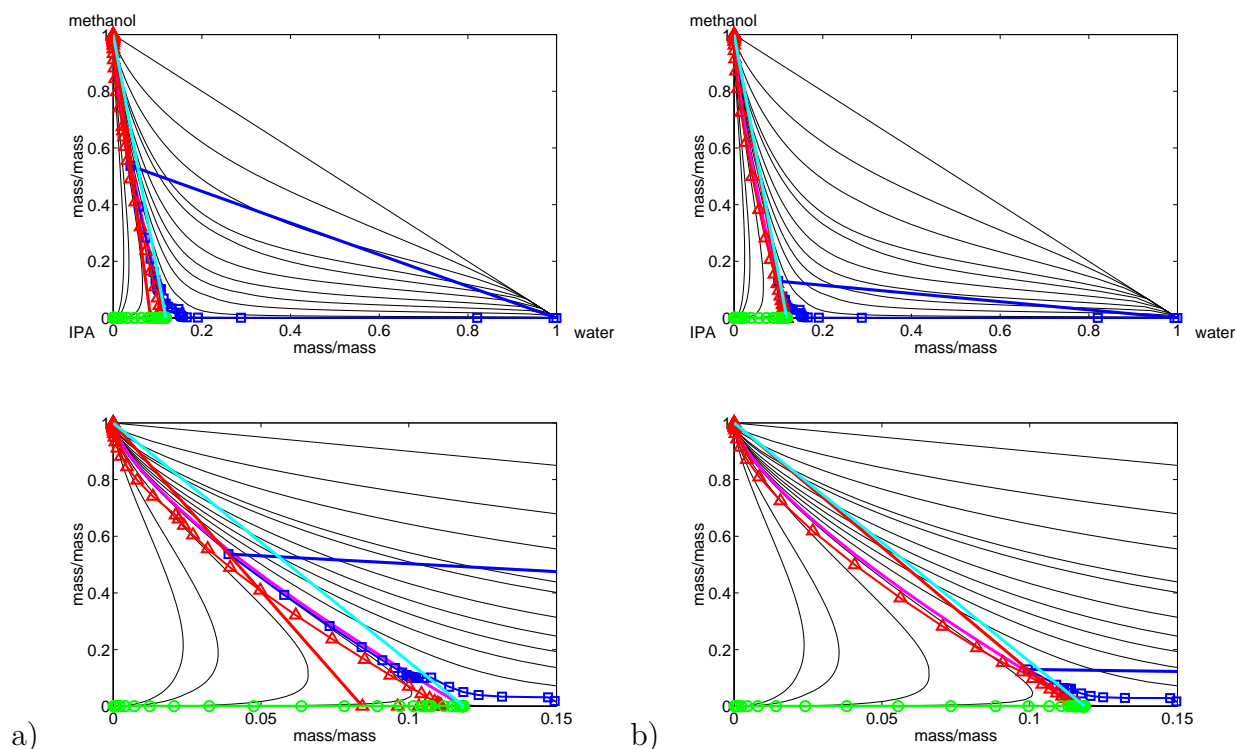


Figure B.11: Two different operation points for $R_2 = 1$ kg/h with parameters listed a) in Table B.1 and b) in Table B.2.

B.2.3 Effect of the Recycle R_2

The mapping of R_2 on $x_{methanol}^{D_1}$ for x^{D_3} in the non-convex set (Figure 5.25) corresponds to an output multiplicity: there are two $x_{methanol}^{D_1}$ (output) for a given R_2 (input). In particular, there are two solutions for the base case feed for $R_2 = 1$ kg/h. Figure B.11 shows the resulting column profiles with the operation parameters listed in Table B.1 for the higher branch and in Table B.2 for the lower branch. The two solutions are not for the optimal setup, but for an earlier over-refluxed setup calculated with Wilson-IG. One solution is for $D_3 = 0.8135$ kg/h. Another solution is around $D_3 \approx 8.5$ kg/h. Using the Aspen Plus steady state solver leads to D_3 decreasing from step to step for $R_3 = 8.581$ kg/h as initial value and to increasing D_3 above $R_3 = 8.583$ kg/h as initial value. This gives the hint that there might be an unstable equilibrium between these values because this is similar to a discrete time system with perfect composition control of the three columns. As mentioned above, a sensitivity study for R_2 is extremely difficult because convergence is hardly reached. This indicates the expected movement of a pole as a result of the output

Table B.1: Operation parameters for a point on the higher branch (stable operation point); base feed (Table 6.1).

D_1	2.482 kg/h	L_1	12.2 kg/h	$x_{water}^{D_1}$	0.0390
B_1	0.334 kg/h	Q_1	4.000 kW	$x_{water}^{B_1}$	0.9998
R_2	1.000 kg/h			$x_{methanol}^{D_1}$	0.5371
D_2	1.333 kg/h	L_2	5.91 kg/h	$x_{methanol}^{D_2}$	0.9998
B_2	1.148 kg/h	Q_2	2.209 kW	$x_{methanol}^{B_2}$	0.00005
D_3	0.816 kg/h	L_3	6.51 kg/h	$x_{water}^{D_3}$	0.11865
B_3	0.333 kg/h	Q_3	1.746 kW	$x_{2-propanol}^{B_3}$	0.9998

Table B.2: Operation parameters for a point on the lower branch (proposed to be unstable); base feed (Table 6.1).

D_1	10.25 kg/h	L_1	5.73 kg/h	$x_{water}^{D_1}$	0.0994
B_1	0.334 kg/h	Q_1	4.000 kW	$x_{water}^{B_1}$	0.9998
R_2	1.000 kg/h			$x_{methanol}^{D_1}$	0.1301
D_2	1.333 kg/h	L_2	17.9 kg/h	$x_{methanol}^{D_2}$	0.9998
B_2	8.917 kg/h	Q_2	5.854 kW	$x_{methanol}^{B_2}$	0.00005
D_3	8.585 kg/h	L_3	20.4 kg/h	$x_{water}^{D_3}$	0.11865
B_3	0.333 kg/h	Q_3	6.915 kW	$x_{2-propanol}^{B_3}$	0.9998

multiplicity.

B.2.4 Continuum of Solutions

B.2.4.1 Validation of Continuous Output Multiplicities

For ternary feeds, it was found for the II-I-II profile that a set of concentrations of x^{D_1} and x^{D_3} is possible for constant flow rates (section 5.3.2.2). These continuous multiplicities are not only possible for the II-I-II profile, but also for a III-I-III profile. This is validated here for the methanol/2-propanol/water mixture using a binary feed of $x_{2-propanol}^{FC} = 0.5$ kg/kg

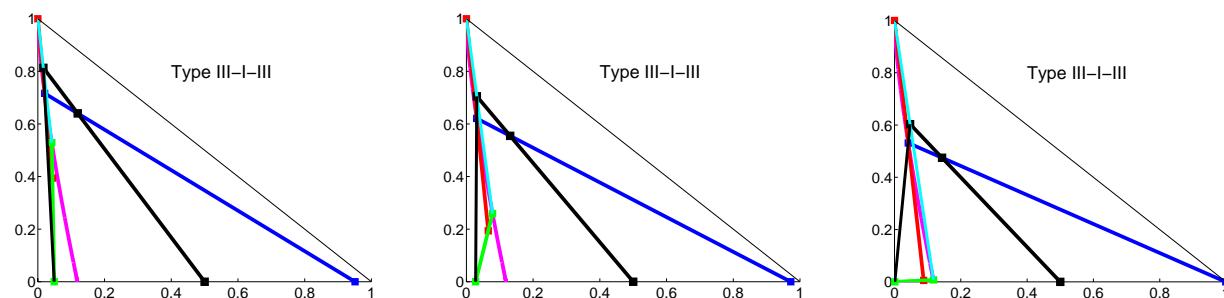


Figure B.12: Mass balances for a III-I-III profile for three different cases for $D_1 = 4.196$ kg/h, $D_2 = 2.224$ kg/h, and $D_3 = 1.472$ kg/h ($F_C = 1$ kg/h) to illustrate the continuum of solutions.

and $x_{water}^{F_C} = 0.5$ kg/kg at $F_C = 1$ kg/h and the Wilson-IG parameter set. The column configuration was already shown in Figure 2.6. This ∞/∞ column sequence has 3 degrees of freedom. For a set a flow rates ($D_1 = 4.196$ kg/h, $D_2 = 2.224$ kg/h, and $D_3 = 1.472$), Figure B.12 shows the mass balances for the III-I-III profile in the residue curve map. From the continuum of solutions, three specific cases are shown. The key point here is that for a fixed set of flow rates, the concentrations x^{D_1} and x^{D_3} may vary along the boundary while x^{B_1} and x^{B_3} vary along the binary edge. For this particular case, the compositions of the flow rates leaving the system (x^{B_1} and x^{B_3}) change for fixed flow rates. In terms of the self-optimizing control concept, the three flow rates are bad controlled variables because they do not uniquely define the product compositions. The impact of this on a finite sequence is the following.

If all three columns are operated with a large reboiler duty and fixed distillate flow rates (very similar to the ∞/∞ case), then the solver will converge to different solutions based on the initial conditions of for example the tear streams (this is an effect of the AspenPlus solver which uses a block oriented approach and tear streams have to be converged). This is validated with simulations of a three column system with 48 stages per column operated at 200 kW reboiler duty. Figure B.13 shows the bottom compositions of all three columns as a function of the water content of x^{D_3} , which is varied along the residue curve boundary, for the ∞/∞ case and the AspenPlus simulations. Though all degrees of freedom are fixed (the three distillate flow rates for the infinite case and in addition the three reboiler duties in the finite case), the external product compositions x^{B_1} and x^{B_3} differ. A closer

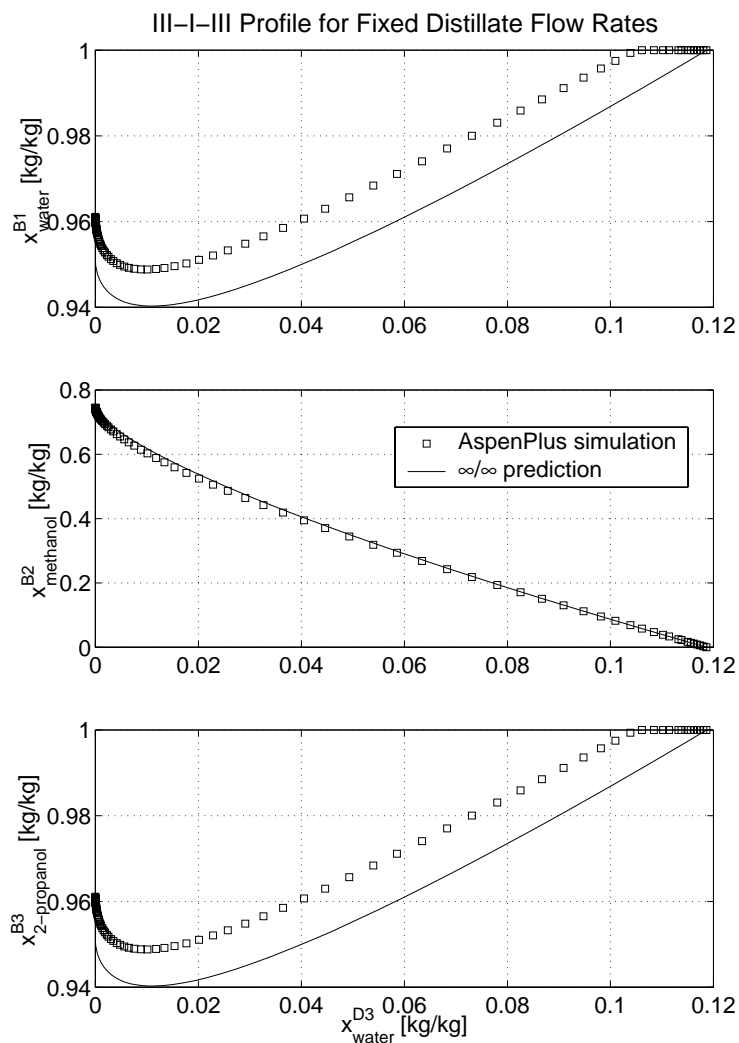


Figure B.13: Different solutions for $D_1 = 4.196$ kg/h, $D_2 = 2.224$ kg/h, and $D_3 = 1.472$ kg/h ($F_C = 1$ kg/h) the III-I-III profile and AspenPlus simulations.

investigation of the solutions reveals that there is a methanol loss which differs from steady state to steady state for the finite columns and a binary feed. For these highly refluxed columns, the methanol loss through B_1 and B_3 is that small that it lies well below the convergence criterion. In this case, these “multiple” solutions are actual a case of extreme sensitivity towards the methanol makeup. Figure B.14 shows the two bottom compositions x^{B_1} and x^{B_3} and the methanol holdup of the system as a function of the methanol makeup for the cases study shown in Figure B.13. Small changes in the makeup lead to a completely different solution with completely different feed compositions and column holdups. Hence, in operation of the three column system with a binary feed, the initial methanol holdup

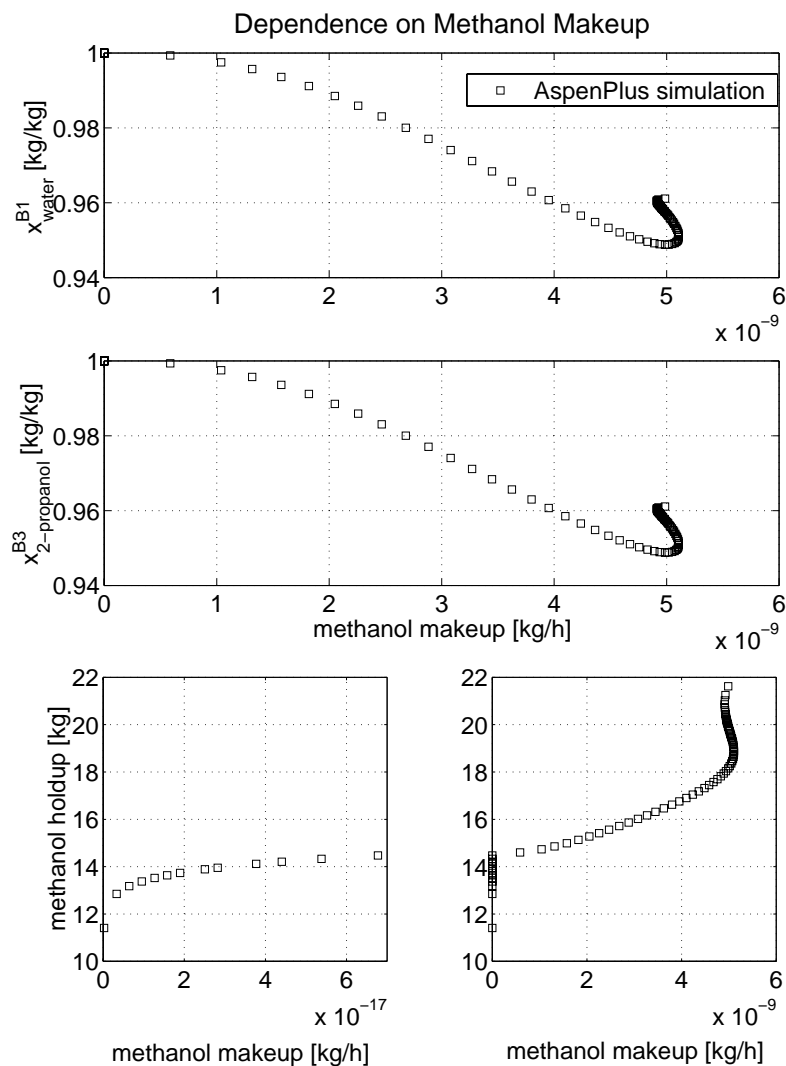


Figure B.14: The compositions x^{B_1} and x^{B_3} and the methanol holdup of the system as a function of the methanol makeup.

plays a central role for the reachability of the desired steady state.

For ∞/∞ columns, there is no methanol in B_1 and B_3 by definition. Hence, the sensitivity disappears and there is a continuum of solutions. The same effect is also possible for a III-III-III profile as shown in Figure B.15. Figure B.16 shows the comparison of the ∞/∞ prediction with AspenPlus simulations with a reboiler duty of 20 kW per column.

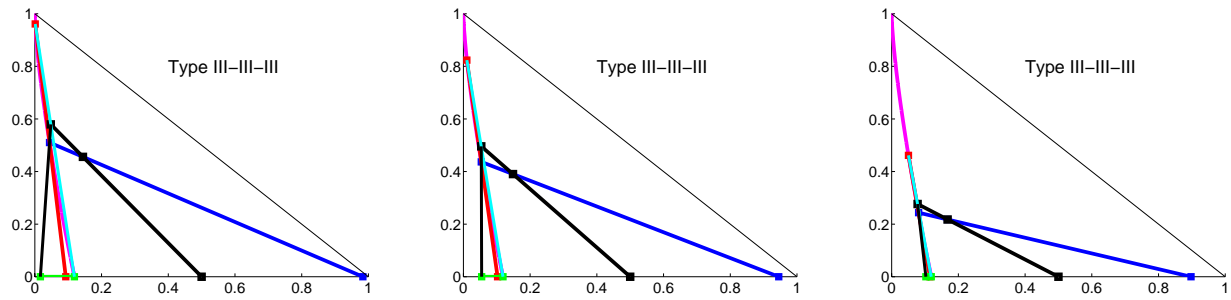


Figure B.15: Mass balances for a III-III-III profile for three different cases for $D_1 = 4.196$ kg/h, $D_2 = 2.224$ kg/h, and $D_3 = 1.472$ kg/h ($F_C = 1$ kg/h) to illustrate the continuum of solutions.

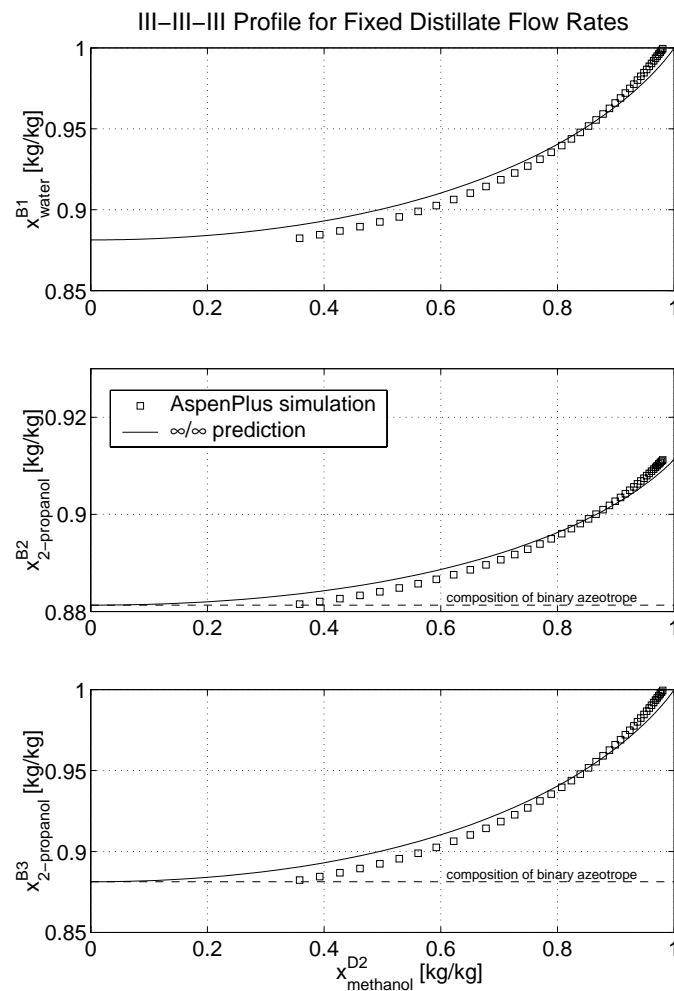


Figure B.16: Different solutions for $D_1 = 4.196$ kg/h, $D_2 = 2.224$ kg/h, and $D_3 = 1.472$ kg/h ($F_C = 1$ kg/h) for the III-III-III profile and AspenPlus simulations.

Table B.3: Two different solutions for the same set of controlled variables for $x^{F_C} = [0.358; 0.308; 0.334]$ and $F_C = 1$ kg/h for the NRTL-IG parameter set.

controlled variable		man. variable	solution 1	solution 2
$x_{water}^{B_1}$	0.9998 kg/kg	B_1	0.334 kg/h	0.334 kg/h
L_1/D_1	1.3	D_1	2.1415 kg/h	1.9897 kg/h
$x_{methanol}^{D_1}$	0.617	R_2	0.895337 kg/h	0.869777 kg/h
$x_{methanol}^{D_2}$	0.9998 kg/kg	D_2	1.2534 kg/h	1.2278 kg/h
L_2/D_2	4.05	$\mathbf{x}_{methanol}^{B_2}$	0.076762 kg/kg	9.24 10⁻⁵ kg/kg
$x_{2-propanol}^{B_3}$	0.9998 kg/kg	B_3	0.333 kg/h	0.333 kg/h
L_3/D_3	5.1	$\mathbf{x}_{water}^{D_3}$	0.105078 kg/kg	0.125096 kg/kg

B.2.4.2 Implications for Simulation and Operation

The above reported continuum (high sensitivity) is a definite effect of the recycles of the system. If the open loop system is analyzed (D_2 and D_3 are feeds to column 1 together with F_C and no product recycles), then there will be three column operated with constant distillate flows but varying feed compositions. As a result of a specific topology of the residue curve, there exists an infinite number of product composition combinations of the two distillates D_2 and D_3 that allow to close the recycles while fulfilling the overall mass balance.

These effects will disappear immediately if compositions such as x^{D_1} , x^{B_2} , and x^{D_3} are specified as done for set 1 of controlled variables. As also discussed in section 6.5 and validated in section 6.6, the reflux-to-distillate ratios are also good controlled variables. However, the uniqueness of solutions can disappear for set 2; at least in the simulations. In a case study for set 2, the block oriented solver did not converge the tear streams. When the next case was initialized with the unconverged solution, the solver found solution 1 for the given controlled variables as listed in Table B.3. Using a different strategy, it was possible to converge to the desired solution (solution 2 in Table B.3).

This is no proof at all that there is really a continuum of solutions in the finite case; this might again be a parametric sensitivity as discussed above in section B.2.4. However, again

Table B.4: Specifications and manipulated variables (in Aspen Plus simulator) for the direct heterogeneous sequence for the base feed (Table 6.1).

specified variable	value	manipulated variable	value
$x_{methanol}^{D_1}$	0.9998 kg/kg	D_1	0.333 kg/h
$x_{methanol}^{B_1}$	0.0001	Q_1^{reb}	1130 W
$x_{2-propanol}^{B_2}$	0.9998 kg/kg	B_2	0.333 kg/h
$x_{water}^{B_3}$	0.9998 kg/kg	B_3	0.334 kg/h
—	—	L_3	1.5 kg/h

the solutions differ significantly. The implications of this for operation of the sequence are that concentration measurements of all the external products are necessary to ensure that the sequence really operates where it should be. This also plays a role for the startup of the sequence (which is not further investigated in this thesis, but is an interesting subject to study).

B.3 Simulations of the Direct Heterogeneous Sequence

For the binaries cyclohexane/2-propanol, cyclohexane/water and 2-propanol/water, NRTL parameters of Wang et al. (1998) were used. For the other binaries, NRTL-IG was used.

B.3.1 Methanol-Free B_1

The most difficult separation is the removal of methanol. Therefore, the longest column was chosen for this separation task. The other two columns have 30 stages to compare it well to the homogeneous schemes. The straightforward specifications for the process are listed in Table B.4 (column 2 has just one degree of freedom, see section 3.2.1 for details, L_3 has to be above minimum reflux). As for the other example system, the feed stages were found by systematically varying the feed stage for the given specifications. The feed stage with the minimum reboiler duty was chosen. For column 1, varying crude feeds and

specifications showed that the optimal feed stage depends on the specifications, but not on the crude feed compositions. The optimal stage is stage 25.

Concerning column 2 and 3, the recycle loop, R_3 is open for the specifications listed in Table B.4. Snowball effects can take place, the solution depends on the initial estimate of F_2 , which is the tear stream to be converged. This problem is the same as observed for binary feeds in the boundary separation scheme. The solution is also the same: the recycle flow R_3 has to be a manipulated variable. For this, a buffer tank has to be added in the recycle loop (also in the steady state simulation to manipulate R_3 independent of D_3). The optimal point is found by minimizing the recycle streams.

Assuming a finite/ ∞ column as introduced in section 3.2.3, the reboiler duty of the heterogeneous column directly depends on the distillate flow D_2 which is a measure for the recycle flow. D_2 is minimal when it is closest to water pure water on the binodal. This is the case when V^T is at the ternary azeotrope. This gives a cyclohexane content of 0.0725 kg/kg in D_2 . For a given feed to the direct sequence, the entrainer feed (the recycle D_3 in this case) has to be adjusted such that F_2 lies on the mass balance line connecting the desired D_2 and B_2 .¹ In the following, the column 2 is operated at this point.

As for column 1, the feed stage of column 2 was varied. The optimal feed stage is stage 3. For column 3, the specification of the reflux L_3 is a bit loose: The column has to be operated with a high enough reflux such that D_3 lies on or at least close to the residue curve boundary. Here, reflux and feed stage are varied. The reboiler duty is nearly independent of the feed stage for different refluxes. Hence, the middle, stage 15, is chosen as feed stage. Varying the refluxes of column 3 for feed stage 15 showed that the sum of the reboiler duties for the two columns in the recycle loop (2 and 3) goes through a minimum. The reason is that for increasing L_3 the distillate moves closer to the boundary. This reduces

¹This is similar to the result of section 3.2 which also explains why the feed forward of the entrainer makeup in the papers of Rovaglio and coworkers works, despite the fact that the entrainer does not really leave the system. From the analysis in this these, it follows more directly that the recycle stream has to be manipulated. By this, the entrainer holdup in the sequence can be varied which is important for the success of the operation of the scheme, as was correctly recognized by Rovaglio and coworkers. However, their scheme lacks the possibility of removing entrainer from the sequence. This could be enabled by placing a buffer tank between the entrainer recovery column and the azeotropic column with decanter.

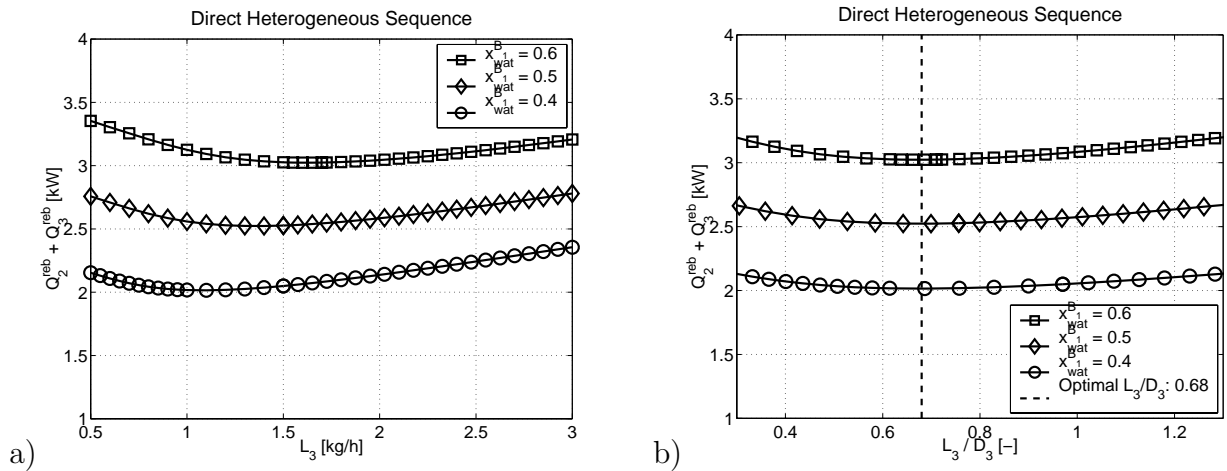


Figure B.17: Sums of the reboiler duties as a function of a) L_3 and b) L_3/D_3 for different feed compositions x^{B_1} at $B_1 = 0.667$ kg/h.

the recycle flows and hence the necessary reboiler duty of column 2. Hence, Q_3 increases and Q_2 decreases for increasing L_3 . Figure B.17 shows the sums of the reboiler duties for the optimal location of D_2 as a function of L_3 for different feed compositions to the recycle loop at a flow rate of 0.667 kg/h. The minimum is a function of the water content in the feed. However, the reflux-to-distillate ratio L_3/D_3 is independent of the water content at the optimal point: 0.68

The reason is that the water flow of F_c determines D_2 and since x^{D_2} is constant, D_3 is also given by the water flow of F_c . Hence, the recycle flow $R_3 = D_3$ only depends on the water flow rate in F_c .

B.3.2 Methanol polluted B_1

Simulations of column operated at high reflux with a pinch at the ternary azeotrope (no decanter on top) for no methanol in the feed showed for increasing methanol contents in the feed that the distillate composition moves to the binary methanol-cyclohexane azeotrope. This validates that there is no quaternary azeotrope present. Figure B.3 (enlargement in Figure B.4) shows the path of the distillate composition including the resulting LLE in a quaternary residue curve diagram. Note that only the boundaries were plotted for the two

ternary subsystems methanol/2-propanol/water and methanol / cyclohexane/2-propanol. From the LLE tielines follows that the aqueous phase in the decanter contains much more methanol than the organic phase. For example, a composition of the boundary with 4% methanol gives 13% methanol in the aqueous phase at 0.5 % in the organic phase. At a methanol content of about 35 %, the phase split disappears giving over 57 % methanol in the aqueous phase. Hence, methanol can be accumulated in the cycle to a significant amount and purged. However, if methanol accumulates, the water content in D_2 decreases from 19% at 4% methanol to 0.5 % at 35 % methanol in the overhead vapor. The water flow that has to pass through D_2 is given. Hence, D_2 has to increase for decreasing water content in D_2 caused by increasing methanol contents. There is a slight methanol loss through B_3 for high methanol contents in the sequence which might be enough to pretend further accumulation of methanol. If not, some of D_2 has to be purged. However, the increase in reboiler duties is significant: The sum of the reboiler duties nearly double from 2.5 kW for no methanol to 4 kW for 0.000006 methanol content in B_1 . For that value, 20 % Methanol in D_2 is required. This high methanol content in D_2 , which is the feed to column 3, leads to a high enough loss of methanol through B_3 .

B.4 Simulations of the Indirect Heterogeneous Sequence

For the binaries cyclohexane/2-propanol, cyclohexane/water and 2-propanol/water, NRTL parameters of Wang et al. (1998) were used. For the other binaries, NRTL-IG was used.

B.4.1 Methanol-Free B_1

The optimal operation point is found by minimizing the recycle streams. As for the direct sequence, the recycle flows are minimal when the top of column 2 is at the ternary azeotrope assuming a methanol-free feed to the recycle loop. Following a similar argumentation as for the direct sequence, R_2 has to be used to manipulate F_2 such that D_3 lies on the line

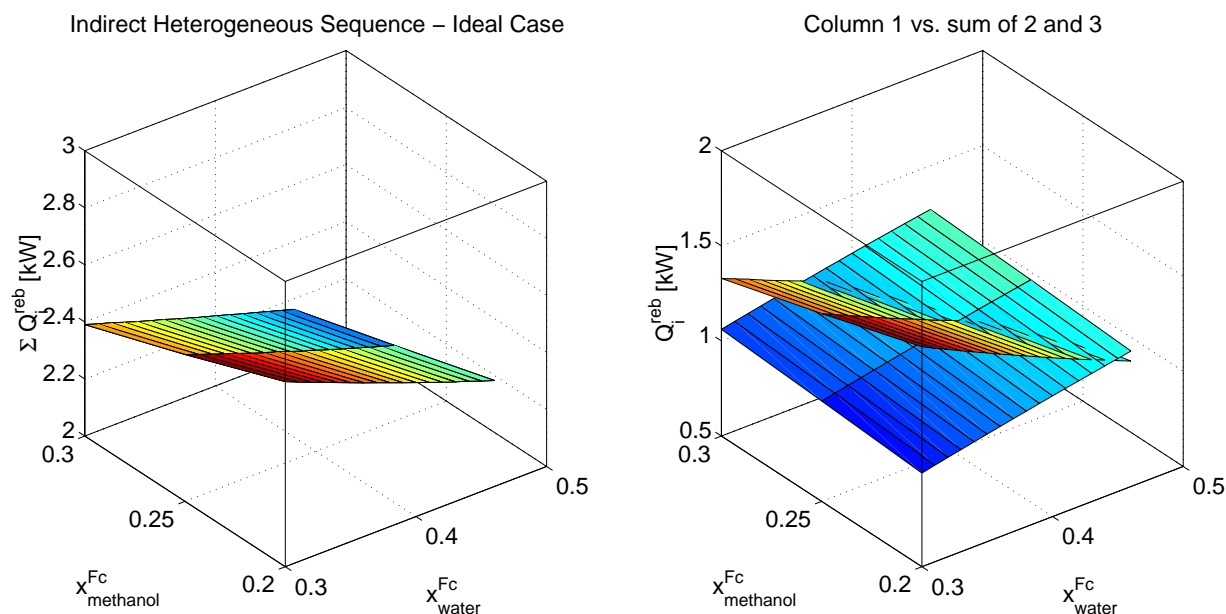


Figure B.18: Reboiler duties for the indirect sequence for the specifications listed in Table 7.5 with $x_{cyc.}^{D_3} = 0.10$.

connecting D_2 with B_2 .

Concerning the simulations in Aspen, it is more difficult to converge the indirect scheme: For column 2, the reflux is a function of the overhead vapor composition (this follows from the decanter policy). For column 3, it is a degree of freedom which can also be manipulated to control the composition of D_3 . Actually, this second degree of freedom is needed because specifying the cyclohexane content for D_2 gave one point on the binodal curve. For D_3 , also one point has to be specified but this time, two compositions have to be defined to uniquely identify the point. Hence, reflux L_3 and R_2 are needed. It turned out that the simulations just converged for a constant reflux $L_3 = 1.36 \text{ kg/h}$. The convergence was also difficult for an $x_{cyc.}^{D_3}$ that would correspond to $x_{cyc.}^{D_2} = 0.0725$. They converged for $x_{cyc.}^{D_3} = 0.038$ which corresponds to $x_{cyc.}^{D_2} = 0.0775$ for the base case. Calculation for the direct sequence with $x_{cyc.}^{D_2} = 0.0775$ showed that $Q_2^{reb} + Q_3^{reb}$ increase by 6% increase for the base case.

However, simulations of the whole 3 column sequence did not converge for varying crude feed compositions for $x_{cyc.}^{D_3} = 0.038$, the scheme only converged for $x_{cyc.}^{D_3} = 0.10$ which corresponds to $x_{cyc.}^{D_2} = 0.138$. The results are shown in Figure B.18. (Since the reflux of

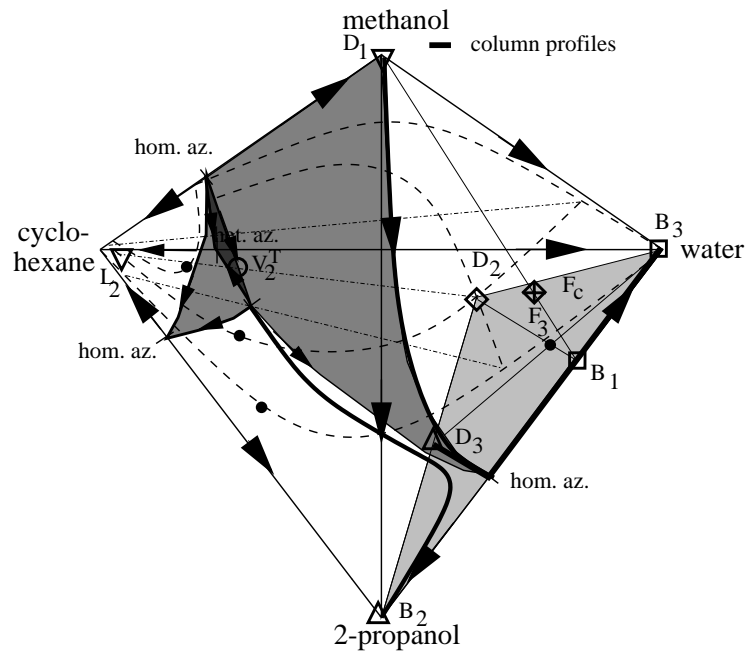


Figure B.19: Indirect heterogeneous sequence for the system methanol /2-propanol/water using cyclohexane as entrainer with a high methanol content in D_2 .

column 2 depends directly on the water content (reflux-to-distillate ratio defined by the LLE phase split and distillate proportional to the water content), the reflux of column 2 might get below the minimum reflux which results in no convergence.

$L_3 = 1.36$ and $x_{cyclohexane}^{D_3} = 0.10$, which corresponds to $x_{cyclohexane}^{D_2} \approx 0.1375$. Specifying the water content with L_3 lead to no convergence.

B.4.2 Methanol polluted B_1

Figure B.19 shows the four component residue curve tetrahedron with the column profiles for a high methanol content in the recycle loop. One problem here is that it is not immediately clear whether the line connecting B_1 and D_2 really intersects the mass balance line of column 3. This is however always the case for the ∞/∞ columns. B_1 does not contain any methanol and B_2 and B_3 are pure 2-propanol and pure water, respectively. A plane spanned by D_2 , B_2 and B_3 contains also D_3 and B_1 because both lie on lines that interconnect these three points. Hence, the line connecting B_1 and D_2 and the mass balance line of

column 3 also lie in this plane and so does F_3 . QED. By changing D_2 , it is possible to place x^{D_2} on the binodal which results from the residue curve boundary connecting the ternary azeotrope with the unstable node, the binary methanol-cyclohexane azeotrope (compare Figure B.3). This is an input multiplicity because the outputs (B_2 and B_3) remain the same, but different methanol/cyclohexane inventories are necessary.

Appendix C

Simple Examples for Illustration

C.1 Quadratic Residue Curve Boundary for the BSS

For the example, the Residue Curve Boundary (RCB) is given by a simple quadratic equation:

$$x_L^{RCB} = 2 \left(x_H^{RCB} \right)^2 - 3 x_H^{RCB} + 1 \quad (\text{C.1})$$

All the calculations are done in the two dimensional space with x_H and x_L as coordinates. The residue curve was shown in Figure 5.13a for these coordinates.

C.1.1 Sequence B

The recycle flows D_3 can be calculated using the mass balance around column 2 and 3:

$$D_1 = D_2 B_3 + D_3 \quad (\text{C.2})$$

$$x^{D_1} D_1 = x^{D_2 B_3} D_2 B_3 + x^{D_3} D_3 \quad (\text{C.3})$$

The overall mass balance gives for a II-I-II profile:

$$D_2 B_3 = (1 - x_H^{F_C}) F_C \quad (\text{C.4})$$

Combining these two equations gives as a function of the H content of the products:

$$D_3 = \frac{x_H^{D_1} - x_H^{D_2 B_3}}{x_H^{D_3} - x_H^{D_1}} (1 - x_H^{F_C}) F_C \quad (\text{C.5})$$

By definition, $x_H^{D_2B_3} = 0$ and x^{D_1} lies on the mass balance line MB23 connecting $x^{D_2B_3}$ with x^{D_3} . This can be written as:

$$x_L^{MB23} = a x_H^{MB23} + b \quad , \quad a = -\frac{x_L^F}{x_H^{D_3}(1-x_H^F)} \quad , \quad b = \frac{x_L^F}{(1-x_H^F)} \quad (\text{C.6})$$

If the residue curve boundary is not given in an explicit form, x^{D_1} has to be found by iteration. Here, the residue curve boundary is given in an explicit form, equation C.1. Equating it with equation C.6 gives:

$$2(x_H^{D_1})^2 - (3+a)x_H^{D_1} + 1 - b = 0 \quad (\text{C.7})$$

This can be solved to:

$$(x_H^{D_1})_{1,2} = \frac{3+a}{4} \pm \sqrt{\left(\frac{3+a}{4}\right)^2 - \frac{1-b}{2}} \quad (\text{C.8})$$

If x^F is in the feasible region, the left (smaller) root is smaller than $x_H^{D_3}$, as required for the calculation of the recycle flow D_3 . The right root is equal to $x_H^{D_3}$. If the left root is $x_H^{D_3}$, x^F is outside the feasible region. Inserting equation C.8 into equation C.5, the recycle flows can be calculated for each given feed x^F inside the feasible region.

C.1.2 Sequence C: Setup 1

C.1.2.1 Optimal Composition of D_1

For a II-I-II profile and the residue curve boundary as given by equation C.1, $x^{D_2} = [0; 1]$ and $x^{D_3} = [1/2; 0]$. Hence, the normal vector as defined by equation 5.25 is:

$$n = \begin{bmatrix} 0 & -1 \\ 1 & 0 \end{bmatrix} \left(\begin{bmatrix} 0 \\ 1 \end{bmatrix} - \begin{bmatrix} 1/2 \\ 0 \end{bmatrix} \right) = \begin{bmatrix} -1 \\ -1/2 \end{bmatrix} \quad (\text{C.9})$$

For $x_L^{D_1}$ the equation for the residue curve boundary is used. Hence:

$$d_1 = [-1 \quad -1/2] \begin{bmatrix} x_H^{D_1} - 1/2 \\ 2(x_H^{D_1})^2 - 3x_H^{D_1} + 1 \end{bmatrix} \quad (\text{C.10})$$

$$d_1 = -x_H^{D_1} + 1/2 - (x_H^{D_1})^2 + 3/2 x_H^{D_1} - 1/2 \quad (\text{C.11})$$

$$d_1 = -(x_H^{D_1})^2 + 1/2 x_H^{D_1} \quad (\text{C.12})$$

$$\frac{d d_1}{d x_H^{D_1}} = -2 x_H^{D_1} + 1/2 \stackrel{!}{=} 0 \quad (\text{C.13})$$

$$\implies x_H^{D_1, opt} = 1/4 \quad (\text{C.14})$$

$$x_L^{D_1, opt} = 2/16 - 3/4 + 1 = 3/8 \quad (\text{C.15})$$

C.1.2.2 Tangent to RCB for x^{D_3}

The tangent of a curve in one point x_0 for a function $f(x)$ is:

$$T(x) = f'(x_0) (x - x_0) + f(x_0) \quad (\text{C.16})$$

Here, f' is the first derivative of f with respect to x . To determine the feasible region for $R_2 = 0$, the tangent to the RCB for a given x^{D_3} has to be calculated:

$$f(x) = 2x^2 - 3x + 1 \quad (\text{C.17})$$

$$f'(x) = 4x - 3 \quad (\text{C.18})$$

$$T(x) = (4x_0 - 3)(x - x_0) + 2x_0^2 - 3x_0 + 1 \quad (\text{C.19})$$

$$T(x_H^{D_3}) = (4x_0 - 3)(x_H^{D_3} - x_0) + 2x_0^2 - 3x_0 + 1 \stackrel{!}{=} x_L^{D_3} \quad (\text{C.20})$$

Reformulation gives:

$$x_0 = x_H^{D_3} \pm \sqrt{(x_H^{D_3})^2 - 3/2 x_H^{D_3} + 1/2} \quad (\text{C.21})$$

Again, only the left root is of interest. x_0 determines the x -coordinate of the point on RCB.

C.1.3 Sequence C: Setup 2

The mass balance for the subsystem column 2 and 3 gives:

$$x^{F_C} F_C + x^{D_1} D_1 = x^{D_2^x} D_2 + x^{B_3} B_3 + x^{F_1} F_1 \quad (\text{C.22})$$

Further:

$$x^{F_1} F_1 = x^{D_2} R_2 + x^{D_3} D_3 \quad (\text{C.23})$$

With:

$$D_1 = R_2 + D_3 - B_1 \quad \text{and} \quad D_3 = D_1 + B_1 - R_2 \quad (\text{C.24})$$

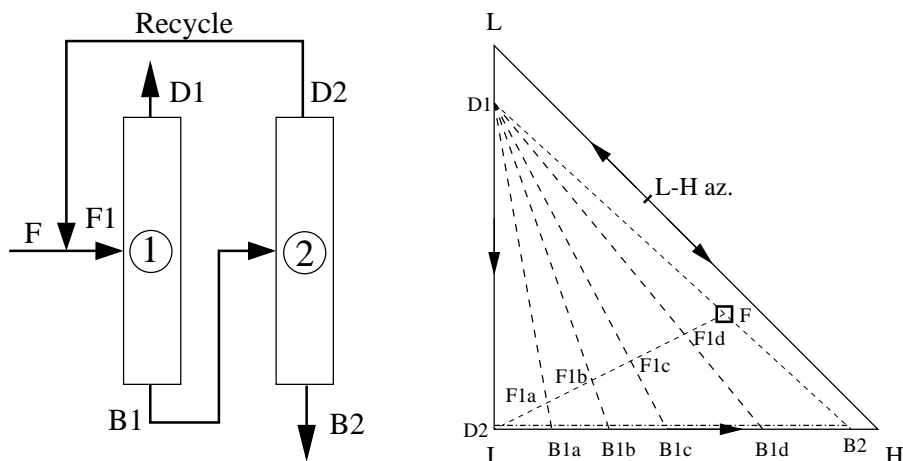


Figure C.1: Intermediate Entrainer Sequence: III-III profile.

follows after rearrangement:

$$(x^{D_3} - x^{D_1}) D_1 + (x^{D_2} - x^{D_3}) R_2 = x^{F_C} F_C - x^{D_3} B_1 - x^{D_2^{ex}} D_2 - x^{B_3} B_3 \quad (C.25)$$

For $x^{D_1, opt} = [0.25; 0.375]$ and $x^{D_3} = [0.5; 0]$ follows for the II-I-II profile:

$$D_1 = 8 x_H^{F_C} F_C \quad \text{and} \quad R_2 = 3 x_H^{F_C} F_C \quad (C.26)$$

$$D_2 = 3 x_H^{F_C} F_C + x_L^{F_C} F_C \quad \text{and} \quad D_3 = 6 x_H^{F_C} F_C \quad (C.27)$$

C.2 Intermediate Entrainer State Multiplicities

Figure C.1 shows that a continuum of recycle streams is possible for constant outputs (flow rates and compositions). Different recycle flow rates D_2 result in e.g. F1a to F1d that all fulfill the overall mass balance.

C.3 Models for Input and Output Multiplicities

The existence of input and output multiplicities has attracted many researchers. A good overview about the capability of models representing input and output multiplicities is given by Pearson (1999) and Pearson and Pottmann (2000). Here, input multiplicities can

be caused by a static nonlinearity before the dynamic system (Hammerstein model) or after the dynamic system (Wiener model). In both cases, just the steady-state gain changes sign as a result of the nonlinearity, but the dynamics remain unchanged. Output multiplicities can be either caused by a nonlinear feedback (Lure model) or by the general NARMAX (Nonlinear AutoRegressive Moving Average eXogenous) models. The latter can also cause input multiplicities. If there is an output multiplicity, the pole of the linearized system crosses the imaginary axis. This is the definition of a fold bifurcation. There are numerous examples for this, which are listed in Dorn (2000). Output multiplicities exist for azeotropic distillation columns (Bekiaris et al., 1993; Bekiaris et al., 1996) and the instability is caused by the topology of the residue curve map (Dorn and Morari, 2002a; Dorn and Morari, 2002b). A simple example is the following:

$$\dot{x}_1 = -x_1^2 + x_1 - 1.25 + u \quad (\text{C.28})$$

$$\dot{x}_2 = -x_1 - 2x_2 \quad (\text{C.29})$$

$$y = x_2 \quad (\text{C.30})$$

For $u = 1.25$, there are two steady states possible.

SS1 (stable): $x_1 = 1$, $x_2 = -0.5$, and $y = -0.5$. The transfer function of the linearized system is:

$$G_{SS1}(s) = \frac{-1}{s^2 + 3s + 2} \quad (\text{C.31})$$

SS2 (unstable): $x_1 = 0$, $x_2 = 0$, and $y = 0$. The transfer function of the linearized system is:

$$G_{SS2}(s) = \frac{-1}{s^2 + s - 2} \quad (\text{C.32})$$

Different to output multiplicities, input multiplicities usually do not affect the dynamic behavior. Two examples (Wiener and Hammerstein structure) illustrate an input multiplicity without an effect on the system dynamics:

Hammerstein Structure

$$\dot{x}_1 = -x_1 + u^2 \quad (\text{C.33})$$

$$\dot{x}_2 = x_1 - 2x_2 \quad (\text{C.34})$$

$$y = x_2 \quad (\text{C.35})$$

For $u = 0.5$, the steady state is at $x_1 = 0.25$, $x_2 = 0.125$, and $y = 0.125$. The transfer function of the linearized system is:

$$G_{u=0.5}(s) = \frac{1}{s^2 + 3s + 2} \quad (\text{C.36})$$

For $u = -0.5$, the steady state is at $x_1 = 0.25$, $x_2 = 0.125$, and $y = 0.125$. The transfer function of the linearized system is:

$$G_{u=-0.5}(s) = \frac{-1}{s^2 + 3s + 2} \quad (\text{C.37})$$

For decreasing u , the steady-state gain of the transfer function of the linearized system moved from positive to negative values being 0 at $u = 0$. The poles remain unchanged.

Wiener Structure

$$\dot{x}_1 = -x_1 + u \quad (\text{C.38})$$

$$\dot{x}_2 = x_1 - 2x_2 \quad (\text{C.39})$$

$$y = x_2^2 \quad (\text{C.40})$$

Here, the static nonlinearity is just shifted from the input (Hammerstein structure) to the output (Wiener Structure). For $u = 0.5$, the steady state is at $x_1 = 0.5$, $x_2 = 0.25$, and $y = 0.0625$. The transfer function of the linearized system is:

$$G_{u=0.5}(s) = \frac{0.5}{s^2 + 3s + 2} \quad (\text{C.41})$$

For $u = -0.5$, the steady state is at $x_1 = -0.5$, $x_2 = -0.25$, and $y = 0.0625$. The transfer function of the linearized system is:

$$G_{u=-0.5}(s) = \frac{-0.5}{s^2 + 3s + 2} \quad (\text{C.42})$$

Despite that, general dynamic systems such as NARMAX models can have input multiplicities that affect the system dynamics. The following arbitrary system has an input multiplicity and the change of the sign of the steady-state gain of the linearized system

results from a transfer function zero moving from the left-half plane into the right-half plane. This introduces a non-minimum phase behavior, which is known to significantly influence the controller performance. The nonlinear system is given as:

$$\dot{x}_1 = -2x_1 + 18x_2^2 - 9x_2 + 2.5 + u \quad (\text{C.43})$$

$$\dot{x}_2 = -3x_2 + u \quad (\text{C.44})$$

$$y = x_1 \quad (\text{C.45})$$

For $u = 0.6$, the steady state is at $x_1 = 1.01$, $x_2 = 0.2$, and $y = 1.01$. The transfer function of the linearized system is:

$$G_{u=0.6}(s) = \frac{s + 1.2}{s^2 + 5s + 6} \quad (\text{C.46})$$

For $u = 0.4$, the steady state is at $x_1 = 1.01$, $x_2 = 0.1333$, and $y = 1.01$. The transfer function of the linearized system is:

$$G_{u=0.4}(s) = \frac{s - 1.2}{s^2 + 5s + 6} \quad (\text{C.47})$$

For decreasing u , the zero the transfer function of the linearized system moved from the left-half plane to the right-half plane, crossing the imaginary axis for $u = 0.5$.

Input and Output MSS

$$\dot{x}_1 = -x_1^2 + x_1 - 1.25 + u \quad (\text{C.48})$$

$$\dot{x}_2 = -x_1 - 2x_2 + u \quad (\text{C.49})$$

$$y = x_2 \quad (\text{C.50})$$

The only difference to model 3 is that the input u also affects directly the second state (x_2). For $u = 1.09$, there are two steady states:

SS1 (stable): $x_1 = 0.8$, $x_2 = 0.145$, and $y = 0.145$. The transfer function of the linearized system is:

$$G_{SS1}(s) = \frac{s - 0.4}{s^2 + 2.6s + 1.2} \quad (\text{C.51})$$

SS2 (unstable): $x_1 = 0.2$, $x_2 = 0.445$, and $y = 0.445$. The transfer function of the linearized system is:

$$G_{SS2}(s) = \frac{s - 1.6}{s^2 + 1.4s - 1.2} \quad (\text{C.52})$$

SS3 (stable): For $y = 0.145$, there are also two steady states. One for $u = 1.09$ (SS1) and the other one for $u = 1.49$ (SS3): $x_1 = 1.2$, $x_2 = 0.145$, and $y = 0.145$. The transfer function of the linearized system is:

$$G_{SS3}(s) = \frac{s + 0.4}{s^2 + 3.4s + 2.8} \quad (\text{C.53})$$

The differences in the behavior can be well explained with the different structure of the A , B , and C matrices of the linearized dynamic system. By this, it can be easily recognized why the pole and the zero have to move for the different linearized systems.

This behavior could be used to explain the observed non-minimum phase behavior in the operation of the heavy entrainer scheme (Andersen et al., 1991; Andersen et al., 1995) for which Zheng et al. (1998) report an input multiplicity.

C.4 Inverse Response Behavior

A possible control scheme could be to fix all the interconnecting flows (D_1 , D_2 , and D_3) and to ensure the bottom purities of column 1 and 3 by manipulating the reboiler duties. Even though this is against the common rule that an external flow rate should never be kept constant (manual) in one-point control of distillation columns (Skogestad, Lundström and Jacobsen, 1990), it seems tempting for the startup of the process to reach the desired steady state. For this scheme, an inverse response of the bottom purity for step changes in the reboiler duty is possible for some operation points. This can be shown by a simple model as shown in Figure C.2. Using rigorous dynamic simulations of a three column system (50 stages each column), the following step answer was obtained (Figure C.3).

It can be shown by simple linear models that it is then not possible to find a proportional-integral feedback controller that allows stable operation.

$$\begin{bmatrix} \Delta x^{D_1} \\ \Delta x^{B_1} \end{bmatrix} = \begin{bmatrix} g_{11} & g_{12} \\ g_{21} & g_{22} \end{bmatrix} \cdot \begin{bmatrix} \Delta x^F + \Delta x^{R_2} \\ \Delta Q_1 \end{bmatrix} \quad (\text{C.54})$$

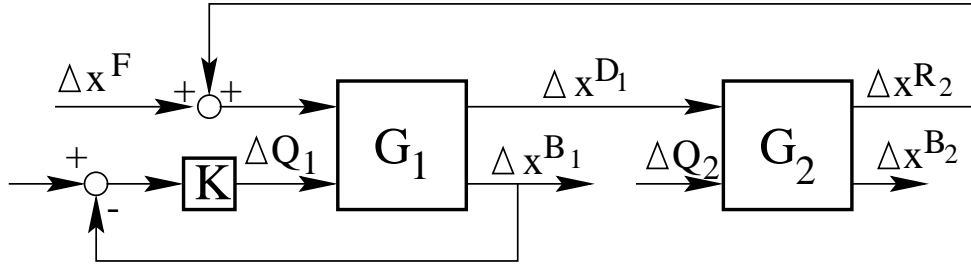


Figure C.2: A reduced linear model for a two column process of the boundary separation scheme operated at constant flow rates.

$$\begin{aligned} g_{11} &= \frac{1}{2s+1} \quad , \quad g_{12} = \frac{-1}{0.2s+1} \\ g_{21} &= \frac{1}{2s+1} \quad , \quad g_{22} = \frac{1}{0.2s+1} \end{aligned} \quad (\text{C.55})$$

$$\begin{bmatrix} \Delta x^{R_2} \\ \Delta x^{B_2} \end{bmatrix} = \begin{bmatrix} g_{33} & g_{34} \\ g_{43} & g_{44} \end{bmatrix} \cdot \begin{bmatrix} \Delta x^{D_1} \\ \Delta Q_2 \end{bmatrix} \quad (\text{C.56})$$

With k varying.

$$\begin{aligned} g_{33} &= \frac{k}{2s+1} \quad , \quad g_{34} = \frac{1}{0.2s+1} \\ g_{43} &= \frac{1-k}{2s+1} \quad , \quad g_{44} = \frac{-1}{0.2s+1} \end{aligned} \quad (\text{C.57})$$

$$G(s) = \frac{1}{0.2s+1} \frac{4s^2 + 4s + 1 - 2k}{4s^2 + 4s + 1 - k} \quad (\text{C.58})$$

The position of the poles and zeros depends on the parameter k .

- For $0 < k < 0.5$, all poles and zeros are in the left-half plane.
- For $k = 0.5$, one zero is in the origin, the other zero and all poles are in the left-half plane.
- For $0.5 < k < 1$, one zero is in right-half plane, the other zero and all poles are in the left-half plane.
- For $k > 1$, one pole also moved to the right-half plane inducing unstable behavior.

If ΔQ_1 is used to control x^{B_1} , there does not exist a PI controller, which operates stable for $k < 0.5$ and for $k > 0.5$.

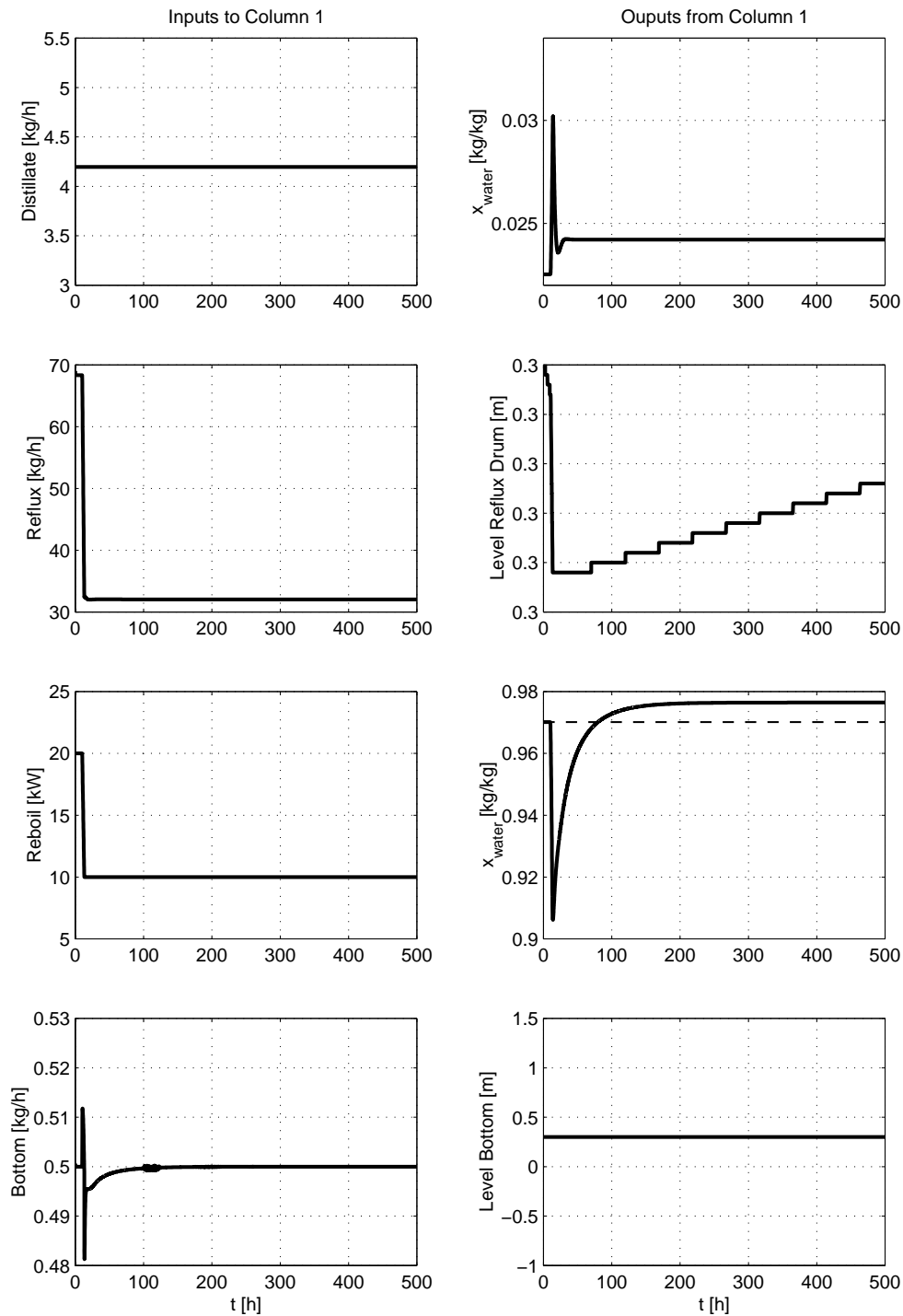


Figure C.3: Dynamic Simulation of a step change in Q_1^R for the boundary separation scheme with DQ^R control scheme for all columns at constant distillate flow rates (locked material balances).

Curriculum Vitae of Jan Ulrich

- born January 18, 1972, Frankfurt/Main, Germany
- citizen of Germany

Education

8/1978 – 7/1982: Albert-von-Reinach-Schule (primary school), Kelkheim/Ts., Germany

8/1982 – 6/1991: Bischof–Neuman–Schule (high school), Königstein/Ts., Germany

10/1992 – 1/1998: Chemical Engineering, University of Karlsruhe, Germany

- **5/1997 – 12/1997:** Diploma–thesis with Solvay fellowship: *Measurements of Aqueous Protein Interactions from Low–Angle Laser–Light Scattering and Molecular Thermodynamics of Salt–Induced Protein Precipitation*, advisors: Prof. J. M. Prausnitz, Prof. H. W. Blanch, Department of Chemical Engineering, University of California, Berkeley, USA, and Prof. E.–U. Schlünder, Institute for Thermal Process Engineering, University of Karlsruhe
- **1/1998:** Diplom (graduation)

3/1998 – 11/2002: Swiss Federal Institute of Technology (ETH) Zürich, Switzerland

- PhD student: *Operation and Control of Azeotropic Distillation Column Sequences*, advisor Prof. Morari, Automatic Control Laboratory, ETH Zürich

Practical Work

7/1991 – 9/1992: civil services, Malteser Hilfsdienst, Kelkheim/Ts., Germany

10/1994 – 6/1996: assistant of Prof. Oellrich, Institute for Thermodynamics and Refrigeration, University of Karlsruhe, Germany

2/1996 – 4/1996: internship at Bayer AG, Leverkusen, Germany

3/1998 – 11/2002: research and teaching assistant at the Automatic Control Laboratory, Department of Information Technology and Electrical Engineering, ETH Zürich

11/1999 – 6/2002: laboratory informatics coordinator at the Automatic Control Laboratory, Department of Information Technology and Electrical Engineering, ETH Zürich